

University of Louisville

## ThinkIR: The University of Louisville's Institutional Repository

---

Electronic Theses and Dissertations

---

12-2011

### Functionalized nanoparticles for AMF-induced gene and drug delivery.

Souvik Biswas  
*University of Louisville*

Follow this and additional works at: <https://ir.library.louisville.edu/etd>

---

#### Recommended Citation

Biswas, Souvik, "Functionalized nanoparticles for AMF-induced gene and drug delivery." (2011). *Electronic Theses and Dissertations*. Paper 112.  
<https://doi.org/10.18297/etd/112>

This Doctoral Dissertation is brought to you for free and open access by ThinkIR: The University of Louisville's Institutional Repository. It has been accepted for inclusion in Electronic Theses and Dissertations by an authorized administrator of ThinkIR: The University of Louisville's Institutional Repository. This title appears here courtesy of the author, who has retained all other copyrights. For more information, please contact [thinkir@louisville.edu](mailto:thinkir@louisville.edu).

**FUNCTIONALIZED NANOPARTICLES FOR  
AMF-INDUCED GENE AND DRUG DELIVERY**

By

Souvik Biswas

A Dissertation

Submitted to the Faculty of the

Graduate School of the University of Louisville

in Partial Satisfaction of the Requirements

for the Degree of

Doctor of Philosophy

in

Chemistry

Department of Chemistry

University of Louisville

Louisville, Kentucky

December 2011

**FUNCTIONALIZED NANOPARTICLES FOR  
AMF-INDUCED GENE AND DRUG DELIVERY**

By

Souvik Biswas

A Dissertation Approved on

12<sup>th</sup> November, 2011

by the following Dissertation Committee:

---

Thesis Director: Dr. Michael H. Nantz

---

Dr. Christopher T. Burns

---

Dr. Geoffrey J. Clark

---

Dr. Francis P. Zamborini

**Dedicated to my Parents**

**Mrs. Chitra Biswas and Mr. Santosh K. Biswas**

## ACKNOWLEDGEMENT

“Some see a hopeless ending, while some see an endless hope”. My thesis mentor Dr. Michael H. Nantz has always inspired me to be one of them who can dream of achieving new goals in the life. I was really fortunate to be a part of *Nantz Team* and also thankful to him for letting me start a new project in his laboratory. His great enthusiasm and brilliant style of teaching organic chemistry made my thesis research very enjoyable. Throughout my graduate study, Dr. Nantz provided me an immense amount of encouragement, lots of unique ideas, the best possible research facilities, and sound advice. More importantly, he showed complete faith in my ability and made me understand the true essence of research. Dr. Nantz has been instrumental in mentoring me on my scientific writing and presentation skills. I am indebted to him for his continuous guidance and without his help I would never been able finish my thesis.

I sincerely thank my committee members, Dr. Christopher T. Burns, Dr. Geoffrey J. Clark, and Dr. Francis P. Zamborini for their valuable suggestions during graduate study.

I would like to thank Dr. Amarnath Maitra (University of Delhi, India), who inspired me to pursue research in the field of drug delivery during my M.Sc. research.

I am grateful to all of my laboratory colleagues: Sadakat Gori Ali, Xuan Huang, Ralph Knipp, Sébastien Laulhé and Stephanie Mattingly for their support and

providing a stimulating environment in the laboratory that was full of fun during my graduate research. I also want to thank Dr. Archana Massey and Dr. Bhaskar Polla for their valuable training during my initial days in the laboratory. I would like to acknowledge Stephanie Mattingly and Dr. Bogdan Bogdanov for performing HRMS spectroscopy measurements at very short notice. I thank Ralph Knipp for helping me in one of the projects and also thank Sébastien for constantly reminding me to complete my thesis writing on time. I also thank Xuan's great advices for any kind of trouble shooting.

I also thank our collaborator Dr. Geoffrey J. Clark (Brown Cancer Center, University of Louisville) for his faith on my project and providing me all the facilities for the completion of biological studies to fulfill my thesis research. I am really grateful to Laura Gordon for training me with all the biological experimental procedures.

I also thank our collaborators Dr. Xiao-An Fu (Chemical Engineering, University of Louisville) and Dr. Sven-U. Gorr (School of Dentistry, University of Minnesota) for testing my synthesized compounds in their research projects.

I would like to thank the Department of Chemistry, University of Louisville for accepting me in the Ph.D. program and providing the best possible academic environment.

I want to thank my brother Mr. Rana Biswas for his valuable guidance. I would like to express my deepest gratitude to my wife Munmun Banerjee for her patience and un-wavering support during the entire stretch of my graduate study.

Finally, and most importantly, I wish to thank my parents, Mrs. Chitra Biswas and Mr. Santosh K. Biswas. They bore me, raised me, taught me, and loved me. Without their support I would not be what I am today.

## **ABSTRACT**

### **FUNCTIONALIZED NANOPARTICLES FOR AMF-INDUCED GENE AND DRUG DELIVERY**

12<sup>th</sup> November, 2011

SOUVIK BISWAS

The properties and broad applications of nano-magnetic colloids have generated much interest in recent years. Specially, Fe<sub>3</sub>O<sub>4</sub> nanoparticles have attracted a great deal of attention since their magnetic properties can be used for hyperthermia treatment or drug targeting. For example, enhanced levels of intracellular gene delivery can be achieved using Fe<sub>3</sub>O<sub>4</sub> nano-vectors in the presence of an external magnetic field, a process known as ‘magnetofection’. The low cytotoxicity, tunable particle size, ease of surface functionalization, and ability to generate thermal energy using an external alternating magnetic field (AMF) are properties have propelled Fe<sub>3</sub>O<sub>4</sub> research to the forefront of nanoparticle research.

The strategy of nanoparticle-mediated, AMF-induced heat generation has been used to effect intracellular hyperthermia. One application of this ‘magnetic hyperthermia’ is heat activated local delivery of a therapeutic effector (e.g.; drug or polynucleotide). This thesis describes the development of a magnetic nano-vector for AMF-induced, heat-activated pDNA and small molecule delivery.



The use of heat-inducible vectors, such as heat shock protein (*hsp*) genes, is a promising mode of gene therapy that would restrict gene expression to a local region by focusing a heat stimulus only at a target region. We thus aimed to design an Fe<sub>3</sub>O<sub>4</sub> nanoparticle-mediated gene transfer vehicle for AMF-induced localized gene expression. We opted to use ‘click’ oximation techniques to assemble the magnetic gene transfer vector. Chapter 2 describes the synthesis, characterization, and transfection studies of the oxime ether lipid-based nano-magnetic vectors **MLP** and **dMLP**. The synthesis and characterization of a novel series of quaternary ammonium aminoxy reagents (**2.1-2.4**) is described. These cationic aminoxy compounds were loaded onto nanoparticles for ligation with carbonyl groups and also to impart a net positive charge on the nanoparticle surface. Our studies indicated that the non-toxic magnetoplexes (magnetic nanoparticle + pDNA complex) derived from **dMLP** deliver pDNA into mammalian cells even without external magnetic assistance. To date, **dMLP** is the only polymer-free magnetic gene delivery system that can deliver pDNA without any magnetic assistance.

Chapter 3 of this thesis outlines the synthesis and characterization of other oxime ether lipids and details studies using derived-lipoplexes. These lipids were evaluated in pDNA and siRNA transfection studies in various mammalian cell lines. This work constitutes the first use of an oxime ether as the linking domain in cationic transfection lipids. These biocompatible oxime ether lipids can be readily assembled by click chemistry through ligation of hydrophobic aldehydes with quaternary ammonium aminoxy salts. Our studies showed that the oxime ether lipids

transfected pDNA and siRNA efficiently in MCF-7, H 1792, and in PAR C10 cells comparable to and in some cases better than commercial transfection lipids.

Chapter 4 describes the design and characterization of a nano-magnetic delivery system for AMF-induced drug (doxorubicin) release. In efforts to develop a magnetic formulation free from thermosensitive materials, such as hydrogels, we synthesized three nanoparticle-based doxorubicin formulations using charge interactions as the key associative force. To do so, we synthesized and characterized a novel cationic oxime ether conjugate at C-13 of doxorubicin. Our investigation indicated that the positive charge of the oxime ether drug conjugate tended to bind better to the negatively charged nanoparticle than did the other formulations prepared in stepwise manner. Our findings show that the nano-magnetic formulations remained essentially inactive at body temperature (37.5 °C) and released a majority of the cargo only when exposed to an external AMF. Our designed magnetic drug delivery platform is the first example of an AMF-inducible system that does not depend on the inclusion of thermosensitive materials.

Finally, we have developed a bioanalytical application of the highly chemoselective oximation chemistry using aminoxy reagent **2.1**. Chapter 5 describes a silica microchip containing micropillars coated with cationic aminoxy reagent **2.1**. The microchip captures gaseous ketones and aldehydes from exhaled human breath. A brief description of microchip fabricated breath analyzer and breath analysis is described in Chapter 5. Our studies showed that the acetone capture efficiency of the aminoxy-loaded microchip was 98%.

## TABLE OF CONTENTS

<b>Contents</b>	<b>Page</b>
Acknowledgement	iv
Abstract	vii
List of Tables	xii
List of Figures and Schemes	xiii
<b>CHAPTER 1: Magnetic Nanoparticles for Drug Delivery</b>	<b>1</b>
1.1. Introduction	2
1.2. Magnetic Vectors for Polynucleotide Delivery	4
1.3. Magnetic Hyperthermia-Induced Drug Delivery	17
<b>CHAPTER 2: AMF-Induced <i>hsp</i>-Promoted Gene Therapy Using Nano-Magnetic Vectors</b>	<b>25</b>
2.1. Introduction	26
2.2. Results and Discussion	30
2.3. Conclusion and Future Directions	53
<b>CHAPTER 3: Cationic Oxime Ether Lipids: A Versatile Class of Gene Carriers</b>	<b>55</b>
3.1. Introduction	56
3.2. Results and Discussion	58
3.3. Conclusion and Future Directions	74

<b>CHAPTER 4: Iron Oxide Nanoparticle-Mediated, AMF-Triggered Drug Delivery</b>	<b>76</b>
4.1. Introduction	77
4.2. Results and Discussion	80
4.3. Conclusion and Future Directions	100
<b>CHAPTER 5: Bioanalytical Applications of Cationic Aminoxy Reagents</b>	<b>101</b>
5.1. Introduction	102
5.2. Results and Discussion	105
5.3. Conclusion	113
<b>CHAPTER 6: Experimental Procedures</b>	<b>115</b>
6.1. Index of Experimental Procedures	116
6.2. Experimental Procedures of Chapter 2	120
6.3. Experimental Procedures of Chapter 3	131
6.4. Experimental Procedures of Chapter 4	137
<b>REFERENCES</b>	<b>144</b>
<b>APPENDIX A: NMR spectra and other figures obtained</b>	<b>158</b>
<b>APPENDIX B: Patent and Publications</b>	<b>181</b>
B.1. List of Patent and Publications	182
B.2. Title Pages of Patent and Publications	183-189
<b>CURRICULUM VITAE</b>	<b>190</b>

## LIST of TABLES

<b>Table</b>	<b>Content</b>	<b>Page</b>
1.1	List of the most recent nano-magnetic gene carriers	16
4.1	Zeta potential and drug loading measurements of nanoparticle formulations	87

## LIST OF FIGURES AND SCHEMES

	Content	Page
Figure 1.1	Barriers to gene transfer	6
Figure 1.2	Cationic gene delivery systems	9
Figure 1.3	Chemical structure of DOTMA and DOTAP	10
Figure 1.4	Multifunctional nanoparticles for theranostic applications	13
Figure 1.5	Schematic representation of magnetofection	14
Figure 1.6	Picture of NanoActivator <sup>TM</sup> : AMF applicator for humans	19
Figure 1.7	Mechanism of heat-activated drug release from thermosensitive materials	23
Figure 2.1	Heat-stimulated <i>hsp</i> -promoted gene expression	29
Scheme 2.1	Strategy for designing cationic magnetic carriers for gene delivery	31
Figure 2.2	Panel of cationic aminoxy reagents	32
Scheme 2.2	Synthesis of quaternary ammonium aminoxy reagents	34
Figure 2.3	<sup>1</sup> H NMR spectra of phthaloyl protected salt and <b>2.1</b>	35
Figure 2.4	SEM micrograph of fluidMAG-DX	36
Scheme 2.3	Synthesis of cationic fluidMAG-DX (CFM)	37
Scheme 2.4	Synthesis of <b>NP•1</b> and <b>NP•FITC2</b>	39
Figure 2.5	UV spectra of FTIC-loaded nanoparticle formulations	40

Scheme 2.5	Synthesis of <b>MLP</b> and <b>dMLP</b>	41
Figure 2.6	Structure of oxime ether lipid formed at the nanoparticle lipid bilayer formation.	42
Figure 2.7	Magnetofection of MCF-7 cells using <b>MLP</b> -derived magnetoplex	43
Figure 2.8	TEM micrograph of <b>dMLP</b>	44
Figure 2.9	Magetofection and transfection of <b>dMLP</b> -derived magnetoplexes in MCF-7 cells	46
Figure 2.10	Zeta potential of <b>MLP</b> - and <b>dMLP</b> -magnetoplexes	48
Figure 2.11	Cell viability assay of MCF-7 cells transfected with <b>MLP</b> - and <b>dMLP</b> -magnetoplexes	49
Figure 2.12	Heat inducible luciferase expression in MCF-7 cells	51
Figure 3.1	Common structure of cationic lipids	56
Scheme 3.1	Synthesis of oxime ether lipid panel ( <b>3.1-3.4</b> )	59
Figure 3.2	<sup>1</sup> H NMR spectrum of <b>3.2</b>	60
Figure 3.3	Zeta potential and mean particle size measurements of oxime:DOPE liposomes	62
Figure 3.4	Size determination of oxime ether-derived lipoplexes	63
Figure 3.5	Transfection activity of oxime ether-derived lipoplexes	65
Figure 3.6	Luciferase expression of <b>3.2</b> -derived lipoplexes using 1 µg pDNA in MCF- cells	66

Figure 3.7	GFP expression in MCF-7 cells of oxime ether-derived lipoplexes	67
Figure 3.8	GFP expression in PAR C10 cells of oxime ether-derived lipoplexes	69
Figure 3.9	siRNA transfection in PAR C10 cells using <b>3.2</b> -derived lipoplexes	71
Figure 3.10	Relative cytotoxicity of oxime ether lipid-derived lipoplexes in MCF-7, H1792 and in PAR C10 cells	73
Figure 3.11	Strategy of developing cell specific targeting lipid <b>3.6</b>	74
Figure 4.1	Schematic illustration of laser-controlled drug release from gold nano cage	77
Figure 4.2	Chemical structure of doxorubicin•HCl (Dox•HCl)	78
Scheme 4.1	Stepwise loading of Dox on the iron oxide nanoparticles	80
Scheme 4.2	Synthesis of <b>Dox•AO</b>	81
Scheme 4.3	Preparation of <b>dNP•AO•Dox</b> and <b>NP•Dox</b>	82
Figure 4.3	<sup>13</sup> C NMR spectra comparison of <b>Dox•HCl</b> and <b>Dox•AO</b>	84
Figure 4.4	Schematic representation of <b>Dox•AO</b> attachment	85
Figure 4.5	AMF-induced nanoparticle heating	88
Figure 4.6	Drug release profile of nanoparticle formulations	90-91
Figure 4.7	Image of AMF generator: EasyHeat, Ameritherm Inc., NY	92



Figure 4.8	NCI 60-cancer cell line screening results	94
Figure 4.9	Experimental setup of AMF-induced drug release in MCF-7 cells and cytotoxicity results	95
Figure 4.10	Fluorescence images of MCF-cells during cytotoxicity studies using drug loaded nanoparticle formulations and AMF exposure	97
Figure 4.11	Fluorescence intensity of <b>Dox•HCl</b> and <b>NP•Dox</b>	98
Figure 4.12	Fluorescence intensity of Dox and <b>NP•Dox</b>	99
Figure 5.1	Schematic diagram of acetone- $d_6$ capture using cationic aminoxy reagent <b>2.2</b>	105
Figure 5.2	FT-ICR-MS spectrum of eluted aminoxy ( <b>2.2</b> )-acetone- $d_6$ adduct	106
Figure 5.3	Optical micrograph of fabricated microreactor	107
Scheme 5.1	Illustration of gaseous ketone and aldehyde capture on cationic aminoxy reagent <b>2.1</b> silical micropillars.	108
Figure 5.4	Setup for preconcentration of ketones and aldehydes by the microreactor	109
Figure 5.5	FT-ICR-MS spectra of preconcentrated acetone- $d_6$ from microreactor and exhaled breath preconcentrated by the <b>2.1</b> -coated microreactor	111
Figure 5.6	Structure of AMA ( <b>5.1</b> )	113

# **CHAPTER 1**

## **MAGNETIC NANOPARTICLES FOR DRUG DELIVERY**

---

### **1.1 . Introduction**

### **1.2 . Magnetic Vectors for Polynucleotide Delivery**

### **1.3 . Magnetic Hyperthermia-Induced Drug Delivery**

---

## 1.1 Introduction

The recent and widespread development of nanoscale technologies is beginning to change the foundations of disease diagnosis, treatment, and prevention. These technological innovations can be grouped into a new field known as nanomedicine, and this field can be defined as an offshoot of nanotechnology featuring highly specific medical interventions at the molecular scale for curing disease or repairing damaged tissues, such as bone, muscle, or nerve” (National Institute of Health, Bethesda, MD).<sup>1</sup> Nanomedicine thus covers a large interdisciplinary scientific research area. This includes nanoparticles that have been engineered as bio-mimics (e.g., functionalized carbon nanotubes), nanomachines (e.g., those made from interchangeable DNA parts and DNA scaffolds), nanoconstructs as biomaterials (e.g., nanofibers of peptides and peptide amphiphiles for tissue engineering), and nanoscale microfabrication-based devices (e.g., silicon microchips for drug release and disease analysis).<sup>2</sup> Furthermore, there is a huge array of intriguing nanoparticulate-based platforms that is capable of delivering genetic materials (pDNA, siRNA), drugs, or diagnostic agents to the desired site of therapy. Among these nano-entities, inorganic nanoparticle-based delivery systems have emerged as an attractive field of research in recent years. Inorganic nanoparticles have two key advantages as a delivery system: ease of preparation with defined size, and they can serve as multifunctional carriers by attaching, for example, both reactive and contrast elements.<sup>3</sup>

Inorganic nanomaterials generally include gold nanoparticles, magnetic nanoparticles (mainly  $\text{Fe}_3\text{O}_4$  and  $\gamma\text{Fe}_2\text{O}_3$ ), silica nanoparticles and various quantum

dots (QD). Magnetic iron oxide nanoparticles, especially magnetite or  $\text{Fe}_3\text{O}_4$  and maghemite or  $\gamma\text{-Fe}_2\text{O}_3$  ( $\gamma$ -phase defined by a cubic crystal structure) show great potential in biomedical research. In addition to being non-toxic,<sup>4, 5</sup> flexibly functionalized and colloidally stable under physiological conditions, iron oxide nanoparticles can be magnetized at the nanoscale range by an external magnetic field. This facilitates their purification and also assists in magnetic targeting of the carriers to the desired site of therapy.<sup>6</sup> These properties make iron oxide nanoparticle formulations promising candidates for gene and drug delivery applications.

Magnetic nanoparticles generate thermal energy when induced with an alternating magnetic field (AMF) through the magnetic oscillation of their magnetic moments. This is due to what is known as Neel and Brownian relaxation (detailed discussion in section 1C). The heat generated in this manner has been effectively used for non-invasive, hyperthermia-based tumor therapy.<sup>7</sup> Iron oxide nanoparticles also can be used as  $T_2$ -weighted<sup>8</sup> magnetic resonance imaging contrast agents. In fact, the commercial formulation Feridex I.V.<sup>TM</sup> was approved for used as an MRI contrast agent in humans. However, for unknown reasons this formulation was been discontinued by the manufacturer (AMAG Pharmaceuticals, Lexington, MA) after November 2008. Combidex<sup>TM</sup> (Advanced Magnetics, Inc., MA) is another iron oxide nanoparticle-based formulation used as an MRI contrast agent. Combidex<sup>TM</sup> is now in Phase III clinical trials.<sup>9</sup> The hyperthermic effects and the  $T_2$ -weighted magnetic resonance imaging make iron oxide nanoparticles an ideal candidate for theranostic (therapeutic + diagnostic) applications.

This dissertation will describe the present status of magnetic nanoparticle-mediated gene and drug delivery and my efforts to improve the efficiencies of these methods. Specially, my thesis research is aimed at developing an efficient magnetic nanoparticle-mediated drug delivery system that can release its cargo in response to the heat generated by an externally applied AMF stimulus.

## **1.2. Magnetic Vectors for Polynucleotide Delivery**

### **Gene Therapy**

According to the American Society of Gene Therapy, gene therapy can be defined as the “use of genetic material to modify a patient's cells for the treatment of an inherited or acquired disease.” The therapy involves the introduction and uptake of exogenous genetic material into a cell, with incorporation and expression of the gene (i.e., transgene) in the nucleus to provide a desired therapeutic effect. For acquired diseases like cancer, gene therapy uses genes to directly or indirectly cause the demise of the cancerous cells. Various therapeutic effects have been realized with the delivery of genes capable of inducing apoptosis, immunogenic responses against the host cell, or inactivating oncogenes.

Despite the original promise, gene therapy remains very inefficient. This inefficiency of transfection (i.e., combined output of gene transfer and expression) is directly related to the pathway via which DNA makes the journey from delivery to nuclear translocation. This mechanism is well studied.<sup>10, 11</sup> The ultimate fate of exogenous DNA depends on the ability to overcome the barriers during the transgene delivery, and these barriers include: (1) stability in the extracellular space, association

with plasma membrane, and importantly cellular internalization via endocytosis, (2) intra-cellular trafficking including endosomal release, (3) cytosolic diffusion, and (4) nuclear localization (Figure 1.1). The driving force behind much gene therapy research is to overcome these barriers. In comparison to most small molecule drugs, nucleic acids have poor bioavailability due to the chemical composition of cell membranes, which have a net anionic surface potential.<sup>12</sup> The anionic ribophosphate backbone of DNA is electrostatically repulsed from the cellular surface. In addition, the immune system may react to exogenous DNA or RNA, which will cause rapid enzymatic degradation of the polynucleotide. Therefore, for most gene therapy applications, DNA must be delivered to the cell surface in a system that promotes cellular internalization while also protecting the DNA from degradation. The ideal vector must be able to condense DNA into discrete particles that protect the transgene from degradation and provide sufficient delivery into the target cell and its nucleus. The vector must be nontoxic, non-immunogenic and should be easy and inexpensive to produce. Presently there are three modes of gene delivery: uncomplexed DNA/siRNA delivery or “naked” polynucleotide delivery, viral-mediated gene delivery, and non-viral mediated gene delivery.

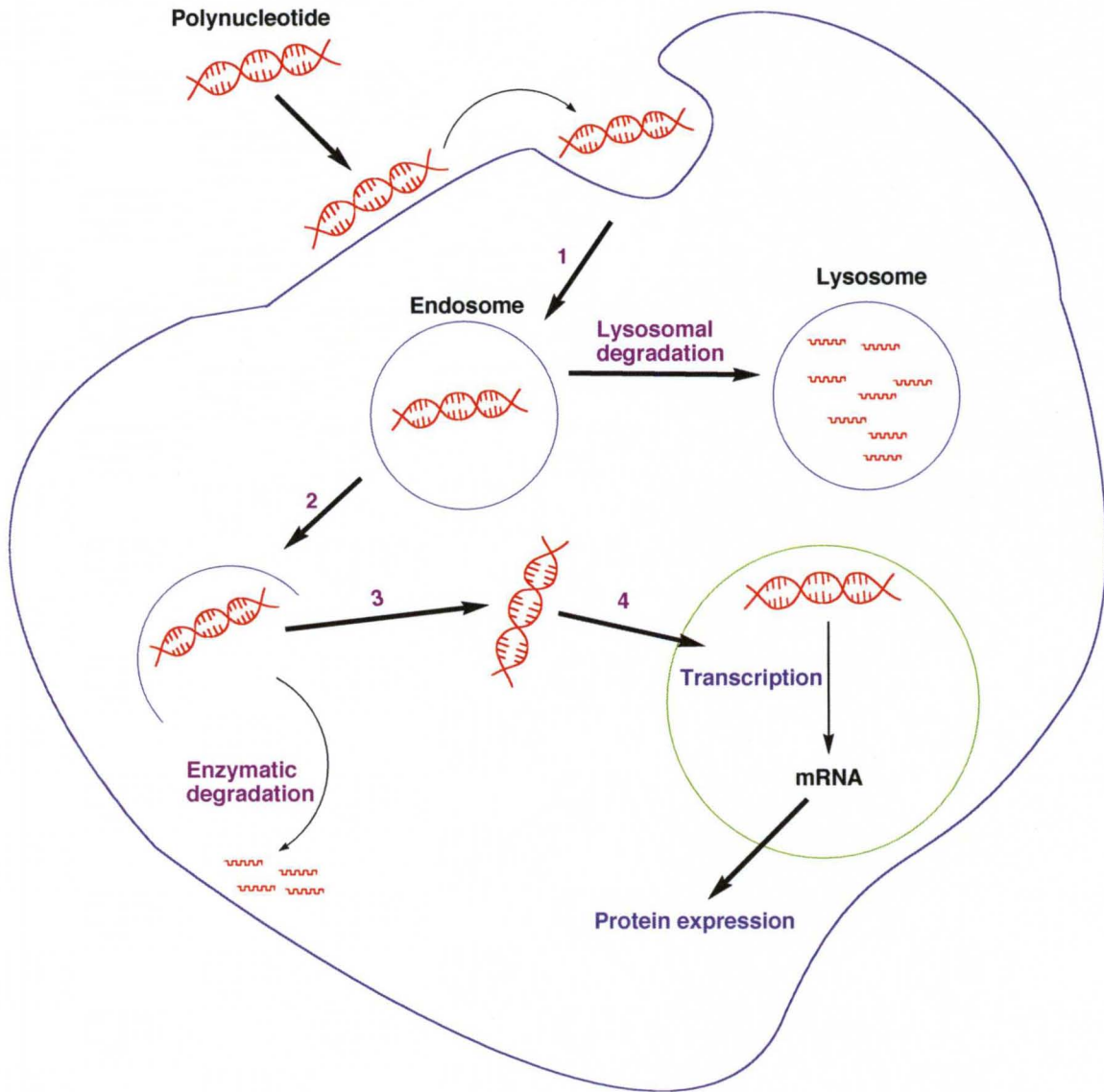


**Figure 1.1. Barriers to effective gene transfer:** after association with cellular membrane, (1) endocytosis, (2) intracellular trafficking and endosomal escape, (3) cytosolic diffusion and (4) translocation to the nucleus and access into the nucleus.

## **Naked DNA (or siRNA) delivery**

The simplest gene delivery strategy is injection/inhalation of ‘naked’ (uncomplexed) nucleic acids (e.g. pDNA, siRNA). This method has attracted researchers due to its simplicity and lack of toxicity observed for naked pDNA. Several pre-clinical and clinical trials have shown that this strategy is useful for delivery of pDNA into skin, muscle, liver, lungs and into some solid tumors.<sup>13, 14, 15</sup> However, the direct injection of naked nucleic acids into tissue or blood is ineffective and limited to a few tissues due to following reasons: first, nucleic acids generally undergo rapid enzymatic degradation by nucleases *in vivo*. Secondly, naked nucleic acids cannot reach many organs by systemic injection because the liver rapidly sequesters them. Due to its relatively smaller size, kidneys clear siRNA rapidly. Finally, the net negative charge of a cellular membrane may repel oligonucleotides or pDNA and cause low efficiency of cellular uptake. To overcome these limitations, it is necessary to develop gene delivery vectors to safely transport DNA/RNA into targeted cells.

## **Viral vectors**

Although my thesis research is focused on developing non-viral gene delivery vectors, a brief discussion on viral-based gene delivery systems is necessary to provide a better perspective of the field. Viruses are nature’s most effective candidates to infect cells with genetic material. Once the immunological component of a virus is dismantled, the viral machinery may be exploited. Likewise, removing replication factors from the virus avoids the potential side effects due to non-targeted



distribution of the viral-vectors. Manipulation of viruses and engineering viral vectors have become major branch of gene therapy.<sup>16</sup>

Retrovirus vectors (RV) are one of the most effective means for gene transfer. Nusbaum *et al.* in 2000 demonstrated for the first time the proof of concept of retroviral gene therapy by treating a genetic disease.<sup>17</sup> Adenovirus is also commonly used for viral transduction and it is capable of infecting both dividing and quiescent cells.<sup>18</sup> Although viral vectors for gene transfer fulfill the requirement of efficient gene transfer, virus mediated transduction suffers from drawbacks, such as like strong immune responses,<sup>19</sup> nonspecific transduction,<sup>20</sup> limited polynucleotide carrying capacity and high cost of production.<sup>21, 22</sup>

### **Non-viral gene delivery**

Non-viral gene delivery utilizes synthetic carriers to mimic viral transfection without the associated side effects. Commonly used non-viral vectors are cationic lipids (CL), polymers, and various inorganic nanomaterials. Generally, non-viral gene delivery vectors possess positive charge density on their surface to facilitate binding to the negatively charged phosphates of the polynucleotide backbone (i.e., electrostatic attractions) to form a complex (Figure 1.2). The cationic liposome-polynucleotide complex is known as a lipoplex and the polymeric counterpart is known polyplex (Figure 1.2).

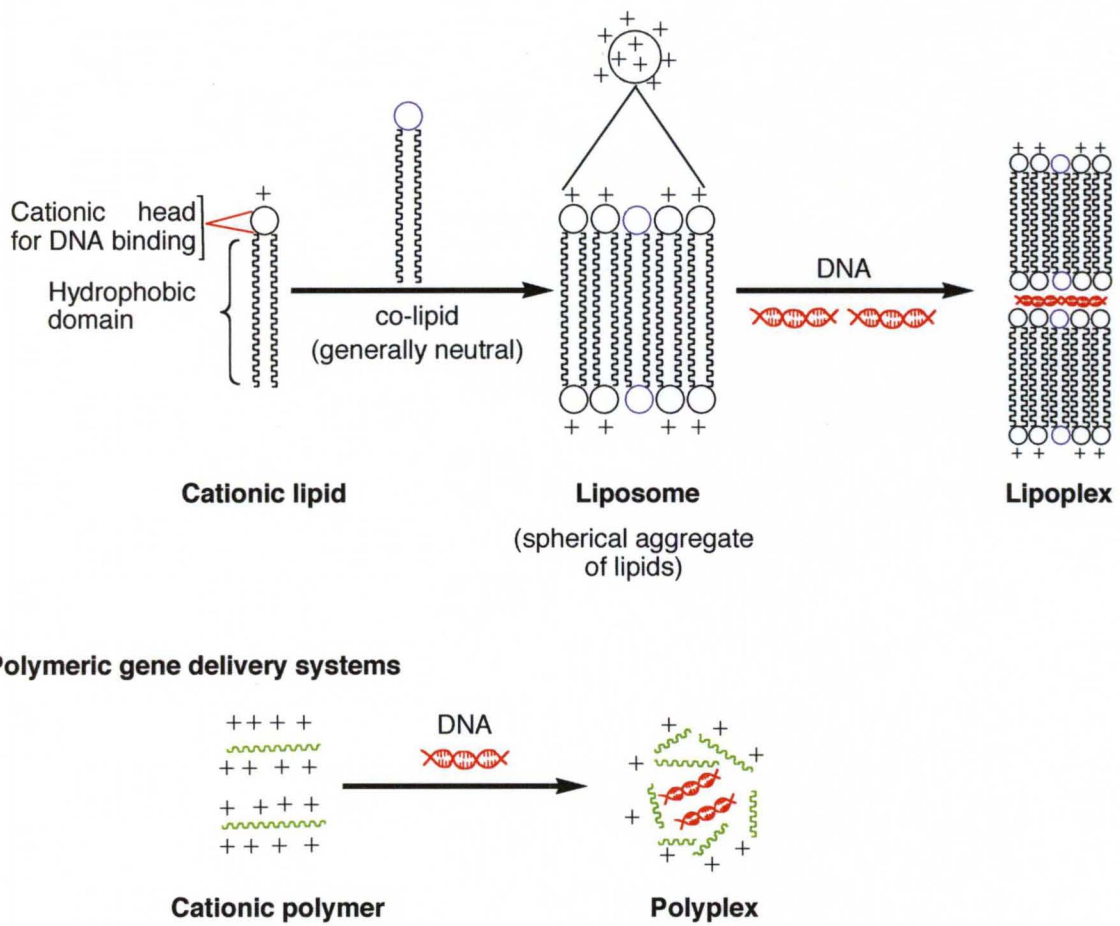


**Figure 1.2. Cationic gene delivery systems:** formulation of cationic lipid- and polymer-based delivery systems.

The advantages of low immunogenicity, the ability to transfect RNA or DNA of nearly unlimited size,<sup>23, 24</sup> and the relative ease of lipoplex (cationic lipid-plasmid DNA/RNA complex) formulation continue to attract interest aimed at developing safer and more efficient cationic lipids. Typically a cationic lipid, like 1,2-di-*O*-octadecenyl-3-trimethylammonium propane (DOTMA)<sup>25</sup> and *N*-[1-(2,3-dioleoyloxy)propyl]-*N,N,N*,-trimethylammonium chloride (DOTAP)<sup>26</sup> has a positively charged head group for DNA/RNA binding connected to a dual chain hydrophobic domain via functional linker (Figure 1.3). Cationic lipids are co-formulated with a

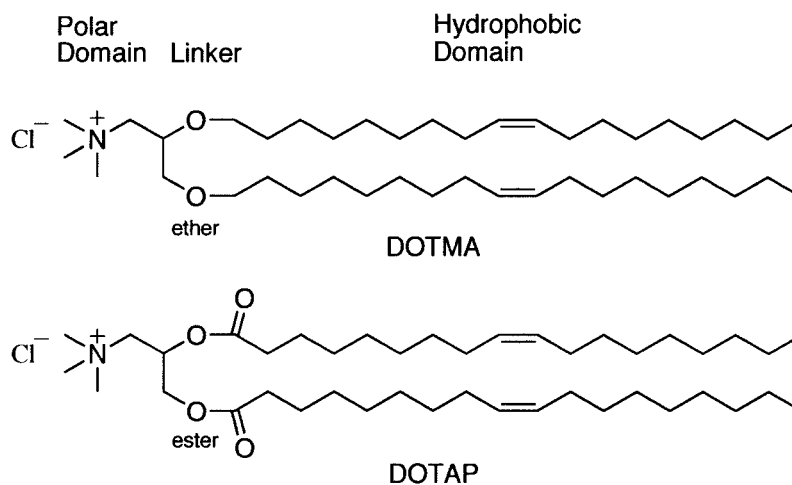


**Figure 1.3.** Chemical structure of DOTMA and DOTAP.

neutral lipid or co-lipid, such as 1,2-dioleoyl-*sn*-glycero-3-phosphoethanolamine (or DOPE), to form a cationic liposome (Figure 1.2). The liposome then condenses the DNA/RNA spontaneously to form a lipoplex (Figure 1.2). The lipid bilayer prevents the DNA/RNA from degradation by extracellular nuclease. Co-lipids can enhance endosomal escape of DNA during transfection.<sup>27</sup> The polynucleotide to CL ratio for lipoplex formulation must be separately optimized, but generally the lipoplexes are formulated with an excess positive charge to provide better interaction with the cell

membrane.

Cationic polymer-based gene delivery vectors are also becoming very promising in nonviral gene therapy research. Cationic polymers, e.g., poly-L-lysine (PLL),<sup>28</sup> polyethylenimine (PEI),<sup>29</sup> polyamidoamine dendrimers (PMAM),<sup>30</sup> and chitosan<sup>31</sup> can bind with the polynucleotide backbone to form a polymer/DNA or siRNA complex or a polyplex (Figure 1.2). In contrast to other polymers, PEI does not require an endosomolytic agent due to its intrinsic endosomolytic property. This ability to facilitate endosomal escape makes PEI superior to other transfection active agents. The PEI backbone consists of repeating ‘-CH<sub>2</sub>CH<sub>2</sub>NH-‘ ethylenimine motifs that provide excellent solubility. Roughly 20% of the nitrogens are protonated at physiological pH.<sup>32</sup> PEI forms a dense polyplex.<sup>33</sup> Due to its “proton sponge” effect, polyplexes derived from PEI avoid lysosomal trafficking and enzymatic degradation,<sup>34</sup> and this usually results in better transfection than other polymers. Although PEI is one of the best polymers for gene transfer, *in vivo* applications using PEI suffer from toxicity. The high positive charge density of PEI disrupts the cellular membrane.<sup>35</sup> Thus, complications arising from vector toxicity affect many PEI-based gene therapy approaches.<sup>36</sup>

### **Inorganic nanoparticle-based vectors for gene delivery**

Inorganic nanoparticles are becoming very popular due to their biocompatibility, simple method of synthesis, size controllability and ease of surface functionalization for various biomedical applications. Inorganic nanoparticles can be coated with biocompatible polymers, and linkers can be attached to their surface to tether various entities (e.g., targeting elements) for different applications. A

hydrophobic drug can be attached to these nanoparticles for delivery purpose and simultaneous cell specific targeting can be achieved when these drug-loaded nano-carriers conjugated to a targeting moiety (e.g., peptides or antibodies, Figure 1.4). Nanoparticles can behave like a multifunctional platform for theranostics when the surface of the particle is further conjugated to a radionucleotide tracer for positron emission tomography (PET imaging) or when linked to a fluorescent-active molecule for bioimaging. The magnetic nano core makes the nanoparticles MRI active. Therapeutic agents, like hydrophilic drugs or nucleic acids, can also be encapsulated into the hydrophilic coating shell (Figure 1.4).

For gene delivery purposes nucleic acids are mostly loaded onto gold nanoparticles (GNP) through thiol linkages or electrostatic interaction with cationic gold nanoparticles.<sup>37, 38, 39, 40</sup> Elbakry *et al.* first developed the PEI/siRNA/PEIAuNP system to deliver siRNA into cells and knock down the expression of a target gene based on the self-assembly layer-by-layer technology.<sup>36</sup> Due to its high transfection capacity, PEI coated mesoporous silica nanoparticles (PEI-MSNP) are very common vectors for nucleic acid delivery to mammalian cells.<sup>41, 42, 43</sup> In addition to their ability to increase the plasmid concentration at the cell surface via sedimentation,<sup>44</sup> the mesopore structures provide the possibility to carry additional elements such as drugs,<sup>45</sup> magnetic tags,<sup>39</sup> and chromophores (to monitor drug delivery or the intracellular trafficking of nanoparticles).<sup>46</sup> Simple DNA coated calcium phosphate nanoparticles (CaP),<sup>47, 48</sup> bisphosphonate stabilized CaP<sup>49</sup> and cationic lipid coated CaPs<sup>50</sup> have been used for cellular delivery of exogenous DNA. Ca<sup>2+</sup> ion plays an important role in boosting transfection activity for these systems. Also, the Ca<sup>2+</sup>

presumably promotes endosomal escape, increases cytosolic stability, and enhances nuclear uptake of the DNA.<sup>51</sup> However, CaP-based gene carriers suffer from poor reproducibility of transfection activity. Stabilizing CaP carriers with lipids is currently underway to solve this issue.<sup>47</sup> Recent studies have reported that carbon nanotubes (CNTs) can deliver therapeutic agents, including DNA and RNA, to target

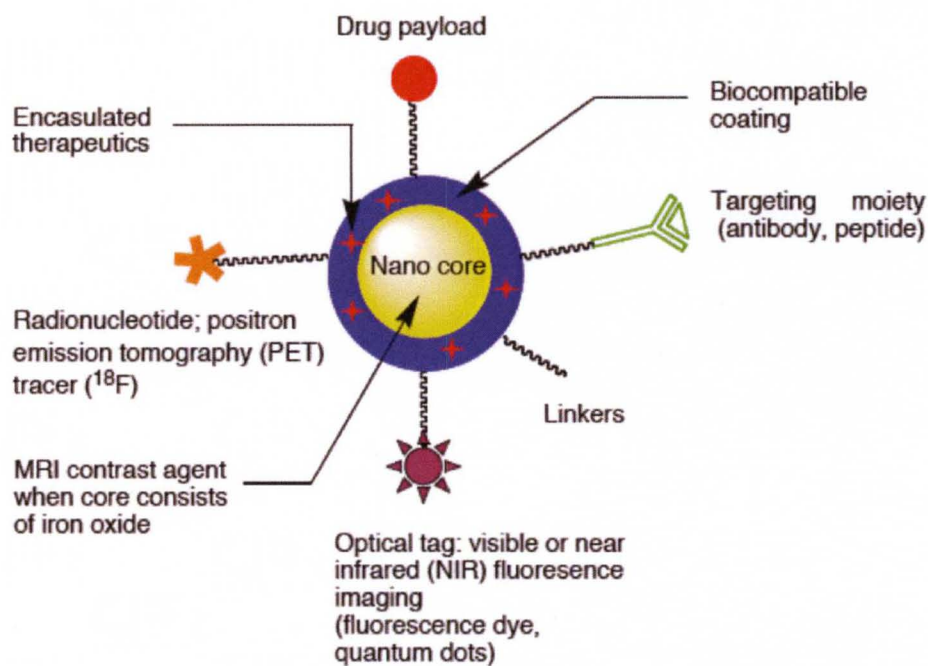


**Figure 1.4.** Example of multifunctional nanoparticles for theranostic applications.

disease sites. Most recently Al-Jamal *et al.* demonstrated delivery of siRNA *in vivo* to central nervous system by using ammonium salt functionalized CNTs.<sup>52</sup>

## Magnetic nanoparticles for gene transfer

Mah's group first demonstrated external magnet-assisted enhancement of viral transduction using magnetic nanoparticles.<sup>53</sup> Nucleic acid delivery assisted by an external magnetic field is now commonly known as magnetofection (Figure 1.5).<sup>54</sup> Although oxide nanoparticles, like  $\text{CoFe}_2\text{O}_4$ ,  $\text{NiFe}_2\text{O}_4$ , and  $\text{MnFe}_2\text{O}_4$  exhibit superior magnetic properties, their use in biomedical applications is challenged by the toxicity of these systems.<sup>55</sup> In contrast, iron oxide nanoparticles, such as  $\text{Fe}_3\text{O}_4$  (magnetite) or

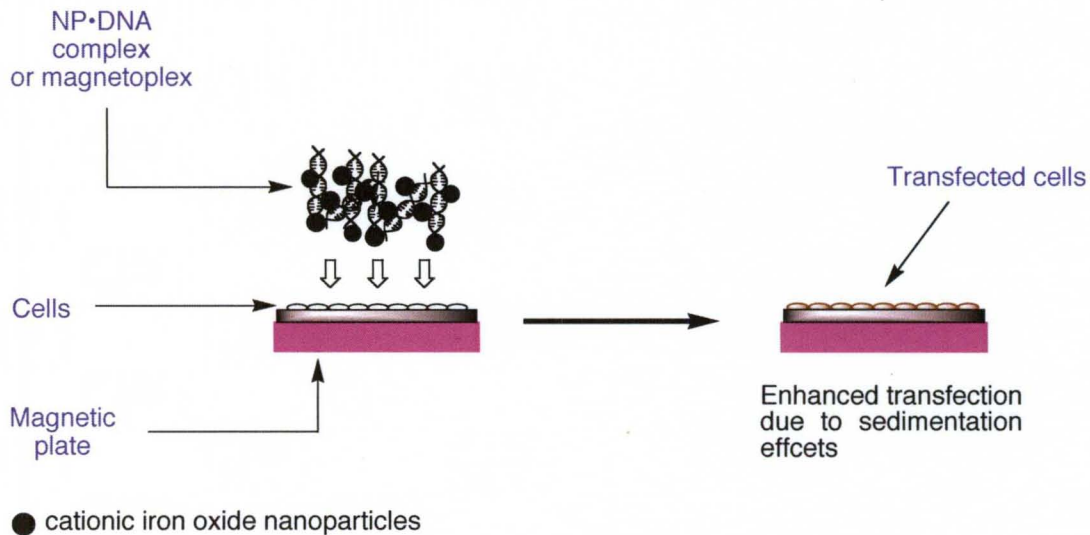


**Figure 1.5.** Magnetofection: External magnetic field assisted transfection.

$\gamma\text{-Fe}_2\text{O}_3$  (maghemite), are relatively safe and have been used in humans use as MRI contrast agents (Feridex I.V.). Many research groups, such as Lee *et al.*<sup>54</sup> have modified the surface to increase the transfection efficacy and reduce the cytotoxicity. To achieve enhanced transfection activity with minimized toxicity, investigators used various surface adjuvants, such as anionic surfactants (oleic acid),<sup>56</sup> polymers (PEG, poly-L-lysine, dendrimers),<sup>57, 58, 59</sup> carbohydrates (chitosan),<sup>60</sup> silica particles (MCM48),<sup>61</sup> proteins (serum albumin),<sup>53, 62</sup> phospholipids,<sup>63</sup> cationic cell penetrating

peptide (TAT peptide),<sup>64</sup> transfection reagents (lipofectamine 2000),<sup>65</sup> and even viruses.<sup>50, 51, 66</sup> These surface modifiers prevent agglomeration and add functionality that may be further used to conjugate other polymers, such as PEI. Most of the researchers employ PEI or a modified PEI coating technology to impart a positive charge density to the magnetic nanoparticles.<sup>63, 67, 68</sup> Huth *et al.* reported that the mechanism of magnetofection using a PEI-based magnetic vectors, followed essentially the same endocytosis process as the related PEI-based polyplexes. Release of the genetic material also occurred in similar manner via the “proton sponge” effect.<sup>69</sup> The same group also reported that the accelerated nucleic acid sedimentation when using the magnetic nanoparticles is the chief force behind the success of magnetofection.<sup>66</sup> The most noted and recent magnetic nanoparticle mediated gene delivery literature is summarized in Table 1.1 (adopted from Reference 65). Although magnetic assistance enhances DNA/siRNA transfection activity many fold, the transfection activity of these magnetic vectors suffers severely when the magnetic field is absent. This is likely to be problematic for gene transfer *in vivo*. Li *et al.*<sup>55</sup> very recently reported successful delivery of pDNA to a lung tumor model in mice without magnetic assistance using a PLL-coated magnetic vector. A second major concern of these PEI coated magnetic carriers is their cytotoxicity, which is associated with the toxic effects of PEI.



Year	Magnetic nanoparticles	Modifying agent	Cells/tissue	Magnetic assistance	Reference
2011	Fe <sub>3</sub> O <sub>4</sub>	PEI, streptavidin	NIH3T3, HeLa	Yes	63
2011	Fe <sub>3</sub> O <sub>4</sub>	Poly(propyleneimine) dendrimers	Saos-2 osteoblasts	Yes	56
2010	Polymag <sup>a</sup>	Tat peptide	U251	Yes	61
2010	Fe <sub>3</sub> O <sub>4</sub>	Silica	NCI-H292	Yes	58
2009	Fe <sub>3</sub> O <sub>4</sub>	Oleic acid, phospholipids	HSC-45	Yes	60
2009	Fe <sub>3</sub> O <sub>4</sub>	Poly-L-lysine	Lung tissue	No	55

**Table 1.1.** Most recent and noted magnetic nanoparticle mediated gene delivery literature (adopted from reference 65). *a*. Commercial PEI-coated iron oxide nanoparticles (Oz Biosciences, France).

Chapter 2 of this thesis is focused on designing a PEI-free nano-magnetic vector that can transfer pDNA into host cells without external magnetic force. Ultimately, we aimed to achieve an AMF-stimulated, heat-induced transgene expression using a magnetoplex (magnetic nanoparticle•DNA complex) containing heat shock protein (*hsp*) pDNA, which will be discussed in Chapter 2 of this thesis. To accomplish our goal, we hypothesized using “click” oximation techniques to coat the iron oxide nanoparticle surface with cationic moieties that facilitate pDNA delivery.

As a part I of thesis, we aimed to achieve: **(a)** the design, synthesis and characterization of cationic iron oxide nanoparticles for efficient gene delivery, and **(b)** the evaluation of a heat-activated, *hsp*-promoted gene expression using thermal energy generated by a magnetic vector under an external AMF-stimulus.

### 1.3. Magnetic hyperthermia-induced drug delivery

#### Magnetic hyperthermia

According to the National Cancer Institute (Bethesda, MD), hyperthermia (Greek for ‘overheating’) is a type of cancer treatment in which body tissue is exposed to high temperatures (up to 45 °C). Research has shown that high temperatures can damage and kill cancer cells, usually with minimal injury to normal tissues.<sup>70</sup> By killing cancer cells or damaging proteins and structures within cancer cells,<sup>71</sup> hyperthermia may shrink tumors. Thermoablation is another form of thermotherapy where the temperature range is 46-56 °C. The higher temperature in this case leads to direct tumor destruction by cell necrosis and carbonization.<sup>72</sup> The notion of hyperthermia is as old as anti-cancer medicine itself. Indeed, heat therapy was first mentioned as a treatment of breast cancer more than 5000 years ago.<sup>73</sup> Since hypoxic (poorly oxygenated) cancerous cells are much more resistant to radiation therapy than that of euoxic (well oxygenated) cancerous cells, and since hypoxic cancerous cells are more heat sensitive than euoxic cells,<sup>74</sup> the combination of heat and radiation therapy is a promising therapeutic modality.<sup>75</sup>

The main sources of thermal energy to induce hyperthermia fall into three categories: (a) contact with externally heated liquids, (b) contactless applicator (e.g., irradiation using ultrasound, microwave, radiofrequencies, or infrared devices) and (c) use of an inserted heating source (probes, laser fibers, and mediators).<sup>76</sup> Unlike other inserted heating sources, mediators convert the electromagnetic energy into heat when exposed to an external electric or magnetic field. Macroscopic mediators are inserted within the body via surgical procedure, whereas micro- or nano-scaled

mediators are injected as particle dispersions. These mediators are heated either by a captive applicator, or by applying an inductive applicator to magnetizable particles, where the electric component (E-field), which can lead to uncontrollable heating of the tissue, is lowered to the benefit of magnetic field (H-field) to generate heat energy.<sup>77</sup> Inductive mediators seem to be more useful because cells do not contain any intrinsic magnetic materials that could generate uncontrolled heat in an alternating magnetic field. For patient comfort, the frequency of an alternating magnetic field (AMF)-induced hyperthermia should be higher than 50 kHz to avoid neuromuscular stimulation and less than 10 MHz for the appropriate penetration depth of the frequency-field.<sup>78</sup> Surgically inserted ferromagnetic rods have been placed into tumors to serve as interstitial macroscopic mediators.<sup>79</sup> The basic limitations of this technique are stressful surgical interventions, lack of accessibility to tumors, potential migration of the rods, and non-uniform temperature patterns.

The most recent magnetic hyperthermia models are based on micro- or nano-sized mediators in the form of an injectable colloidal dispersion of magnetic particles. Magnetic nanoparticle-mediated heating occurs via two main mechanisms: **(a)** external AC magnetic field supplies energy and assists magnetic moment rotation by overcoming the energy barrier ( $E = KV$ ; K is the anisotropy constant, and V is volume of the magnetic core) so that energy is dissipated when the particle moment relaxes to an equilibrium orientation, a phenomenon known as Néel relaxation; and **(b)** rotational Brownian motion can also generate heat from magnetic nanoparticles within a carrier liquid due to the torque generated on the magnetic moment by an AMF.<sup>73</sup> The prerequisite criterion for clinical application is nontoxicity of the

magnetic nanoparticles. To date, magnetite ( $\text{Fe}_3\text{O}_4$ ) and maghemite ( $\gamma\text{-Fe}_2\text{O}_3$ ) nanoparticles with satisfactory biocompatibility have been under intensive investigation. Gilchrist reported the first application of iron oxide mediated hyperthermia *in vivo* in 1957. The first Phase I clinical trial of magnetic hyperthermia was done by MagForce Nanotechnology Co. (Berlin, Germany) in 2005 with 14 patients suffering from glioblastoma. In this trial, the feasibility of magnetic



**Figure 1.6.** AMF applicator for humans: NanoActivator<sup>TM</sup>, MagForce Nanotechnologies AG, Berlin. A fiber-optic thermometry unit is part of the applicator. Image was taken from Magforce website.

hyperthermia as a therapy was evaluated using a 100 kHz AMF applicator (NanoActivator<sup>TM</sup>, MagForce, Germany, Figure 1.6) and aminosilane-coated iron oxide nanoparticles (NanoTherm<sup>TM</sup>, MagForce).<sup>80</sup> Hyperthermia was well tolerated with radiation and with minor or little side effects. Signs of local tumor control were observed.<sup>6</sup> The Phase II trial of this study is in progress with 65 patients.<sup>81</sup> In fact, this hyperthermia therapy was cleared for the market in European Union countries last year, and has begun the treatment in patients in Germany under "an individual

patient agreement." Investigators in Japan also have reported the clinical application of magnetic hyperthermia for melanoma treatment.<sup>82</sup>

In summary, there is exciting evidence that raises the prospect of therapeutic application of magnetic-hyperthermia in humans. The continuous effort in building proper AMF generators for inducing magnetic hyperthermia in humans, gaining idea of biodistribution of these nanoparticles, and acquiring knowledge of magnetic nanoparticle toxicity is definitely strengthening the belief that AMF-induced magnetic nanoparticle-mediated thermotherapy will be a viable treatment option.

### **Magnetic hyperthermia-triggered drug release**

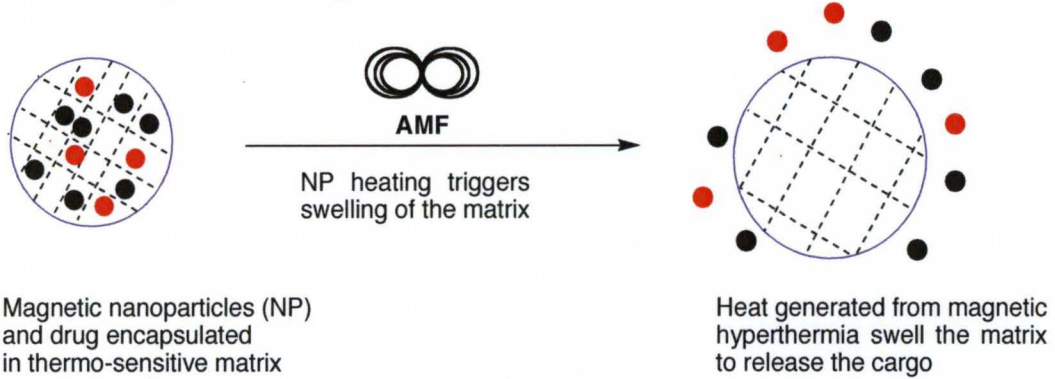
Magnetic hyperthermia opened a new avenue in stimuli-triggered non-invasive drug delivery technology whereby drugs encapsulated within thermo-sensitive polymers, gels, or lipids containing magnetic nanoparticles (for generating thermal energy to change the conformation of the carrier matrix) could be stimulated by exposure to an AMF to cause the release. Once at the target site, a drug is released from the carrier upon AMF-induction to create a local high concentration of drug resulting reduced side effects. To date, the AMF-triggered or magnetic hyperthermia-induced drug release platforms rely on two basic principles: magnetic heating (or magnetic hyperthermia) of nanoparticle and a thermally responsive or (-rupturable) coating.

Magnetic nanoparticles that are designed with the proper composition and size to achieve heating using an AC magnetic field are generally placed inside a thermally-responsive matrix. A polymer can also be coated directly onto the nanoparticle, or a self-assembled structure (e.g., micelles, liposomes or

polymersomes) can be devised to encapsulate the nanoparticles. For biomedical applications, the coating must open or partially rupture to release a drug when heated above physiological temperatures. There are three mechanisms in which heat energy can cause the structural change in matrix to release the drug (Figure 1.7). Generated heat can swell the matrix and that can cause the release (Figure 1.7A).<sup>83</sup> In squeezing-controlled release (Figure 1.7B), an already hydrated gel collapses rapidly when heated, exuding water and much of the imbedded drug with the water.<sup>84, 85</sup> Liu *et al.*<sup>82</sup> encapsulated doxorubicin (Dox, an anti-cancer drug) and iron oxide nanoparticles inside of Pluronic F127 (F127) matrix and demonstrated Dox release by AMF induction. Considerable volume shrinkage of F127 matrix due to heat generated by magnetic hyperthermia causes the instantaneous release of Dox. This system, however, is not suitable for *in vivo* applications because cargo release occurs at 35 °C, which is lower than the body temperature (37.5 °C). In another example, Chaubey *et al.* used a naturally occurring genipin cross-linked gelatin nanoparticles for encapsulating Fe<sub>3</sub>O<sub>4</sub> nanoparticles and Dox. Drug release was observed when the above system was induced by an AMF and this system is based on swelling controlled release.<sup>80</sup> Iron oxide nanoparticles and drug encapsulated alginate microsphere are also developed for magnetically controlled heat-responsive drug release.<sup>86, 87</sup> In these cases, nanoparticle-induced thermal energy twists and shakes the molecular chains, resulting in an increase of wall permeability that causes increased diffusion of the drug (Figure 1.7C).<sup>84</sup> Brüle *et al.*<sup>86</sup> observed cytotoxicity of this carrier even before AMF-pulse, indicating premature drug release at 37.5 °C. Because squeezing-based hydrogel systems would release a drug when heated, they

are preferred over swelling-controlled systems for the development of magnetothermally-triggered drug delivery systems. However, when a hydrogel is placed in an aqueous environment (such as the human body), the gel will swell, leaving the mesh open for drug diffusion and release prior to the triggering event, so a squeezing-controlled release platform is not ideal for delayed triggering events. Hsu *et al.* encapsulated lipophilic drug tetracaine and  $\gamma\text{-Fe}_2\text{O}_3$  nanoparticles (size 5-25 nm) in a solid lipid nanoparticle (SLNP) matrix. Drug release was observed when the vehicle was stimulated with a 25 kHz (frequency), 60 kA/m AMF.<sup>88</sup> Lipid transition change was induced by heat generated from NP heating which caused diffusion of the drug from the matrix. The low frequency of the AMF and high temperature rise (37-50 °C in 20 min) may face challenges in *in vivo* studies. Very recently Thomas *et al* developed a smartly engineered magnetic core (Zn-doped iron oxide nano crystal)-silica shell nano-system in which the anti cancer drug doxorubicin was entrapped via diffusion. The mesopores then were blocked by curcubit[6]uril (a macrocyclic amination) to prevent nonresponsive drug leakage at 37.5 °C.<sup>89</sup> The valves opened and released the drug efficiently when an AMF-stimulus was applied.

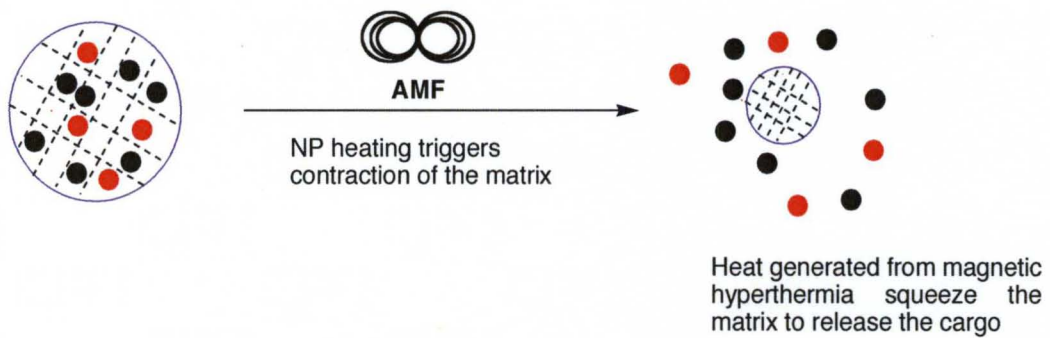
**A. Thermo-responsive swelling**



Magnetic nanoparticles (NP) and drug encapsulated in thermo-sensitive matrix

- Magnetic nanoparticles (NP)
- Encapsulated cargo

**B. Thermo-responsive squeezing**



**C. Thermo-responsive opening of grafts**

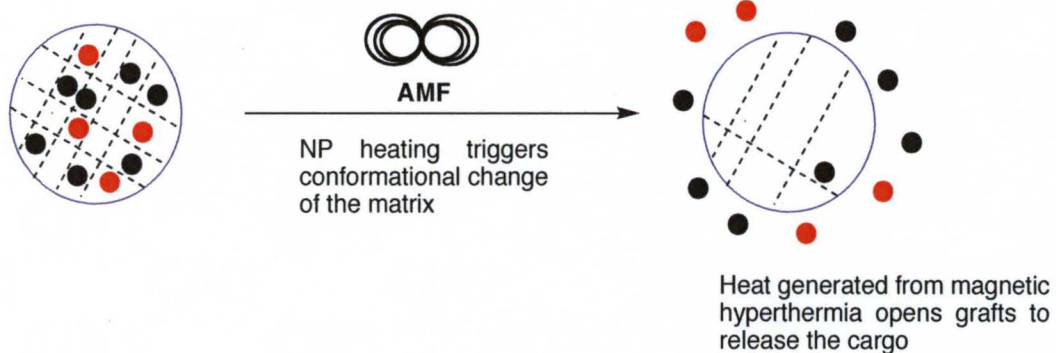


**Figure 1.7.** Thermo-sensitive formulations for controlled release of payloads. **A.** swelling, **B.** squeezing, and **C.** change in molecular conformation of matrix.



To address the challenge of premature cargo release, we aimed to design magnetic nano vehicle for AMF-controlled release that does not rely on a thermosensitive material. As part II of my thesis, we set out to assemble a simple drug-conjugated nano-sized magnetic drug delivery platform using “click” oximation chemistry. Our final objective is to demonstrate AMF-induced drug release from our custom magnetic vector. Chapter 4 of my thesis will describe the development of the first magnetic thermo-sensitive polymer-independent delivery system to address the above stated challenges.

## **CHAPTER 2**

### **AMF-INDUCED *hsp*-PROMOTED GENE THERAPY USING NANO-MAGNETIC VECTORS**

---

#### **2.1. Introduction**

#### **2.2. Results and Discussion**

#### **2.3. Conclusion and Future Directions**

---

## 2.1. Introduction

Logically, the control of therapeutic gene expression within tumors would enhance the therapeutic impact of gene therapy. Along these lines, inducible plasmid promoters to control gene expression would make the spatial and temporal targeting of therapy more feasible.<sup>90,91</sup> One smart strategy for induced gene expression is based on chemical signaling. Examples include tetracycline-inducible or -suppressible gene expression systems based on bacterial tetracycline operon.<sup>92</sup> Disease-specific gene activation systems have also been reported for induced gene therapy.<sup>93, 94</sup> However, two major obstacles of this strategy are: **(a)** tumor specific promoters must be identified for each individual tumor, and **(b)** the ability to switch off the transgene expression on demand is still problematic.<sup>95</sup>

Among the various inducible gene expression systems, external stimuli-induced systems have some unique advantages. Chief among them is the ability to focus the inducing agent in a spatially targeted region. Such a system has been described using gamma radiation and the Egr-1 promoter.<sup>96, 97</sup> Targeting was achieved either by radiotherapy or by systemic injection of radioisotopes accumulating in the tumor cells. However, radiotherapy has the disadvantage of using ionizing radiation. In another approach, thermal energy can be used to trigger gene expression in an inducible gene expression system. Among the most commonly used heat-inducible promoters are the heat shock protein (*hsp*) genes, such as the *hsp70* family. Their transcription is upregulated in response to a toxic insult to the cell, particularly exposure to heat.<sup>98</sup> Importantly, the basal expression of genes controlled by an *hsp70* promoter region is nearly undetectable, whereas heat-induced

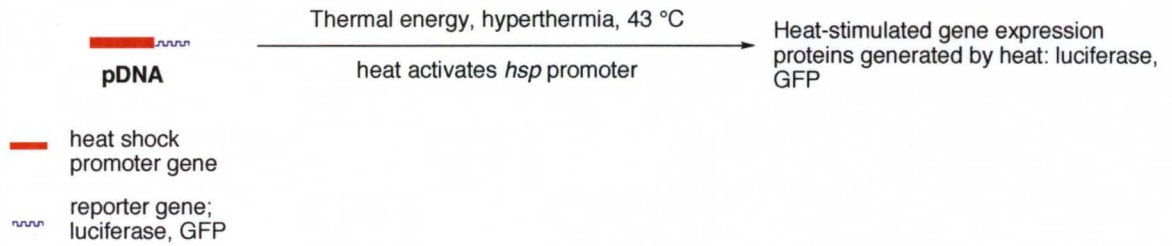
expression is comparable to that observed with the popular cytomegalovirus early (CMV) promoter.<sup>99</sup> Thus, it is feasible to restrict gene expression to a local region by focusing the heat stimulus only on the target region (Figure 2.1A). It has been demonstrated that hyperthermia generated heat can be used for non-invasive and non-toxic alternative regulator for local gene expression using a thermo-inducible promoter.<sup>100</sup> One of the main advantages of hyperthermia over radiotherapy is that hyperthermia is potentially suitable for diseases other than cancer. There appear to be long-term side effects in experimental cancer treatments using hyperthermia, particularly in the temperature range that is most effective for heat-induced gene induction. Among many examples, Huang *et al.*<sup>95</sup> have demonstrated that *in vitro* expression of a heterologous gene with a heat shock protein 70 promoter could be elevated 500 to 1000-fold over background by heat generated from a hot water bath (39-43 °C). Verkis *et al.*<sup>101</sup> demonstrated *in vitro* GFP (green fluorescent protein) reported expression using thermo-inducible *hsp* promoter at 43 °C. Duration of hyperthermia in this study was 30 min. Moonen *et al.* used the same heat shock promoter and GFP reporter plasmid for heat-induced gene expression using MRI-guided focused ultra sound technique to generate thermal shock in the tumor tissue.<sup>102</sup> In another study Smith *et al.*<sup>103</sup> activated an *hsp*-promoted luciferase reporter construct for heat-induced gene expression using ultrasound-based hyperthermia.

The main obstacle with hot water bath hyperthermia is to generate enough heat energy in tumors located deep within the body. This somewhat invasive therapy may also face challenges in *in vivo* clinical applications. Ultrasound-mediated hyperthermia suffers with undesirable temperature rise at the muscle-bone interface.

An alternative strategy to avoid whole body hot water bath hyperthermia or ultrasound-induced hyperthermia for heat inducible gene therapy system is to apply magnetic nanoparticle-mediated intracellular AMF-stimulated hyperthermia technology to induce localized gene expression (Figure 2.1B). Ito *et al.* have combined TNF- $\alpha$  gene therapy driven by a heat-inducible *hsp70* (heat shock protein 70) promoter with hyperthermia produced by AMF-irradiation of cationic liposome-iron oxide nanoparticle formulations.<sup>104</sup> Tang *et al.* also developed a heat-inducible gene expression system in which thermal energy generated by PEI coated Mn-Zn ferrite magnetic nanoparticles under an alternating magnetic field (AMF) was used to activate gene expression.<sup>105</sup> They also used the *hsp70* promoter. The NPs in this system are challenged with biocompatibility issues due the composition of the Mn-Zn and due to the PEI coating. In this experiment, however, authors injected a second dose of nanoparticle formulation (2.6 mg or 4.6 mg of magnetic particles) before AMF-induction, which might cause aggregation of particles in a particular zone of the tumor and might result in non-uniform heating in tumor during clinical applications.

The successful fusion of PEI-free magnetic nanoparticle-mediated gene transfer, AMF-induced intracellular nanoparticle heating and heat-induced apoptotic gene expression would constitute a non-invasive, localized treatment of cancer. This is our goal at the onset of my thesis research.

**A. Heat shock-promoted gene expression**



**B. AMF-induced heat-activated gene expression**

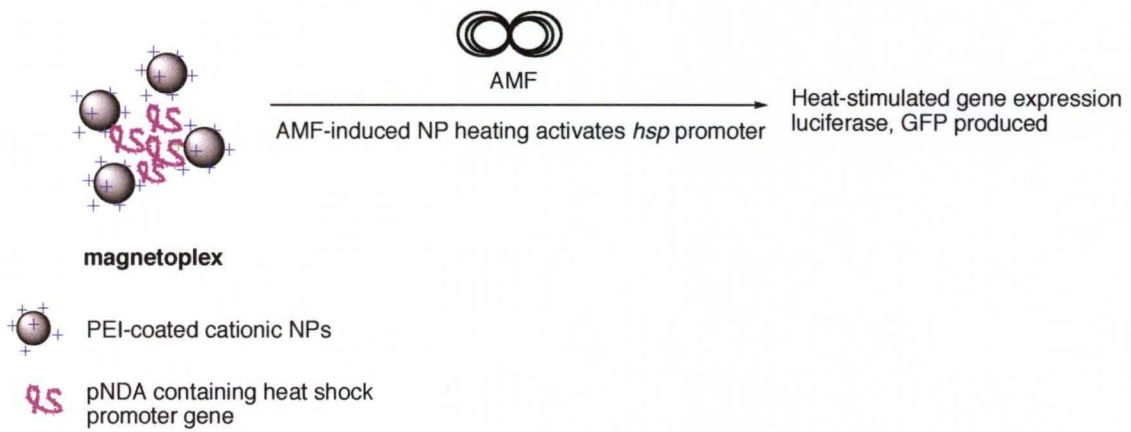


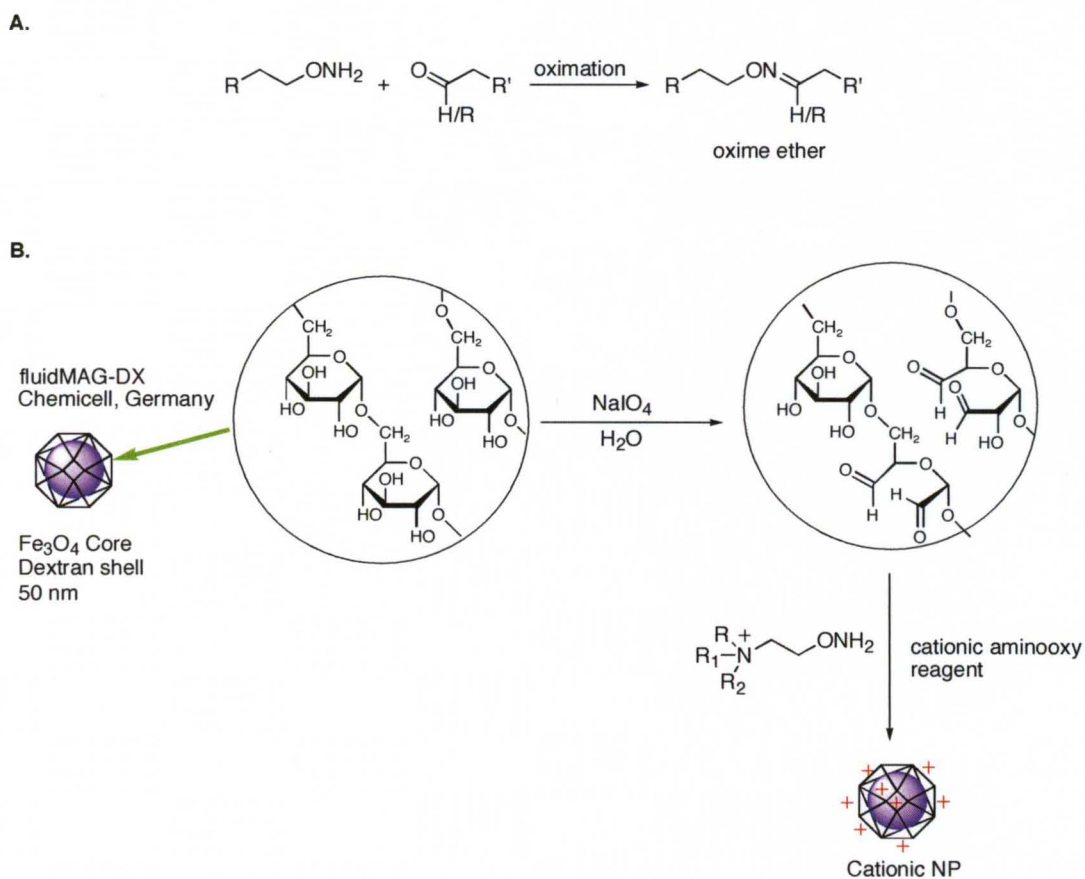
**Figure 2.1.** Heat-stimulated *hsp*-promoted controlled gene expression. **A.** Thermal energy controlled (e.g., hyperthermia) heat-activated *hsp*-promoted gene expression. **B.** Noninvasive AMF-induced NP heating triggered heat-stimulated gene expression.

## 2.2. Results and discussion

To achieve our goal, we first set out to design a biocompatible PEI-free cationic iron oxide ( $\text{Fe}_3\text{O}_4$ ) nanoparticle (NP) formulation to function as an efficient pDNA delivery vehicles. In keeping with our research theme, we aimed to use “click” oximation technology for NP surface manipulations. Chemoselective click ligation of an aldehyde or ketone carbonyl group with an aminoxy counterpart to form an oxime ether linkage (i.e., oximation, Scheme 2.1A) is a key step in the synthesis of numerous bioconjugates.<sup>106, 107, 108</sup> Oxime ether linkages also are used as a mechanism for pro-drug generation,<sup>109</sup> and are present in FDA-approved pharmaceuticals, such as fluvoxamine.<sup>110</sup> Very recently (May, 2011), Cho *et al.*<sup>111</sup> published a report in which they conjugated an aminoxy terminated 30 kDa PEG linker to human growth hormone using oximation technique. This modified hormone (**ARX201**) bearing oxime ether linkage was synthesized to achieve a molecular size suitable for minimizing renal clearance yet maintaining acceptable viscosity for enhanced therapeutic effect. In fact, **ARX201** is now in Phase II clinical trials.

Our first strategy was to pursue the surface modification of commercially available dextran-coated NPs (fluidMAG-DX, Chemicell, Berlin, Germany) using an oximation approach. We hypothesized that dextran-coated magnetic iron oxide nanoparticles (50 nm) could be activated for conjugation to cationic aminoxy reagents by cleaving the vicinal diol groups of the carbohydrate domain. Thus, periodate oxidation of fluidMAG-DX would generate multiple surface aldehyde sites (Scheme 2.1B) for reaction with cationic aminoxy reagents. We planned to condense cationic quaternary ammonium aminoxy salts with the aldehyde groups to generate a

positive charge density on the NPs for ultimate DNA-binding and for subsequent transfection applications.



**Scheme 2.1.** **A.** Chemoselective "click" oximation between aminoxy and the carbonyl group of either a ketone or aldehyde. **B.** Strategy for synthesizing a cationic NP: generate aldehyde groups by periodate oxidation, and then react the oxidized NP with a cationic aminoxy reagent.



To initiate our above stated plan we first synthesized and characterized a panel of novel quaternary ammonium aminoxy salts (Figure 2.2, **2.1-2.4**) for use in the final oximation step.<sup>112</sup> We adapted Grochowski's methodology to synthesize these cationic aminoxy reagents.<sup>113</sup> The cationic aminoxy reagents can serve as nucleophilic reagents to access cationic materials more readily than their electrophilic counterparts<sup>114, 115</sup> because the chemospecific oximation reaction between aminoxy and aldehyde/ketones is expected to be facile. Our interest in gene transfer<sup>116, 117</sup> and the fact that hydroxyethylated polar domains enhance the transfection efficiency led us to prepare hydroxyethyl-functionalized analogs **2.3** and **2.4**. Consequently, we devised a general synthetic route of the novel nucleophilic cationization reagents **2.1-2.4**.<sup>112</sup>

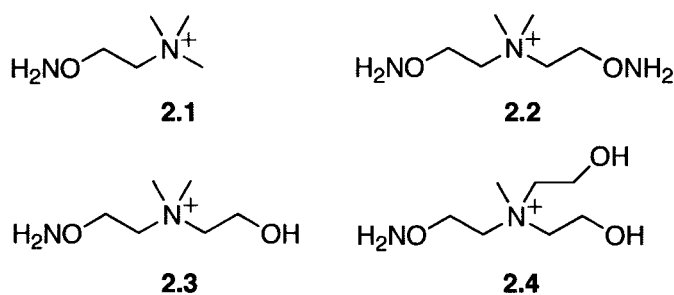


**Figure 2.2.** Panel of quaternary ammonium aminoxy reagents.

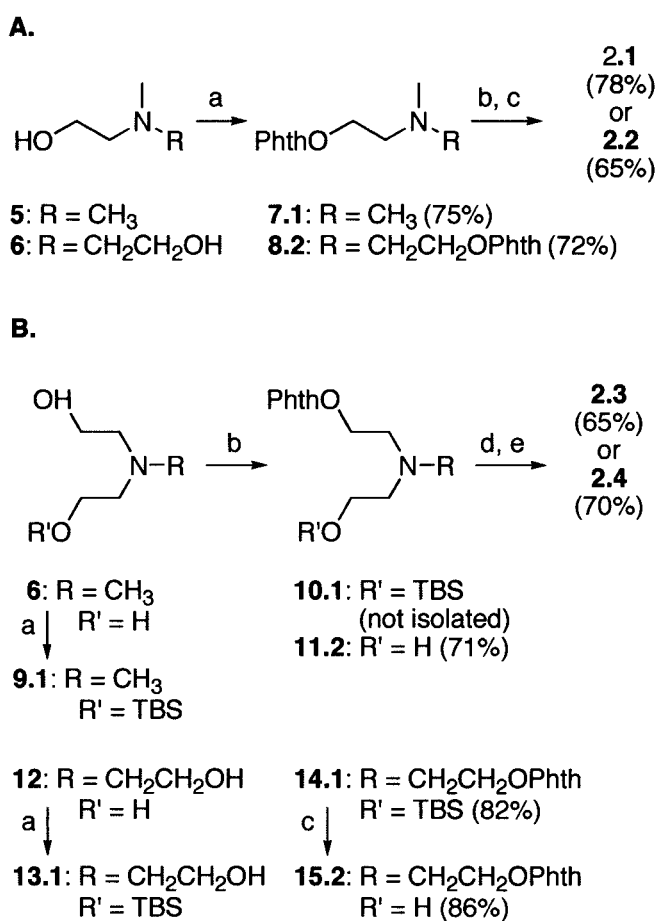
### Synthesis of quaternary aminoxy salts

Reaction of the commercially available ethanolamines **5** and **6** (Scheme 2.2A) with *N*-hydroxyphthalimide (NHP) under Mitsunobu conditions (equimolar amounts of NHP/PPh<sub>3</sub>/DIAD) furnished phthaloyloxy amines **7.1** and **8.2**, respectively. Amine quaternization was best accomplished by gently warming the amines in

methyl iodide (*ca.* 0.2 M). The resultant, crude ammonium iodides were treated directly with hydrazine in ethanol to cleave the phthaloyl groups. Aminoxy reagents **2.1** and **2.2** were purified and isolated as filtrate from hot acetonitrile in good overall yield.

Monosilylation of di- (**6**) and triethanolamine (**12**) was accomplished by reacting an excess of each ethanolamine with TBSCl as the limiting reagent. The resultant, mono-protected ethanolamines **9.1** and **13.1** (Scheme 2.2B) were then transformed to the corresponding *N*-(2-hydroxyethyl)-functionalized aminoxy reagents (**2.3** and **2.4**) using the path established for synthesis of reagents **2.1** and **2.2**. Desilylation of the more polar phthaloyloxy amine **10.1** proceeded smoothly on work-up by stirring with aq. HCl, this approach did not work for phthaloyloxy amine **14.1**. In fact, reaction with aqueous HF instead of TBAF ultimately furnished the desired final target **2.4**. My laboratory colleague, Mr. Xuan Huang, synthesized the reagent **2.4**.

The  $^1\text{H}$  NMR and  $^{13}\text{C}$  NMR clearly indicated that phthaloyl group was cleaved during hydrazinolysis process and aminoxy or  $-\text{ONH}_2$  group was generated.  $^1\text{H}$  NMR spectra of phthaloyl protected quaternary ammonium salt and **2.1** are included (Figure 2.3).



**Scheme 2.2.** Synthesis of cationic aminoxy reagents. Reagents and conditions: **A.** Phth = phthalimidoyl; (a) *N*-hydroxyphthalimide, PPh<sub>3</sub>, DIAD, THF, 0 °C – rt, 12 h; (b) CH<sub>3</sub>I, sealed tube, 45 °C, 2 h; (c) H<sub>2</sub>NNH<sub>2</sub>·H<sub>2</sub>O, EtOH, rt, 12 h. **B.** TBS = *t*-BuMe<sub>2</sub>Si; (a) TBSCl (0.2 eq), Et<sub>3</sub>N (1 eq), CH<sub>2</sub>Cl<sub>2</sub>; (b) *N*-hydroxyphthalimide, PPh<sub>3</sub>, DIAD, THF, 0 °C – rt, 12h; (c) 48% aq. HF, THF, 0 °C – rt, 12h; (d) CH<sub>3</sub>I, sealed tube, 60 °C, 2h; (e) H<sub>2</sub>NNH<sub>2</sub>·H<sub>2</sub>O, EtOH, rt, 12h.

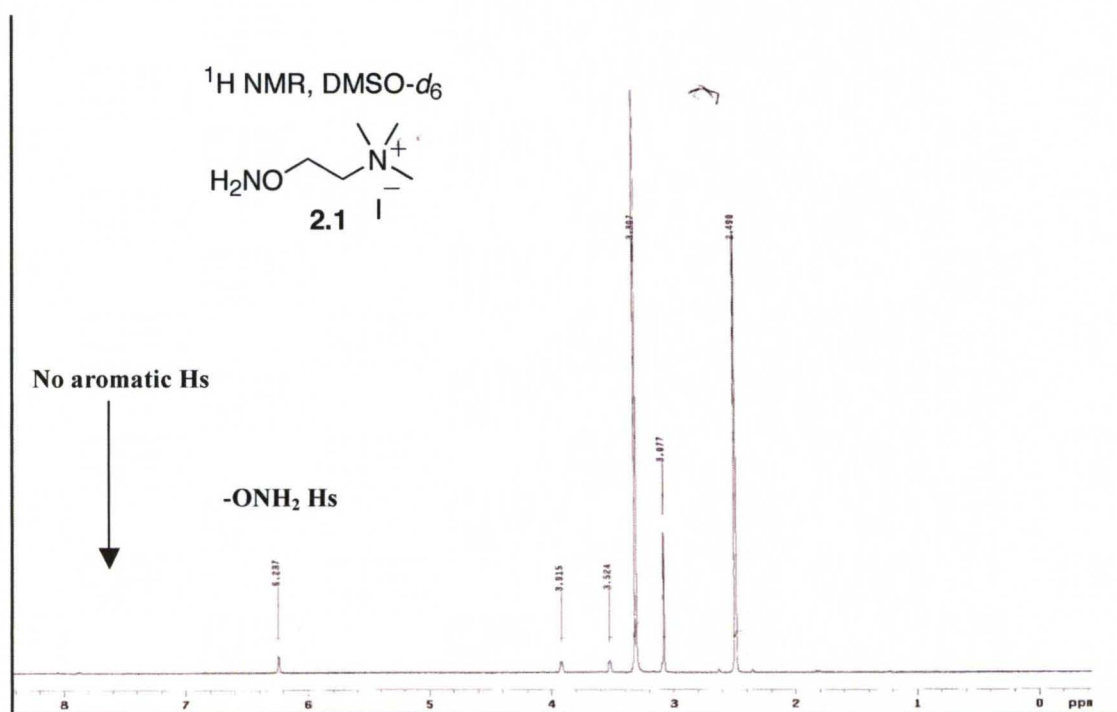
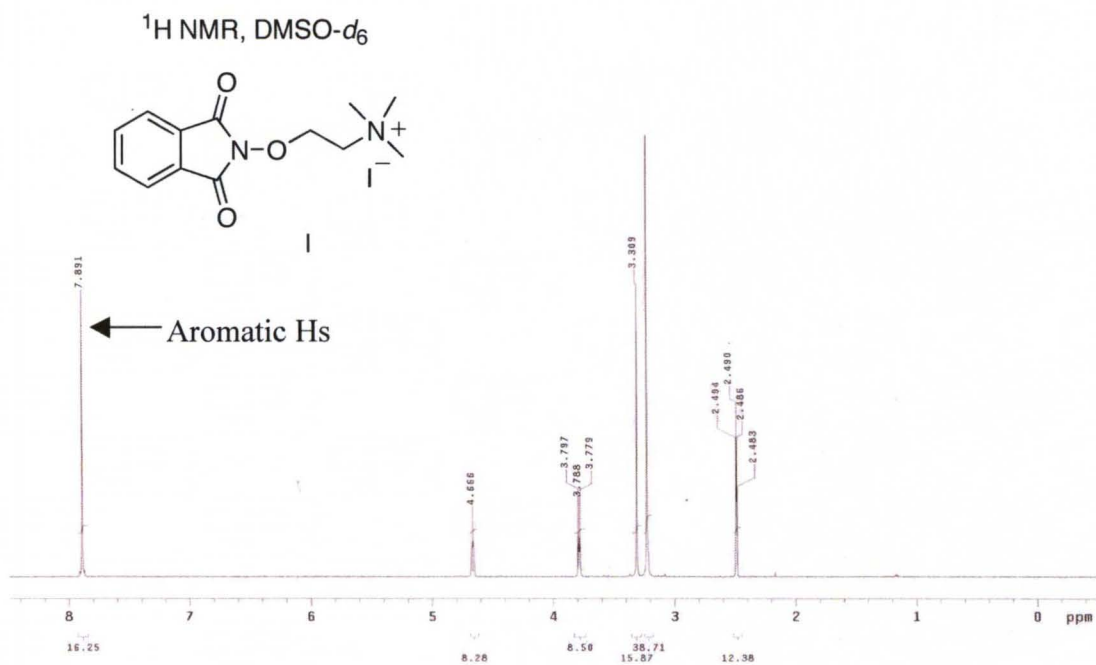


**Figure 2.3.** <sup>1</sup>H NMR spectra of phthaloyl protected salt and 2.1 in DMSO-*d*<sub>6</sub>.

## Preparation of cationic fluidMAG

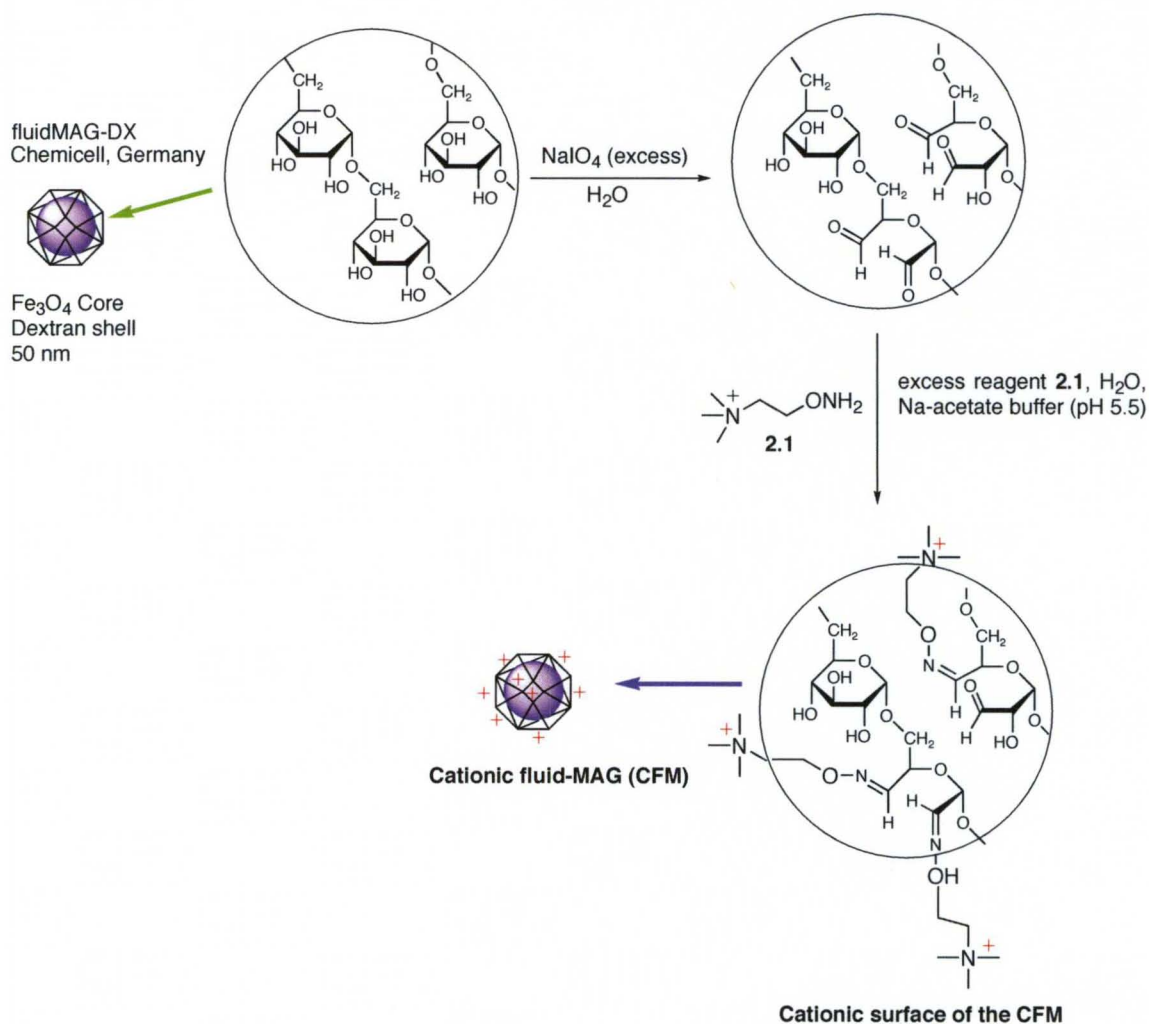
We performed  $\text{NaIO}_4$  oxidation on the fluidMAG-DX NPs to form aldehyde groups at NP surface (Scheme 2.3).<sup>118</sup> Although elemental analysis data of the oxidized fluidMAG-DX initially indicated the presence of aldehyde groups at the NP surface, inconsistent elemental analysis values also indicated poor reproducibility of this step. This raised a concern about the consistency of the quality of the commercial fluidMAG-DX. Oximation then was employed to conjugate the cationic mono-aminoxy reagent **2.1** to add positive charge density at the NP surface to



**Figure 2.4.** SEM micrograph of commercial fluidMAG-DX.

furnish cationic fluidMAG (**CFM**, Scheme 2.3). According to elemental analysis data, we could succeed to conjugate only ~1.0% nitrogen after oximation to the **CFM**, whereas theoretical %N in **CFM** was approximately 6%. The functionalized particles prepared from this strategy never showed encouraging magnetofection or transfection activity in studies using breast cancer cells (MCF-7). Lack of nitrogen content at the NP surface indicated lack of cationic head group, which is the reason of poor transfection activity of the fluidMAG-DX derived formulation. In fact, we noticed inconsistent chemical behaviors of the commercial fluidMAG-DX from batch

to batch. Size determination using Scanning Electron Microscopy revealed that the size of the commercial particles were larger than the vendor's claim (Figure 2.4). SEM images of these particles also demonstrated a large size distribution. For these reasons, we abandoned the strategy of functionalization of commercial material.



**Scheme 2.3.** Synthesis of cationic NPs. Aldehyde moieties are formed at the surface of the fluidMAG-DX NPs by periodate oxidation. Subsequent oximation using cationic aminoxy reagent **1** then inputs a net positive charge to the particles.

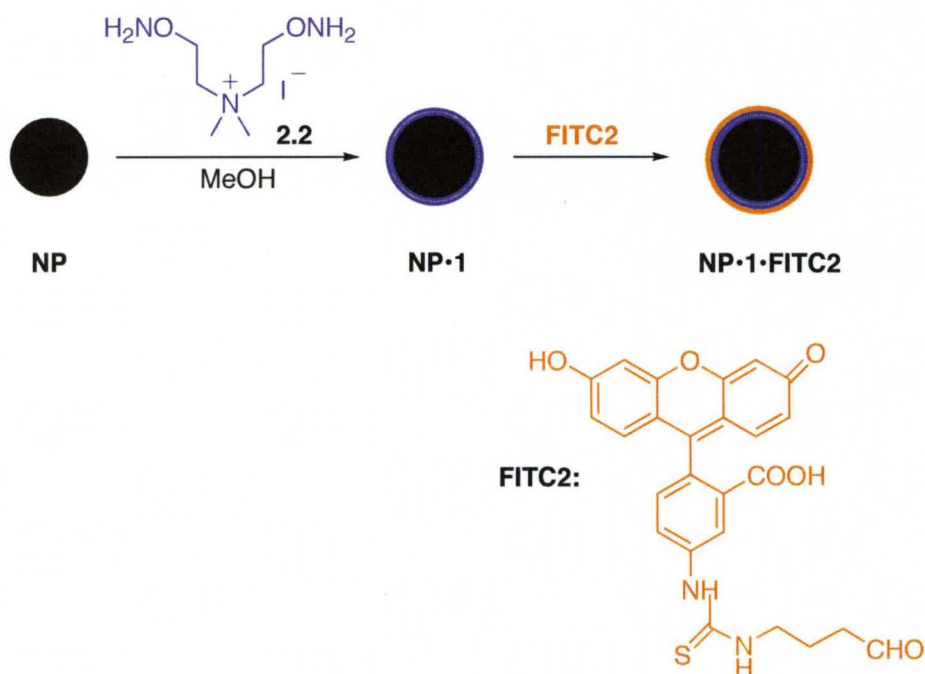
## Development of magnetic lipid particles (MLPs)

Unhappy with the quality of the commercial fluidMAG-DX preparation, we decided to develop our own custom nano-magnetic delivery vector for polynucleotide delivery. To initiate our new plan, we first synthesized negatively charged Fe<sub>3</sub>O<sub>4</sub> nanoparticles (NP) according to a co-precipitation method described by Mikhaylova *et al.*<sup>119</sup> Zeta potential measurements revealed the NPs had a surface charge of -32 mV. X-Ray Diffraction (XRD) and Energy-Dispersive X-Ray Spectroscopy (EDX) measurements confirmed Fe<sub>3</sub>O<sub>4</sub> magnetite and Transmission Electron Microscopy (TEM) indicated particles with an average 5-10 nm diameter.

Without the aid of established transfection lipids and their co-lipid formulations, the use of lipid coated nanoparticle vectors for gene transfer remains largely unexplored. Our research group's interest in oximation and program on developing non-viral gene delivery systems<sup>116, 120, 121, 122</sup> led us to devise a flexible method for stepwise construction of a transfection-active lipid coating directly on the surface of iron oxide nanoparticles. Inspired by the nanoparticle 'click' conjugate work of Miller<sup>123</sup> and Mirkin,<sup>124</sup> we sought to harness click chemistry to attach lipid side chains onto aminoxy functionalized NPs using oximation methodology

To functionalize the NP surface with an aminoxy layer, the NPs were treated with an excess (*ca.* 3.3 wt. equivalents) of cationic aminoxy reagent **2.2** (Scheme 2.4). The resultant aminoxy-coated nanoparticles (**NP•1**) were readily isolated by magnet-assisted sedimentation and, using this method repeatedly, were washed 2X to remove any unassociated aminoxy compound. Dry weight measurements consistently indicated a deposition of **2.2** on the surface of **NP•1** in the range of 1.27-

1.30  $\mu\text{mol}/\text{mg}$ , which is nearly  $2 \times 10^4$  aminoxy groups/particle. We hypothesized that the close association of **2.2** with the nanoparticles presumably is driven by a combination of hydrogen bonding and electrostatic interactions.<sup>125</sup> The relative extent of these associative interactions is unclear. The observed reduction in zeta potential for **NP•1** to -16 mV reflected a partial neutralization of surface charge by the ammonium ion of **2.2**.



**Scheme 2.4.** Synthesis of **NP•1** and conjugation of **FITC2** to the **NP•1**.

We evaluated the availability of aminoxy groups on **NP•1** by performing a labeling experiment. We used an aldehyde fluorescent probe **FITC2** for this study (Scheme 2.4). After mixing the particles with **FITC2**, conjugated were magnetically separated and washed 2X with methanol to furnish **NP•1•FITC2**. **FITC2** was mixed with only **NP** in a same way to prepare **NP•FITC2** that served as a control. The UV



measurements indicated the aldehyde substrate **FITC2** is bound to the nanoparticle only when compound **2.2** is present (Figure 2.5). **FITC2** was not bound unless compound **2.2** was loaded onto the **NP** first, implicating the oxime ether linkage as the tethering functionality.

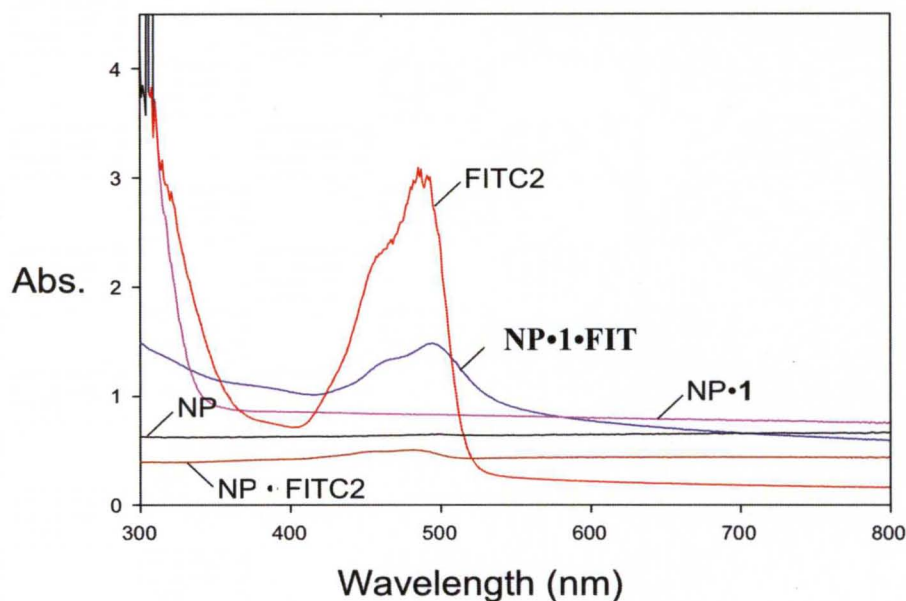
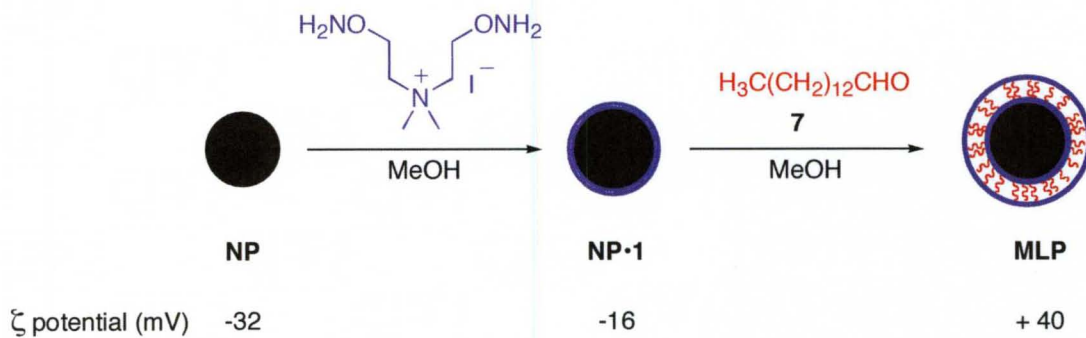


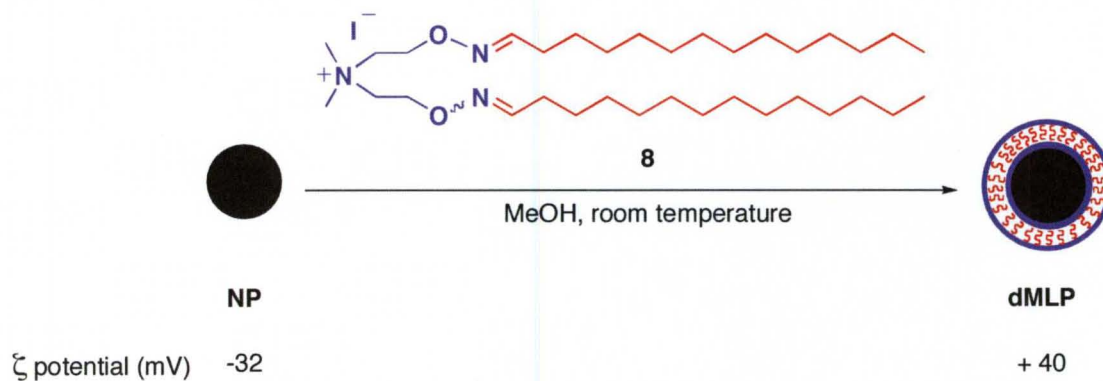
**Figure 2.5.** UV-visible spectrum of NP-loaded with FITC2, NP•1 and NPs. UV-Visible spectroscopy measurements were taken of NP, NP•1, NP•1•FITC2 and FITC2 at concentrations of 0.025 mg NP/mL (water). As a control, unmodified NPs were reacted with FITC2.

We were gratified to find that reaction of **NP•1** with excess myristaldehyde (**7**, Scheme 2.5A) resulted in smooth attachment of hydrophobic chains via oximation to give the corresponding magnetic lipid particles (**MLP**, Scheme 2.5A). The **MLP** formulation demonstrated a significantly more positive zeta potential than **NP•1**. Weight analyses indicate roughly one equivalent of myristaldehyde is attached during the oximation step, suggesting that single chain lipid **8.1**, or likely a mixture of lipids **8.1** and **8** (Figure 2.6A), is bound at the **MLP** surface and possibly as a surrounding bilayer (Figure 2.6B), is most likely reason for the shift in zeta potential (+ 40 mV).

**A. Stepwise method**



**B. Direct method**



**Scheme 2.5.** Strategies for synthesis of lipid coated nano-magnetic carriers. Conditions: Each functionalization step was done in methanol at room temperature for 12 h; isolation and purification were performed via magnetic separation. Surface charge ( $\zeta$ -potential) measured in  $\text{H}_2\text{O}$ . **A.** Preparation of magnetic lipid particles (MLP) using a stepwise oximation approach. **B.** Preparation of dMLP via direct loading of oxime ether lipid.

Evaluation of the transfection efficiency of **MLP** in MCF-7 breast cancer cells was done using a luciferase reporter gene assay (Figure 2.7). MLP-magnetoplexes

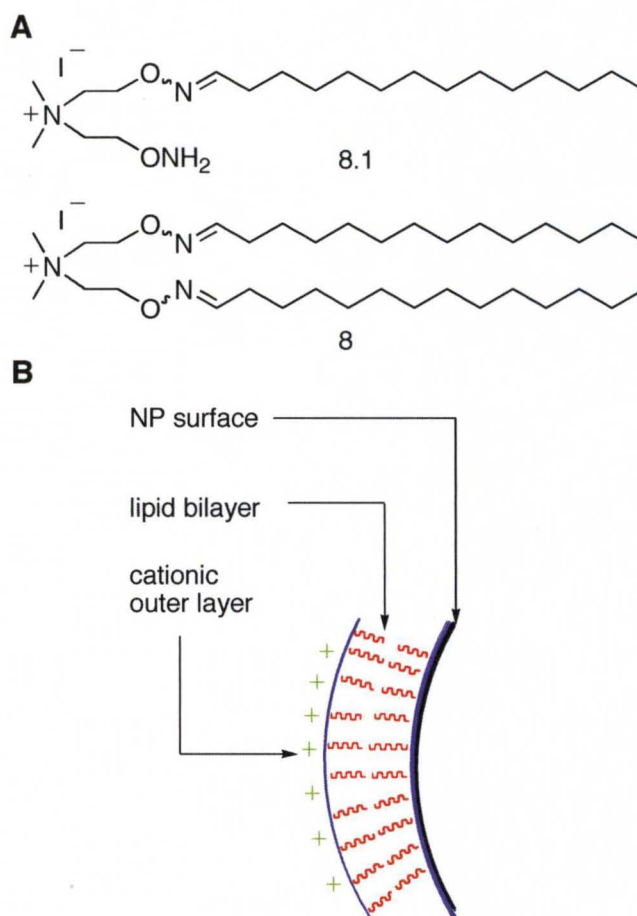


**Figure 2.6. A.** Cationic oxime ether formed on reaction with meristaldehyde at the NP surface. **B.** Schematic representation of bilayer formation at NP surface.

(MLP•DNA complex) were prepared at various weight ratios by direct mixing with the luciferase pDNA followed by application to cells in the presence of a static magnetic field. The data (Figure 2.7) indicated that **MLP** transfection efficiency is roughly equivalent or slightly higher than that of the commercial transfection agent Lipofectamine 2000 (positive control) at magnetoplex weight ratios exceeding 120,

while activity drops off rapidly at higher ratios. Not unexpectedly, given the negative zeta potential of NP•1, magnetoplexes derived from NP•1 did not transfect (400-600 RLU).

Unfortunately, as with most magnetic nanoparticle delivery systems, removal of the magnetic field resulted in substantial loss of transfection activity for the MLP-magnetoplexes.

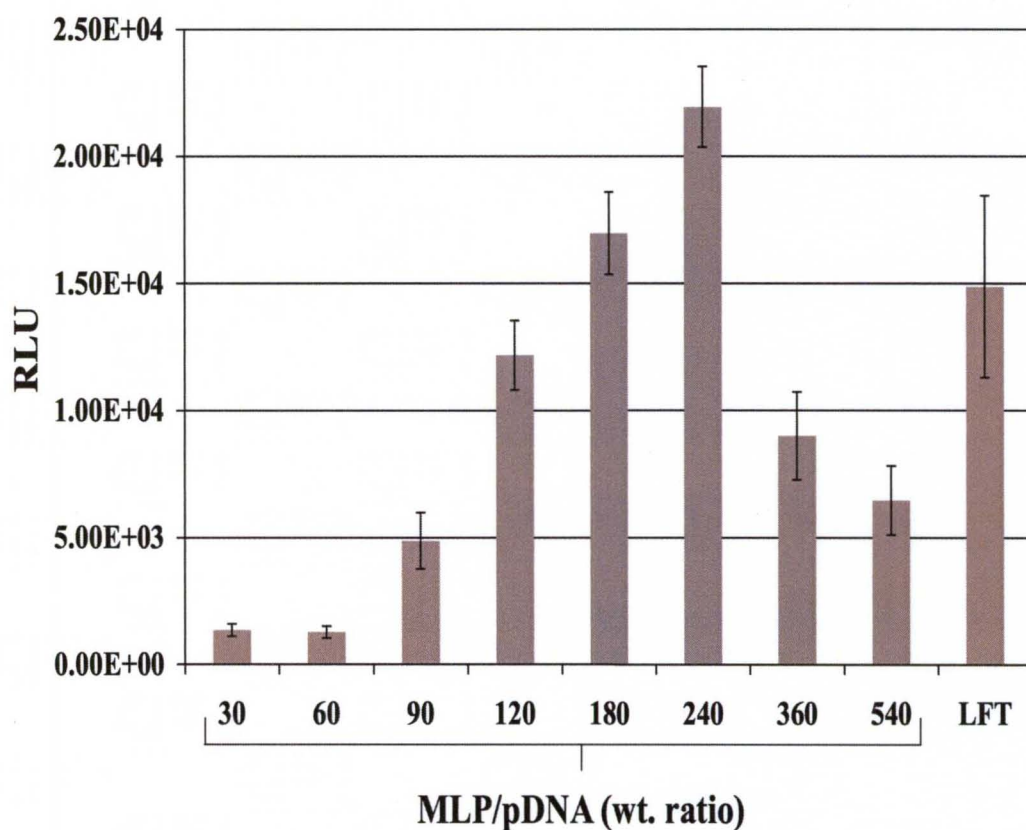


**Figure 2.7.** Magnetofection of MCF-7 cells using MLP-derived magnetoplexes in presence of 10% FBS. Results are expressed as total relative light units (RLU). Transfections were performed in 24-well tissue culture plates using 0.025 mg luciferase reporter construct (pCMVLuc) per well with 18 h transfection time. Each data point reflects the mean value of three separate transfections and the standard deviation from the mean. LFT = Lipofectamine 2000.

Since additional myristaldehyde could not be attached by further reaction with **MLP**, we probed whether direct attachment of the dual-chain lipid **8**<sup>112</sup> to iron oxide nanoparticles could be accomplished. Reaction of excess **8** with the NPs followed by our washing protocol delivered **dMLP**, magnetic lipid particles formed on direct exposure to the cationic oxime ether lipid. Lipid loading was measured at 1.25-1.35  $\mu\text{mol/mg}$ . The TEM micrograph of **dMLP** (Figure 2.8) shows spherical shaped nanocrystalline particles around 5-10 nm in diameter.

Evaluation of **dMLP** in the transfection of MCF-7 cells (Fig. 2.9) revealed notable differences in comparison to transfections using **MLP**. Under magnetofection conditions (Figure 2.9A) and in the presence of serum, **dMLP**-magnetoplexes are considerably more active than **MLP**-magnetoplexes at all

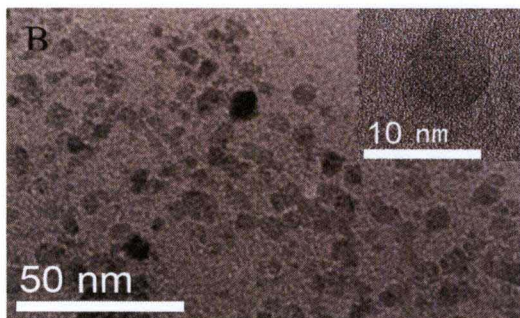


**Figure 2.8.** TEM micrograph of **dMLP**.

magnetoplex ratios and substantially more efficacious. The optimal **dMLP**-magnetoplex-120 exhibits more than three orders of magnitude higher transfection activity (*ca.* 1425-fold) than the transfection standard Lipofectamine 2000. More remarkable are the activities of **dMLP**-magnetoplexes in the absence of a magnet (Figure 2.9B). The **dMLP**-derived magnetoplexes are not dependent on magnet-assisted sedimentation for their activity, unlike **MLP**-magnetoplexes. At magnetoplex ratios between 90 and 540, the data indicate **dMLP** significantly

promotes transfection relative to the positive control (e.g., magnetoplex-180 exhibits >40-fold higher activity than Lipofectamine 2000). We also examined if the observed activity of **dMLP** is due to any unattached lipid **8** acting independently as a transfection agent. We examined **8** at various lipid:DNA ratios without any helper lipid and found it to be essentially inactive.

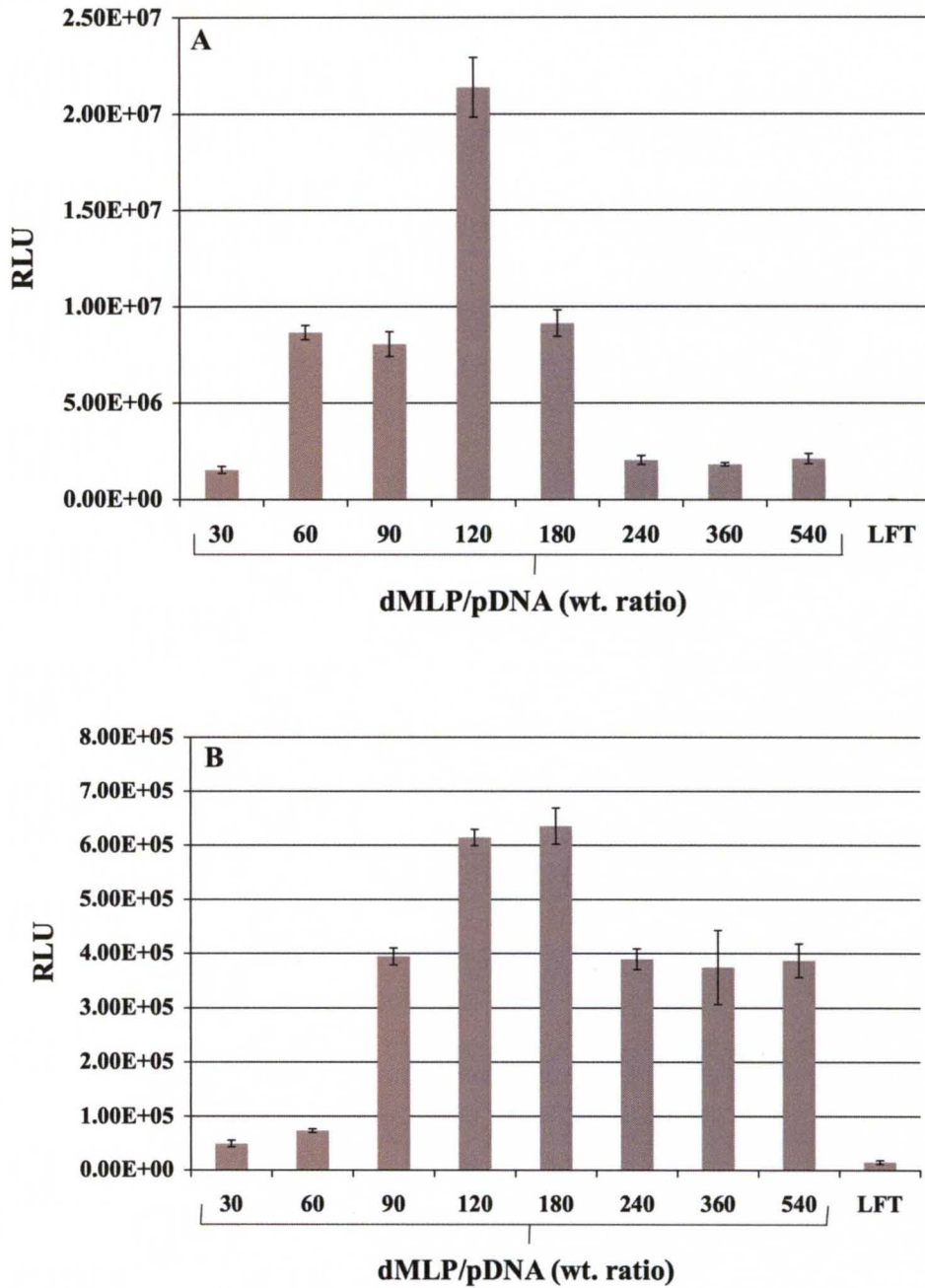


**Figure 2.9.** Magnetofection (A) and transfection (B, no magnet) of MCF-7 cells using dMLP-derived magnetoplexes in presence of 10% FBS. The results are expressed as total relative light units (RLU). Transfections were performed in 24-well tissue culture plates using 0.025 mg luciferase reporter construct (pCMVLuc) per well with 18 h transfection time. Each data point reflects the mean value of three separate transfections. Error bars show the standard deviation from the mean. LFT = Lipofectamine 2000.

Comparison of the measured zeta potentials for MLP- and dMLP-magnetoplexes (Figure 2.10) indicates different plasmid-binding properties. The dMLP formulations achieved net positive magnetoplexes at lower particle concentrations. Furthermore, the use of dMLP results in a fairly uniform magnetoplex charge over a wide range of formulation ratios as reflected by the consistent transfection activities observed for the dMLP-magnetoplexes, particularly in the absence of a magnet, which is in agreement with transfection activities.

A cell viability assay was performed to evaluate the cytotoxicity of dMLP-magnetoplexes using alamarBlue kit (Invitrogen Corporation, CA). The cytotoxicity study revealed that magnetoplexes derived from dMLP were less toxic towards MCF-7 cells than Lipofectamine (Figure 2.11).



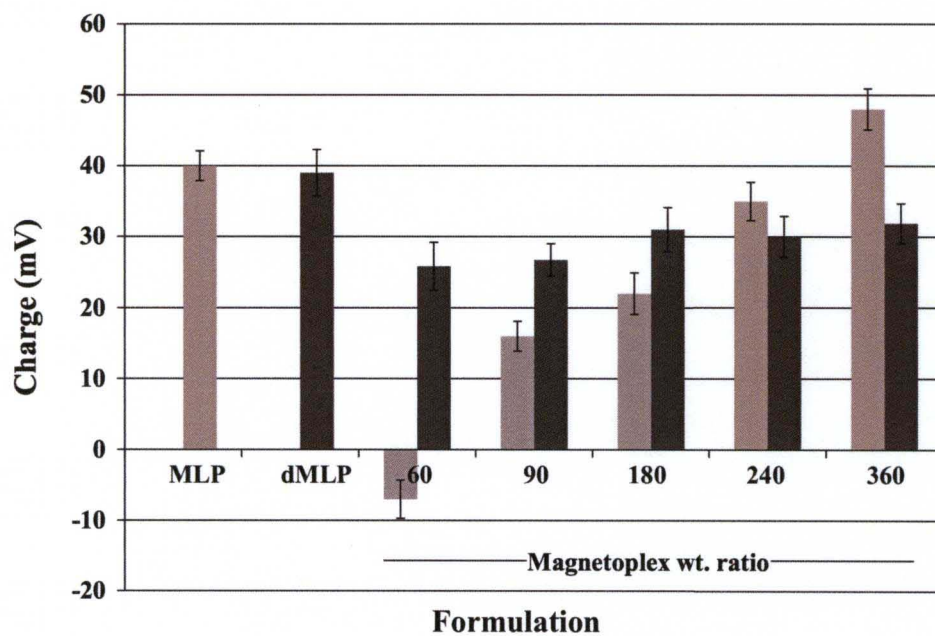


**Figure 2.10.** Zeta potential measurements ( $H_2O$ ) of MLP- (light bars) and dMLP-magnetoplexes (dark bars) at various nanoparticle to pDNA ratios; the concentration of NP in the aqueous particle samples was 0.1 mg/mL; magnetoplexes were formulated at a concentration of 0.5  $\mu$ g pDNA/formulation;  $n = 3$ .

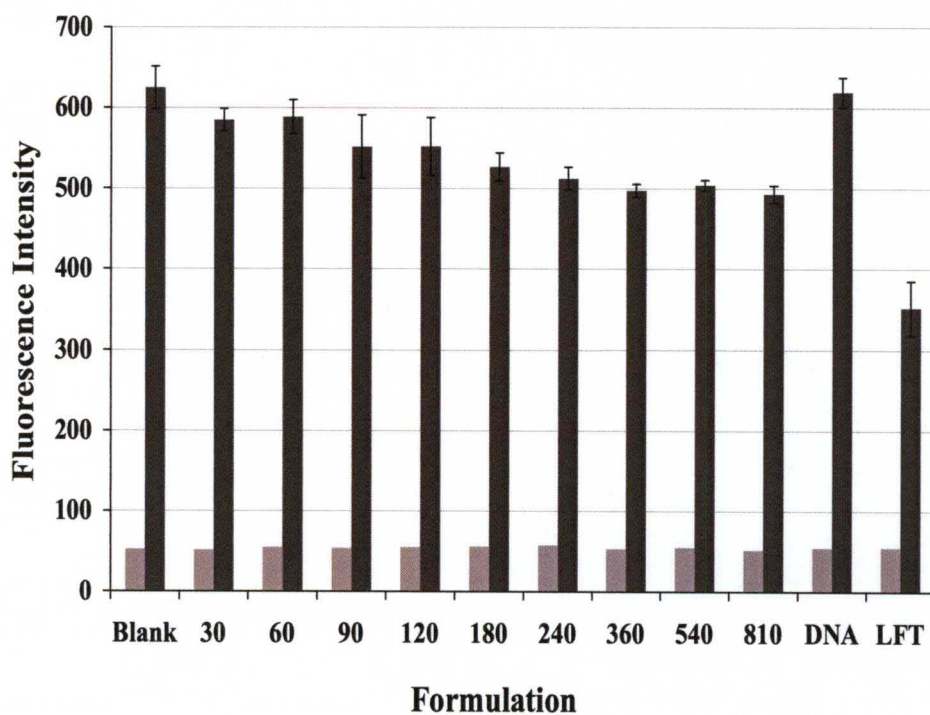


**Figure 2.11.** Cell viability study of MCF-7 cells transfected with DNA alone (DNA), Lipofectamine 2000 (LFT) and dMLP-magnetoplexes at various dMLP:pDNA ratios. At 18 h post transfection, alamarBlue® was added to cells and the fluorescence intensity (arbitrary fluorescent units) was measured at the onset (light bar) and then measured again at 4 h post addition (dark bar, n=3).

### **AMF-induced *hsp* gene-promoted gene expression**

With an efficient route to synthesize positively charged, lipid-coated magnetic nanoparticles (dMLP) in hand, and having carefully optimized transfection conditions *in vitro*, we next sought to develop a heat-inducible gene expression system in which the thermal energy generated by dMLP under an AMF-stimulus would be used to activate the gene expression. To pursue our goal we first purchased an *hsp70*-luciferase reporter plasmid (*hsp70-luc*, SwitchGear Genomics, Menlo Park, CA, product number S112961). At first we wanted to examine the level of gene expression when cells transfected using this *hsp*-construct were heated at 43 °C in an incubator (no AMF) and then compare the transfection levels to those of cells incubated at constant 37.5 °C. Commercial transfection lipid Lipofectamine 2000 was used to transfect the *hsp70* gene-promoted plasmid into the MCF-7 cells. Transfected cells were heated at 43 °C for 1 h according to the vendor's protocol and a luciferase assay was then performed to evaluate the transfection efficiency 24 h post heat-induction. Unfortunately we did not observe any encouraging promotion of gene expression due to the heat-induction (only ~ 3X higher levels of expression for the heat-treated cells, Figure 2.12).

The primary problem with this *hsp-luc* vector is related to the prolonged heat shock of 1 h required to produce protein expression. This is likely to be a major obstacle for NP-mediated AMF-induced gene expression. One hour AMF-induction even in cell culture would cause cell death due to over heating from NPs, as internalized NP surface will be at much higher than 43 °C. Also long time AMF-irradiation in animal study would face technical problems.

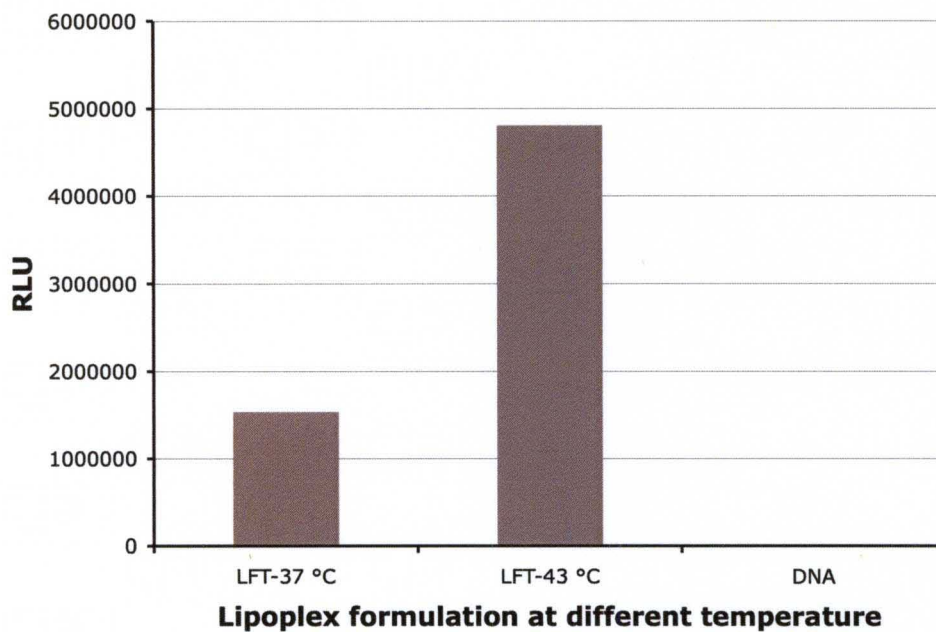


**Figure 2.12.** Heat-inducible luciferase expression in MCF-7 cells. Transfection was performed in 30 mm dish using 0.5  $\mu\text{g}$  pDNA/dish. Transfection activity was expressed as RLU. Lipofectmaine 2000 was used to transfect at vendor's ratio. Cells incubated at 37 °C was used as a control. LFT-37/43 °C is the lipoplex formulation incubated at 37 ° or at 43 °C. Transfection activity was evaluated using a luciferase assay kit according to the vendor's protocol after 24 h of transfection. Transfection experiment was performed in duplicates.

Thus, the *hsp* promoter gene is not potent enough to show very high level of expression when transfected cells received a heat-induction. Verkis *et al.*<sup>101</sup> reported 80-90% GFP expression after 30 min of heat treatment when the cells were transfected by their *hsp*-GFP construct. In their study *hsp* was taken from the plasmid pD3SX, which was purchased from Stressgen Biotechnologies, Victoria, Canada. In the work of Smith *et al.*,<sup>103</sup> *hsp*-luc (luciferase reporter) construct showed 53 fold enhancement of luciferase expression when cells were induced with heat (temperature 43 °C) for 11 min than the transfected cells incubated at constant 37.5 °C. They also used the same source of plasmid to construct the heat shock promoter from Stressgen Biotechnologies. Unfortunately, when we pursued obtaining the same vector we found that Stressgen Biotechnologies had merged with Enzo Life Sciences, Inc., NY and the *hsp*-vector was discontinued. Our collaborator Dr. Geoffrey Clark (Brown Cancer Center, University of Louisville, KY) also tried to contact various authors, who had used the vector, but we did get not favorable responses.

However, further cloning technique could be required to re-engineer the present plasmid to improve its expression efficacy at 43 °C before use in AMF-induced *hsp*-promoted gene expression studies.

At this stage of the research, we turned our focus to a more achievable goal of using AMF-induced hyperthermia to cause drug release from magnetic carriers. The details of this research are discussed in Chapter 4.

### 2.3. Conclusion and future directions

To our knowledge, the **MLP** and **dMLP** nano-magnetic gene delivery system discussed in this chapter are the first demonstration of attaching lipid sidechains onto iron oxide nanoparticles using click oximation methodology. Elaboration of the aminoxy-coated particles **NP•1** described herein into a magnetofection-active vector avoids the use of PEI and requires only simple mixing with a hydrophobic aldehyde. Using an even more direct approach, we demonstrated that reacting an ammonium ion-based oxime ether lipid with iron oxide nanoparticles generated a highly active, non-cytotoxic, magnetic transfection vector. Notably, the resultant lipid-coated nanovector **dMLP** functioned in the presence of serum to transfect a representative cancer cell line without the assistance of a magnet. According to our literature search, our custom made **dMLP** NPs at present are the only polymer free magnetic vectors that can transfect pDNA without magnetic assistance. The poly-L-lysine (PLL) coated magnetic vector prepared by Li *et al.* (Chapter 1, Table 1.1) is the only other reported transfection-active magnetic particle-based formulation that does not require magnetofection condition. Under magnetofection conditions, **dMLP** was orders of magnitude more active in MCF-7 cells based on luciferase assay than the industry-standard transfection agent. The results of our study demonstrate that  $\text{Fe}_3\text{O}_4$  nanoparticles can function as transfection enhancers for an otherwise transfection-inactive material.

Given the emerging field of *in vivo* applications, the development of a magnetic vector that does not require a magnet for the transfection stage may enable applications previously thwarted by less-effective magnetofection.

Given a suitable plasmid construct that operates within 15-20 min of heat activation, **dMLP** derived magnetoplexes would lead to AMF-induced heat-actuated localized gene expression.

## **CHAPTER 3**

### **CATIONIC OXIME ETHER LIPIDS: A VERSATILE CLASS OF GENE CARRIERS**

---

#### **3.1 Introduction**

#### **3.2 Results and Discussion**

#### **3.3 Conclusion and Future Directions**

---



### 3.1. Introduction

Cationic lipids and their derived liposomes have become the most well-studied and widely used synthetic, nonviral gene delivery systems since Felgner *et al.*<sup>126</sup> first demonstrated DOTMA mediated gene transfer in 1987.<sup>127, 128</sup> As discussed in Chapter 1, the major limitations of viral vectors, such as associated immune responses, limited polynucleotide carrying capacity and high cost,<sup>129, 130</sup> make cationic lipids a promising alternative in modern gene therapy. The advantages like

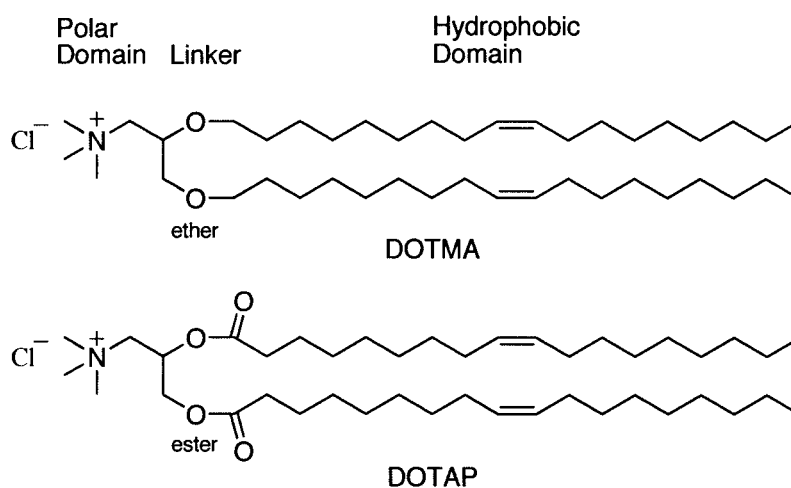


**Figure 3.1.** Common structural domain of cationic lipids.

low immunogenicity, the ability to transfect RNA or DNA of nearly unlimited size,<sup>131, 132</sup> and ease of formulation techniques of cationic lipid-polynucleotide complexes (lipoplex)<sup>133</sup> continue to attract interest aimed at developing safer and more efficient cationic lipids for use as transfection agents.<sup>134</sup>

Typical cationic lipid molecules, such as the dual chain lipids DOTMA and DOTAP (Figure 3.1), contain a polar, positively charged (DNA binding) head group connected to a hydrophobic domain via a linking functionality. These three principal structural components of cationic glycerol-type lipids have been extensively studied

in efforts to improve lipid-mediated intracellular delivery of polynucleotides to mammalian cells.<sup>135</sup>

Over the years many structure–activity relationships have been determined<sup>136, 137</sup> to understand the contribution of the hydrophobic domain to transfection efficiency, including the variables of chain length, degree of unsaturation, and domain asymmetry.<sup>138</sup> Although the linker determines conformational flexibility, degree of stability, and biodegradability of the cationic lipid, fewer direct structural comparisons of changes in the cationic lipid backbone, or linking domain, have been reported. The most well-known comparison being that of the diether DOTMA versus the diester DOTAP. Among the most studied chemical functionalities comprising the linking domain of transfection lipids are the ether, ester, ortho ester,<sup>139, 140</sup> carbamate,<sup>141</sup> amide,<sup>142, 143</sup> and phosphono<sup>144</sup> moieties.

The use of oxime ether linkers in chemical biology and medicinal chemistry have been discussed in Chapter 1 of this thesis. Oxime ether research has increased dramatically in the past several years as the benefits of chemoselectivity and methods for their exploitation have become better understood. Although oximation has been used to attach ligands to transfection lipids, such as the ligation of carbohydrates,<sup>145</sup> and although an oxime ether-based assembly for siRNA delivery has been reported,<sup>146</sup> no studies have examined the use of the robust yet biodegradable oxime ether linkage as the backbone feature of cationic lipids for DNA delivery.

Our research group's long-term interest on developing lipid-based gene delivery vectors<sup>139, 147, 148</sup> and interest in click chemistry<sup>149, 150</sup> inspired us to use oximation as a facile approach to prepare non-toxic cationic oxime ethers and

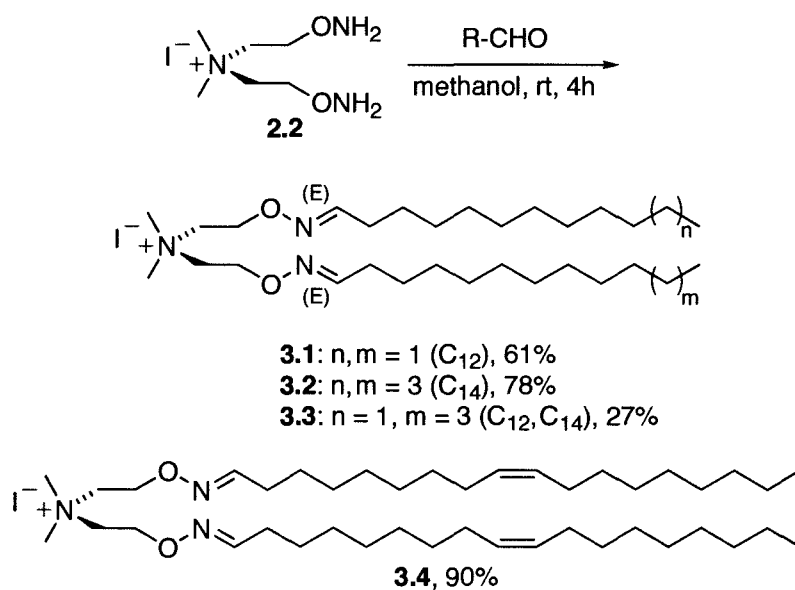
evaluate their transfection activity in several mammalian cells. Based on the promising transfection results using the oxime ether lipid coated NPs (MLPs) discussed in Chapter 2, we prepared a panel of oxime ether lipids and evaluated their gene expression activity using a conventional co-lipid formulation. A series of novel oxime ether lipids were prepared (Scheme 3.1), containing different length of hydrophobic chains to study the structure-transfection activity relationships in various mammalian cells. The synthesis, characterization and transfection activity of these novel oxime ether lipids is presented below.

## 3.2. Results and Discussion

### Synthesis

We prepared a panel of cationic oxime ether lipids by reacting bis-(aminoxy) ammonium salt **2.2**<sup>151</sup> with the hydrophobic aldehydes dodecanal, tetradecanal, or (*Z*)-octadec-9-enal (oleyl aldehyde) in methanol at room temperature to afford oxime ethers **3.1**, **3.3** and **3.5**, respectively (Scheme 3.1). In each case, the lipid was obtained as a mixture containing two stereoisomers (diastereomeric ratio ranging from approximately 2.3:1 to 5.3:1). The major diastereomer has (*E*)-stereochemistry about each oxime C=N bond (as depicted in Scheme 3.1). The minor diastereomer has an (*E*)-oxime ether as well as a (*Z*)-oxime ether linkage. The (*E,E*):(*E,Z*) ratio was readily measured by integration of the well separated oximyl proton shifts in the <sup>1</sup>H NMR spectra (Figure 3.2). For example, the oximyl proton shift for the (*E*)-oxime ether side chain in **3.2** occurs at  $\delta = 7.45$  ppm, while the (*Z*)-isomer shift appears at  $\delta = 6.79$  ppm. The isomer ratio was found to be susceptible to a variety of factors including exposure to mild acid and heat. The stereochemical integrity of the oxime

ether lipids is inconsequential in that isomerization can be expected *in vivo*. Of greater interest, however, is that the oximation approach used to prepare these compounds delivers the lipids with intrinsic asymmetry in the hydrophobic domain. Nantz *et al.*<sup>147</sup> and others<sup>152</sup> have recently noted the beneficial influence of unsymmetrical hydrophobic domains in cationic lipid-mediated DNA transfection. Consequently, we used the oxime ether lipids as obtained directly in transfection experiments. To probe further the influence of an unsymmetrical hydrophobic



**Scheme 3.1.** Synthesis of oxime ether lipid panel via oximation route.

domain, we also prepared unsymmetrical analogue **3.4** (Scheme 3.1) by successively condensing **2.2** with dodecanal and tetradecanal. The yield of **3.4** was poor (27%) compared to others. The yield was not so great in the first step due to formation of both bis- and mono-oxime ether lipids and then finally during attachment of the second hydrophobic C<sub>14</sub>- or C<sub>12</sub>-chain to the isolated mono oxime ether we observed that column purified fraction was a mixture of **3.1**, **3.2**, and **3.3**. Although, proton

NMR looked good, HRMS measurement indicated that the final compound was mixture of above three lipids. After careful purification we could only get 27% yield of **3.3**. Hydrophobic oxime ethers **3.1-3.4** were formulated as cationic liposomes using equimolar quantities of colipid dioleoylphosphatidylethanolamine (DOPE) for subsequent studies.

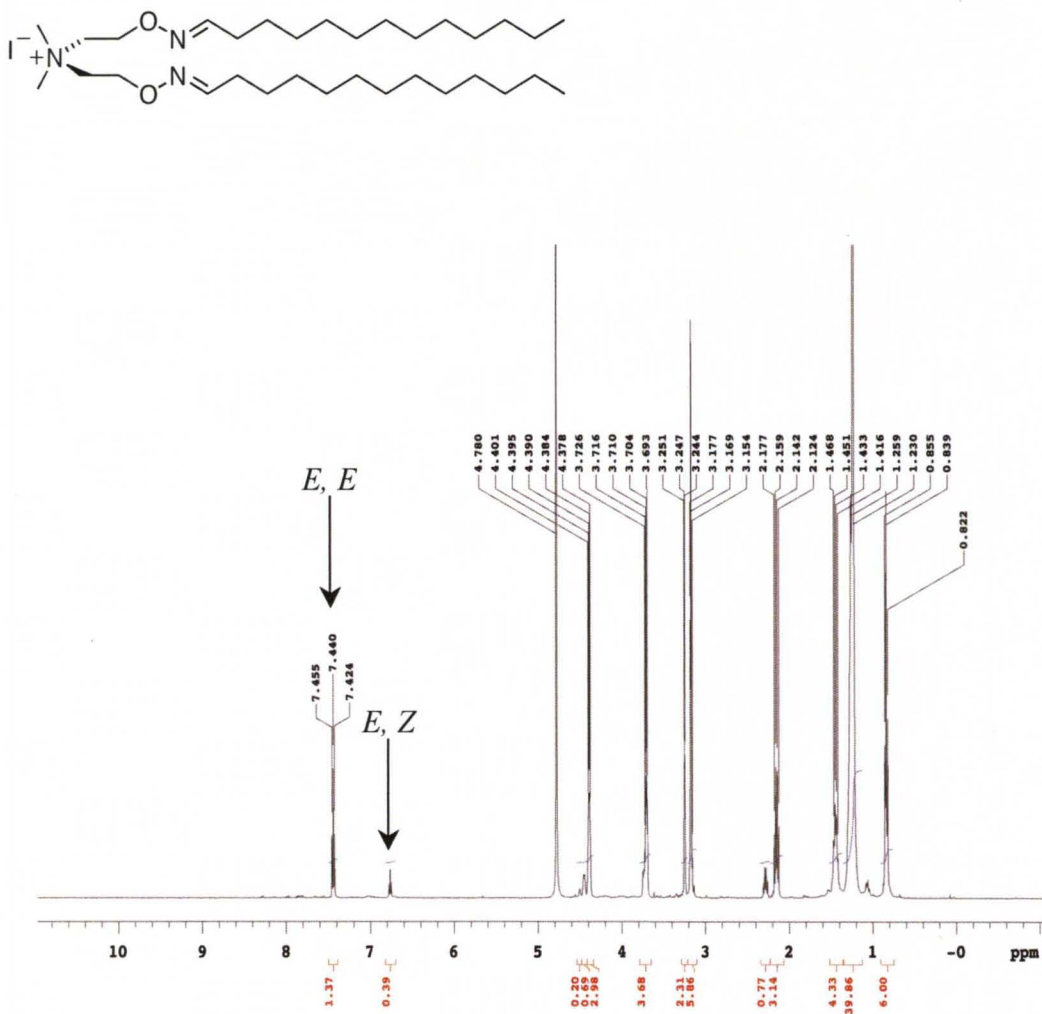


**Figure 3.2.**  $^1\text{H}$  NMR of **3.2** in  $\text{CD}_3\text{OD}$ . Oximyl proton shift of *E, E* isomer: 7.45 ppm and *Z, Z* isomer: 6.79 ppm.

### **Size and charge characterization**

Particle size and zeta potential measurements on the oxime ether liposome suspensions revealed that the particles were net positively charged with electrostatic potentials in the range of 45-66 mV (Figure 3.3A). Liposomes derived from bis-C<sub>18</sub> lipid **3.4** were the largest, with particle diameters exceeding 200 nm, and the most highly charged. Not unexpectedly, the liposomes derived from the shortest oxime ether lipids **3.1** and **3.3** i.e., lipids prepared using dodecanal, had the smallest mean diameters, near 150 nm. The trend in particle size versus particle charge correlates well for this series of lipids.

The net charge of lipoplexes derived for the cationic lipids-DOPE, and pDNA significantly influence the transfection activity of lipoplex formulation.<sup>153, 154</sup> Complexation of the oxime ether/DOPE liposomes with pDNA (pCMV-Luc) at different ammonium nitrogen/DNA phosphate ratios (N:P ratio) gave the corresponding lipoplexes. Zeta potential measurements of the oxime ether-derived lipoplexes at N:P ratios of 3, 5 and 7 showed high positive values in the range of 31-53 mV (Figure 3.3B). We observed that at these electrostatic potentials, minimal lipoplex aggregation ensued. The oxime ether/DNA lipoplex suspensions were stable at concentrations up to 0.33 mg oxime ether lipid per mL beyond one week. Particle size measurements of the lipoplexes (Figure 3.3) indicated that the mean effective diameter for all N:P formulations remained under 250 nm. Lipoplex size mirrored closely the precursor liposome, with the lipoplex generally having an increase in diameter by 20-50 nm (Figure 3.4).

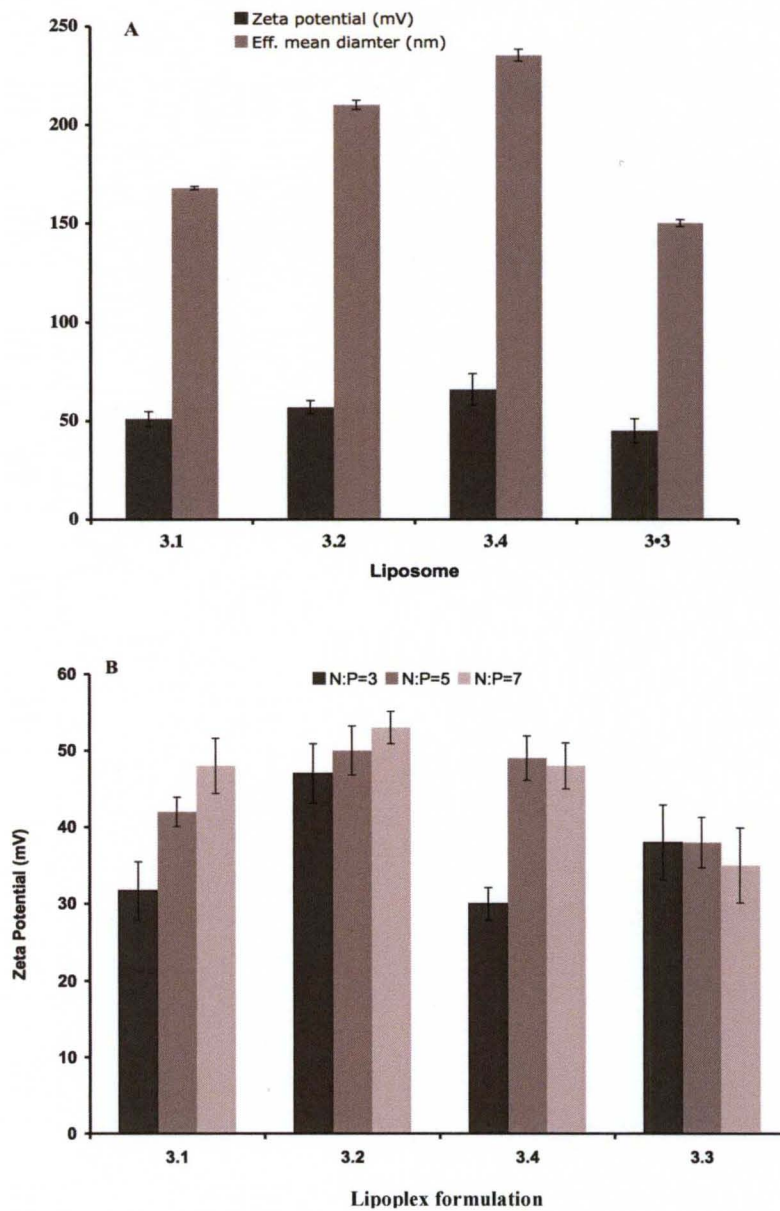


**Figure 3.3.** **A.** Zeta potential and mean particle size measurements for oxime ether:DOPE liposomes (0.1 mg cationic lipid per mL H<sub>2</sub>O). **B.** Lipoplex zeta potential measurements (lipoplexes were formulated at 0.1 mg cationic lipid per mL H<sub>2</sub>O with pDNA (pCMV-Luc) at different N:P charge ratios). Results are expressed as the mean values of n = 3 measurements.

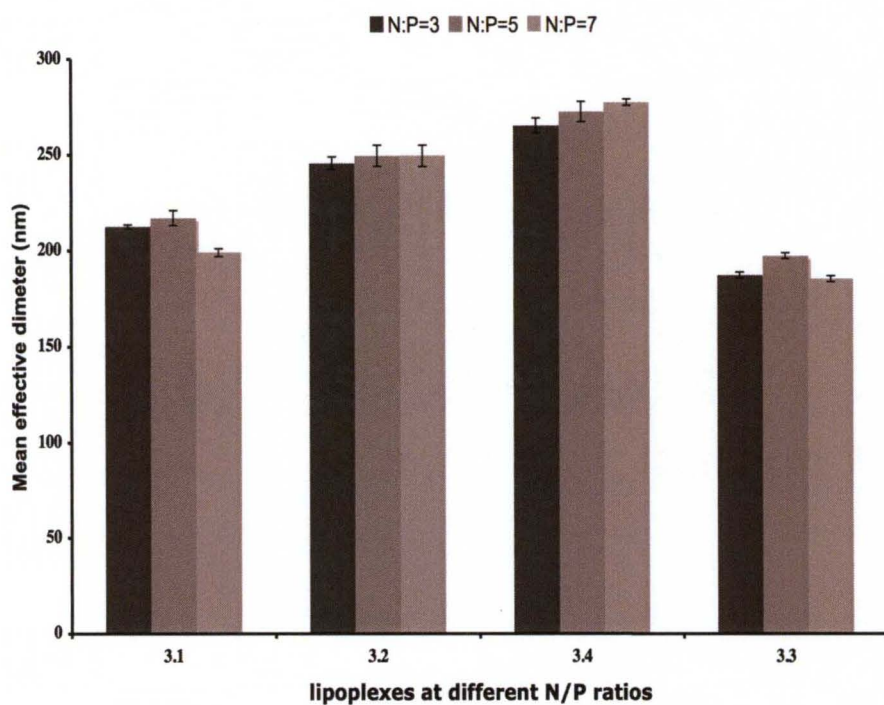


**Figure 3.4.** Size determination of lipoplexes. Lipoplexes were formulated at 0.1 mg cationic lipid/mL H<sub>2</sub>O with pDNA (pCMV-Luc) at different N:P charge ratios.



## Transfection activity

After synthesis and thorough characterization of the lipids **3.1-3.4**, and their derived lipoplexes, we evaluated the transfection activity of the lipid panel in human breast cancer (MCF-7) and human lung cancer (H1792) cells using a CMV-luciferase reporter plasmid in the presence of serum (Figure 3.5). Whereas the shortest chain lipid **3.1** was essentially ineffective at all N:P formulations examined in MCF-7 cells ( $2000 \pm 225$  RLU), our studies revealed that transfection efficiency of lipid **3.2** in this cell line at an N:P ratio of 7 was notably superior (greater than 2.5 orders of magnitude higher activity than the commercial standards) to the commercial transfection standard lipofectamine 2000 ( $3500 \pm 990$  RLU) as well as to the popular transfection formulation jetPrime ( $2500 \pm 209$  RLU) (Figure 3.5A). The unsaturated lipid **3.4** was also found to be efficacious in MCF-7 cells, although we observed greater deviation in the measurement of transgene expression at the higher N:P ratios using this lipid (Figure 3.5A). We did not observe an additional boost in transfection activity on further amplifying the hydrophobic domain asymmetry by using dissymmetric lipid **3.3**, relative to the activities of lipids **3.2** and **3.4** in this cell line (Figure 3.5A).

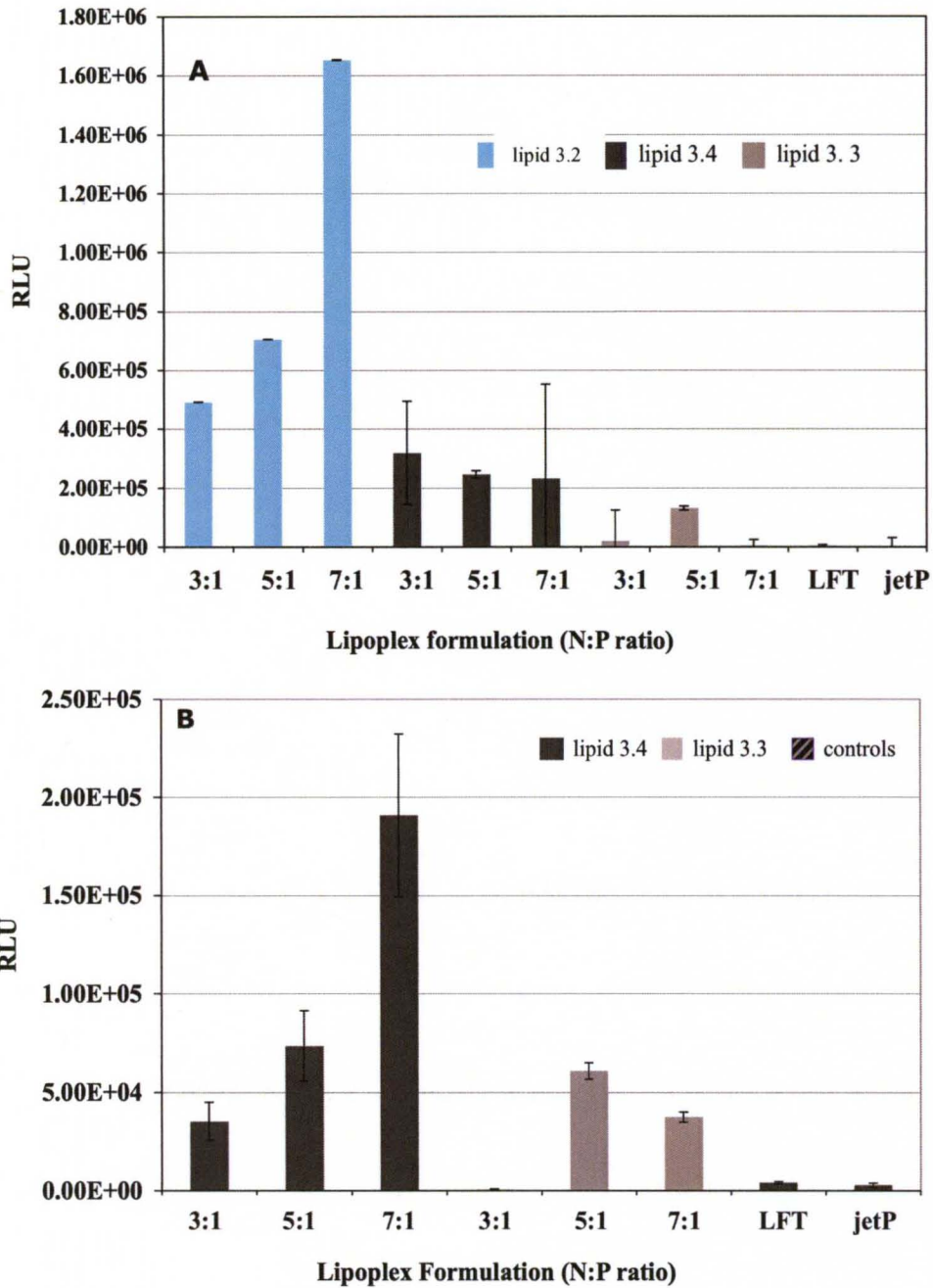


**Figure 3.5.** Transfection of cells using lipoplexes formulated at different N:P charge ratios: **A.** MCF-7 cells and **B.** H1792 cells. Results are expressed as total relative light units (RLU). Transfections were performed in 24-well tissue culture plates using luciferase reporter construct (pCMV-Luc; 0.025  $\mu$ g / well) with 18 h transfection time. Each data point represents the mean value of three separate transfections. Error bars show the standard deviation (SD) from the mean. LFT=lipofectamine 2000, jetP=jetPRIME.

Only lipids **3.3** and **3.4** led to high transgene expression in H1792 cells (Figure 3.5B). In agreement with the observation reported by Nantz *et al.*<sup>155</sup> and Fletcher *et al.*<sup>156</sup> on lung cell transfections, the presence of unsaturation in the hydrophobic domain, such as is present in lipid **3.4**, proved to be beneficial for activity (Figure 3.5B). Lipoplexes derived from lipid **3.4** effectively transfected H1792 cells relative to the commercial controls (60-fold higher activity at N:P=7, Figure 3.5B). Interestingly, the enhanced asymmetry of lipid **3.3** resulted in improved transfection of this cell line relative to the other saturated lipids examined (Figure 3.5B).

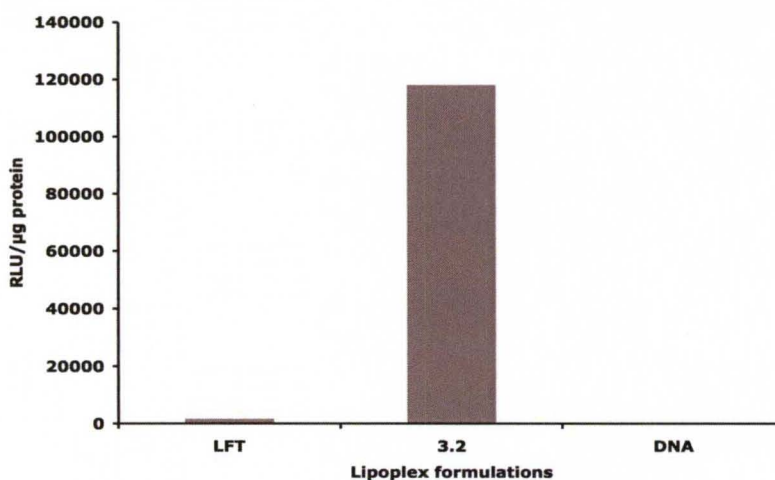


**Figure 3.6.** Transfection activity of lipid 3.2 in MCF-7 cells using 1 μg pDNA/well at N:P = 7. Transfection experiment performed in duplicate.

On a scale of 1 μg DNA per well, transfection of MCF-7 cells in a six-well format using lipoplexes derived from lipid **3.2** at an N:P ratio of 7:1 gave approximately a 70-fold higher luciferase expression (as assessed by RLU per mg protein) the lipofectamine 2000-derived lipoplexes (Figure 3.6). This result shows that the most potent oxime ether lipid **3.2** is effective in high dose and wide range of DNA doses in MCF-7 cells.

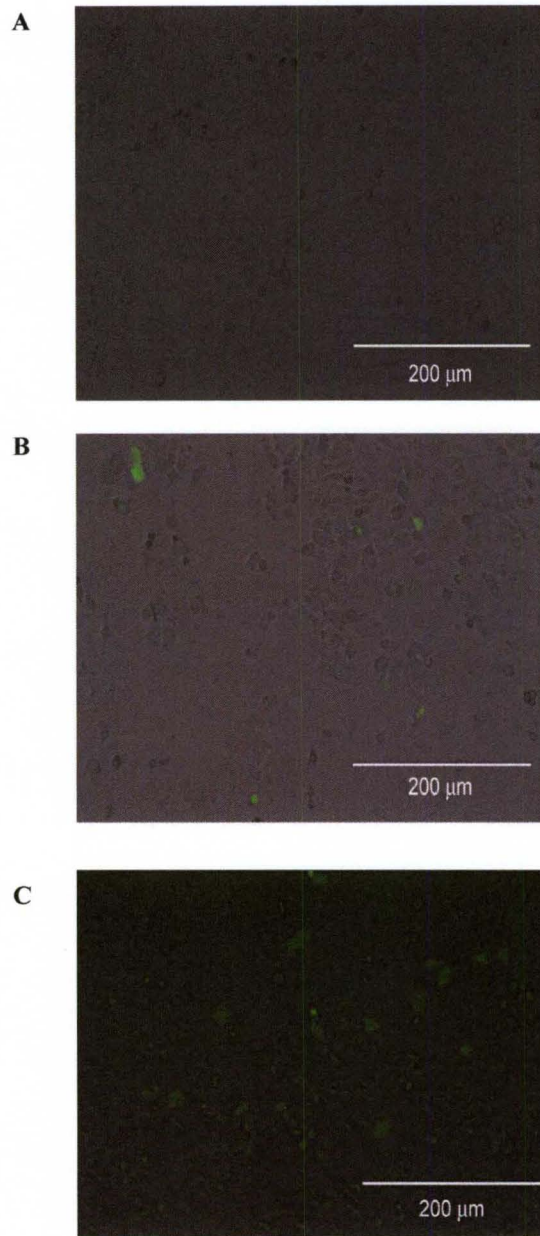


**Figure 3.7.** MCF-7 cells were transfected with a GFP expression plasmid (0.1  $\mu\text{g}$  per well in a 24-well plate). Figure are presented as an overlay of green fluorescence (visualized by fluorescent microscopy after 20 h of transfection) over the phase contrast image: **A.** Cells treated with pDNA (negative control); **B.** Cells transfected with lipoplexes derived from lipofectamine 2000 (positive control; vendor-recommended dose=0.25 mL); **C.** Cells transfected with lipoplexes derived from lipid 3 at N:P=7.

We also examined the gene-transfer capability of lipids with an oxime ether linker domain using a green fluorescent protein (GFP) reporter vector to estimate the transfection efficiency in MCF-7 cells (Figure 3.7). Examination of cells by fluorescence microscopy using an EVOS fluorescent microscope determined that the results were in agreement with those of the luciferase assay.

### **Salivary gland cell transfection**

To test the lipids in a non-cancer epithelial cell line, GFP was expressed in the salivary gland cell line PAR C10. This study was completed with the collaboration of Professor Sven Gorr's research group at the University of Minnesota, School of Dentistry. Lipoplexes were formulated at an N:P ratio of 1.5, the optimal ratio determined for lipids **3.1-3.4** in this cell line. GFP expression was evaluated 48 h post-transfection. The fraction of transfected cells was quantified by flow cytometry. Lipid **3.2** (C<sub>14</sub>) transfected approximately 40% of the cells, lipid **3.1** transfected about 20%, while lipids **3.3** and **3.4** exhibited less than 10% cell transfection (Figure 3.8A). Lipofectamine was slightly more effective in this cell line when used in excess (>3X recommended dose; Figure 3.8A) and comparable to lipid **3.2** when used at the vendor-recommended dose (Figure 3.8B). These results suggest that lipids with an oxime ether linker domain are suitable for the pDNA transfection of epithelial cell lines and, depending on hydrophobic domain composition, competitive with the transfection standard lipofectamine.

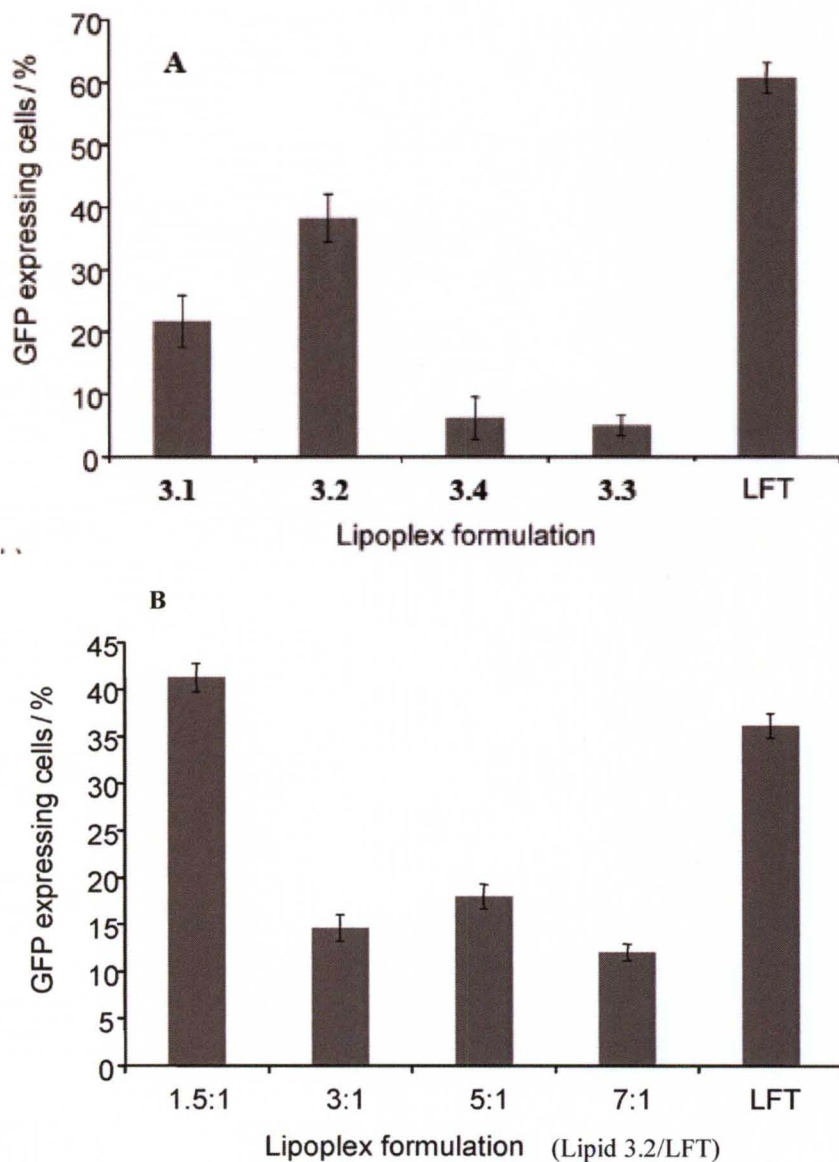


**Figure 3.8.** GFP expression in PAR C10 cells. **A.** Cells were transfected (0.2  $\mu$ g GFP reporter construct) with lipoplex formulations derived from lipids 3.1-1.4 (N:P=1.5) and excess lipofectamine 2000 (LFT; positive control; 1.6  $\mu$ L); **B.** Comparison of lipid 3.2 formulations at the indicated N:P ratio with LFT at the vendor-recommended dose (0.5  $\mu$ L). The transfection percentage of GFP expressing cells was analyzed by flow cytometry 48 h post-transfection; n = 3.

## **siRNA Transfection**

RNA interference (RNAi) gained a tremendous attention since Fire, Mello and colleagues first discovered the ability of double-stranded RNA to silence gene expression in 1998.<sup>157</sup> Tuschl and co-workers published their celebrated proof-of-principle experiment demonstrating that synthetic small interfering RNA (siRNA) could achieve sequence-specific gene knockdown in a mammalian cell line in 2001<sup>158</sup> and the first successful use of siRNA for gene silencing in mice was demonstrated for a hepatitis C target shortly after.<sup>159</sup> Theoretically, when using appropriately designed siRNA, the RNAi machinery can be exploited to silence nearly any gene in the body, giving it a broader therapeutic potential than typical small-molecule drugs.<sup>160</sup> Indeed, it has already been reported that synthetic siRNAs are capable of knocking down targets in various diseases in vivo, including hypercholesterolaemia,<sup>161</sup> hepatitis B virus (HBV),<sup>162</sup> human papilloma virus,<sup>163</sup> ovarian-cancer<sup>164</sup> and bone cancer.<sup>165</sup> In order for these advances to be implemented in a clinical setting, safe and effective delivery systems must be developed.

We tested the ability of our lipids to transfect epithelial cells with siRNA. The previous study revealed that only lipid **3.2** transfected efficiently in PARC10 cells, so cellular “housekeeping” gene glyceraldehyde-3-phosphate dehydrogenase was determined by measuring the reduction in GAPDH activity. GAPDH assay is a rapid, convenient, fluorescence-based method for measuring the enzymatic activity of glyceraldehyde-3 phosphate dehydrogenase (GAPDH) in cultured cells derived from human, mouse, and rat. GAPDH is a tetrameric enzyme, composed of 36 kD protein subunits. It catalyzes the oxidative phosphorylation of glyceraldehyde-3-phosphate

(G-3-P) to bisphosphoglycerate (BPG). The GAPDH gene is generally recognized as an ideal target for siRNA. GAPDH gene expression can be readily knocked down in many different cell types by delivery of a validated control GAPDH siRNA (e.g.,

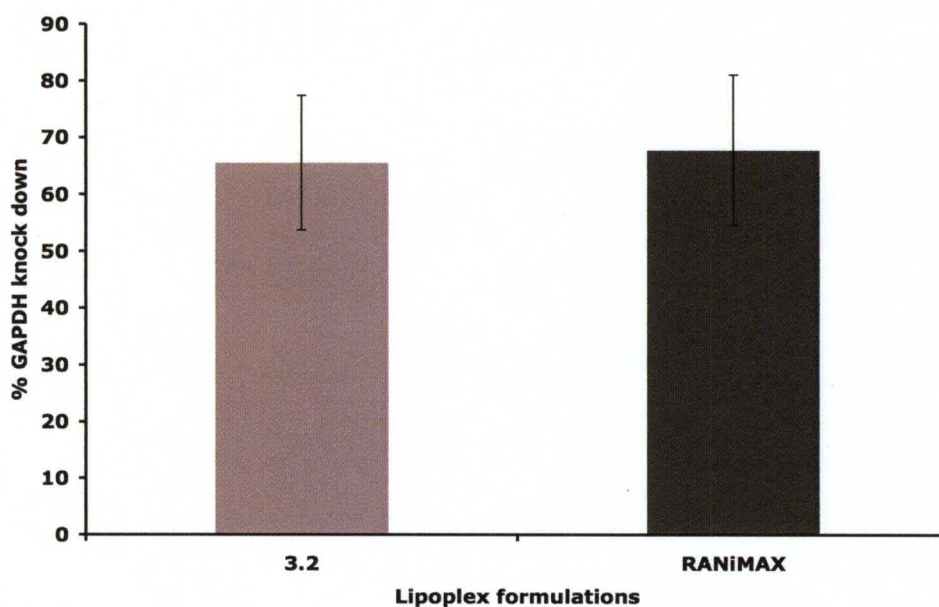


**Figure 3.9.** Par C10 cells were transfected with siRNA for GAPDH and silencer negative control. The enzyme activity was quantified 72 hr after transfection. Each data point reflects the mean value of three independent experiments (n=9). Error bars show the standard deviation from the mean.

Silencer® GAPDH Control siRNA). Thus, the efficiency of siRNA delivery can be monitored by measuring the reduction in GAPDH mRNA or protein levels in cells transfected with GAPDH siRNA relative to cells transfected with a negative control siRNA.

Lipoplexes derived from **3.2** reduced GAPDH activity by 55±9% (mean±SEM), while the control lipid, commercial lipofectamine RNAiMAX, reduced GAPDH activity by 71±6% (n=9, Figure 3.9). This difference was not statistically



significant ( $p=0.23$ ). These results suggested that lipid **3.2** effectively introduces siRNA into epithelial cells.

### **Cytotoxicity Evaluation**

We evaluated cytotoxicity of the lipids in MCF-7 and H1792 cells using vital dye trypan blue to stain the dead cells. The number of live cells remaining after treatment was calculated as a percentage over the untreated control (Figure 3.10A). Our lipids were found to be less toxic than lipofectamine and jetPrime in both cell lines (Figure 3.10A), with cell viability comparable to untreated cells at all N:P formulations examined.

For PAR C10 cells, the viability was determined by reduction of alamar blue (Figure 3.10B). None of the lipids reduced cell viability significantly compared with untreated cells, confirming the low toxicity of lipids with an oxime ether linker domain.

The PARC10 cell transfection experiments were done by Dr. Nandula in Prof. Gorr's laboratory and it is worth mentioned that performance of these lipids were reproducible, which is very promising for liposomal formulation. Also, in course of our transfection evaluation studies we found that our cationic liposome formulations are stable for six months at 4 °C.

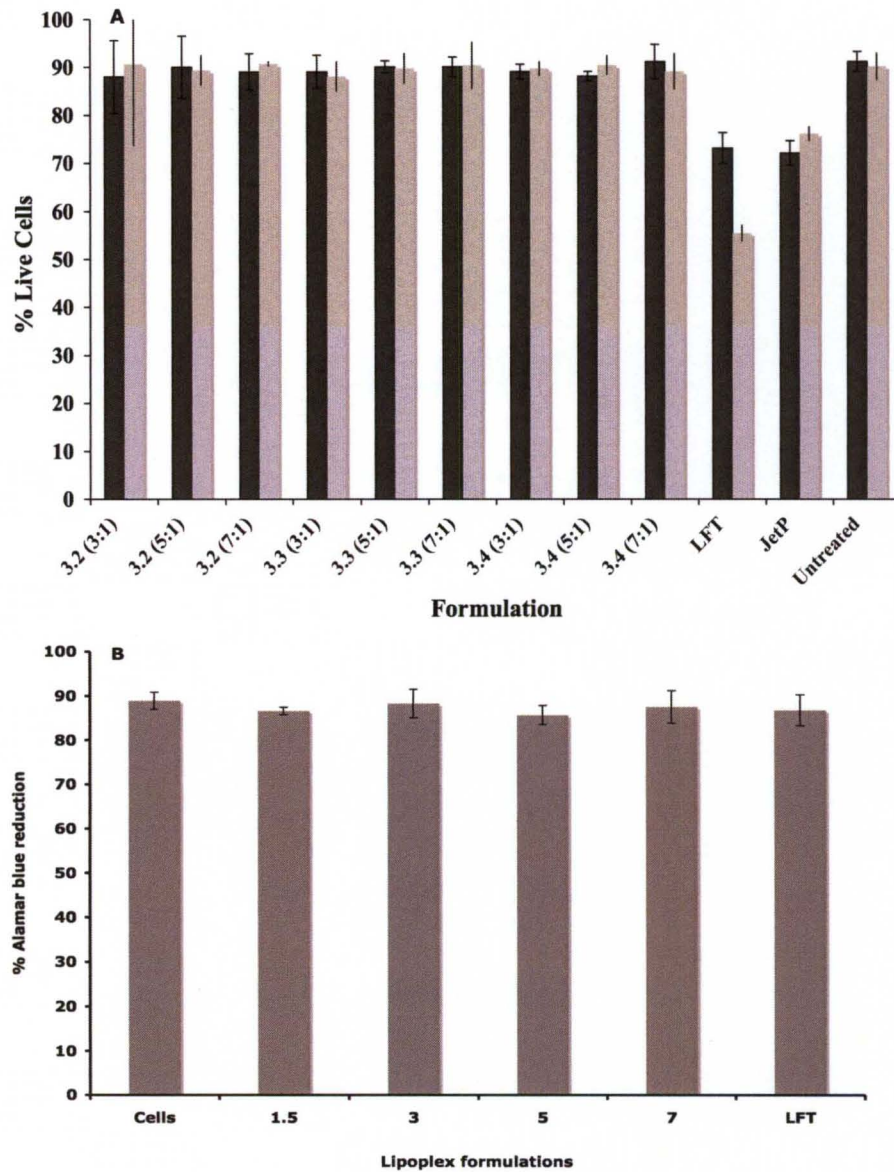


**Figure 3.10. A.** Relative cytotoxicity. MCF-7 (dk. bar) and H1792 cells (lt. bar) were transfected using either lipofectamine 2000 (LFT), jetPrime (JetP) or oxime ether lipoplexes at the specified N:P ratio (value in parenthesis). Transfections were performed in a 96-well format. Dead and live cells were counted 18 h post transfection using a trypan blue stain (n=3); **B.** Cell viability assay. PAR C10 cells were transfected (N:P=1.5) with lipoplex formulations derived from lipids 2–5 and lipofectamine 2000 (LFT; 1.6 mL). After 48 h, the cell viability was measured by calculating the percentage reduction of alamar blue dye. n = 3

### 3.3. Conclusion and Future Directions

We have demonstrated that the facile aminoxy-carbonyl click reaction can be used to rapidly assemble transfection lipids furnished with asymmetric hydrophobic domains.<sup>117</sup> The data show that lipids containing an oxime ether linking domain are well tolerated by both cancerous and noncancerous epithelial cells. Furthermore, with appropriate tuning of hydrophobic domain composition and N:P formulation,

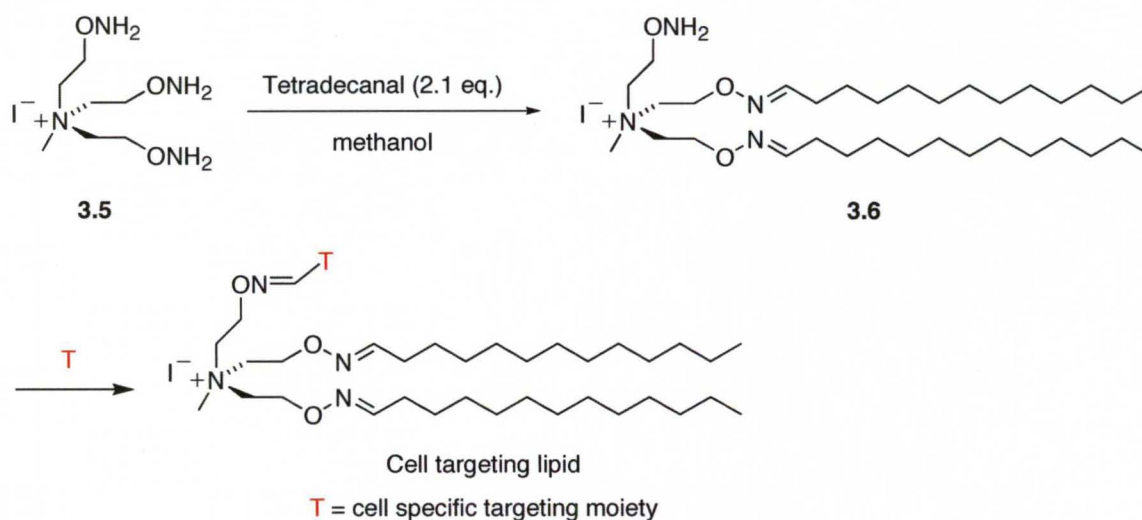


**Figure 3.11.** Synthesis of prototype oxime ether lipid for cell specific targeting.

lipoplexes derived from oxime ether lipids readily transfect representative epithelial cell lines with excellent activity relative to established transfection agents. Our research using the cationic oxime ether lipid panel shows that this functionality is a suitable choice for linker domain. Given the biological compatibility of oxime ethers and their ease of formation, this functional group should find much application in the future design of transfection vectors. The ability to transfect epithelial cells could have clinical applications, as epithelial surfaces are readily accessible and attractive targets for gene therapy protocols that aim to express therapeutic proteins *in vivo*. In

fact, *in vivo* study of siRNA delivery in salivary gland using the lipid **3.2** is presently undergoing at the Professor Sven Gorr's laboratory. The ability to simultaneously transfect pDNA and siRNA with a single reagent now opens potential applications to express therapeutic proteins in cells that are simultaneously modified by gene knockdown.

In regards to future direction, we have designed a prototype dual chain oxime ether lipid (**3.6**) that has a free aminoxy group for attaching targeting ligands or elements for cell specific delivery (Figure 3.11). The potential of this lipid for targeted gene delivery will be evaluated in near future.

## **CHAPTER 4**

### **IRON OXIDE NANOPARTICLE-MEDIATED, AMF-TRIGGERED DRUG DELIVERY**

---

**4.1. Introduction**

**4.2. Results and Discussion**

**4.3. Conclusion and Future Goals**

---

## 4.1. Introduction

For therapeutic applications, an external and noninvasive technique of actuation can be beneficial to achieve a desired therapeutic effect. The best-known examples of such a strategy include using gold nanocages, hollow gold nanospheres, or other GNP-based platforms for drug delivery. These vehicles have been used as heat-induced drug delivery systems.<sup>166</sup> They represent a class of nano-architectures with a hollow interior and/or porous walls that undergo a photothermal effect while absorbing strongly at near-infrared region to generate heat while retaining their

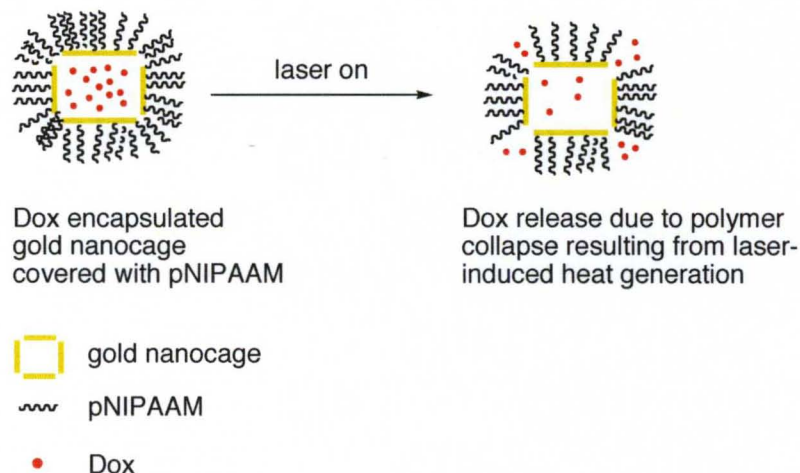


**Figure 4.1.** Schematic illustration of laser-controlled drug release.<sup>1</sup>

shape.<sup>167</sup> For example, Yavuz *et al.*<sup>166</sup> encapsulated the doxorubicin (Dox) into a gold nanocage covered with a thermosensitive poly(*N*-isopropylacrylamide) (pNIPAAAM) derivative. On exposure to a laser beam with a wavelength that matched the absorption peak of the Au nanocage, light was absorbed and converted into thermal energy. These researchers showed that the heat dissipated into the surroundings, and the rise in temperature caused the polymer chains to collapse and expose the pores in the nanocage causing release of the pre-loaded Dox (Figure

4.1). They also demonstrated that when the laser was turned off, heating immediately ceased and the temperature drop brought the polymer back to its original, extended conformation, closing the pores and stopping the release.

In another example, Yang *et al.*<sup>168</sup> reported a delivery system consisting of a poly(lactic-co-glycolic acid) (PLGA) matrix containing (Dox) and a gold over-layer on a polymer matrix that also undergoes of a photothermal effect. The temperature of the carrier increased due to the surface plasmon resonance (SPR) effect of the gold

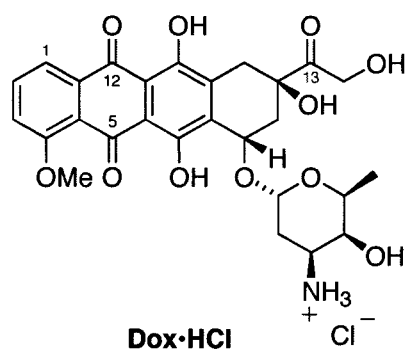


**Figure 4.2.** Structure of doxorubicin.

layer when irradiated by near-infra red (NIR) light, and the resultant heat effected cargo release from the softened PLGA matrix.

The concept of heat-triggered drug delivery using hyperthermia generated from nano-magnetic carriers has already been discussed in Chapter 1. One important advantage of magnetic hyperthermia-stimulated drug delivery using magnetic nanoparticles over gold nanoparticle-mediated laser-induced delivery, such as described above, is that magnetic particles can easily be viewed by MRI. Secondly, laser-induction has the problem of shallow tissue penetration<sup>169</sup>. Where as alternating magnetic field (AMF) can penetrate deep into tissue. More importantly, laser-

induced nanoparticle heating can generate uncontrolled heating (50-70 °C).<sup>169</sup> Magnetic hyperthermia is less risky and more controllable than laser-induced heating. Given the fact that magnetic hyperthermia already has been examined in clinical trials,<sup>170, 171</sup> AMF-induced drug delivery holds immense potential as an externally controlled drug delivery platform.

The recently developed magnetic carriers for AMF-activated drug release are described in Chapter 1. In most of the examples, the vehicle consists of a magnetic nanoparticle encapsulated in a thermo-sensitive material. The AMF-induced hyperthermia (i.e., external stimulus) caused structural changes in these materials and these in turn result in cause cargo release (Chapter 1, Figure 1.7) from the vehicles.<sup>86, 172, 173, 174, 175</sup> One problem of these systems is that many thermo-responsive material-based magnetic carriers suffer from pre-mature drug release at body temperature (37 °C). Depending on the cargo, this may cause non-specific toxicity *in vivo*.

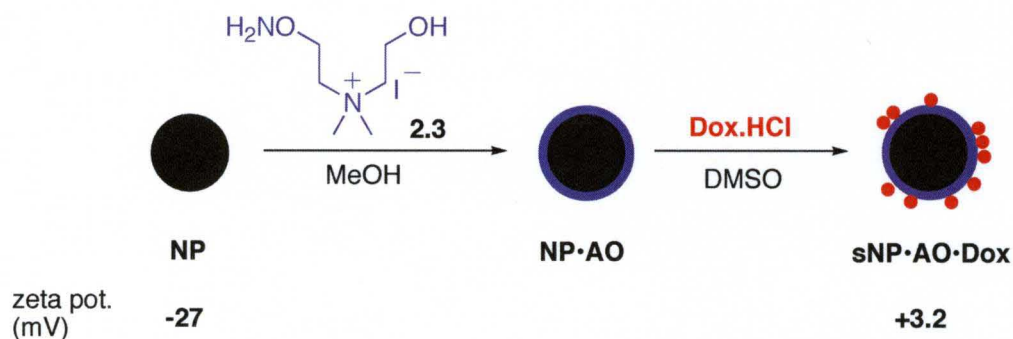
To address the challenge of premature cargo release, we aimed to assemble a Fe<sub>3</sub>O<sub>4</sub> nanoparticle (NP)-based delivery platform functions without the need for a third component's structural or conformational change. In other words, our goal is to design a thermosensitive, polymer matrix-free magnetic drug carrier that will respond to an external AMF-stimulus to cause magnetic hyperthermia-triggered drug release. Thus, the key innovation over existing carriers is vehicle simplification — no thermo-responsive materials will be incorporated.



## 4.2. Results and Discussion

### Development of magnetic carriers

We have chosen the potent, anti-cancer drug doxorubicin (Dox, Figure 4.2) as our model drug. Dox is an anthracycline antibiotic that consists of an aglycone, hydroxylated quinone, and daunosamine sugar residue. Dox is a leading anti-cancer drug because of its potent and broad spectrum of activity against diverse types of cancer.<sup>176</sup> However, the efficacy of Dox treatments are severely impeded due to its significant cardiotoxicity<sup>177, 178</sup> and nephrotoxicity.<sup>179</sup>

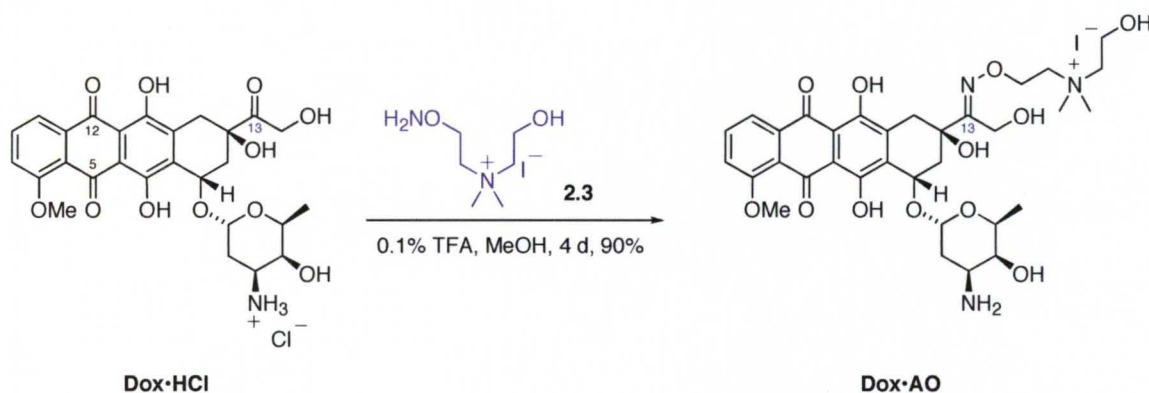


**Scheme 4.1.** Stepwise loading of Dox on the NP.

To achieve our goal we strategized three routes to load Dox onto the  $\text{Fe}_3\text{O}_4$  NP surface. As learned from our MLP/dMLP-mediated gene delivery program, we first devised a stepwise loading of Dox onto the NP surface. In this route (Scheme 4.1), we first coated the NPs with the quaternary ammonium aminoxy reagent **2.3** to synthesize **NP•AO** by simple mixing of the NPs with excess **2.3** (ca. 3.5 wt. equivalents). Absorption of charged ligands on nanoparticle surfaces are well known in the literature.<sup>180, 181, 182</sup> Recently Berret *et al.*<sup>183</sup> demonstrated that negatively charged  $\gamma\text{-Fe}_2\text{O}_3$  nanoparticles can be coated and consequently stabilized using block copolymers containing a cationic quaternary ammonium group. The mechanism is

based on electrostatic attraction between the oppositely charged entities. Alcoholic hydroxyl groups are also well known for stabilizing iron oxide nanoparticles, e.g., dextran coated nanoparticles are well characterized and even commercially available.

We hypothesize that the positive charge of the cationic aminoxy reagent as well as its hydroxyl groups are responsible for the efficient surface coating, specially since the NPs are negatively charged ( $\zeta$ -potential = -30 mV).  $\zeta$ -potential measurement of **NP•AO** revealed that particles were partially neutralized at -19 mV. We demonstrated previously (Chapter 2) that cationic aminoxy reagents can be used as surface modifiers of NPs and that the aminoxy groups are available for ligation applications. The presence of **2.3** at the NP surface provides aminoxy moieties for

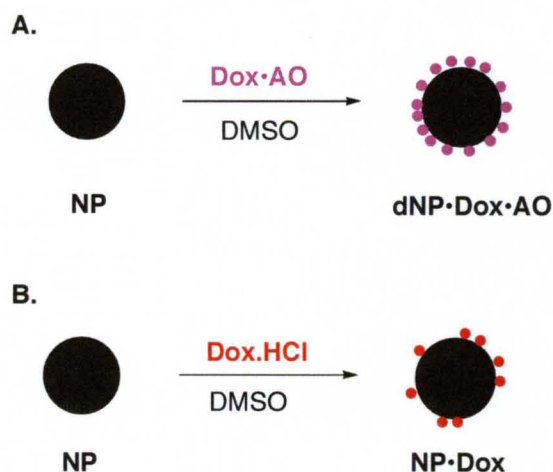


**Scheme 4.2.** Synthesis of Dox•AO.

subsequent conjugation of Dox via an oximation reaction to yield sNP•AO•Dox (Scheme 4.1). Dox has multiple carbonyl groups for reaction with aminoxy functionality.

The fact that cationic oxime ether lipids tend to bind well to our NPs (Chapter 2), inspired us to devise our second formulation route. We first synthesized a novel cationic oxime ether conjugate of Dox at the C-13 ketone position (**Dox•AO**, Scheme

4.2). To synthesize **Dox•AO** we modified the method described for synthesizing a Dox-maleimide conjugate at C-13 position as described by Krüger *et al.*<sup>184</sup> In brief, **2.3** and Dox were reacted in 0.1% trifluoro acetic acid in anhydrous methanol for 96 h at room temperature under nitrogen. The solvent was evaporated and **Dox•AO** was purified via recrystallization from hot acetonitrile. **Dox•AO** was characterized by <sup>1</sup>H NMR, <sup>13</sup>C NMR and HRMS. <sup>13</sup>C NMR spectroscopy revealed that oximation had occurred at C-13 as expected. The <sup>13</sup>C NMR chemical shift of C-13 changed from



**Scheme 4.3.** Preparation of Dox loaded magnetic nanoparticle formulations. **A.** Direct loading of Dox•AO. **B.** Only Dox. loading.

213.2 ppm in Dox•HCl to 162.6 ppm in the conjugate. In contrast, the <sup>13</sup>C NMR chemical shifts of the quinone carbonyl carbons (C-12 and C-5) were essentially unchanged (Figure 4.3). The two extra signals between 50 and 55 ppm and three extra signals between 60 and 70 ppm (Figure 4.3) correspond to the added carbons of **2.3**. Also, chemical shift of alpha carbon to the amine group of the Dox•HCl and **Dox•AO** remain essentially unchanged. HRMS analysis revealed the existence of  $M/z = 1$  species. After synthesizing **Dox•AO**, we loaded this cationic analog onto

the NPs directly (Scheme 4.3A) to furnish **dNP•AO•Dox**. Reaction of **NP** and **Dox•AO** in DMSO at room temperature for 12 h, followed by two magnetic separations provided **dNP•AO•Dox**. After the first magnetic separation, the isolated NPs were washed with methanol, and after the second wash we did not observe any red colored supernatant indicative of free Dox-conjugate.

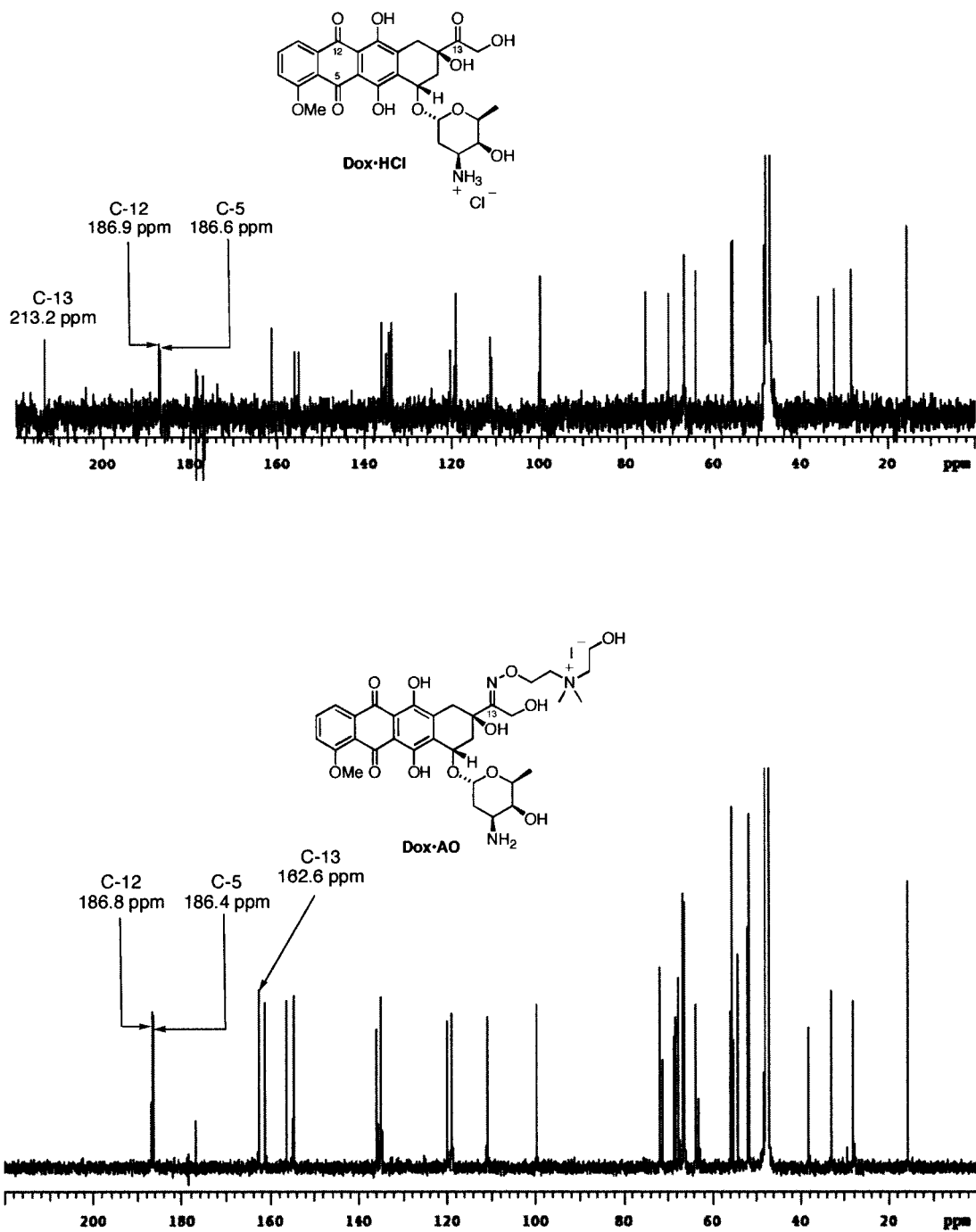


**Figure 4.3.** Comparison of the  $^{13}\text{C}$  NMR spectra of Dox•HCl and Dox•AO in  $\text{CD}_3\text{OD}$ .

The fact that Dox•HCl (Figure 4.1) is a hydrochloride salt and has a sugar moiety encouraged us to examine a third strategy, the preparation of NP•Dox (Scheme 4.3B).

We loaded Dox•HCl directly onto NPs assuming that the innate charge attraction, and hydrogen bonding would be sufficient to keep Dox associated with the NPs.

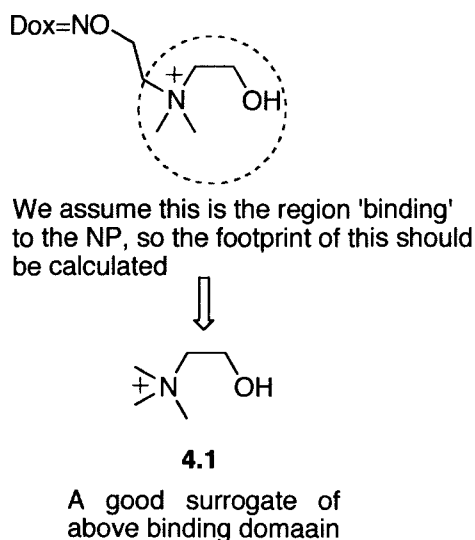


**Figure 4.4.** Possible binding domain of Dox•AO.

In each of the NP functionalization steps we purified and isolated end-functionalized particles by employing a magnetic separation technique that involved a methanol washing followed by another magnetic separation. The collected supernatant that contained un-separated drug-loaded NP colloids were centrifuged at 10000 rpm (4 °C for 15 min) to purify from unreacted **Dox•AO** and resultant NP-pellet was mixed with magnetically separated NPs. The dry weight of purified (i.e., multiple washed) drug-loaded formulation provided the loading efficiencies. The direct formulation (**dNP•AO•Dox**) showed maximum loading efficiency (~ 0.37

$\mu\text{mol}/\text{mg}$  NP). A considerable amount of conjugate was also associated with the NPs using the stepwise method ( $\sim 0.3 \mu\text{mol}/\text{mg}$  NP, Table 4.1). The **NP•Dox** formulation also indicated loading of Dox onto NP surface ( $\sim 0.15 \mu\text{mol}/\text{mg}$  NP, Table 4.1). Loading calculation revealed that nearly 580 **Dox•AO** molecules/NP. Loading calculation revealed  $\sim 580$  **Dox•AO** molecules/NP. A footprint calculation of **Dox•AO** (number of molecules/ NP surface area), assuming the ammonium ion head group binds to the NP surface, (Figure 4.4) revealed that approximately 1450 **Dox•AO** molecules can be attached to the NP surface. We hypothesize that the Dox molecules likely are not lying flat on the particle surface, but actually are attached to the surface via the polar linker groups (Figure 4.4). Thus, we calculated the footprint using surface area of a close surrogate **4.1** (Figure 4.4) of binding moiety of **Dox•AO**. Since the aminoxy domain is smaller than the Dox molecule, more drug molecules are predicted to be bound to the NP surface. This accounts in part for the smaller quantity of Dox that was measured in the **NP•Dox** formulation relative to the **NP•AO•Dox** formulations.

## Zeta potential measurements

We performed zeta ( $\zeta$ ) potential measurements to evaluate the surface charge of the Dox-loaded nano-magnetic drug carriers (Table 4.1). Surface potential of **sNP•AO•Dox** was increased to slightly positive (+3 mV) from -27 mV (NP surface potential) and it became moderately positive in **dNP•AO•Dox** to +17 mV (Table 4.1). Dox•HCl attachment onto the NP surface also partially neutralized the NP surface

Formulation	Zeta potential (mV)	Average loading $\mu$ mol/mg NP	Average loading (no. of drug conjugate molecules/NP)	Loading footprint: no. of drug molecules/NP surface area
NP	-27 $\pm$ 1.7	—	—	—
NP•Dox	-20 $\pm$ 2.3	0.15	235	587
sNP•AO•Dox	3 $\pm$ 2.1	0.3	470	1175
dNP•AO•Dox	17.1 $\pm$ 3.1	0.37	580	1450

**Table 4.1.** Zeta potential of NPs and drug loaded NPs (concentration: 0.3 mg NP/mL PBS, n=3); and average loading of Dox as determined by weight differentials.

potential to -20 mV. Charge neutralization of NPs indicated better attachment of cationic oxime ether Dox analog to the negatively charged NP surface.

## AMF-induced NP heating

Next we evaluated the AMF-stimulated heating of our NP-drug formulations. Local temperature of surrounding media containing NP-formulation suspension increased when **dNP•AO•Dox** (2.5 mg/ mL NP by wt.) was subjected to an external AMF (EasyHeat, Amritherm; frequency: 203 kHz, power: 350 A, 5 turn coil with 5 cm ID) for 18 min. The AMF parameters were chosen by noting previously reported magnetic NP-derived hyperthermia-induced drug delivery demonstrations. Brulé *et al.*<sup>86</sup> applied 700 kHz frequency to release Dox from an alginate-based magnetic microsphere. Zink and coworkers demonstrated cargo release from magnetic carriers



using an AMF applicator at 500 kHz.<sup>185</sup> Importantly, frequencies greater than 400 kHz are known to cause nonspecific heating in tissue.<sup>186</sup> Finally, Jordon *et al.*<sup>187</sup> Reported achieving intracellular hyperthermia in humans using a 100 kHz AMF frequency.

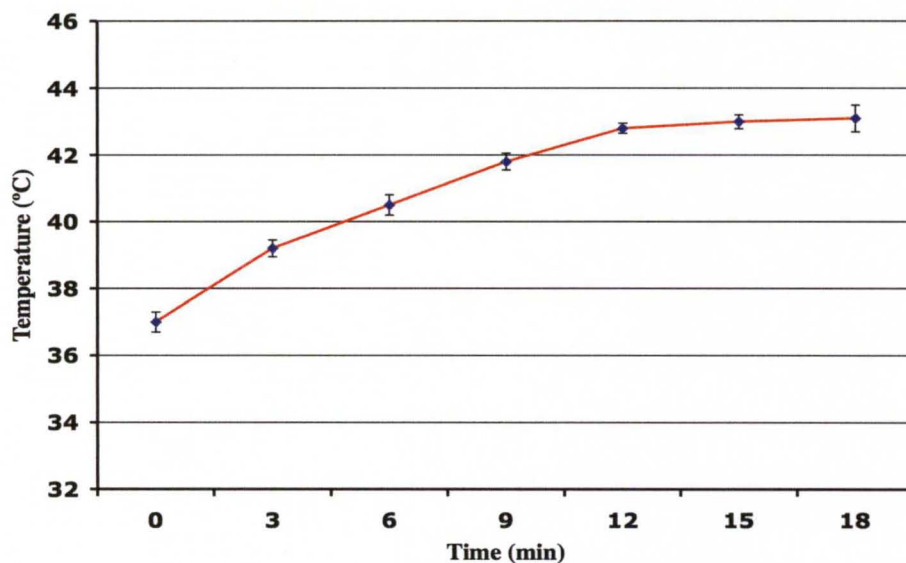


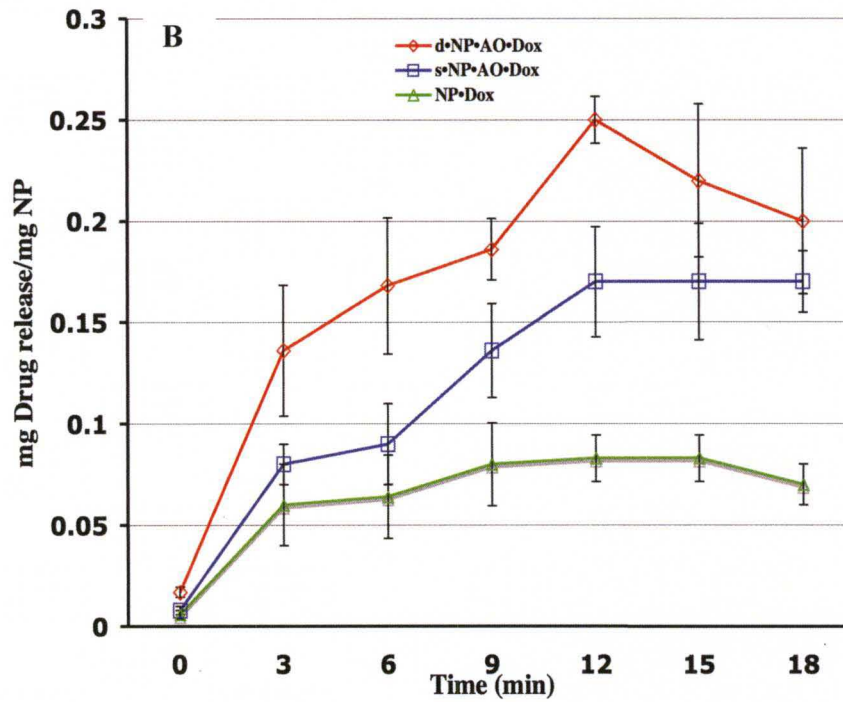
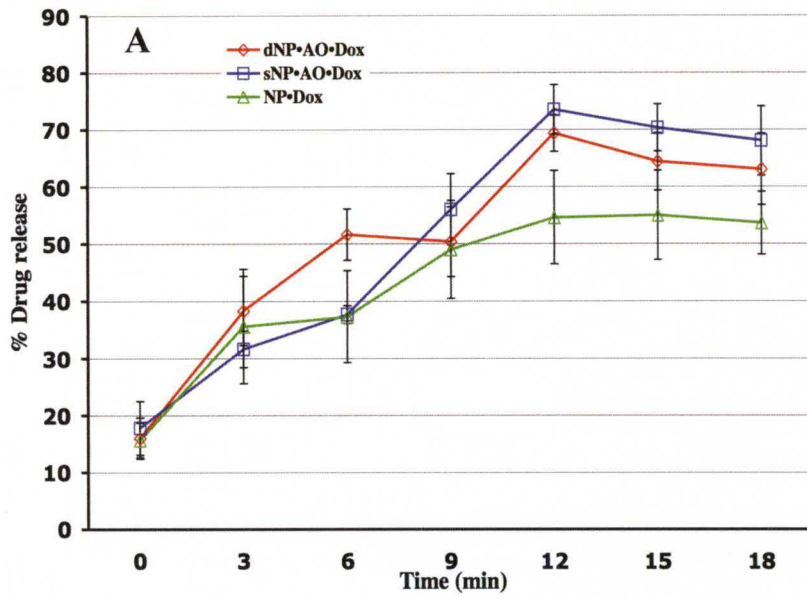
**Figure 4.5.** AMF-induced hyperthermia of dNP•AO•Dox in PBS (2.5 mg NP by wt.)/mL. Temperature of the surrounding solution was measured every 3 min using a fiber optic temperature probe. n = 3.

With above demonstration, we decided to use an intermediate frequency of 200 kHz that can be generated readily using our 5-turn coil AMF applicator. The power (350 A) was automatically set for this frequency. AMF-induction was started after temperature of the medium reached at 37.0 °C and the temperature of the surrounding solution was measured at every 3 min using an optical fiber temperature probe (Neoptix Inc., Québec, Canada). Our studies showed that the thermal energy generated by the NP formulation on AMF-exposure elevated the solution temperature from 37 °C to ~43 °C within 12 mins. Little change occurred on continued AMF-exposure (Figure 4.5).

### **AMF-induced Dox release**

Drug release studies using our NP formulations were performed following the same AMF parameters as mentioned above. The Dox conjugate release study was performed according to methods described in papers published by Brulé<sup>175</sup> and Luo *et al.*<sup>188</sup> Dox release was estimated every 3 min using a UV-spectrophotometer measurements taken at 480 nm. 480 nm is the Dox absorbance of the quinone system. Every 3 min 10 µL of supernatant was aliquoted and diluted to 1 mL for spectrometric reading.

We observed that an AMF-stimuli considerably increases Dox or Dox-conjugate release from the magnetic carriers (Figure 4.6A) than what was released by mere incubation at 37.5 °C. Both the **dNP•AO•Dox** and **dNP•AO•Dox** formulations released ~65% of their payload by 12 mins of AMF induction. The **NP•Dox** formulation released ~55% of cargo at the same point of time (Figure 4.6A, green line). Although **s/dNP•AO•Dox** released same average % of drug conjugate, they released different amounts of drug since the loadings differed (Figure 4.6B). According to our observations, no substantial drug release was detected at 37.5 °C from the carrier (Figure 4.6C). It is evident from AMF-induced NP heating and drug release studies that maximum average local temperature of 43 °C can be achieved at 12<sup>th</sup> mins, and this duration of AMF-exposure can trigger ~65% of cargo release from the nano-magnetic vehicles. We also predicted that these NP formulations would not exhibit cytotoxicity due to their lack of their at 37 °C, and thus the formulations might well function as ‘prodrug’.



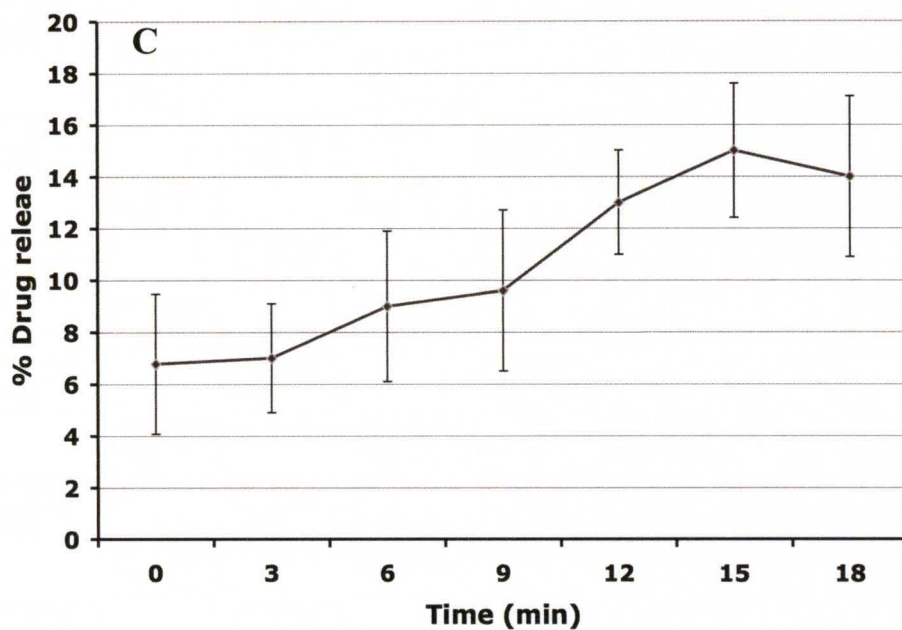


**Figure 4.6.** Drug release profile. **A.** % of AMF-induced Dox and Dox•AO. Drug release was calculated every 3 min using UV-spectrophotometer measurements taken at 480 nm. Every 3 min, 10  $\mu$ L of supernatant was removed and diluted to 1 mL for spectrometric measurement (n = 3). **B.** mg of Dox released per mg of NP during AMF-stimulation (n = 3). **C.** Drug release at 37.5  $^{\circ}$ C; no AMF-induction (n = 3)

## Cytotoxicity studies

Encouraged by our AMF-promoted NP heating and drug release studies we set out to investigate AMF-induced cytotoxicity of the NP formulations in a breast cancer cell line (MCF-7). MCF-7 cells plated in a 30 mm dish at  $4 \times 10^5$  cells/ dish were grown to 50-60% confluence. After treatments with varying amounts of the NP formulations (0.25 mg, 0.5 mg and 0.75 mg NPs./ dish), the cells were incubated for 1 h at 37.5 °C before exposure to the AMF. Dishes containing cells treated with NP•drug formulations and untreated (control) were placed at the center of the



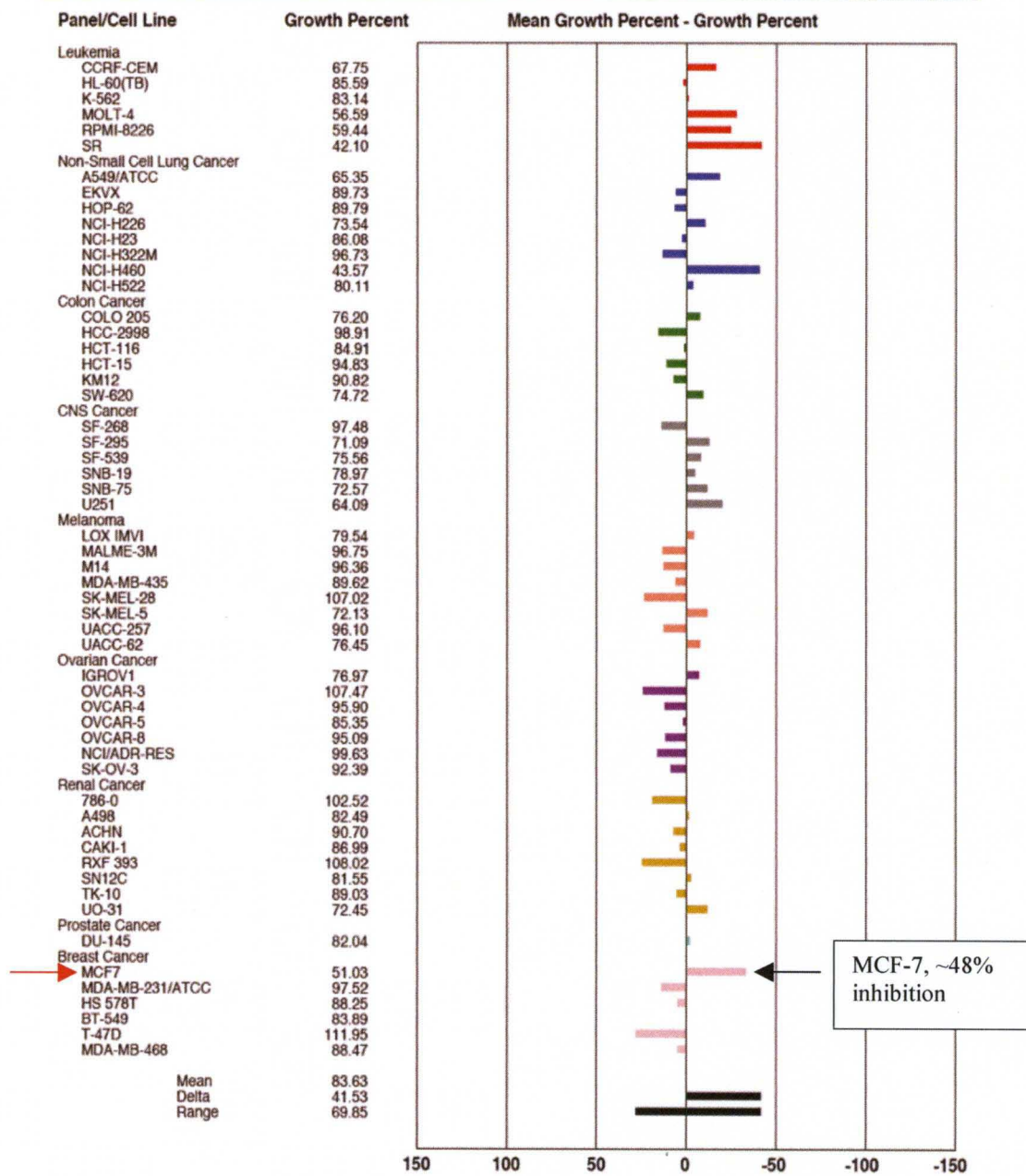
**Figure 4.7.** AMF generator: EasyHeat, Ameritherm, NY.

induction heater coil (Figure 4.7). Each dish was then subjected to an AMF for 15 min using the same parameters as described above. Cells treated with Dox (0.5  $\mu$ mol) and **Dox•AO** (0.5  $\mu$ mol) served as positive controls.

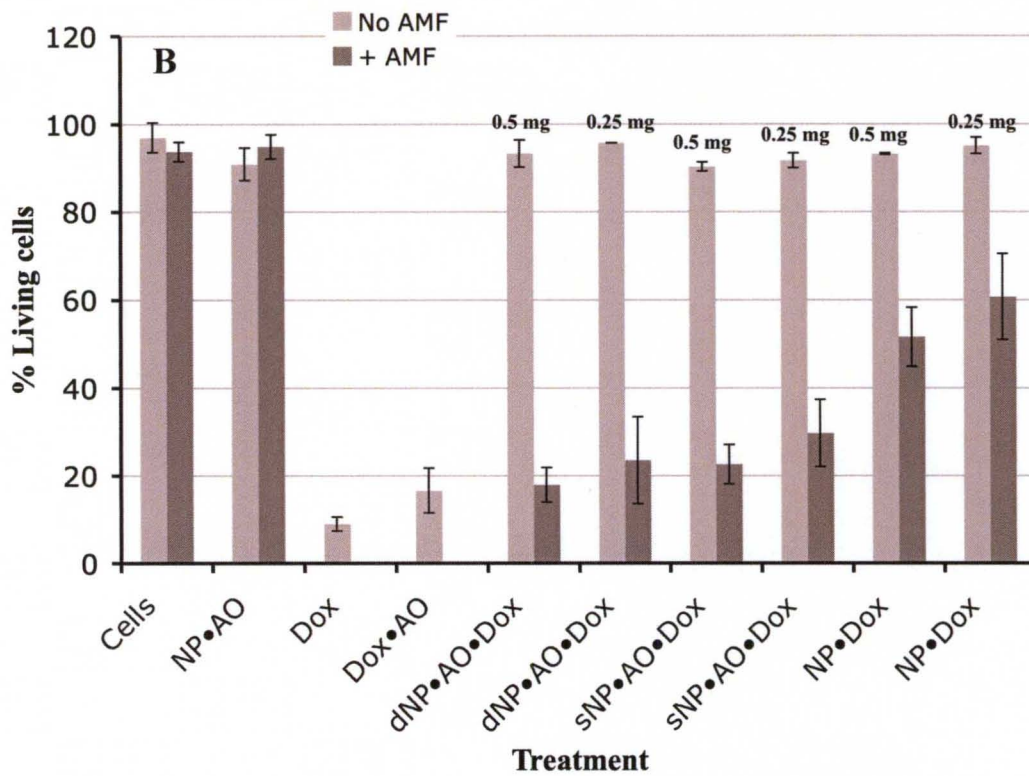
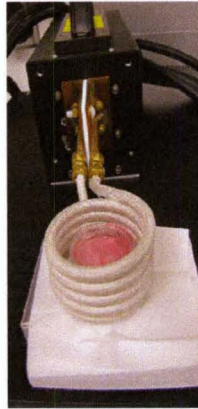
As determined by the assay using the National Cancer Institute (Frederick, MD) 60-cancer cell line screen, we found that **Dox•AO** was cytotoxic towards MCF-7 cells (Figure 4.8 and Figure 4.9B). In regards to the other control experiments, cells treated with NP formulations were incubated at 37.5 °C for 48 h to evaluate the

cytotoxicity in the absence of AMF-exposure. We did not observe any abnormal behavior of the untreated cells towards AMF induction (Figure 4.9B). Also, aminoxy coated NPs (**NP•AO**) were found to be nontoxic and surprisingly showed no cytotoxicity even in the presence of AMF-exposure. Our studies indicated that none of the NP-based Dox formulations (**s/dNP•AO•Dox** or **NP•Dox**) were cytotoxic in the *absence of AMF-exposure*; however all the NP formulations displayed significant cytotoxicity upon AMF treatment (Figure 4.9B). We found that the 0.5 mg dose (NP by wt.) was the most effective dose for AMF-induced cell death. Cells treated with same amount of **s/dNP•AO•Dox** (NP by wt.) and exposed to an AMF showed different levels of cytotoxicity. With AMF-exposure cell viability decreased to ~15% when the cells were treated with **dNP•AO•Dox** at the 0.5 mg NP dose whereas cell viability decreased to ~27% when cells were treated with **sNP•AO•Dox** at the same dose. As discussed previously, **dNP•AO•Dox** has more conjugate (in terms of mg) loaded on the NP surface than stepwise formulation, which in turn released more conjugate on AMF-irradiation. Releasing more drug-conjugate from **dNP•AO•Dox** than **sNP•AO•Dox** makes **dNP•NP•Dox** more cytotoxic in the presence of AMF-induction. We also hypothesized that the higher positive  $\zeta$ -potential of the **dNP•AO•Dox** promoted its cellular internalization. The **NP•Dox** formulation was also active and demonstrated ~50% cell inhibition when stimulated by AMF (Figure 4.9B). The 0.75 mg NP dose showed aggregation in the cellular media and was not evaluated further.

Developmental Therapeutics Program One Dose Mean Graph	NSC: D-755124 / 1	Conc: 1.00E-5 Molar	Test Date: Dec 13, 2010
	Experiment ID: 1012OS71		Report Date: Jan 13, 2011



**Figure 4.8.** NCI 60-cancer cell line screen of **Dox•AO** (We thank Dr. Paul Grothaus (NCI) for assistance with these data).

**A**

**Figure 4.9.** AMF-induced cytotoxicity in MCF-7 cells. **A.** Experimental setup of AMF-induced drug release in MCF-cells; cells were plated in 30 mm dish. **B.** Cell viability; Control groups (cells treated with NP formulations but no AMF-induction) were incubated at 37.5 °C for 48 h. NP formulation treated cells and only cells were induced by AMF for 15 min with same parameter as before. 0.5 and 0.25 mg formulation (NP by wt.)/ dish was added to cells; 0.5  $\mu$ mol of Dox and Dox•AO were positive controls. Cell viability was evaluated after 48 h of treatment using trypan blue assay.



Finally we monitored Dox and **Dox•AO** release in the MCF-7 cells pre-AMF and post-AMF exposure using fluorescence microscopy (EVOS, Advanced Microscopy Group, WA). Dox is easily observed using fluorescence microscopy due its red fluorescent color and it appears as a bright red signal. Figure 4.10B shows the fluorescence image of MCF-7 cells treated with Dox. Figure 4.10C suggests there is no Dox release from NP•Dox before AMF-treatment. As clear from Figure 4.10D, AMF exposure triggers Dox release from the magnetic vector.

Very interestingly, when the above experiment was performed using **dNP•AO•Dox** we did not observe any indication of **Dox/Dox•AO** release in the cells (Figure 4.10E) post-AMF treatment, but significant cell death occurred suggesting release had occurred. This incident of fluorescent quenching was also observed when cells were treated with only **Dox•AO** (Figure 4.10F). We explain this phenomenon by hypothesizing that **Dox•AO** binds its intracellular target DNA more effectively than Dox,<sup>189, 190</sup> which ultimately quenches the fluorescence of **Dox•AO** more effectively. The fluorescence quenching is not due to the formation of the cationic oxime ether linkage. The fluorescence intensity of both Dox and **Dox•AO** at the same concentration is similar (Figure 4.11). Our results indicated that fluorescence intensity was same for Dox and **Dox•AO** (Figure 4.11). Further more, when we analyzed the supernatant from AMF-induced **dNP•AO•Dox** using HRMS, data indicated the presence of only **Dox•AO** (M/z=2).

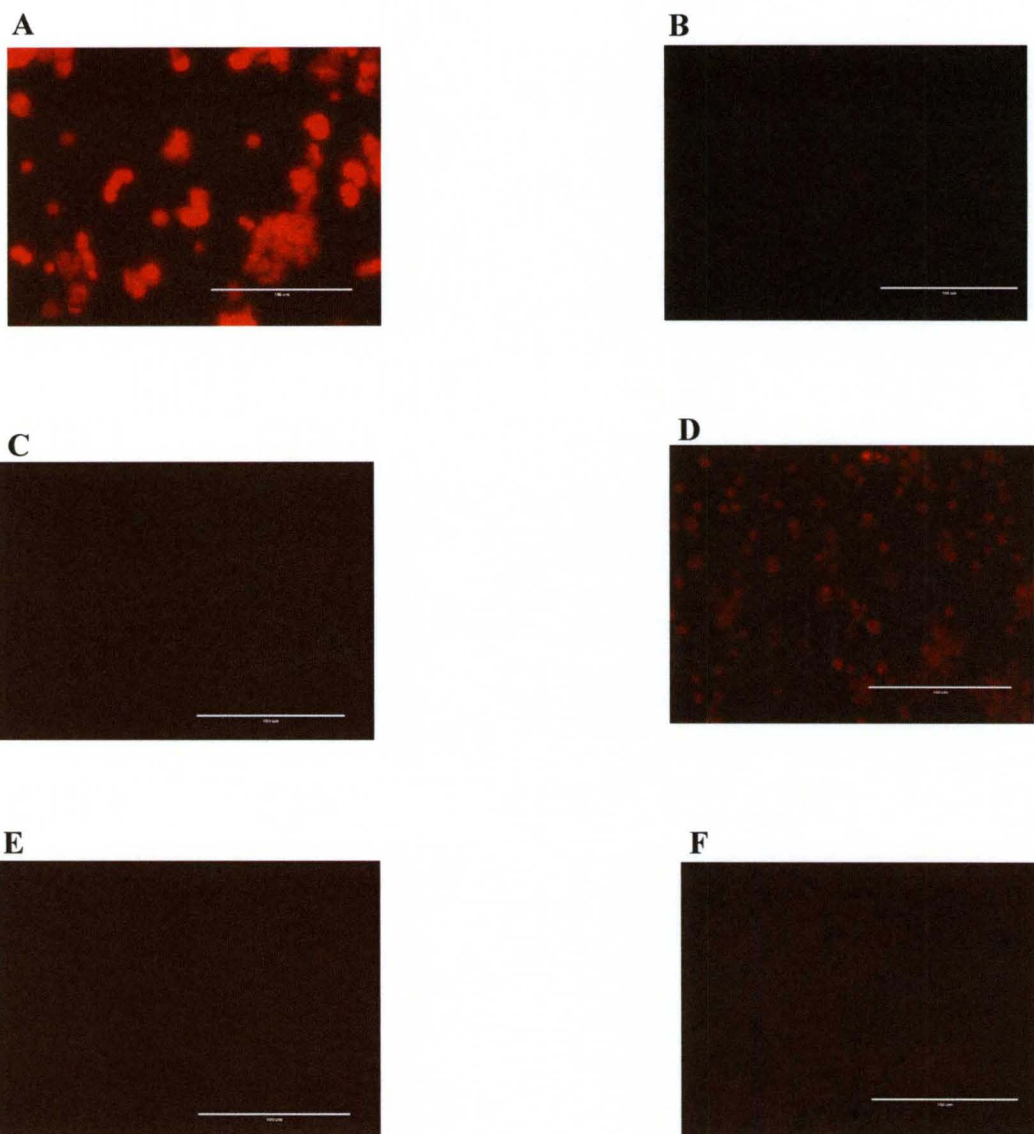


**Figure 4.10.** Fluorescence images of MCF-7 cells. A. Cells treated with Dox. B. Cells treated with Dox•AO. C. Cells treated with NP•Dox (No AMF). D. Post-AMF treated with Np•Dox. E. Cells treated with dNP•AO•Dox (0.5 mg NP by wt., No AMF). F. Post-AMF treated with dNP•AO•Dox (0.5 mg NP by wt.). 0.5  $\mu$ mol of Dox and Dox•AO was added to the cells. Fluorescence images were taken after 6h of treatment using a fluorescence microscopy (ex/em = 480/590 nm)

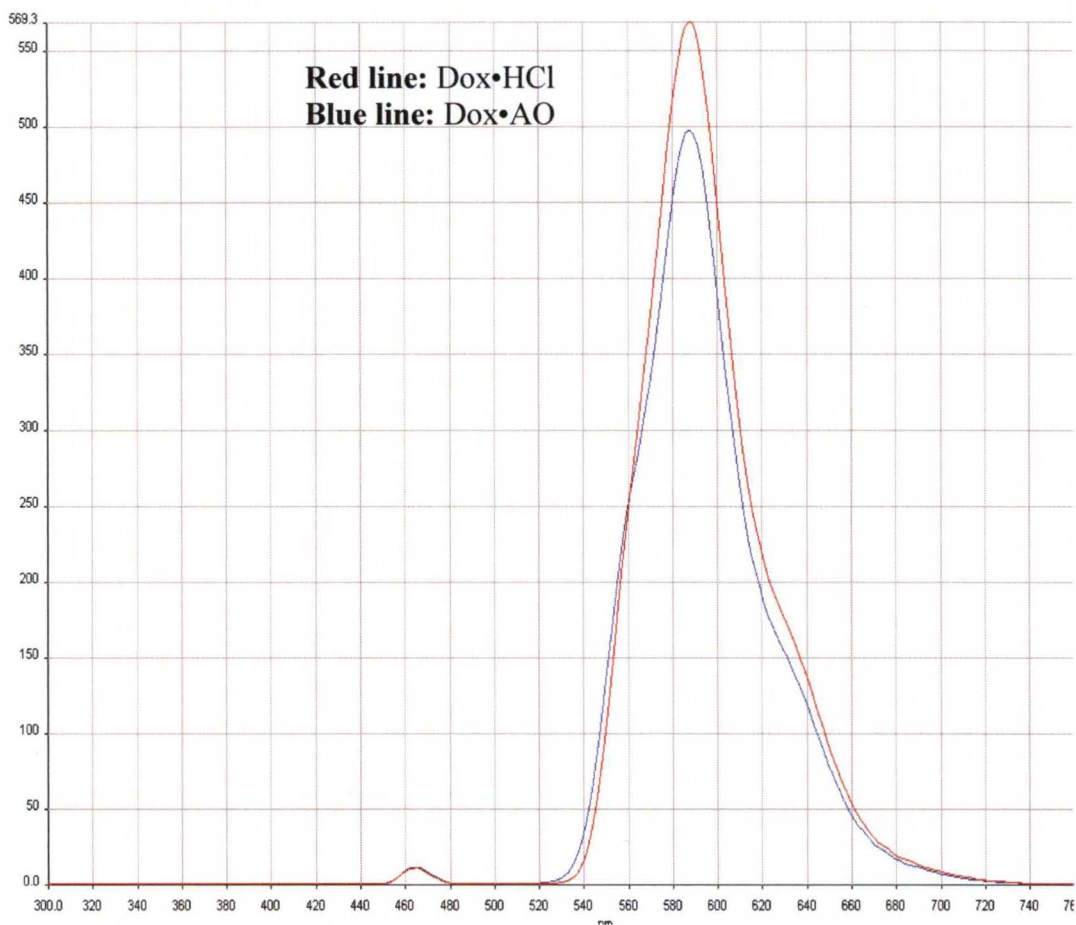


**Figure 4.11.** Fluorescence spectra of Dox•HCl and Dox•AO (1 mmol in methanol). Y-axis: fluorescent intensity and X-axis: wave length (nm).

We performed a fluorescence measurement of the **NP•Dox** formulation. After synthesizing **NP•Dox**, fluorescence activity was measured in ethanol using a fluorescence plate. The fluorescence intensity of **NP•Dox** was 41% less than the fluorescent intensity measured for free Dox•HCl (Figure 4.12). We hypothesize that the reduction is in part due to the spherical nature of particles, and one would expect the edges of the sphere would receive less excitation than the face directly positional toward the excitation signal.

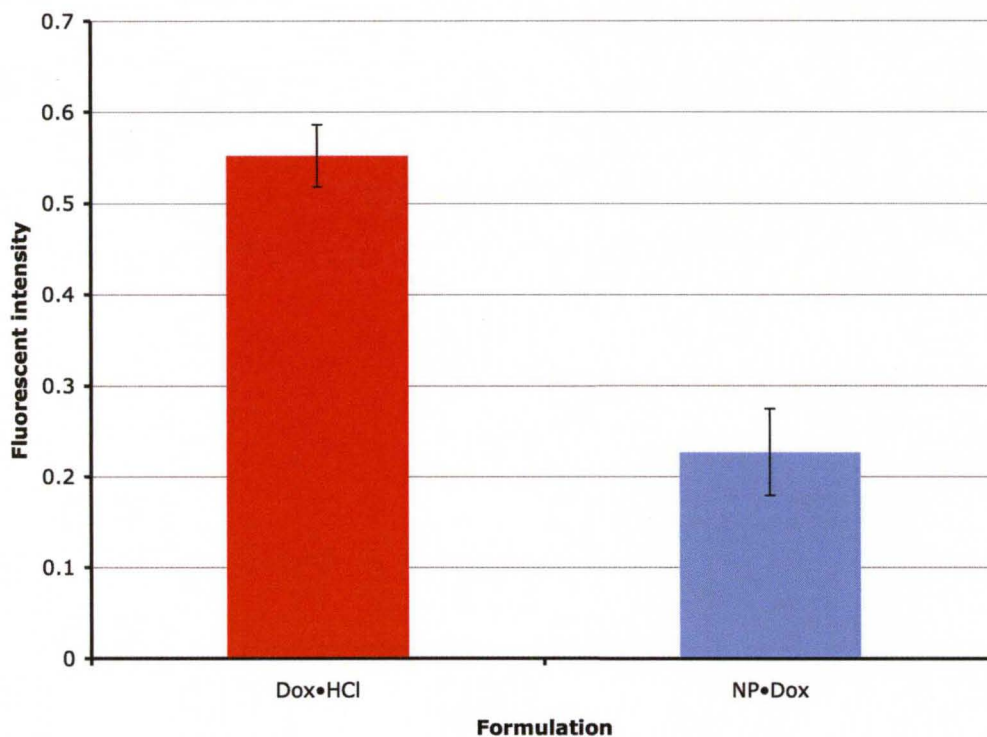


**Figure 4.12.** Fluorescence intensity of Dox and NP•Dox. 1 mmol/L Dox in ethanol.

### 4.3. Conclusion and future directions

We developed a binary (NP + pharmaceutically active coating) external stimuli-responsive magnetic drug delivery system in which a drug conjugate is loaded onto NPs via simple electrostatic attraction and hydrogen bonding. Subsequent AMF exposure breaks the electrostatic attraction forces as the NPs heat, thus constituting a stimuli-responsive drug release. The temperature of NP surface is high enough (> 43 °C) to promote ammonium drug conjugate release from NP surface.<sup>191</sup> This binary nano-platform does not depend on a third variable, e.g., structural change of polymer due to NP heating for cargo release.

We demonstrated that the cationic oxime ether analog of doxorubicin can be attached to Fe<sub>3</sub>O<sub>4</sub> NPs via simple mixing. The loaded NP formulations are nontoxic to cells. However, on application of an AMF, the Dox payload released from the particles. The magnetic nanoparticle delivery system was functionally demonstrated using MCF-7 cells and shown to be effective when the external AMF stimulus was applied. Our AMF-applicator parameters are well within the safe range for treatment of mammals as described previously and in present<sup>189</sup> clinical trials of magnetic hyperthermia.

The future of our magnetic delivery system largely depends on animal studies. Effect of various oxime ether drug-conjugates (e.g.; one, two, or three hydrooxy ethyl groups on cationic aminoxy reagents) on drug loading and release will be performed in near future. The effect of AMF-applicator parameters on NP heating also remained to be optimized in near future, as the focus of the research shifts to animal studies.

## **CHAPTER 5**

### **BIOANALYTICAL APPLICATIONS OF CATIONIC AMINOOXY REAGENTS**

---

**5.1. Introduction**

**5.2. Results and Discussion**

**5.3. Conclusion**

---

## 5.1. Introduction

This chapter describes my contributions to a collaborative bioengineering project focused on the development of a microchip-based human breath analyzer for detection of volatile organic compounds (VOCs). The project is a collaboration among three research groups, those of Professors Nantz and Higashi (Chemistry) and Fu (Chemical Engineering). Although this project is not directly related to my thesis focus of drug delivery, the research does exploit the cationic aminoxy compounds described earlier.

The microreactor fabrication, functionalization, and breath analyses were performed by Dr. Xian Fu and his graduate student Mingxiao Li (Chemical Engineering, University of Louisville).

Analysis of exhaled breath has become an important research arena because of its potential and applicability in noninvasive health diagnosis, metabolite bioinformatics, and drug discovery.<sup>192, 193, 194, 195, 196</sup> The gaseous portion of breath is a complex mixture of atmospheric gases, water vapor, and trace volatile organic compounds (VOCs). In 1971, Pauling reported the first gas-chromatographic analysis of breath, and the study revealed the presence of a large number of VOCs in human breath.<sup>197</sup> A number of recent publications<sup>198, 199, 200, 201</sup> suggest that the analysis of exhaled breath promises to be a non-invasive diagnosis for early detection of particulate cancers since some VOCs in exhaled breath represent metabolic output of cancer tissues and cells.

One of the most critical challenges for the analysis of VOCs in exhaled breath is ultra-trace concentrations of VOCs and interference of complex gas mixtures.

Exhaled breath contains more than 200 VOCs. Recently, several reports indicate that some ketones and aldehydes in exhaled breath could be used for the diagnosis of lung cancer at an early stage.<sup>195, 196</sup>

Carbonyl metabolites are produced in biochemical pathways as intermediates and some can be unique to a given pathway or process. However, even common carbonyl metabolites can be attributed to specific processes when stable isotope labeled substrates are metabolized (e.g. by human subjects) and detected by mass spectrometry or NMR.<sup>202, 203</sup> Volatile ketones and aldehydes are also generated from damaging oxidative reactions, such as lipid peroxidation.<sup>204, 205</sup> Therefore, development of a new method for analysis of ketone and aldehyde VOCs in exhaled breath has a tremendous potential to fulfill the breath analysis promises.

Ketones and aldehydes can be detected by proton transfer reaction mass spectrometry (PTR-MS),<sup>206, 207, 208</sup> or selected ion flow tube mass spectrometry (SIFT-MS) without any preconcentration process.<sup>209, 210</sup> Most recently, solid phase microextraction (SPME) with adsorbed *O*-2,3,4,5,6-(pentafluorobenzyl)hydroxylamine hydrochloride (PFBHA) has been used for analysis of aldehydes in exhaled breath by gas chromatography-mass spectrometry (GC-MS).<sup>195, 196</sup> SPME is a popular preconcentration method introduced a decade ago as a rapid extraction technique for analysis of volatile compounds from a variety of matrices.<sup>211</sup> However, the smaller surface area of the SPME polymer extraction phase and physical adsorption of aldehyde PFBHA onto SPME for its capture makes it is also extremely difficult to improve upon, or even determine the volume of air that is actually sampled by the SPME fiber. The quality of the fibers depends on the



manufacturer, and the performance varies from batch to batch. Derivatization of ketones and aldehydes by reaction with 2,4-dinitrophenylhydrazine has also been used for analysis of carbonyl compounds in exhaled breath,<sup>212</sup> which has the advantage of converting volatile aldehydes and ketones into stable, easy-to-handle non-volatile analytes. However, this class of reagents was not designed to aid in detection by modern ultra-sensitive ion sources such as nanoelectrospray FT-ICR-MS.

To address the above stated problems, we aspired to design a breath analyzer based on a microreactor approach to capture gaseous ketones and aldehydes from exhaled breath using a chemoselective oximation technique.

## 5.2. Results and Discussion

### Proof of concept

To engineer a breath analyzer silica microchip-based aminoxy loaded, we first designed a simple bench top proof-of-concept experiment, wherein silica gel (1.5 g) was first loaded with cationic bis-aminoxy reagent **2.2** (35 mg, 0.12 mmole) in 1:5 MeOH:dichloromethane (steps **a** and **b**; Scheme 5.1). An ampoule of acetone- $d_6$  (1 mL) was placed inside of the RB containing dried silica gel coated with quaternary aminoxy salt **2.2** and then RB was sealed to protect the functionalized silica gel from laboratory ambient acetone (or other vapors containing ketones or aldehydes). After 18 h, the acetone- $d_6$  ampoule was removed and silica was analyzed

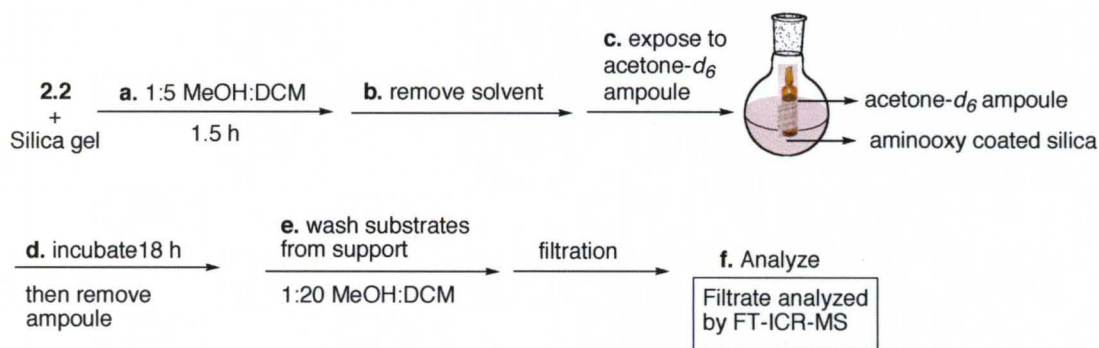


**Figure 5.1.** Schematic diagram of acetone- $d_6$  capture.

for adducts by first eluting all materials from silica (stage **e** and **f**, Scheme 5.1) and then analyzed by FT-ICR-MS. MS analysis revealed that the aminoxy-coated silica gel indeed captured acetone- $d_6$  vapor efficiently (Figure 5.2).

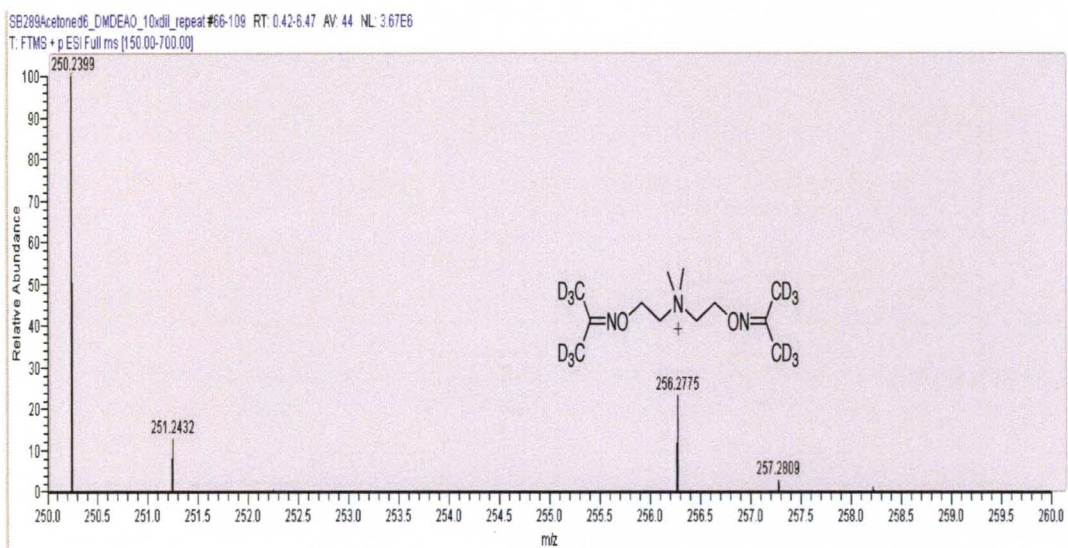


**Figure 5.2.** FT-ICR-MS spectrum of eluted aminioxy-acetone- $d_6$  adduct.

## Microreactor design

With this result in hand, Dr. Xian Fu's research group prepared a microreactor fabricated on 4 inch-silicon wafer using standard microelectro-mechanical systems (MEMS) fabrication technology.<sup>213</sup> Figure 5.3 shows an optical micrograph of the fabricated microreactor. The fabricated microreactor is the size of a penny (Figure 5.3B).

The micropillars have high-aspect-ratio with dimensions of  $50\ \mu\text{m} \times 50\ \mu\text{m} \times 250\ \mu\text{m}$  created by dry reactive ion etching silicon. The distances from center to center of the micropillars are  $100\ \mu\text{m}$ . The flow channel size is  $7\ \text{mm} \times 5\ \text{mm}$ . The

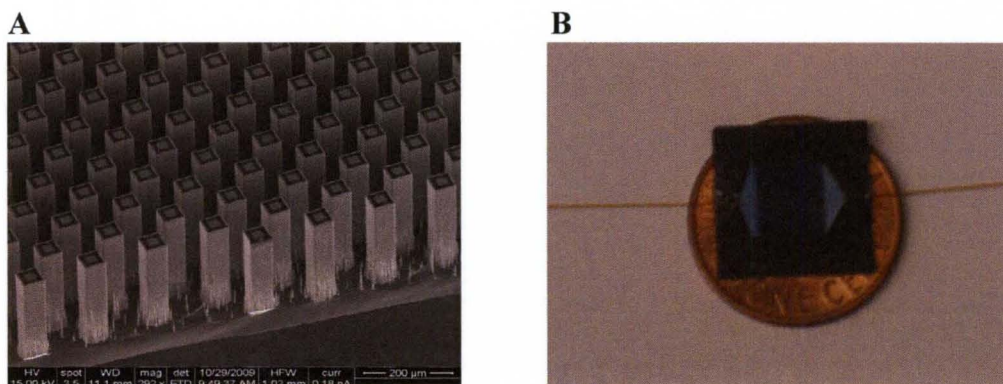


**Figure 5.3.** A. Optical micrograph of a fabricated microreactor with thousands internal micropillars. B. Fabricated micropillar on a silicon wafer.

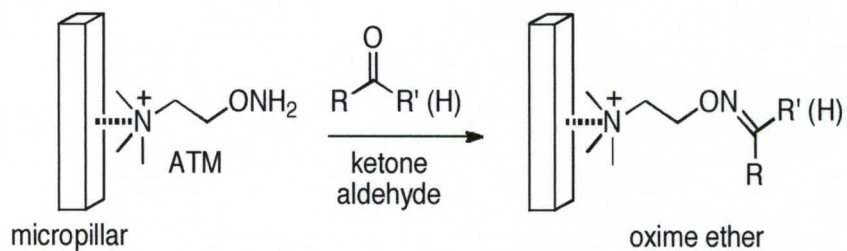
total empty space in the microreactor is about  $5\ \mu\text{L}$ . There are more than five thousand square micropillars within the microreactor corresponding to a total micropillar surface area of about  $260\ \text{mm}^2$ . For introduction of the capture coating and eventual gaseous samples, the inlet and outlet of the microreactor were connected with  $190\ \text{mm}$  O.D.,  $100\ \text{mm}$  I.D. deactivated fused silica tubes using a silica-based bonding agent.

## Surface coating

The surface of the micropillars was functionalized using quaternary ammonium aminoxy salt **2.1**<sup>151</sup> (abbreviated as ATM in this collaboration) for chemospecific ketone or aldehyde capture (Scheme 5.1). The surface functionalization of the channels and micropillars by ATM ions was performed by infusing a known amount of the ATM iodide salt in methanol solution into the microreactor channel from one connection port followed by evaporation of the solvent under vacuum. The slightly negative surface charge of silicon oxide micropillars enforces the close association of ATM with the solid support, which is a benefit of including the quaternary ammonium group in the design.

## Capture efficiency

To test the capture efficiency of the microreactor, measured amounts of deuterated acetone, acetone or propanal in the microliter range or lower (diluted in



**Scheme 5.1.** ATM oximation traps ketones and aldehydes in the microreactor.

methanol) were injected into a high purity (99.9999%) helium gas flow stream passing through the microreactor. As illustrated in Scheme 5.1, the adsorbed ATM on the micropillars react with gaseous ketones and aldehydes via oximation to capture the analytes as oxime ether adducts.

Figure 5.4 shows the schematic test setup for preconcentration of ketones and aldehydes by the microreactor. In brief, various quantities of deuterated acetone, from 0.271 nmole to 0.271 mmole in methanol, were added to the 20 mL vial to evaporate into helium flowing through the vial and then the microreactor. The vial had a Teflon lined rubber septum connected to both helium source and the microreactor by the silica capillary tubing. Acetone- $d_6$  was used in these tests to

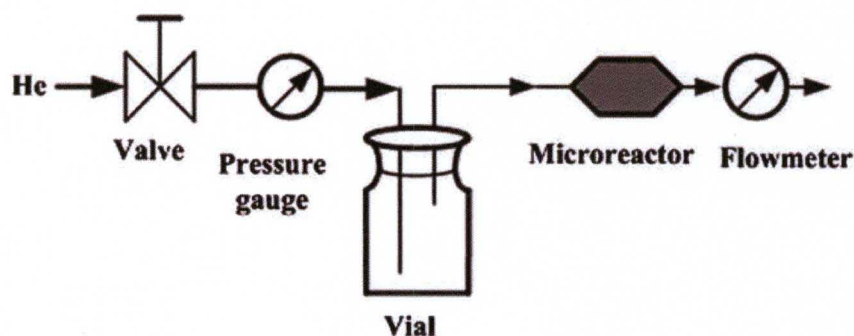


**Figure 5.4.** Schematic flow diagram of the preconcentration setup.

avoid bias from any environmental trace acetone contamination. The microreactor operated at an inlet helium pressure from 15 to 25 psi. The flow rate of helium through the microreactor was 2 to 5 mL/min. After addition of acetone- $d_6$  to the vial, helium flowed for at least 30 min to allow completion of the acetone- $d_6$  transfer into the microreactor. After preconcentration, the microreactor was disconnected from the setup. Then, the microreactor was eluted by flowing 10  $\mu$ L methanol portions through the microreactor into a septum-sealed glass vial; each aliquot was analyzed separately to gauge elution efficiency via mass balance. The collected elution solutions were directly analyzed by nanoelectrospray FT-ICR-MS for 5 min.

Figure 5.5A shows a typical FT-ICR-MS spectral region that has oximation product of ATM with acetone- $d_6$  (165.18688m/z ion) as well as unreacted ATM

cations (119.11793 m/z ion). Greater than 98% of total reacted ATM and unreacted ATM was collected from the microreactor with the first 10 mL methanol aliquot. There was no trace detectable ATM and ATM-acetone- $d_6$  after flushing a total 40  $\mu$ L methanol through the microreactor. Thus, the transfer efficiency exceeded 98% for a rapid 5 min, 10  $\mu$ L elution at the benchtop, requiring no specialized equipment other than septum-capped vials and a syringe. The total analytical recovery of the acetone- $d_6$  dosage was >98%. Figure 5.5A also indicates that trace acetone contamination from ambient air was very low.

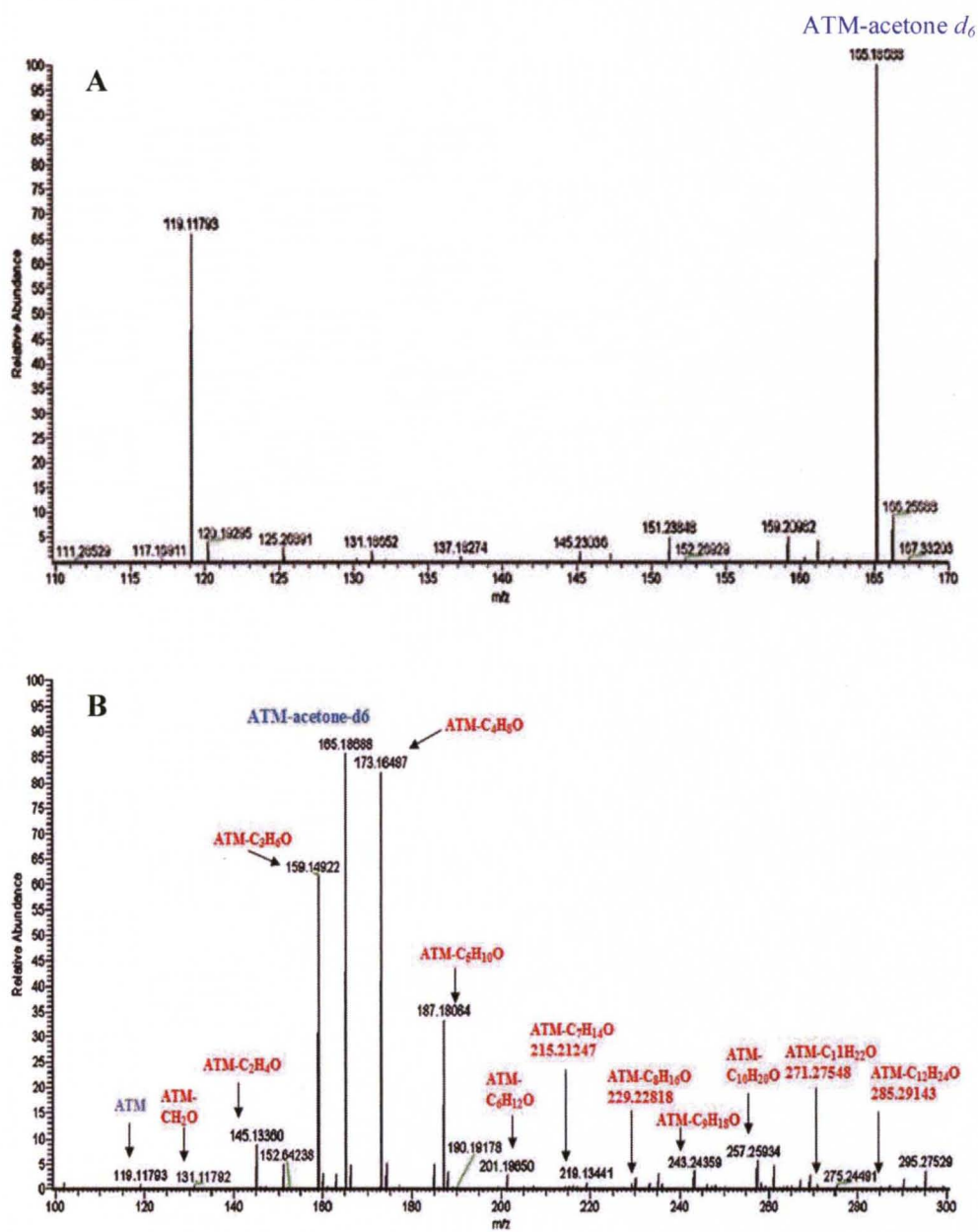


**Figure 5.5.** A. Positive-ion nanoelectrospray FT-ICR-MS spectrum of pre-concentrated deuterated acetone from the microreactor. B. A typical FTICR-MS spectrum of an exhaled breath pre-concentrated by the ATM-coated microreactor.



## **Ketone and aldehyde capture in exhaled human breath**

Further testing was performed using exhaled breath as a prelude to future non-invasive health diagnosis methods. After approval by the Internal Review Board at the University of Louisville and after having obtained written informed consent, exhaled breath samples were collected from nine voluntary healthy non-smoking subjects in the age range from 20 to 40. The subjects breathed 1L breath air into one liter Tedlar bags. A mixed alveolar breath and non-alveolar breath was collected. The Tedlar bags were purchased from Supelco (Bellefonte, PA, USA). The bags were tested free of ketone and aldehyde contamination. After collecting exhaled breath, the sample bag was connected to the inlet of the microreactor through septa and the silica tube. The outlet of the microreactor was connected to an oil free vacuum pump. Each microreactor was loaded with 365 nmole ATM. After the breath air in the sample bag was evacuated, the microreactor was disconnected from the flow line and then eluted with methanol as described above. A 8mL solution containing 2.32 nmole acetone- $d_6$  completely reacted with ATM in methanol was added into each eluted sample for analysis by FT-ICRMS. The ATM-acetone- $d_6$  adduct served as the internal reference to estimate captured amounts of ketones and aldehydes. Fig. 5.5B shows a typical FT-ICR-MS spectrum of exhaled breath.  $C_1$  to  $C_{12}$  ketones and aldehydes were detected.

### 5.3. Conclusion

The results of this work show that a microreactor-based aminoxy coating efficiently oximates gaseous carbonyl species for practical analysis of ketone and aldehyde VOCs. The designed microreactor features thousands of micropillars that uniformly distribute gas flow to maximize the interactions with ketones and aldehydes in the gas flow, resulting in capture efficiencies higher than 98%. Moreover, the key inclusion of a quaternary ammonium group in the design of the coating of the micropillar surface greatly enhances electrospray MS analyses. Simple elution of the entire microreactor coating including all captured analytes eliminates sample transfer problems that have plagued previous preconcentration approaches. This complete elution is enabled by the use of direct infusion nanoelectrospray FTICR-MS, which has the resolution to avoid interference of analytes by the capture phase.

Since the FT-ICR-MS instrument is very expensive (present price \$ 1M) and not common in many diagnosis facilities, we also considered applying this approach

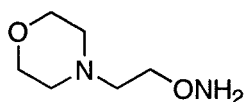


**Figure 5.6.** Structure of AMA (5.1).

to the more widely used GC-MS technique. To make the microreactor-based breath analyzer more available and cheap, we have functionalized microreactors using the commercial neutral aminoxy reagent ortho-(2-morpholin-4-yl-ethyl)-hydroxylamine (or AMA, 5.1, Figure 5.6) to detect the oximated adduct by less expensive GC-MS.

Initial studies revealed that capture efficacy of **5.1** is comparable to ATM. This work is ongoing.

Various cationic and neutral aminoxy-based reagents will be synthesized and will be tested for ketone/aldehyde capture using microreactor. The ATM-loaded microchip is now being tested for analyzing vapor generated from the lung cancer tissue and cell culture samples. The micrometer size of the chip can be advantageous for testing various unique atmospheres of cells. Due to the high sensitivity and easy engineering, this chemoselective microreactor-based vapor analyzer has great potential for explosive detection, drug testing for athletics, etc.

# **CHAPTER 6**

## **EXPERIMENTAL PROCEDURES**

---

**6.1. Index of Experimental Procedures**

**6.2. Experimental Procedures of Chapter 2**

**6.3. Experimental Procedures of Chapter 3**

**6.4. Experimental Procedures of Chapter 4**

---

## 6.1. Index of Experimental Procedures

<b>Description</b>	<b>Page</b>
Synthesi of <b>2.1</b> .....	120
Synthesis of <b>2.2</b> .....	122
Synthesis of <b>2.3</b> .....	123
Synthesis of <b>9.1</b> .....	124
Synthesis of <b>11.2</b> .....	125
Synthesis of <b>8 or 3.2</b> .....	126
Synthesis of Fe <sub>3</sub> O <sub>4</sub> <b>NPs</b> .....	127
Synthesis of <b>NP•1</b> .....	127
Synthesis of <b>NP-FITC</b> conjugates.....	127
Synthesis of <b>MLP and dMLP</b> .....	128
Labeling study.....	128
TEM, XRD, and EDX measurements of <b>NPs</b> and <b>dMLPs</b> .....	129
Zeta potential measurements of <b>NP, NP•1, MLP</b> and <b>dMLP</b> .....	129
Lucciferase expression using <b>MLP/dMLP</b> -derived magnetoplexes.....	130
Cytotoxicity assay using <b>MLP/dMLP</b> -derived magnetoplexes.....	130
Synthesis of <b>3.1</b> .....	131
Synthesis of <b>3.3</b> .....	132
Synthesis of <b>3.4</b> .....	133
ζ potential and liposome size measurements.....	133

Liposome formulation.....	134
Luciferase assay using oxime ether lipid-derived lipoplexes.....	135
GFP expression using oxime ether lipid-derived lipoplexes.....	136
Cytotoxicity assay using oxime ether lipid-derived lipoplexes.....	136
Synthesis of <b>Dox•AO</b> .....	137
Synthesis of <b>sNP•AO•Dox</b> .....	138
Synthesis of <b>dNP•AO•Dox</b> .....	139
Synthesis of <b>NP•Dox</b> .....	139
TEM micrograph of <b>dNP•AO•Dox</b> .....	139
<b>Dox•AO</b> loading calculation.....	140
$\zeta$ -potential measurements of <b>NP</b> , <b>dNP•AO•Dox</b> , <b>sNP•AO•Dox</b> and <b>NP•Dox</b> .....	140
AMF-induced NP heating.....	140
Drug release studies.....	141
Cytotoxicity evaluation of AMF-induced drug delivery.....	142
Fluorescence imaging of cells.....	143

## Experimental procedures

### Chemistry

All solvents and reagents used in this thesis were reagent grade and were used as received unless otherwise indicated. All nanoparticles and nanoparticle formulations were synthesized using HPLC grade methanol (Sigma-Aldrich). Dry THF and CH<sub>2</sub>Cl<sub>2</sub> were obtained from SPBT-101 Bench Top Solvent Purification System (LC Technology Solutions, Inc., USA). Anhydrous DMSO and methanol were purchased from Sigma-Aldrich. Doxorubicin (Dox•HCl) was purchased from Selleck Chemicals (TX, USA).

Column chromatography was conducted on silica gel (SiO<sub>2</sub>, Mesh size: 230-400 mesh, EMD Silica Gel 60). Thin layer chromatography was performed on precoated silica plates (EMD Silica Gel 60 F<sub>254</sub>). UV active compounds were visualized by UV light (254 nm). The TLC plates were stained using iodine, or p-anisaldehyde, or with phosphomolybdic acid. High performance liquid chromatography (HPLC) purification was performed using a Waters Delta 600 with a dual wavelength (214 and 254 nm detector) UV detector (Waters 2487 Dual Wavelength Absorbance Detector).

NMR spectra were recorded with a Varian MR (<sup>1</sup>H 400 MHz, <sup>13</sup>C 125 MHz) or with a Varian Inova (<sup>1</sup>H 500 MHz, <sup>13</sup>C 100 MHz) spectrometer. <sup>1</sup>H and <sup>13</sup>C NMR spectra of Dox•HCl and **Dox•AO** were recorded using a Varian VNMRS 700 spectrometer (<sup>1</sup>H 700 MHz, <sup>13</sup>C 176 MHz). Infrared spectra were recorded on a Mattson Galaxy Series FTIR 5000 spectrometer. Fluorescent spectrometric measurements were performed using a Perkin Elmer LS55 Fluorescence

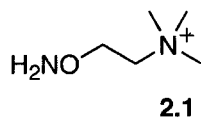
Spectrometer. High resolution mass spectrometry (HRMS) of the compounds were performed at the University of Louisville, Center for Regulatory and Environmental Analytical Metabolomics (CREAMM) facility using Thermo LTQ-FT instrument.

Liposome and nanoparticle formulations were prepared in ultra pure water (Milipore). Sonication was performed using bath sonicator purchased from Laboratory Supplies Co., Inc., Ithica, NY. Zeta potential and particle size analyses were conducted using ZetaPALS dynamic light scattering detector (Brookhaven Instruments Corporation; Model 90 Plus).



## 6.2. Experimental procedure of Chapter 2

### Synthesis



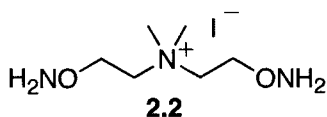
#### *N*-(2-(aminooxy)ethyl)-*N,N,N*-trimethylammonium iodide (2.1)

To a solution of triphenylphosphine (15.3 g, 58.3 mmol) and *N*-hydroxyphthalimide (9.50 g, 58.3 mmol) in THF (200 mL) at 0 °C was added dropwise *N,N*-dimethyl-ethanolamine (**5**) (4.33 g, 48.6 mmol). After stirring 30 min, diisopropyl azodicarboxylate (DIAD) (11.5 mL, 58.3 mmol) was added slowly via syringe. The reaction mixture was stirred an additional 30 min at 0 °C and then allowed to warm to room temperature. After 12 h, the solvent was removed by rotary evaporation. EtOAc (150 mL) was added to dissolve the residue followed by successive washings with saturated aq. NaHCO<sub>3</sub> (3 X 100 mL), water (50 mL), and brine (3 X 100 mL). The organic layer then was dried (Na<sub>2</sub>SO<sub>4</sub>), filtered, and concentrated to ~50 mL by rotary evaporation. The organic layer was cooled using an ice bath and cold 5% aq. HCl (30 mL) was added. On complete addition, the mixture was warmed to room temperature and stirred 20 min. The aqueous layer was separated, washed with Et<sub>2</sub>O several times, cooled to 0 °C, and then made alkaline by slowly adding saturated aq. NaHCO<sub>3</sub>. The alkaline aqueous layer was extracted using chloroform (3 X 50 mL). The combined organic phase was dried (Na<sub>2</sub>SO<sub>4</sub>), filtered, and the solvent removed by rotary evaporation to afford aminooxy phthalimide **7.1** (8.53 g, 75%) as a light yellow solid which required no further purification for use in

the next step;  $^1\text{H}$  NMR (DMSO- $d_6$ , 500 MHz)  $\delta$  7.82 (d,  $J = 5.0$  Hz, 4H), 4.21 (t,  $J = 5.0$  Hz, 2H), 2.60 (t,  $J = 5.0$  Hz, 2H), 2.17 (s, 6H);  $^{13}\text{C}$  NMR (DMSO- $d_6$ )  $\delta$  163.7, 135.3, 129.2, 123.8, 76.1, 57.4, 45.9.

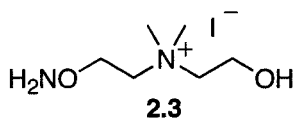
The phthalimide **7.1** (0.50 g, 2.13 mmol) was placed in a sealed tube and iodomethane (6.5 mL) was added. The mixture was degassed using a stream of nitrogen and then the tube was sealed and warmed to 50 °C. After 2 h, the sealed tube was cooled, opened, and the solvent was evaporated (caution: fume hood required) to afford the crude ammonium iodide as a light yellow solid;  $^1\text{H}$  NMR (DMSO- $d_6$ , 500 MHz)  $\delta$  7.89 (s, 4H), 4.67 (br s, 2H), 3.8 (t,  $J = 5.0$  Hz, 2H), 3.24 (s, 9H);  $^{13}\text{C}$  NMR (DMSO- $d_6$ )  $\delta$  164.0, 135.9, 129.4, 124.3, 72.3, 64.2, 54.2.

The crude iodide salt was dissolved in a mixture of EtOH (5 mL) and H<sub>2</sub>O (0.05 mL). Hydrazine monohydrate (1.13 mL, 14.9 mmol) was added and the reaction mixture was stirred 4 h at room temperature. The solvents were removed by rotary evaporation and acetonitrile (10 mL) was added to the residue. The resultant white turbid solution was warmed to 40 °C for 10 min and filtered through a cotton plug. Filtrate was evaporated and dried under high vacuum to furnish **2.1** (0.41 g, 78%) as a light yellow amorphous solid: mp 97-99 °C; IR (DRIFT) 3236, 3008, 1480, 963  $\text{cm}^{-1}$ ;  $^1\text{H}$  NMR (DMSO- $d_6$ , 500 MHz)  $\delta$  6.23 (s, 2H), 3.91 (br s, 2H), 3.52 (br s, 2H), 3.07 (s, 9H);  $^{13}\text{C}$  NMR (DMSO- $d_6$ )  $\delta$  69.3, 64.1, 54.0. HPLC analysis (C<sub>18</sub> 5 $\mu\text{m}$  column, gradient elution using 100% H<sub>2</sub>O to 100% CH<sub>3</sub>CN over 10 min at a flow rate of 1 mL/min) indicated excellent sample homogeneity (98% purity,  $t_r = 1.88$  min). The elution profile was monitored by UV absorbance at 214 nm. HRMS calculated for C<sub>5</sub>H<sub>15</sub>N<sub>2</sub>O<sup>+</sup> (M<sup>+</sup>): 119.1179, found: 119.1178.



***N,N*-bis(2-aminooxyethyl)-*N,N*-dimethylammonium iodide (2.2)**

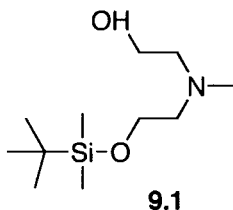
Using the procedure described for synthesis of **2.1**, *N*-methyl-diethanolamine (**6**) (2.0 g, 16.8 mmol) was transformed into the corresponding bis-(phthaloyloxyethyl)amine **8.2** (4.94 g, 72%); <sup>1</sup>H NMR (DMSO-*d*<sub>6</sub>, 500 MHz) δ 7.81 (s, 8H), 4.19 (t, *J* = 5.0 Hz, 4H), 2.79 (t, *J* = 5.0 Hz, 4H), 2.30 (s, 3H); <sup>13</sup>C NMR (DMSO-*d*<sub>6</sub>) δ 164.0, 135.6, 129.5, 124.1, 76.4, 55.9, 43.0. A portion of this material (0.50 g, 1.22 mmol) then was treated with iodomethane in the manner described above to afford the corresponding ammonium iodide; <sup>1</sup>H NMR (DMSO-*d*<sub>6</sub>, 500 MHz) δ 7.87 (s, 8H), 4.71-4.73 (m, 4H), 3.96-3.98 (m, 4H), 3.37 (s, 6H); <sup>13</sup>C NMR (DMSO-*d*<sub>6</sub>) δ 164.0, 135.9, 129.4, 124.3, 72.1, 63.3, 52.7. The crude ammonium iodide was treated with hydrazine as previously described to give the crude aminoxy product. Purification of **2.2** was accomplished by following the same procedure as described for **2.1**. **2.2** was isolated as a light yellow solid (0.23 g, 65% yield): mp 105-107 °C; IR (DRIFT) 3294, 1469, 960, 929 cm<sup>-1</sup>; <sup>1</sup>H NMR (DMSO-*d*<sub>6</sub>, 500 MHz) δ 6.24 (s, 4H), 3.92 (br s, 4H), 3.57 (br s, 4H), 3.08 (s, 6H); <sup>13</sup>C NMR (DMSO-*d*<sub>6</sub>) δ 69.1, 63.0, 52.3; HRMS calculated for C<sub>6</sub>H<sub>18</sub>N<sub>3</sub>O<sub>2</sub><sup>+</sup> (M<sup>+</sup>): 164.1394, found: 164.1394.



***N*-(2-aminooxyethyl)-*N*-(2-hydroxyethyl)-*N,N*-dimethylammonium iodide (2.3)**

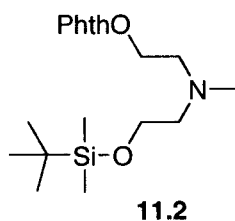
In a sealed tube, mono-phthalimide **11.2** (0.60 g, 2.28 mmol) was dissolved in iodomethane (10 mL). The reaction mixture was degassed using a stream of N<sub>2</sub> before sealing the tube. The reaction was heated to 50 °C. After 3 h at 50 °C, the reaction was cooled and the tube opened. The iodomethane was evaporated (Caution: fume hood required) to afford the corresponding ammonium iodide which was used in the next step without further purification; <sup>1</sup>H NMR (DMSO-*d*<sub>6</sub>, 500 MHz) δ 7.88 (s, 4H), 5.29 (br s, 1H), 4.67 (br s, 2H), 3.85 (t, *J* = 5.0 Hz, 4H), 3.56 (br s, 2H), 3.24 (s, 6H); <sup>13</sup>C NMR (DMSO-*d*<sub>6</sub>) δ 164.0, 135.9, 129.5, 124.3, 72.2, 67.0, 63.2, 55.9, 52.6.

To a solution of the crude ammonium iodide in EtOH (5 mL) at room temperature was added hydrazine monohydrate (0.86 mL, 11.3 mmol). After stirring 12 h at room temperature, the solvents were removed by rotary evaporation. The residue was purified using same technique as before to give **2.3** as a white solid (0.40 g, 65%): mp 120-121 °C; IR (DRIFT) 3400, 3238, 1477, 963, 933 cm<sup>-1</sup>; <sup>1</sup>H NMR (DMSO-*d*<sub>6</sub>, 500 MHz) δ 6.24 (s, 2H), 5.24 (br s, 1H), 3.92 (br s, 2H), 3.82 (br s, 2H) 3.58 (br s, 2H), 3.43 (br s, 2H), 3.09 (s, 6H); <sup>13</sup>C NMR (DMSO-*d*<sub>6</sub>) δ 69.2, 66.7, 63.1, 55.9, 52.4; HRMS: calculated for C<sub>6</sub>H<sub>17</sub>N<sub>2</sub>O<sub>2</sub><sup>+</sup> (M<sup>+</sup>): 149.1285, found: 149.1284.



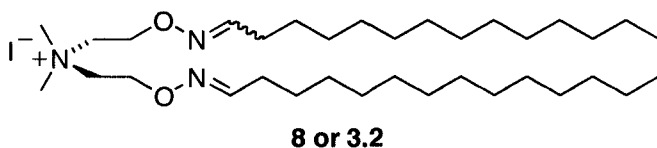
**2-(*N*-methyl-(2-*tert*-butyldimethylsilyloxyethyl)amino)ethanol (9.1)**

To a solution of diethanolamine (**6**) (9.0 mL, 78.4 mmol) and Et<sub>3</sub>N (2.19 mL, 15.7 mmol) in CH<sub>2</sub>Cl<sub>2</sub> (300 mL) at 0 °C was added slowly a solution of *tert*-butyldimethylchlorosilane (2.35 g, 15.7 mmol) in CH<sub>2</sub>Cl<sub>2</sub> (150 mL). On complete addition, the reaction was allowed to warm to room temperature. After 12 h, the reaction mixture was diluted with CH<sub>2</sub>Cl<sub>2</sub>, transferred to a separatory funnel, and washed successively with saturated NaHCO<sub>3</sub> (3 x 150 mL) and brine (3 x 150 mL). The organic layer was dried (Na<sub>2</sub>SO<sub>4</sub>), filtered and the solvent removed by rotary evaporation. The residue was purified by column chromatography (SiO<sub>2</sub>), eluting with a 1:14 mixture of methanol: CH<sub>2</sub>Cl<sub>2</sub> (product R<sub>f</sub> 0.43), to afford silyl ether **9.1** (2.72 g, 75%) as an oil; <sup>1</sup>H NMR (CDCl<sub>3</sub>, 500 MHz) δ 3.68 (t, *J* = 5.0 Hz, 2H), 3.55 (t, *J* = 5.0 Hz, 2H), 2.58-2.59 (m, 4H), 2.31 (s, 3H), 0.85 (s, 9H), 0.02 (s, 6H); <sup>13</sup>C NMR (CDCl<sub>3</sub>) δ 61.2, 59.3, 58.7, 42.6, 26.0, 18.3, -4.90; HRMS: calcd for C<sub>11</sub>H<sub>27</sub>NO<sub>2</sub>SiNa [M+Na]<sup>+</sup> requires 256.1708, found 256.1709.



**2-(*N*-methyl-(2-phthalimidooxyethyl)amino)ethanol (11.2)**

Using the Mitsunobu procedure described above for the synthesis of **2.1**, silyl ether **9.1** (1.0 g, 4.1 mmol) was transformed into the corresponding mono-phthalimide product. After work-up, the crude mono-phthalimide was dissolved in EtOAc (20 mL) and treated with cold 5% aq. HCl (20 mL). After stirring vigorously for 20 min at room temperature, the layers were separated. The aqueous layer then was washed with additional portions of Et<sub>2</sub>O (3 × 30 mL), made slightly alkaline by addition of saturated aq. NaHCO<sub>3</sub>, and extracted with CHCl<sub>3</sub> (3 × 50 mL). The combined chloroform extract was dried (Na<sub>2</sub>SO<sub>4</sub>) and the solvent was removed by rotary evaporation to give **11.2** (0.80 g, 71%) as an oil; <sup>1</sup>H NMR (CDCl<sub>3</sub>, 500 MHz) δ 7.78-7.79 (m, 2H), 7.70-7.72 (m, 2H), 4.28 (t, *J* = 5.0 Hz, 2H), 3.57 (t, *J* = 5.0 Hz, 2H), 2.82-2.85 (m, 2H), 2.61-2.63 (m, 2H), 2.32 (s, 3H); <sup>13</sup>C NMR (CDCl<sub>3</sub>) δ 163.7, 134.7, 129.0, 123.7, 76.4, 59.3, 58.8, 55.7, 42.2.



**Dimethyl-*bis*(2-tetradecylideneaminoxy-ethyl)-ammonium iodide (8 or 3.2)**

Ammonium iodide **2.2** (0.05 g, 0.17 mmol) and tetradecanal (0.80 g, 0.39 mmol) were dissolved in methanol (3 mL) and stirred at room temperature. After 3.5 h, the solvent was removed by rotary evaporation and the residue was purified by column chromatography (SiO<sub>2</sub>), eluting with a 1:33 mixture of methanol:CH<sub>2</sub>Cl<sub>2</sub> to afford **8** (0.09 g, 82%) as a yellow solid (2.7:1 mixture of (*E,E*):(*E,Z*) oxime ether diastereomers); TLC (19:1, CH<sub>2</sub>Cl<sub>2</sub>:MeOH) R<sub>f</sub> = 0.45; mp 59–60 °C; IR (neat) 1703 (C=N), 1467, 968, 920 cm<sup>-1</sup>; <sup>1</sup>H NMR (CD<sub>3</sub>OD, 500 MHz) major diastereomer, δ 7.58 (t, *J* = 5.0, 2H), 4.53 (m, 4H), 3.83-3.85 (m, 4H), 3.4 (s, 6H), 2.30 (appt q, *J* = 5.0 Hz, 4H), 1.58-1.61 (m, 4H), 1.37-1.4 (m, 40H), 0.98 (t, *J* = 5.0 Hz, 3H); <sup>13</sup>C NMR (CD<sub>3</sub>OD) δ 154.9, 67.8, 64.8, 53.2, 33.0, 30.6, 30.3, 27.5, 23.7, 20.1, 14.4; HRMS calculated for C<sub>34</sub>H<sub>70</sub>N<sub>3</sub>O<sub>2</sub><sup>+</sup>(M<sup>+</sup>): 552.5463, found: 552.5467.

### **Preparation Fe<sub>3</sub>O<sub>4</sub> nanoparticles (NPs)**

Fe<sub>3</sub>O<sub>4</sub> nanoparticles (NPs) with an average particle size of 10 nm were prepared without any additional stabilizer according to the procedure described by Mikhaylova *et al.*<sup>119</sup> Typically, 5 mL of a 0.1 M FeCl<sub>2</sub> and 0.2 M FeCl<sub>3</sub> solution were added dropwise into 50 mL of 0.1 M NaOH solution under vigorous stirring for 30 min at room temperature under a N<sub>2</sub> atmosphere. The color of the suspension turned black immediately. The precipitated particles were collected and removed from the solution by applying a magnet (Super Magnetic Plate, Oz Biosciences, France). The supernatant solution was removed from the reaction mixture by decantation. The isolated NPs were dried using a lyophilizer (55 mg, 94.8% yield). The NPs were characterized by TEM, EDX and XRD as described in the following subsections.

### **Synthesis of NP•1**

NPs (5 mg) were suspended in methanol (3 mL) and sonicated 5 min at room temperature. To the suspension was added *N,N*-bis-(2-aminooxyethyl)-*N,N*-dimethylammonium iodide (**2.2**, 15 mg). The reaction mixture was first sonicated for 5 min and then stirred at room temperature. After 12 h, the coated NPs were separated magnetically and washed with methanol. The washing procedure was performed for total three times and then the coated NPs were dried under high vacuum for overnight to obtain NP•1 (6.9 mg, 2X10<sup>4</sup> molecules/NP).

### **Synthesis of NP-FITC conjugates**

**FITC2** was prepared according to the method described by Trévisiolli *et al.*<sup>214</sup> To an aqueous suspension of NP•1 (5 mL, NP•1 concentration at 0.8 mg/mL) was added **FITC2** (15 mg). The mixture was sonicated for 10 min. and then water (5



mL) was added. After stirring at room temperature for 12 h, the NP•1•FITC2 particles were magnetically separated and washed according to the procedure described above using methanol. The separated particles then were isolated after freeze drying to give NP•1•FITC2 (7.5 mg).

### **Synthesis of MLP and dMLP**

To NP•1 (6.9 mg) suspended in methanol (5 mL) was added myristaldehyde (20.0 mg, 0.94 mmol). The suspension was stirred at room temperature. After 12 h, the lipid-coated nanoparticles were isolated by magnetic sedimentation, washed with methanol (2X), and then dried under vacuum 5 h to yield the magnetic lipid particles (MLP; 7.8 mg).

To NP (5.0 mg) suspended in methanol (5 mL) was added *N,N*-dimethyl-bis(2-tetradecylideneaminoxy-ethyl)ammonium iodide (**8**; 11.0 mg, 0.016 mmol) and mixture was sonicated at room temperature for 2 mins. The suspension was stirred 12 h at room temperature. The resultant particles then were isolated by magnet-assisted sedimentation, washed with methanol one extra time, and dried under vacuum 5 h to give dMLP (9.25 mg).

### **Nanoparticle Characterization**

#### **Labeling study**

UV-Visible spectroscopy measurements were taken of NP, NP•1, NP•1•FITC2 and FITC2 at concentrations of 0.025 mg/mL. As a control, unmodified NPs were mixed with FITC2.

### **TEM, EDX, and XRD measurement of NPs and dMLPs**

Methanol suspensions of NP or dMLP samples were deposited on transmission electron microscopy (TEM) Cu grids coated with a carbon film. TEM microstructures and energy dispersive X-ray (EDX) spectra then were measured using a JEOL JEM 3200FS at 300 kV equipped with an EDX detector. X-Ray diffraction (XRD) patterns were obtained using a BRUKER D8 diffractometer with a CuK $\alpha$  radiation source (1  $\frac{1}{4}$  0.15418 nm). The phase identification was performed using JCPDS-ICDD 2000 software (The International Centre for Diffraction Data; ICDD).

TEM, XRD, and EDX measurements of NPs were performed at the Institute for Advanced Materials and Renewable Energy, University of Louisville. TEM images of dMLPs were taken at the Indiana University (TEM facility).

### **Zeta potential measurements**

The zeta potentials of NP, NP•1, MLP, dMLP and derived magnetoplexes were measured in water using a ZetaPALS dynamic light scattering detector (Brookhaven Instruments Corporation; Model 90 Plus). The concentration of iron oxide in the aqueous particle samples was 0.1 mg/mL. Magnetoplexes were formulated at a concentration of 0.5  $\mu$ g pDNA.

### **Transfection and cytotoxicity evaluation**

#### **Cell culture**

Human breast cancer cells (MCF-7) were purchased from American Type Culture Collection VA, USA. Cells were grown to 50-60% confluency in DMEM and 1% Pennstrep (Mediatech, Inc, VA) with 10% FBS (Valley Biomedical, Winchester, VA).

### **Luciferase expression**

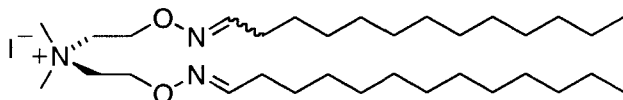
Luciferase transfections were performed in triplicate using 0.025 µg of pDNA (pCMV Luc) /well in MCF-7 cells. MCF-7 cells were seeded up to  $1 \times 10^5$  cells/well in a 24-well plate to 50-60% confluence. Magnetoplexes (MLP•pDNA and dMLP•pDNA) were prepared at nanoparticle:pDNA ratios of 30, 60, 90, 120, 180, 360 and 540 by adding the required volume of aqueous suspension of MLP or dMLP to a pDNA solution (3 mL, 0.025 µg DNA/mL). 200 µL of serum free DMEM then was added to each magnetoplex solution followed by incubation for 30 min at room temperature. The magnetoplex solutions were diluted to 600 µL with serum free DMEM, and then 200 µL of the final magnetoplex formulation were added directly to each well. For magnetofection, the cell plate was placed on top of a magnetic plate (Oz Biosciences) for 1 h at 37.5 °C. After 18 h incubation at 37.5 °C, the cells were lysed and luciferase gene expression was quantified using a commercial kit (Promega) and luminometer according to the vendor's protocol. Lipofectamine 2000 (Invitrogen) was used as a positive control. Transfections were also performed in similar manner without the assistance of a magnet.

### **Cytotoxicity assessment of the dMLP formulations**

Cell cytotoxicity and proliferation of cells treated with dMLP formulations were examined by an alamarBlue assay. After transfection of MCF-7 cells using dMLP derived magnetoplexes (0.025 µg of DNA/well) and incubation for 18 h, cell viability was measured according to the vendor's (Invitrogen) protocol. Fluorescence intensities were measured using a spectrofluorometer (Molecular Devices:Gemini EM) by excitation at 540 nm and emission at 600 nm.

### 6.3. Experimental procedures of Chapter 3

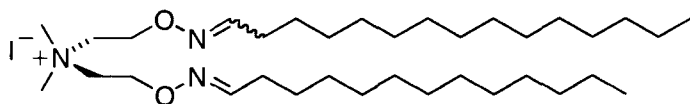
#### Synthesis



**3.1**

#### *N,N*-Dimethyl-*N*-2-((dodecylideneamino)oxy)-(2-((dodecylideneamino)oxy)ethyl)ethanaminium iodide (**3.1**)

Compound **2.2** (26.5 mg, 0.091 mmol) and dodecanal (35.4 mg, 0.19 mmol) were dissolved in MeOH (3 mL) and stirred at RT. After 3.5 h, the solvent was removed in vacuo, and the residue was purified by silica column chromatography (MeOH:CH<sub>2</sub>Cl<sub>2</sub>, 3%) to afford oxime ether lipid **3.1** as a white solid (34.6 mg, 61 %; (E, E):(E, Z), 5.3:1); R<sub>f</sub>=0.52 (CH<sub>2</sub>Cl<sub>2</sub>/MeOH, 9:1); mp: 155 °C (dec); IR (neat): 1735, 1468, 966, 920 cm<sup>-1</sup>; <sup>1</sup>H NMR (400 MHz, CD<sub>3</sub>OD) δ (major diastereomer) 0.86 (t, *J*=6.8 Hz, 6 H), 1.25–1.45 (m, 28H), 1.43–1.48 (m, 4 H), 2.17 (dd, *J*=6.8, 7.2 Hz, 4 H), 3.20 (s, 6 H), 3.73–3.75 (m, 4 H), 4.40–4.41 (m, 4 H), 7.46 ppm (t, *J*=6.0 Hz, 2H); <sup>13</sup>C NMR (100 MHz, CD<sub>3</sub>OD) δ 14.6, 23.9, 27.1, 27.3, 27.7, 30.4, 30.6, 30.9, 33.2, 53.4, 64.9, 68.0, 68.3, 155.0, 155.5 ppm; HRMS: *m/z* [M]<sup>+</sup> calcd for: C<sub>30</sub>H<sub>62</sub>N<sub>3</sub>O<sub>2</sub><sup>+</sup>: 496.4837, found: 496.4839.

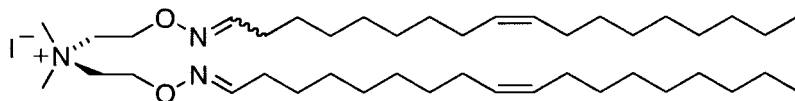


**3.3**

***N,N*-Dimethyl-*N*-2-((dodecylideneamino)oxy)-(2-((tetradecylideneamino)oxy)ethyl)ethanaminium iodide (3.3)**

Compound **2.2** (22.6 mg, 0.078 mmol) and dodecanal (7.2 mg, 0.034 mmol) were dissolved in MeOH (1 mL) and stirred at RT. After 14 h, the solvent was removed in vacuo, and the residue was purified by SiO<sub>2</sub> column chromatography (MeOH:CH<sub>2</sub>Cl<sub>2</sub>, 5%) to afford the intermediate mono-oxime ether as a yellow oil (14.0 mg, 39%; (E, E):(E, Z), 1.7:1): R<sub>f</sub>=0.25 (CH<sub>2</sub>Cl<sub>2</sub>/MeOH, 9:1).

The C<sub>12</sub> mono-oxime ether intermediate (13.1 mg, 0.029 mmol) and tetradecanal (9.1 mg, 0.043 mmol) were dissolved in MeOH (1 mL) and stirred at RT. After 14 h, the solvent was removed in vacuo, and the residue was purified by column chromatography (SiO<sub>2</sub>; MeOH:CH<sub>2</sub>Cl<sub>2</sub>, 3%) to afford unsymmetrical lipid **3.3** as a yellow oil (13 mg, 69%; E: Z, 2.3:1): R<sub>f</sub>=0.48; (CH<sub>2</sub>Cl<sub>2</sub>/MeOH, 9:1); <sup>1</sup>H NMR (400 MHz, CD<sub>3</sub>OD) (major diastereomer) δ 0.84 (t, *J*=6.8 Hz, 6H), 1.23–1.26 (m, 36H), 1.44 (dd, *J*=6.8, 7.2 Hz, 4H), 2.15 (dd, *J*=6.4, 7.2 Hz, 4H), 3.18 (s, 6H), 3.69–3.72 (m, 4 H), 4.38–4.40 (m, 4 H), 7.44 ppm (t, *J*=6.2 Hz, 2H); <sup>13</sup>C NMR (100 MHz, CD<sub>3</sub>OD) δ 14.6, 23.9, 27.1, 27.3, 27.6, 30.4, 30.6, 30.7, 30.8, 30.9, 33.2, 53.3, 64.9, 68.0, 68.4, 155.0, 155.5 ppm; IR (neat): 1728, 1467, 964, 942 cm<sup>-1</sup>; HRMS: *m/z* [M]<sup>+</sup> calcd for: C<sub>32</sub>H<sub>66</sub>N<sub>3</sub>O<sub>2</sub><sup>+</sup>: 524.5150, found: 524.5172.



**3.4**

***N,N*-Dimethyl-*N*-2-((((*Z*)-octadec-9-en-1-ylidene)amino)oxy)-(2-((((*Z*)-octadec-9-en-1-ylidene)amino)oxy)ethyl)ethanaminium iodide (3.4)**

Compound **2.2** (19.7 mg, 0.068 mmol) and *cis*-9-octadecenal (37.8 mg, 0.142 mmol) were dissolved in MeOH (3 mL) and stirred at RT. After 3.5 h, the solvent was removed in vacuo, and the residue was purified by column chromatography (SiO<sub>2</sub>; MeOH:CH<sub>2</sub>Cl<sub>2</sub>, 3%) to afford oxime ether lipid **3.4** as a yellow oil (45.8 mg, 90.0%; (E, E):(E, Z), 3.0:1): R<sub>f</sub>=0.51 (CH<sub>2</sub>Cl<sub>2</sub>/MeOH, 9:1); IR (neat) 1730, 1464, 964, 942 cm<sup>-1</sup>; <sup>1</sup>H NMR (400 MHz, CD<sub>3</sub>OD): (major diastereomer) δ 0.84 (t, *J*=6.8 Hz, 6H), 1.23–1.27 (m, 40H), 1.42–1.47 (m, 4H), 1.96–1.97 (m, 8 H), 2.15 (dd, *J*=6.4, 7.2 Hz, 4H), 3.16 (s, 6 H), 3.68–3.71 (m, 4 H), 4.38–4.39 (m, 4 H), 5.27–5.29 (m, 4H), 7.43 ppm (t, *J*=6.0 Hz, 2H); <sup>13</sup>C NMR (100 MHz, CD<sub>3</sub>OD) δ 14.6, 23.9, 27.6, 28.3, 30.4, 30.5, 30.6, 30.8, 31.0, 33.2, 53.3, 64.9, 68.0, 130.9, 131.1, 155.0 ppm; HRMS: *m/z* [M]<sup>+</sup>: calcd for C<sub>42</sub>H<sub>82</sub>N<sub>3</sub>O<sub>2</sub><sup>+</sup>: 660.6401, found: 660.6395.

**Zeta potential and liposome size measurements**

Measurements of liposome size, lipoplex zeta potential and formulated nanoparticle size were performed using a ZetaPALS dynamic light scattering detector (Brookhaven Instruments Corporation; Model 90 Plus). All measurements were taken in water. Lipoplexes were formulated at a final concentration of 0.1 mg oxime ether lipid per mL water. To formulate lipoplexes at different N:P ratios, 100 mL of

the liposome formulation was added to the required quantity of pDNA (taken from a stock solution of 0.1 mg pDNA per mL) in an Eppendorf tube. After incubating each lipoplex for 15 min, the solutions were diluted to 1 mL by adding ultra-pure water. Measurements were taken within minutes of formulation.

### **Liposome formulation**

An equimolar amount of DOPE from a stock solution (10 mg DOPE per mL CHCl<sub>3</sub>) was added to a solution of oxime ether lipid (1 mg) in CHCl<sub>3</sub> (0.20 mL). The solvent was evaporated, and the resultant thin lipid film was dried under vacuum (4 h). Ultra-pure water (3 mL) was added to the dry lipid film, and the suspension was sonicated (bath sonicator, Laboratory Supplies Co., Inc., Ithica, NY) for 1 min at RT to furnish the liposome formulation (0.33 mg oxime ether lipid / mL).

### **Tissue Culture**

Human breast cancer cells (MCF-7) and lung tumor cells (H1792) were purchased from American Type Culture Collection (Manassas, VA, USA). Cells were grown to 50–60% confluency prior to transfection. MCF-7 cells were cultured in Dulbecco's modified Eagle's medium (DMEM; Invitrogen, Carlsbad, CA, USA), 1% pennstrep (Mediatech Inc., Manassas, VA, USA, 10% fetal bovine serum (FBS; Valley Biomedical, Winchester, VA, USA). H1792 cells were cultured in RPMI (Invitrogen), 1% pennstrep (Mediatech Inc.), 10%FBS.

## **Transfection and cytotoxicity studies**

### **Luciferase assay**

Luciferase transfections in MCF-7 and H1792 cells were performed in triplicate using 0.025 mg of pDNA (pCMVLuc) per well. Cells were seeded up to  $1 \times 10^5$  cells per well in a 24-well plate to give 50–60% confluency, and 400  $\mu$ L of media containing 10% FBS was added to each well. Lipoplexes (lipid•pDNA complex) were prepared at N:P charge ratios of 3, 5 and 7 by adding the required volume of liposome solution to a pDNA solution (3 mL, 0.025 mg DNA per mL) and incubated for 5 min. Serum free DMEM (100  $\mu$ L) was then added to each lipoplex solution followed by incubation for 20 min at RT with occasional gentle vortex mixing. The lipoplex solutions were diluted to 600  $\mu$ L with serum free DMEM, and then an aliquot of the final lipoplex formulation (200  $\mu$ L) was added directly to each well. No additional media containing FBS was added to the cells during transfection. After 18 h incubation at 37.5 °C, the cells were lysed and luciferase expression was quantified using a commercial kit (Promega Corp., Wisconsin, USA) and luminometer according to the vendor's protocol. Lipofectamine 2000 (Invitrogen) and jetPrime (Polyplus Transfection, SA, Illkirch, France) lipoplexes were prepared at the vendor recommended stoichiometry (2  $\mu$ L stock per mg DNA).

Luciferase transfections were also performed in duplicate using 1  $\mu$ g of pDNA (pCMV-Luc)/well in MCF-7 cells as described above. Cells were seeded up to  $4 \times 10^5$  cells/well in a 6-well plate to give 50–60% confluence. Transfection activity of lipid 3 was evaluated at N:P=7. RLU/ $\mu$ g of protein was measured using the BCA protein assay kit (Bio-Rad, USA).



### **GFP expression**

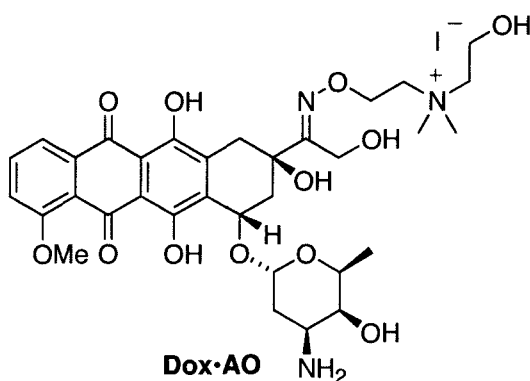
Transfection studies were performed using a GFP reporter gene in MCF-7 cells using 0.1 mg of pEGFP DNA (Clontech Laboratories Inc. WI, USA) per well in a 24-well plate with a similar transfection protocol as described for the luciferase assays. Cells were examined 40 h post transfection by fluorescence microscopy (EVOS, Advanced Microscopy Group, Bothell, WA, USA) and photographed.

### **Cytotoxicity evaluation**

Lipid cytotoxicity was evaluated using the vital dye trypan blue to distinguish between live and dead cells. MCF-7 and H1792 cells were seeded at  $1 \times 10^4$  cells per well and then grown to 50–60% confluency in 96-well plates. Transfections were performed as described above. The media was removed 18 h post transfection. Cells were then trypsinized by adding 100  $\mu$ L trypsin to each well and incubated for 5 min at 37.5 °C. Trypsin was neutralized by adding 1X phosphate-buffered saline (1X PBS), and then 10  $\mu$ L of extract from each well was mixed with 10  $\mu$ L of trypan blue. Dead and live cells were counted under an inverted microscope to determine the percentage cell viability using a hemocytometer.

## 6.4. Experimental procedures of Chapter 4

### Synthesis



**2-(((E)-1-((2R,4S)-4-(((2R,4S,5S,6S)-4-amino-5-hydroxy-6-methyltetrahydro-2H-pyran-2-yl)oxy)-2,5,12-trihydroxy-7-methoxy-6,11-dioxo-1,2,3,4,6,11-hexahydrotetracen-2-yl)-2-hydroxyethylidene)amino)oxy)-N-(2-hydroxyethyl)-N,N-dimethylethanaminium iodide (Dox•AO)**

To a solution of **Dox•HCl** (Selleck Chemicals, Houston, TX, USA; 45.0 mg, 0.077 mmol) in anhydrous methanol (35 mL) at room temperature was added *N*-(2-hydroxyethyl)-*N,N*-dimethyl-2-aminoethylethylammonium iodide (**2.3**, 100 mg, 0.38 mmol) and trifluoroacetic acid (0.5 mL). After stirring the reaction mixture at room temperature for 96 h, the solvent was removed under reduced pressure. Acetonitrile (5 mL) was added to the residue and the suspension was sonicated 1 min at room temperature and then warmed to 40 °C for 5 min. The suspension was then cooled to -20 °C. After storing 18 h at -20 °C, the supernatant was decanted and the remaining precipitate (red solid) was dried under reduced pressure to afford **Dox•AO** (55 mg,

91%): mp: 50-53 °C (dec); <sup>1</sup>H NMR (700 MHz, CD<sub>3</sub>OD) δ 1.296-1.33 (m, 3 H), 1.92 (dd, *J*=8.40, 4.20 Hz 1H), 2.05 (dd, *J*=7.7, 3.5 Hz, 1H), 2.42 (dd, *J*=8.4, 6.3 Hz, 1H), 2.57 (d, *J*=11.2 Hz), 3.15 (d, *J*=14 Hz, 2H), 3.22-3.32 (m, 10H), 3.36-3.62 (m, 2H), 3.63 (s, 1H), 3.72-3-3.86 (m, 3H), 4.03 (d, *J*=21 Hz, 6H), 4.29-4.30 (m, 2H), 4.51-4.61 (m, 4H), 4.87-5.04 (m, 1H), 5.48 (s, 1H), 7.55 (d, *J*=8.4 Hz, 2H), 7.81 (t, *J*=7 Hz, 2H), 7.89 (d, *J*=7.7 Hz, 2H); <sup>13</sup>C NMR (150 MHz, CD<sub>3</sub>OD) δ 15.7, 28.0, 33.09, 38.1, 47.2, 47.3, 47.4, 47.6, 51.8, 54.2, 55.4, 55.8, 63.0, 63.7, 66.4, 66.6, 67.6, 68.5, 71.4, 71.9, 99.6, 110.7, 110.9, 118.9, 119.0, 120.1, 134.9, 135.0, 135.1, 135.9, 154.8, 156.1, 161.0, 162.6, 186.4, 186.8 ppm; HRMS: calculated for: C<sub>33</sub>H<sub>44</sub>N<sub>3</sub>O<sub>12</sub><sup>+</sup> (M)<sup>+</sup>, 674.2920; found: 674.2926.

#### Preparation of sNP•AO•Dox

A suspension of Fe<sub>3</sub>O<sub>4</sub> nanoparticles (5.5 mg) in methanol (1.5 mL) at room temperature was sonicated (1 min) followed by addition of a solution of *N*-(2-hydroxyethyl)-*N,N*-dimethyl-2-aminooxyethylammonium iodide (**2.3**) (30 mg) in methanol (1.5 mL). The reaction suspension was sonicated (1 min) at room temperature and then stirred 12 h. The resultant NP•AO particles were magnetically sedimented to facilitate removal of the supernatant. The particles then were washed with methanol (1 mL, 2X). The washed particles were dried under reduced pressure to afford NP•AO (7.42 mg).

A suspension of NP•AO (7.4 mg) in anhydrous DMSO (1.5 mL) at room temperature was sonicated (1 min). Within 1 min of sonication, a solution of doxorubicin•HCl (10 mg) in anhydrous DMSO (1.5 mL) was added. The reaction suspension then was sonicated (1 min) at room temperature and stirred at room

temperature an additional 12 h. The resultant drug-conjugated particles were magnetically sedimented to facilitate removal of the supernatant. The particles then were washed with DMSO (1.5 mL, 1x). The supernatant was collected and centrifuged for 10 min at 4 °C. The pelleted and magnetically separated particles were combined and dried under reduced pressure to afford **sNP•AO•Dox** (9 mg).

#### **Synthesis of dNP•AO•Dox**

Fe<sub>3</sub>O<sub>4</sub> nanoparticles (**NP**, 7 mg) were suspended in anhydrous DMSO (1.5 mL) at room temperature and sonicated (1 min, room temperature) using an Ultra Sonicator water bath. To the resultant NP suspension, a solution of **Dox•AO** (20 mg) in anhydrous DMSO (1.5 mL) was added. The reaction suspension was further sonicated for 1 min at room temperature and then stirred 12 h. The resultant drug-loaded particles were purified as described above to afford **dNP•AO•Dox** (9.4 mg).

#### **Synthesis of NP•Dox**

A suspension of Fe<sub>3</sub>O<sub>4</sub> nanoparticles (9.0 mg) in anhydrous DMSO (1.5 mL) at room temperature was sonicated (1 min) followed by addition of a solution of **Dox•HCl** (20 mg) in anhydrous DMSO (1.5 mL). This reaction suspension was sonicated (1 min) and then stirred at room temperature for 12h. The loaded particles were isolated using the magnetic separation and washing procedure described above to furnish **NP•Dox** (10 mg).

#### **NP characterization**

##### **Transmission electron micrograph of dNP•AO•Dox**

Methanol suspensions of **dNP•AO•Dox** samples were deposited on transmission electron microscopy (TEM) Cu grids coated with a carbon film. TEM

microstructures and energy dispersive X-ray (EDX) spectra then were measured using a JEOL JEM 3200FS at 300 kV equipped with an EDX detector. TEM measurements were performed at the Indiana University (Bloomington), TEM facility.

### **Dox•AO loading calculation**

Volume of 1 mg NP = mass/density =  $0.001 \text{ (g)}/5.24 \text{ gcm}^{-3} = 0.0002 \text{ cm}^3 \text{ (V)}$

Volume of one NP =  $4/3 \pi r^3 = 5.23 \times 10^{-19} \text{ cm}^3 \text{ (V}_1)$

Number of NPs in 1 mg =  $V/V_1 = 3.82 \times 10^{14} \text{ (X)}$

0.37  $\mu\text{mol}$  **Dox•AO** is attached/ mg NP

Number of **Dox•AO** molecules in 0.37  $\mu\text{mol}$  =  $2.22 \times 10^{17} \text{ (X}_1)$

So, number of **Dox•AO** molecules attached to each NP =  $X_1/X = 580$

Surface area of a single NP =  $4 \pi r^2 = 31428.57 \text{ \AA}^2 \text{ (A)}$

Polar surface area (PSA) of **4.1** =  $21 \text{ \AA}^2$  (PSA was calculated using a software form <http://www.daylight.com/meetings/emug00/Ertl/tpsa.html>)

So, maximum number of **Dox•AO** molecules that can attach on surface side by side of each NP or footprint of **Dox•AO** =  $A/\text{PSA} = 1450$

### **Zeta potential measurements**

The zeta potentials of **NP**, **sNP•AO•Dox**, **sNP•AO•Dox**, **NP•Dox** were measured in 1X PBS using a ZetaPALS dynamic light scattering detector (Brookhaven Instruments Corporation; Model 90 Plus). The concentration of each of the sample was 0.3 mg NP/mL buffer.

### **AMF-induced NP heating**

A suspension of **dNP•AO•Dox** (2.5 mg) in PBS (1 mL) was exposed to a continuous AMF (EASYHEAT™ 8310LI solid state induction power supply,

Ameritherm, Inc., 5 turn coil with ID: 5.0 cm and OD: 6.5 cm, 203 kHz, 350 A) for 18 min. The AMF exposure was started after the temperature of the suspension had reached 37.0 °C. The temperature of the suspension was measured every 3 min using an optical fiber temperature probe (Neoptix Inc., Québec, Canada).

Solution containing AMF-triggered drug was analyzed by HRMS. The supernatant was collected after AMF exposure and diluted to 0.5 µmol for analysis using a FT-ICR-MS (Fourier Transform Ion Cyclotron Resonance Mass Spectrometry).

### **Drug release studies**

#### **AMF-induced drug release**

The drug-loaded nanoparticle formulation were suspended in PBS by sonication (1 min) and then subjected to AMF-exposure (203 KHz) for 18 min. Every 3 min, a 10 µL of aliquot was taken out and diluted to 1 mL for UV measurements at 480 nm.<sup>86</sup> The concentration of drug released was calculated using Beer-Lambert's law. Release study was performed in triplicate.

According to Beer Lambert's law:  $A = \epsilon lc$

Where, A is the absorbance;  $\epsilon$  is the molar absorptivity (a constant); l is path length (1 cm). Thus, if the path length and the molar absorptivity are known and the absorbance is measured, the concentration of the substance or 'c' can be deduced.

#### **Drug release study at 37.5 °C**

**dNP•AO•Dox** (3 mg NP/mL in PBS) was incubated at 37.5 °C for 18 min.

Drug release study was conducted in similar fashion as stated above.

### **AMF-induced drug cytotoxicity in MCF-7 cells**

Human breast cancer cells (MCF-7) were purchased from American Type Culture Collection (VA, USA). Cells were plated in 30 mm dishes at  $\sim 4 \times 10^5$  cells/dish, and then grown up to 50-60% confluency in DMEM, 1% Pennstrep (Mediatech, Inc, VA) and 10% FBS (Valley Biomedical, Winchester, VA).

Stock solutions of the nanoparticle formulations **NP•AO**, **dNP•AO•Dox**, **sNP•AO•Dox**, and **NP•Dox**, were prepared in PBS 1X buffer solution at a uniform  $\text{Fe}_3\text{O}_4$  concentration of 1 mg/mL. To the MCF-7 cells maintained at 37.5 °C were added specific doses (0.1, 0.25 mg or 0.5 mg) of the NP formulations. The required volume of NP formulation was first diluted to 2 mL in DMEM containing 10% FBS. The media was removed and NP formulations were added to the cells. After 1 h of incubation with NP formulation at 37 °C, cells were exposed to a continuous AMF for 15 min using same parameters as described above. **Dox•HCl** (0.5  $\mu\text{mol}$ ) and **Dox•AO** (0.5  $\mu\text{mol}$ ) served as positive controls. Untreated (no NP formulation added) cells were also exposed to an AMF. Cells were also treated with NP formulations but not exposed to an AMF; these served as another control group for the experiment. After AMF exposure, the cells were incubated at 37.5 °C for 48 h. The media was then removed and the cells were trypsinized by adding 500  $\mu\text{L}$  trypsin to each well and incubated for 5 min at 37.5 °C. Trypsin was neutralized by DMEM containing 10% FBS, and then 10  $\mu\text{L}$  of extract from each well was mixed with 10  $\mu\text{L}$  of trypan blue. Dead and live cells were counted under an inverted microscope to determine the percentage cell viability using a hemocytometer.

### **Fluorescence imaging of MCF-7 cells**

A cytotoxicity experiment was performed exactly as described above on MCF-cells using the NP drug formulations. After 6 h of treatment media was removed and 1 ml of 1X-PBS was added to each dish. Then fluorescence images of cells were taken using a fluorescence microscopy (ex/em: 480/590 nm, EVOS, Advance Microscopy Group, WA).



## REFERENCES

1. <http://nihroadmap.nih.gov/nanomedicine/>
2. Moghimi, S. M.; Hunter, A. C.; Murray, J. C. *FASEB J.* **2005**, *19*, 311-330.
3. You, J.; Zhang, G.; Li, C. *ACS Nano* **2010**, *4*, 1033-1041.
4. Gupta, A. K.; Curtis, A. S. G. *Biomaterials* **2004**, *25*, 3029-3040.
5. Mahmoudi, M.; Simchi, A.; Milani, A. S.; Stroeve, P. *J. Colloid Interface Sci.* **2009**, *15*, 510-518.
6. Unger, C.; Haring, B.; Medinger, M.; Dreves, J.; Steinbild, S.; Kratz, F.; Mross, K. *Clin. Cancer Res.* **2007**, *13*, 4858-4866.
7. Moroz, P.; Jones, S. K.; Gray, B. N. *Int. J. Hyperthermia* **2002**, *18*, 267-284.
8. Maeng, Hee J.; Lee, Daneg. D.; Jung, Hee. K.; Bae, Y.; Park, Inn-S.; Jeong, S.; Jeon, Sun-Y.; Shim, Koo-C.; Kim, W.; Kim, J.; Lee, J.; Lee, Mee-L.; Kim, Hee-J.; Kim, Hong-W.; Hong, Sun-S. *Biomaterials* **2010**, *31*, 4995-5006.
9. Tran, N.; Webster, T. J. *J. Mater. Chem.* **2010**, *20*, 8760-8767.
10. Zhou, R.; Geiger, R. C.; Dean, D. A. *Expert Opinion in Drug Delivery* **2004**, *1*, 127-140.
11. Wiethoff, C. F.; Midaugh, C. R. *J. Pharm. Sci.* **2003**, *92*, 203-217.
12. Singer, S. J.; Nicolson, G. L. *Science* **1972**, *175*, 720-731.
13. Hickman, M.A.; Malone, R.W.; Lehmann, B.K.; Sih, T.R.; Knoell, D.; Szoka, F.C.; Walzem, R.; Carlson, D.M.; Powell, J.S. *Hum. Gene.Ther.* **1994**, *5*, 1477-1483.
14. Wolff, J.A.; Malone, R.W.; Williams, P.; Chong, W.; Acsadi, G.; Jani, A.; Felgner, P.L. *Science* **1990**, *247*, 1465-1468.
15. Yang, J.P.; Huang, L. *Gene Therapy* **1996**, *3*, 542-548.

16. Waehler, R.; Russell, S. J.; Curiel, D. T. *Nature Reviews Genetics* **2007**, *8*, 573-587.
17. Cavazzana-Calvo, M.; Hecein-Bey, S.; de Saint Basile, G.; Gross, F.; Yvon, E.; Nusbaum, P.; Selz, F.; Hue, C.; Certain, S.; Casanova, J.-L.; Bousso, P.; Deist, F. L.; Fischer, A. *Science* **2000**, *288*, 669-672.
18. Kochanek, S. *Hum. Gene Ther.* **1999**, *10*, 2451-2459.
19. Chirmule, N.; Probert, K.; Magosin, S.; Qian, Y.; Qian, R.; Wilson, J. *Gene Ther.* **1999**, *6*, 1574-1583.
20. Bett, A. J.; Haddara, W.; Prevec, L.; Graham, F. L. *Proc. Natl. Acad. Sci. USA* **1994**, *91*, 8802-8806.
21. Thomas, C. E.; Ehrhardt, A.; Kay, M. A. *Nature Rev. Genetics* **2003**, *4*, 346-358.
22. Young, L.S.; Searle, P. F.; Onion, D.; Mautner, V. *J. Pathol.* **2006**, *208*, 299-318.
23. Li, S.; Huang, L. *Gene Therapy* **2000**, *7*, 31-34.
24. Kodama, K.; Katayama, Y.; Shoji, Y.; Nakashima, H. *Curr. Med. Chem.* **2006**, *13*, 2155-2161.
25. Felgner, P. L.; Gadek, T.R.; Holm, M.; Roman, R.; Chan, H. W.; Wenz, M.; Northrop, J. P.; Ringold, G. M.; Danielsen, M. *Proc. Natl. Acad. Sci. USA* **1987**, *84*, 7413-7417.
26. Leventis, R.; Silviu, J. R.; *Biochim. Biophys. Acta* **1990**, *1023*, 124-132
27. Farood, H.; Serbina, N.; Huang, L. *Biochim. Biophys. Acta* **1995**, *1235*, 289-295.
28. McKenzie, D. L.; Smiley, E.; Kowk, K. Y.; Rice, K. G. *Bioconjugate Chem.* **2000**, *11*, 901-909.
29. Godbey, W. T.; Wu, K. K.; Mikos, A. G. *J. Biomed. Mater. Res.* **1999**, *45*, 268-275.
30. Haensler, J.; Szoka, F. C., Jr. *Bioconjugate Chem.* **1993**, *4*, 372-379.
31. Mansouri, S.; Lavigne, P.; Corsi, K.; Benderdour, M.; Beaumont, E.; Fernandes, J. C. *Eur. J. Pharm. Biopharm.* **2004**, *57*, 1-8.
32. Suh, J.; Paik, H.-J.; Hwang, B. K. *Bioorg. Chem.* **1994**, *22*, 318-327.

33. Ruponen, M.; Yla-Herttula, S.; Urtti, A. *Biochem. Biophys. Acta* **1999**, *1451*, 331-341.
34. Godbey, W. T.; Barry, M. A.; Saggiu, P.; Wu, K. K.; Mikos, A. G.; *J. Biomed. Mater. Res.* **2000**, *51*, 321-328.
35. Moghimi, S. M.; Symonds, P.; Murray, J. C.; Hunter, A. C.; Debska, G.; Szewczyk A. *Mol. Ther.* **2005**, *11*, 990-995.
36. Lv, H.; Zhang, S.; Wang, B.; Cui, S.; Yan, J. *J. Control Rel.* **2006**, *114*, 100-109.
37. Ghosh, P. S.; Kim, C. K.; Han, G.; Forbes, N. S.; Rotello, V. M. *ACS Nano* **2008**, *2*, 2213–2218.
38. Lee, Y.; Miyata, K.; Oba, M.; Ishii, T.; Fukushima, S.; Han, M.; Koyama, H.; Nishiyama, N.; Kataoka, K. *Angew.Chem. Int. Ed.* **2008**, *47*, 5163–5166.
39. Elbakry, A.; Zaky, A.; Liebk, R.; Rachel, R.; Goepferich, A.; Breunig, M. *Nano Lett.* **2009**, *9*, 2059-2064.
40. Giljohann, D. A.; Seferos, D. S.; Prigodich, A. E.; Patel, P. C.; Mirkin, C. A. *J. Am. Chem. Soc.* **2009**, *131*, 2072–2073.
41. Xia, T.; Kovoichich, M.; Liong, M.; Meng, H.; Kabehie, S.; George, S.; Zink, J. I.; Nel, A. E.; *ACS Nano* **2009**, *10*, 3273–3286.
42. Yiu, H. P.; McBain, S. C.; El Haj, A. J.; Dobson, J. *Nanotechnology* **2007**, *18*, 435601-435607
43. Cebria'n, V.; Yagúe, C.; Arruebo, M.; Saavedra,-F. M. M.; Santamara, J.; Vilaboa, N. *J. Nanopart. Res.* **2011**, *13*, 4097-4108.
44. Gemeinhart, R. A.; Luo ,D.; Saltzman, W. M.; *Biotechnol. Prog.* **2005**, *21*, 532–537.
45. Torney, F.; Trewyn, B. G.; Lin , V. S. Y.; Wang, K. *Nat. Nanotechnol.* **2005**, *2*, 295-300.
46. Yu, J.; Zhao, H.; Ye, L.; Yang, H.; Ku, S.; Yang, N.; Xiao, N. *J. Mater. Chem.* **2009**, *19*,1265-1270.
47. Ynachun, L; Tao, W.; Fangli, H.; Qian, L.; Dexi, Z.; Shuanglin, X.; Shengpei, S.; Jian, Z. *International Journal of Nanomedicine* **2011**, *6*, 721-727.
48. Bisht, S.; Bhakta, G.; Mitra, S.; Maitra, A. N. *Int. J. Pharm.* **2005**, *288*, 157-168.

49. Giger, Elisabeth V.; Puigmarti,-L. J.; Schlatter, R.; Castagner, B.; Dittrich, P. S.; Leroux, J.-C. *J. Controlled Rel.* **2011**, *150*, 87-93.
50. Zhou, C.; Yu, B.; Yang, X.; Huo, T.; Lee, L. J.; Barth, R. F.; Lee, R. J. *International Journal of Pharmaceutics* **2010**, *392*, 201-208.
51. Maitra, A. N. *Expert Review of Molecular Diagnostics* **2005**, *5*, 893-905.
52. Al-Jamal, K. T.; Gherardini, L.; Bardi, G.; Nunes, A.; Guo, C.; Bussy, C.; Herrero, M. A.; Bianco, A.; Prato, M.; Kostarelos, K.; Pizzorusso, T. *Proc. Natl. Acad. Sci. USA* **2011**, *108*, 10952-10957.
53. Mah, C.; Fraites, T.J. Jr.; Zolotukhin, I.; Song, S.; Flotte, T. R.; Dobson, J.; Batic, C.; Byrne, B. J. *Mol. Ther.* **2002**, *6*, 106-112.
54. Scherer F, Anton M, Schillinger U, Henke J, Bergemann C, Krüger. A, Gänsbacherand, B.; Plank, C. *Gene Ther.* **2002**, *9*, 102-109.
55. Mykhaylyk, O.; Antequera, Y. S.; Vlaskou, D.; Plank, C. *Nature Protocols* **2007**, *2*, 2391-2411.
56. Lee, J. H.; Lee, K.; Moon, S. H.; Lee, Y.; Park, T. G.; Cheon, J. *Angew. Chem. Int. Ed. Engl.* **2009**, *48*, 4174-4179.
57. Berry, C. C.; Wells, S.; Charles, S.; Curtis, A. S. *Biomaterials* **2003**, *24*, 4551-7455.
58. Li, Z.; Xiang, J.; Zhang, W.; Fan, S.; Wu, M.; Li, X.; Li, G. *Cancer Gene Ther.* **2009**, *16*, 423-429.
59. Gonzalez, B.; Ruiz-Hernandez, E.; Feito, M. J.; Lopez de Laorden, C.; Arcos, D.; Ramirez-Santillan, C.; Matesanz, C.; Portoles, M. T.; Vallet-Regi, M. *J. Mater. Chem.* **2011**, *21*, 4598-4604.
60. Kievit, F. M.; Veiseh, O.; Bhattarai, N.; Fang, C.; Gunn, J.W.; Lee, D.; Ellenbogen, R.G.; Olson, J. M.; Zhang, M. *Adv. Funct. Mater.* **2009**, *19*, 2244-2251.
61. Yiu, H. H.; McBain, S. C.; Lethbridge, Z. A.; Lees, M. R.; Dobson, J. *J. Biomed. Mater. Res., Part A* **2010**, *92*, 386-392.
62. Hashimoto, M.; Hisano, Y. *J. Neurosci. Methods* **2011**, *194*, 316-320.
63. Namiki, Y.; Namiki, T.; Yoshida, H.; Ishii, Y.; Tsubota, A.; Koido, S.; Nariai, K.; Mitsunaga, M.; Yanagisawa, S.; Kashiwagi, H.; Mabashi1, Y.; Yumoto1, Y.; Hoshina1, S.; Fujise, K.; Tada, N. *Nat. Nanotechnol.* **2009**, *4*, 598-606.

64. Song, H. P.; Yang, J. Y.; Lo, S. L.; Wang, Y.; Fan, W. M.; Tang, X. S.; Xue, J. M.; Wang, S. *Biomaterials* **2010**, *31*, 769-778.
65. Yang, S. Y.; Sun, J. S.; Liu, C. H.; Tsuang, Y. H.; Chen, L. T.; Hong, C. Y.; Yang, H. C.; Horng, H. E. *Artif. Organs* **2008**, *32*, 195-204.
66. Hashimoto, M.; Hisano, Y. *J. Neurosci. Methods* **2011**, *194*, 316-320.
67. Zhang, H.; Lee, M. Y.; Hogg, M. G.; Dordick, J. S.; Sharfstein, S. T. *ACS Nano* **2010**, *4*, 4733-4743.
68. Kami, D.; Takeda, S.; Itakura, Y.; Gojo, S.; Watanabe, M.; Toyoda, M. *Int. J. Mol. Sci.* **2011**, *12*, 3705-2722.
69. Huth, S.; Lausier, J.; Gersting, S. W.; Rudolph, C.; Plank, C.; Welsch, U.; Rosenecker, J. *J. Gene Med.* **2004**, *6*, 923-936.
70. van der Zee, J. *Annals of Oncology* **2002**, *13*, 1173-1184.
71. Hildebrandt B, Wust P, Ahlers O. *Critical Reviews in Oncology/Hematology* **2002**, *43*, 33-56.
72. Jordon, A.; Scholz, R.; Wust, P.; Fähling, H.; Felix, R. *J. Magn. Magn. Mater.* **1999**, *210*, 413-419.
73. Overgaard, J. *Hyperthermic Oncology* **1985**, *2*, 3-8.
74. Hofer, K. G. *Eur. Cell.* **2002**, *3 (suppl. 2)*, 67-69.
75. Dubois, J. B. *Bul Cancer/Radiother.* **1995**, *82*, 207-224.
76. Mornet, S.; Vasseur, S.; Grasset, F.; Duguet, E. *J. Mater. Chem.* **2004**, *14*, 2161-2175.
77. Gel'vich, E. A.; Mazokhin, V. N. *Crt. Rev. Biomed. Eng.* **2001**, *29*, 77-97.
78. Hill, D. A. *Bioelectromagnetics* **1985**, *6*, 33-40.
79. Moroz, P.; Jones, S. K.; Gray, B. N. *Int. J. Hyperthermia* **2002**, *18*, 267-284.
80. Wust, P.; Gneveckow, U.; Johannsen, M.; Böhmer, D.; Henkel, T.; Kahmann, F.; Schouli, J.; Felix, R.; Ricke, J.; Jordan, A. *Int. J. Hyperthermia* **2006**, *22*, 673-685.
81. Zhao, L.; Tang, J.; Feng, S.-S. *Nanomedicine* **2010**, *5*, 1305-1308.

82. Akira, I.; Takeshi, K. *Thermal Med.* **2008**, *24*, 113-129.
83. Chaubey, J.; Bajpai, A. K. *J. Mater. Sci.: Mater. Med.* **2010**, *21*, 1573-1586.
84. Bikram, M.; Gobin, A. M.; Whitmire, R. E.; West, J. L. *J. Control Rel.* **2007**, *123*, 219-227.
85. Liu, T.-Y.; Hu, S.-H.; Liu, K.-H.; Shaiu, R.-S.; Liu, D.-M.; Chen, S.-Y. *Langmuir* **2008**, *24*, 13306-13311.
86. Brulé, S.; Levy, M.; Wilhelm, C.; Letourneur, D.; Gazeau, F.; Ménager, C.; Visage, C. L. *Adv. Mat.* **2011**, *23*, 287-290.
87. Liu, J.; Zhang, Y.; Wang, C.; Xu, R.; Chen, Z.; Gu, N. *J. Phys. Chem. C* **2010**, *114*, 7673-7679.
88. Hsu, M.-H.; Su, Y.-C. *Biomed. Microdevices* **2008**, *10*, 785-793.
89. Thomas, C. R.; Ferris, D. P.; Lee, J.-H.; Choi, E.; Cho, M. H.; Kim, E. Sook.; Stoddart, J. F.; Shin, J.-S.; Cheon, J.; Zink, J. I. *J. Am. Chem. Soc.* **2010**, *132*, 10623-10625.
90. Manome, Y.; Kunieda, T.; Wen, P. Y.; Koga, T.; Kufe, D. W.; Ohno, T. *Hum. Gene Ther.* **1998**, *9*, 1409-1417.
91. Gerner, E. W.; Hersh, E. M.; Pennington, M.; Tsang, T. C.; Harris, D.; Vasanwala, F.; Brailey, J. *Int. J. Hyperthermia* **2000**, *16*, 171-181.
92. Gossen, M.; Bujard, H. *Nucleic Acids Res.* **1993**, *21*, 4411-4412.
93. Hauck W.; Stanners, C. P. *J. Biol. Chem.* **1995**, *270*, 3602-3610.
94. Richards, C. A.; Austin, E. A.; Huber, B. E. *Hum. Gene Ther.* **1995**, *6*, 881-893.
95. Huang, Q.; Hu, J. K.; Lohr, F.; Zhang, L.; Braun, R.; Lanzen, J.; Little, J. B.; Dewhirst, M. W.; Li, C.-Y. *Cancer Res.* **2000**, *60*, 3435-3429.
96. Hallahan, D. E.; Mauceri, H. J.; Seung, L. P.; Dunphy, E. J.; Wayne, J. D.; Hanna N. N.; Toledano, A.; Hellman, S.; Kufe, D. W.; Weichselbaum, R. R. *Nat. Med.* **1995**, *1*, 786-791.
97. Takahashi T.; Namiki, Y.; Ohno, T. *Hum. Gene Ther.* **1997**, *8*, 827-833.
98. Lindquist, S.; Craig, E. A. *Annu. Rev. Genet.* **1988**, *22*, 631-677.

99. Gerner, E. W.; Hersh, E. M.; Pennington, M.; Tsang, T. C.; Harris, D.; Vasanwala, F.; Brailey, J. *Int. J. Hyperthermia* **2000**, *16*, 171-181.
100. Walther, W.; Stein, U.; Schlag, P. *Int. J. Cancer*. **2002**, *98*, 291-296.
101. Verkis, A.; Maurange, C.; Moonen, C. T. W.; Mazurier, F.; Verneuil De. H.; Canioni, P.; Voisin, P. *The Journal of Gene Medicine* **2002**, *2*, 89-96.
102. Guilhon, E.; Voisin, P.; Zwart, de. J. A.; Quesson, B.; Salomir, R.; Maurange, C.; Bouchaud, V.; Smirnov, P.; Verkis, A.; Canioni, P.; Moonen, C. T. W. *The Journal of Gene Medicine* **2003**, *5*, 333-342.
103. Smith, R. C.; Machluf, M.; Bromley, P.; Atala, A.; Walsh, K. *Hum. Gene. Ther.* **2002**, *13*, 697-706.
104. Ito, A.; Shinkai, M.; Honda, H.; Kobayashi, T. *Cancer Gene Ther.* **2001**, *8*, 649-654.
105. Tang, Q.; Zhang, D.; Cong, X.; Wan, M.; Jin, L. *Biomaterials* **2008**, *29*, 2673-2679.
106. Marcaurette, L. A.; Shin, Y.; Goon, S.; Bertozzi, R. C. *Org. Lett.* **2001**, *3*, 3691-3694.
107. Gajewiak, J.; Cai, S.; Shu, X. Z.; Prestwich, G. D. *Biomacromolecules* **2006**, *7*, 1781-1789.
108. Surkau, G.; Böhm, K. J.; Müller, K.; Prinz, H. *Eur. J. Med. Chem.* **2010**, *45*, 3354-3364.
109. Choong, I. C.; Ellman, J. A. *J. Org. Chem.* **1999**, *64*, 6528-6529.
110. Figgitt, D. P.; McClellan, K. J. *Drugs* **2000**, *60*, 925-954.
111. Cho, H.; Daniel, T.; Buechlera, Y. J.; Litzinger, D. C.; Maioa, Z.; Putnama, A.-M. H.; Kraynov, V. S.; Sim, B. C.; Bussell, S.; Javahishvili, T.; Kaphle, S.; Viramontes, J.; Onga, M.; Chu, S.; Lieu, R.; Knudsen, N.; Castiglioni, P.; Norman, T. C.; Axelrod, D. W.; Hoffman, A. R.; Schultz, P. G.; DiMarchi, R. D.; Kimmel, B. E. *Proc. Natl. Acad. Sci. USA*, **2011**, *108*, 9060-9065.
112. Biswas, S.; Huang, X.; Badger, W. R.; Nantz, M. H.; *Tetrahedron Lett.* **2010**, *51*, 1727-1729.
113. Grochowski, E.; Jurczak, J. *Synthesis* **1976**, 682-684.
114. El-Sakhawy, M.; Milichovsky, M. *Polym. Int.* **2000**, *49*, 839-844.

115. Inoue, M.; Akimaru, J.; Nishikawa, T.; Seki, N.; Yamada, H. *Biotechnol. Appl. Biochem.* **1998**, *28*, 207-213.
116. Hauck, E. S.; Zou, S.; Scarfo, K.; Nantz, M. H.; Hecker, J. G. *Mol. Ther.* **2008**, *16*, 1857-1864.
117. Biswas, S.; Knipp, R. J.; Gordon, L. E.; Nandula, S. R.; Gorr, S.-U.; Clark, G. J.; Nantz, M. H. *ChemMedChem* **2011**, *6*, 2063-2069.
118. Hong, X.; Guo, W.; Yuan, H.; Li, J.; Liu, Y.; Ma, L.; Bai, Y.; Li, T. *J. Mag. Mag. Mat.* **2004**, *269*, 95-100.
119. Mikhaylova, M.; Kim, D. K.; Bobrysheva, N.; Osmolowsky, M.; Semenov, V.; Tsakalakos, T.; Muhammed, M. *Langmuir* **2004**, *20*, 2472-2477.
120. Nantz, M. H.; Dicus, C. W.; Hilliard, B.; Yellayi, S.; Zou, S.; Hecker, G.J. *Molec. Pharm.* **2010**, *7*, 786-794.
121. Hecker, G. J.; Berger, G. O.; Scarfo, K. O.; Zou, S.; Nantz, M. H. *ChemMedChem* **2008**, *3*, 1356-1361.
122. Zhu, J.; Munn, R. J.; Nantz, M. H.; *J. Am. Chem. Soc.* **2000**, *122*, 2645-2646.
123. Carmona, S.; Jorgensen, M. R.; Kolli, S.; Crowther, C.; Salazar, F. H.; Marion, P. L.; Fujino, M.; Natori, M.; Thanou, M.; Arbuthnot, P.; Miller, A. D. *Molec. Pharm.* **2009**, *6*, 706-717.
124. Cutler, J. I.; Zheng, D.; Xu, X.; Giljohann, D. A.; Mirkin, C. A. *Nano. Lett.* **2010**, *10*, 1477-1480.
125. Green, J. J.; Chiu, E.; Leshchiner, E. S.; Shi, J.; Langer, R.; Anderson, D. G. *Nano. Lett.* **2007**, *7*, 874-879.
126. Felgner, P. L.; Gadek, T. R.; Holm, M.; Roman, R.; Chan, H. W.; Wenz, M.; Northrop, J. P.; Ringold, G. M.; Danielsen, M. *Proc. Natl. Acad. Sci. USA* **1987**, *84*, 7413-7417.
127. Wasungu, L.; Hoekstra, D.; *J. Controlled Release* **2006**, *116*, 255-264.
128. Mountain, A. *Trends Biotechnol.* **2000**, *18*, 119-128.
129. Thomas, C. E.; Ehrhardt, A.; Kay, M. A. *Nature Rev. Genetics* **2003**, *4*, 346-358.
130. Young, L.S.; Searle, P.F.; Onion, D.; Mautner, V. *J. Pathol.* **2006**, *208*, 299-318.



131. Li, S.; Huang, L. *Gene Ther.* **2000**, *7*, 3-34.
132. Kodama, K.; Katayama, Y.; Shoji, Y.; Nakashima, H. *Curr. Med. Chem.* **2006**, *13*, 2155-2161.
133. Elouahabi, A.; Ruyschaert, J.-M. *Mol. Ther.* **2005**, *11*, 336-347.
134. Montier, T.; Benvegna, T.; Jaffrès, P. A.; Yaouanc, J. J.; Lehn, P. *Curr. Gene Ther.* **2008**, *8*, 296-312.
135. Ilarduya, Tros de. C.; Sun, Y.; Düzgünes, N. *Eur. J. Pharm. Sci.* **2010**, *40*, 159-170.
136. Niculescu-Duvaz, D.; Heyes, J.; Springer, C. J. *Curr. Med. Chem.* **2003**, *10*, 1233-1261.
137. Ewert, K.; Slack, N.L.; Ahmad, A.; Evans, H. M; Lin, A. J.; Samuel, C. E.; Safinya, C. R.; *Curr. Med. Chem.* **2004**, *11*, 133-149.
138. Balasubramaniam, R. P.; Bennett, M. J.; Aberle, A. M.; Malone, G. J.; Nantz, M. H.; Malone, R. W. *Gene Ther.* **1996**, *3*, 163-172.
139. Zhu, J.; Munn, R. J.; Nantz, M. H.; *J. Am. Chem. Soc.* **2000**, *122*, 2645-2646.
140. Chen, H.; Zhang, H.; McCallum, C. M; Szoka, F. C.; Guo, X. *J. Med. Chem.* **2007**, *50*, 4269-4278.
141. Liu, D.; Qiao, W.; Li, Z.; Chen, Y.; Cui, X.; Li, K.; Yu, L.; Yan, K.; Zhu, L.; Guo, Y.; Cheng, L. *Chem. Biol. Drug Des.* **2008**, *71*, 336-344.
142. Byk, G.; Dubertret, C.; Escriou, V.; Frederic, M; Jaslin, G.; Rangara, R.; Pitard, B.; Crouzet, J.; Wils, P.; Schwartz, B.; Scherman, D. *J. Med. Chem.* **1998**, *41*, 224-235.
143. Savva, M.; Chen, P.; Aljaberi, A.; Selvi, B.; Spelios, M. *Bioconjugate Chem.* **2005**, *16*, 1411-1422.
144. Guénin, E.; Hervé, A.-C.; Floch, V. V.; Loisel, S.; Yaouanc, J.-J.; Clément, J.-C.; Férec, C.; Abbayes, des H. *Angew. Chem. Int. Ed.* **2000**, *39*, 629-631.
145. Perouzel, E.; Jorgensen, M, R.; Keller, M.; Miller, A. D.; *Bioconjugate Chem.* **2003**, *14*, 884-898.
146. Carmona, S.; Jorgenson, M. R.; Kolli, S.; Crowther, C.; Salazar, F. H.; Marion, P. H.; Fujino, M.; Natori, Y.; Thanou, M.; Arbuthnot, P.; Miller, A. D. *Molec. Pharm.* **2009**, *6*, 706-713.

147. Nantz, M. H.; Dicus, C. W.; Hilliard, B.; Yellayi, S.; Zou, S.; Hecker, J. G. *Mol. Pharm.* **2010**, *7*, 786-794.
148. Zou, S.; Scarfo, K. A.; Nantz, M. H.; Hecker, J. G. *Int. J. Pharm.* **2010**, *389*, 232-243.
149. Biswas, S.; Gordon, L. E.; Clark, G. J.; Nantz, M. H. *Biomaterials* **2011**, *32*, 2683-2688.
150. Hecker, J. G.; Berger, G. O.; Scarfo, K. O.; Zou, S.; Nantz, M. H. *ChemMedChem* **2008**, *3*, 1356-1361.
151. Biswas, S.; Huang, X.; Badger, W. R.; Nantz, M. H. *Tetrahedron Letters* **2010**, *51*, 1727-1729.
152. Chandrashekar, V.; Srujan, M.; Prabhakar, R.; Reddy, R. C.; Sreedhar, B.; Rentam, K. K. R.; Kanjilal, S.; Chaudhuri, A. *Bioconjugate Chem.* **2011**, *22*, 497-509.
153. Ewert, K.; Slack, N. L.; Ahmad, A.; Evans, H. M.; Lin, A. J.; Samuel, C. E.; Safinya, C. R. *Curr. Med. Chem.* **2004**, *11*, 133-149.
154. Je, J.-Y.; Cho, Y.-S.; Kim, S.-K. *Biomacromolecules* **2006**, *7*, 3448-3451.
155. Balasubramaniam, P.R.; Bennett, M. J.; Aberle, A. M.; Malone, J. G.; Nantz, M. H.; Malone, R. W. *Gene Ther.* **1996**, *3*, 163-172.
156. Fletcher, S.; Ahmad, A.; Perouzel, E.; Heron, A.; Miller, A. D.; Jorgensen, M. R. *J. Med. Chem.* **2006**, *49*, 349-357.
157. Fire, A.; Xu, S.; Montgomery, M. K.; Kostas, S. A.; Driver, S. E.; Mello, C. C. *Nature* **1998**, *391*, 806-811.
158. Elbashir, S. M.; Harborth, J.; Lendeckel, W.; Yalcin, A.; Weber, K.; Tuschl, T. *Nature* **2001**, *411*, 494-498.
159. McCaffrey, A. P.; Meuse, L.; Pham, T. T.; Conklin, D. S.; Hannon, G. J.; Kay, M. A. *Nature* **2002**, *418*, 38-39.
160. Whitehead, K. A.; Langer, R.; Anderson, D. A. *Nature Rev. Drug Discovery* **2009**, *8*, 129-138.
161. Frank-Kamenetsky, M. *et al.* *Proc. Natl Acad. Sci. USA* **2008**, *105*, 11915-11920.

162. Song, E; Lee, S.-K.; Wang, J.; Ince, N.; Ouyang, N.; Min, J.; Chen, J.; Shankar, P.; Lieberman, J. *Nature Med.* **2003**, *9*, 347-352.
163. Niu, X.-Y.; Peng, Z. L.; Duan, W. Q.; Wang, H.; Wang, P. *Int. J. Gynecol. Cancer* **2006**, *16*, 743-751.
164. Halder, J. *et al.* *Clin. Cancer Res.* **2006**, *12*, 4916-4924.
165. Takeshita, F.; Minakuchi, Y.; Nagahara, S.; Honma, J.; Sasaki, H.; Hirai, K.; Teratani, T.; Namatame, N.; Yamamoto, Y.; Hanai, K.; Kato, T.; Sano, K.; Ochiya, T. *Proc. Natl Acad. Sci. USA* **2005**, *102*, 12177-12182.
166. Yavuz, M. S.; Cheng, Y.; Chen, J.; Cobley, C. M.; Zhang, Q.; Rycenga, M.; Xie, J.; Kim, C.; Song, K. H.; Schwartz, A. G.; Wang, L. V.; Xia, Y. *Nature Materials* **2009**, *8*, 935-939.
167. Chen, J.; McLellan, J. M.; Siekkinen, A.; Xiong, Y.; Li, Z.-Y.; Xia, Y. *J. Am. Chem. Soc.* **2006**, *128*, 14776-14777.
168. Yang, J.; Lee, J.; Kang, J.; Oh, S. J.; Ko, H.-J.; Son, J.-H.; Lee, K.; Suh, J.-S.; Huh, M.-H.; Haam, S. *Advanced Materials* **2009**, *21*, 4339-4342.
169. You, J.; Zhang, G.; Li, C. *ACS Nano* **2010**, *2*, 1033-1041.
170. Zhao, L.; Tang, J.; Feng, S.-S. *Nanomedicine* **2010**, *5*, 1305-1308.
171. Akira, I.; Takeshi, K. *Thermal Med.* **2008**, *24*, 113-129.
172. Chaubey, J.; Bajpai, A. K. *J. Mater. Sci.: Mater. Med.* **2010**, *21*, 1573-1586.
173. Liu, T.-Y.; Hu, S.-H.; Liu, K.-H.; Shaiu, R.-S.; Liu, D.-M.; Chen, S.-Y. *Langmuir* **2008**, *24*, 13306-13311.
174. Liu, J.; Zhang, Y.; Wang, C.; Xu, R.; Chen, Z.; Gu, N. *J. Phys. Chem. C* **2010**, *114*, 7673-7679.
175. Hsu, M.-H.; Su, Y.-C. *Biomed. Microdevices* **2008**, *10*, 785-793.
176. Weiss, R. B. *Semin. Oncol.* **1992**, *19*, 670-686.
177. Lefrak, E. A.; Piha, J.; Rosenheim, S.; Gottlieb, J. A. *Cancer* **1973**, *32*, 302-314.
178. Thorburn, A.; Frankel, A. E. *Mol. Cancer Ther.* **2006**, *5*, 197-199.

179. Patil, R. P.; Guhagarkar, S. A.; Devarajan, P. V. *Critical Reviews in Therapeutic Drug Carrier Systems* **2008**, *25*, 1-61.
180. Desset, S.; Spalla, O.; Lixon, P.; Cabane, B. *Langmuir* **2001**, *17*, 6408-6418.
181. Cha, J. N.; Birkedal, H.; Euliss, L. E.; Bartl, M. H.; Wong, M. S.; Deming, T. J.; Stucky, G. D. *J. Am. Chem. Soc.* **2003**, *125*, 8285-8289.
182. Sehgal, A.; Lalatonne, Y.; Berret, J.-F.; Morvan, M. *Langmuir* **2005**, *21*, 9359-9364.
183. Berret, J.-F.; Schonbeck, N.; Gazeau, F.; Kharrat, D. E.; Sandre, O.; Vacher, A.; Airiau, M. *J. Am. Chem. Soc.* **2006**, *128*, 1755-1766.
184. Krüger, M.; Beyer, U.; Schumacher, P.; Unger, C.; Zahn, H.; Kratz, F. *Chem. Pharm. Bull.* **1997**, *45*, 399-401.
185. Thomas, C. J.; Ferris, D. P.; Lee, J.-H.; Choi, E.; Cho, M. H.; Kim, E. S.; Stoddart, J. F.; Shin, J.-S.; Cheon, J.; Zink, J. I. *J. Am. Chem. Soc.* **2010**, *132*, 10623-10625.
186. Akira, I.; Takeshi, K. *Thermal Med.* **2008**, *24*, 113-129.
187. Wust, P.; Gneveckow, U.; Johannsen, M.; Böhmer, D.; Henkel, T.; Kahmann, F.; Sehouli, J.; Felix, R.; Ricke, J.; Jordan, A. *Int. J. Hyperthermia* **2006**, *22*, 673-685.
188. Luo, Y.; Bernshaw, N. B.; Lu, Z-R.; Kopecek, J.; Prestwich, G. D. *Pharmaceutical Research* **2002**, *19*, 396-402.
189. Chambon, M. H.; Viratelle, O. M. *Anal. Biochem.* **1998**, *263*, 198-207.
190. Xiong, G.; Chen, Y.; Arriaga, E. D. *Anal. Chem.* **2005**, *77*, 3488-3493.
191. Humienik, M.-O. *Thermochimica Acta* **2001**, *378*, 102-112.
192. Horvath, I.; Lazar, Z.; Gyulai, N.; Kollai, M.; Losonczy, G. *Eur. Respir. J.* **2009**, *34*, 261-275.
193. Amann, A.; Spanel, P.; Smith, D. *Mini-Rev. Med. Chem.* **2007**, *7*, 115-129.
194. Peng, G.; Hakim, M.; Broza, Y. Y.; Billan, S.; Bortnyak, R.-A.; Kuten, A.; Tisch, A.; Haick, H. *Br. J. Cancer* **2010**, *103*, 542-551. (correct abbrev)
195. Fuchs, P.; Loeseken, C.; Schubert, J. K.; Miekisch, W. *Int. J. Cancer* **2010**, *126*, 2663-2670.

196. Poli, D.; Goldoni, M.; Corradi, M.; Acampa, O.; Carbognani, P.; Internullo, E.; Casalini, E.; Mutti, A. *J. Chromatogr., B: Anal. Technol. Biomed. Life Sci.* **2010**, *878*, 2643-2651.
197. Pauling, L. *Proc. Natl. Acad. Sci., U. S. A.* **1971**, *68*, 2374-2376.
198. Dragonieri, S.; Annema, J. T.; Schot, R.; van der Schee, M. P.; Spanevello, A.; Carratu, P.; Resta, O.; Rabe, K. F.; Sterk, P. J. *Lung Cancer* **2009**, *64*, 166-170.
199. Patterson, S. G.; Bayer, C. W.; Hendry, R. J.; Sellers, N.; Lee, K. S.; Vidakovic, B. *American Surgeon* **2011**, *77*, 747-751.
200. Buszewski, B.; Keszy, M.; Ligor, T.; Amann, A. *Biomed. Chromatogr.* **2007**, *21*, 553-566.
201. Phillips, M.; Altorki, N.; Austin, J. H. M.; Cameron, R. B.; Cataneo, R. N.; Kloss, R.; Maxfield, R. A.; Munawar, M. I.; Pass, H. I.; Rashid, A.; Rom, W. R.; Schmitt, P.; Wai, J. *Clin. Chim Acta*, **2008**, *393*, 76-84.
202. Fan, T. W.; Lane, A. N.; Higashi, R. M.; Farag, M. A.; Gao, H.; Bousamra, M.; Miller, D. M. *Mol. Cancer* **2009**, *8*, 41.
203. Lane, A. N.; Fan, T. W.; Bousamra, M.; Higashi, R. M.; Yan, J.; Miller, D. M. *OMICS* **2011**, *15*, 173-182.
204. Corradi, M.; Rubinstein, I.; Andreoli, R.; Manini, P.; Caglieri, A.; Poli, D.; Alinovi, R.; Mutti, A. *Am. J. Respir. Crit. Care Med.* **2003**, *167*, 1380-1386.
205. Esterbauer, H.; Schaur, R. J.; Zollner, H. *Free Radical Biol. Med.* **1991**, *11*, 81-128.
206. Weihinger, A.; Schmid, A.; Mechtcheriakov, S.; Ledochowski, M.; Grabmer, C.; Gastl, G.; Amann, A. *Int. J. Mass Spectrom.* **2007**, *265*, 49-59.
207. Schwarz, K.; Filipiak, W.; A. Amann, A. *J. Breath Res.* **2009**, *3*, 027002.
208. Riess, U.; Tegtbur, U.; Fauck, C.; Fuhrmann, F.; Markewitz, D.; Salthammer, T. *Anal. Chim. Acta* **2010**, *669*, 53-62.
209. Pysanenko, A.; Wang, T.; Spanel, P.; Smith, D. *Rapid Commun. Mass Spectrom.* **2009**, *23*, 1097-1104.
210. Spanel, P.; Smith, D. *Mass Spectrom. Rev.* **2011**, *30*, 236-267.
211. Arthur, C. L.; Pawliszyn, J. *Anal. Chem.* **1990**, *62*, 2145-2148.

212. Lin, Y.; Dueker, S. R.; Jones, A. D.; Ebeler, S. E.; Clifford, A. J. *Clin. Chem.* **1995** *41*, 1028-1032.
213. Voiculescu, I.; Zaghoul, M.; Harasimhan, N. *TrAC, Trends Anal. Chem.* **2008**, *27*, 327-343.
214. Trévisiol, E.; Defrancq, E.; Lhomme, J.; Laayoun, A.; Cros, P. *European Journal of Organic Chemistry* **2000**, *1*, 211-217.

## **APPENDIX A**

---

**A.1. Index of NMR Spectrums and Other Figures**

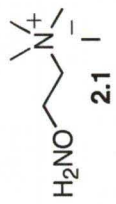
**A.2. NMR Spectra and Other Figures Obtained in Chapters  
2, 3, and 4**

---

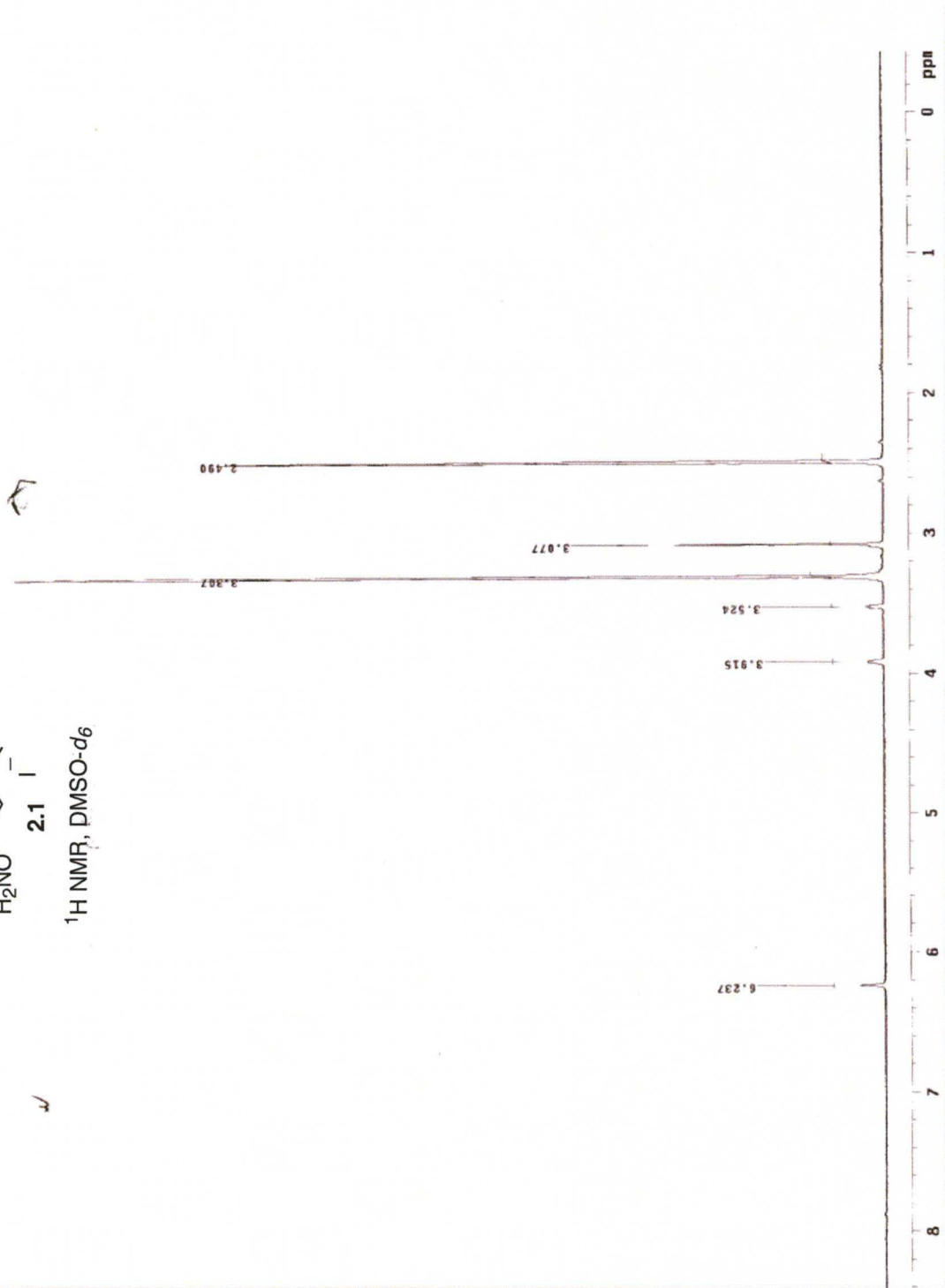
## A.1. Index of NMR Spectra and Other Figures

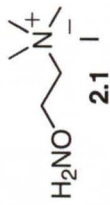
Compound	Description	Page
2.1	<sup>1</sup> H NMR Spectrum	160
	<sup>13</sup> C NMR Spectrum	161
2.2	<sup>1</sup> H NMR Spectrum	162
	<sup>13</sup> C NMR Spectrum	163
2.3	<sup>1</sup> H NMR Spectrum	164
	<sup>13</sup> C NMR Spectrum	165
3.1	<sup>1</sup> H NMR Spectrum	166
	<sup>13</sup> C NMR Spectrum	167
3.2	<sup>1</sup> H NMR Spectrum	168
	<sup>13</sup> C NMR Spectrum	169
3.3	<sup>1</sup> H NMR Spectrum	170
	<sup>13</sup> C NMR Spectrum	171
3.4	<sup>1</sup> H NMR Spectrum	172
	<sup>13</sup> C NMR Spectru	173
3.5	<sup>1</sup> H NMR Spectrum	174
3.6	<sup>1</sup> H NMR NMR Spectrum	175
Dox•AO	<sup>1</sup> H NMR Spectrum	176
	<sup>13</sup> C NMR Spectrum	177
Dox•HCl and Dox•AO	Microscopy images of MCF-7 cells treated with formulations	178
NPs	TEM micrograph	179
NPs	EDX spectra	179
dNP•AO•Dox	TEM micrograph	180



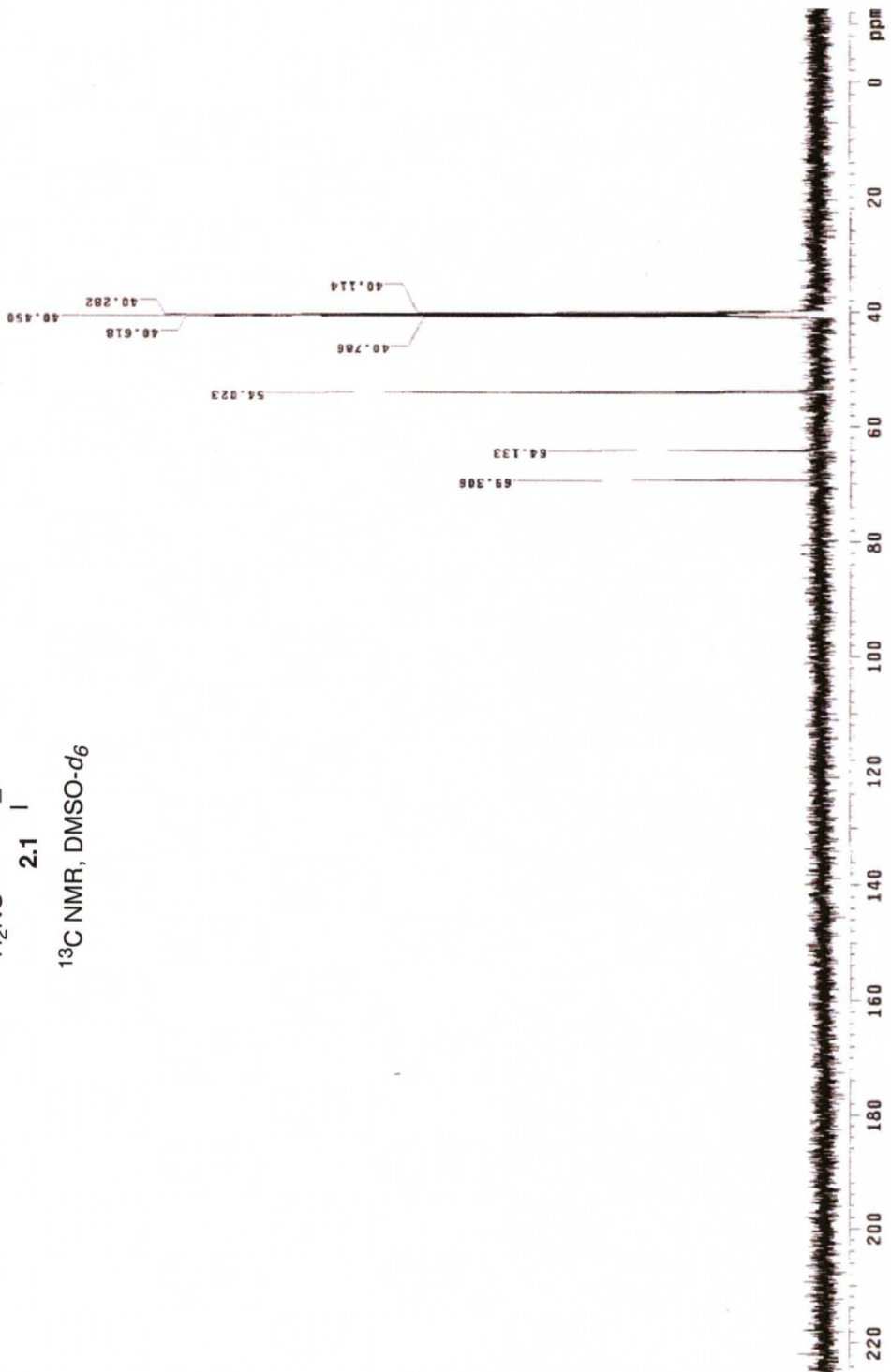


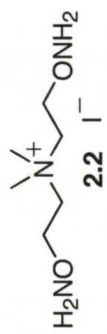
<sup>1</sup>H NMR, DMSO-d<sub>6</sub>



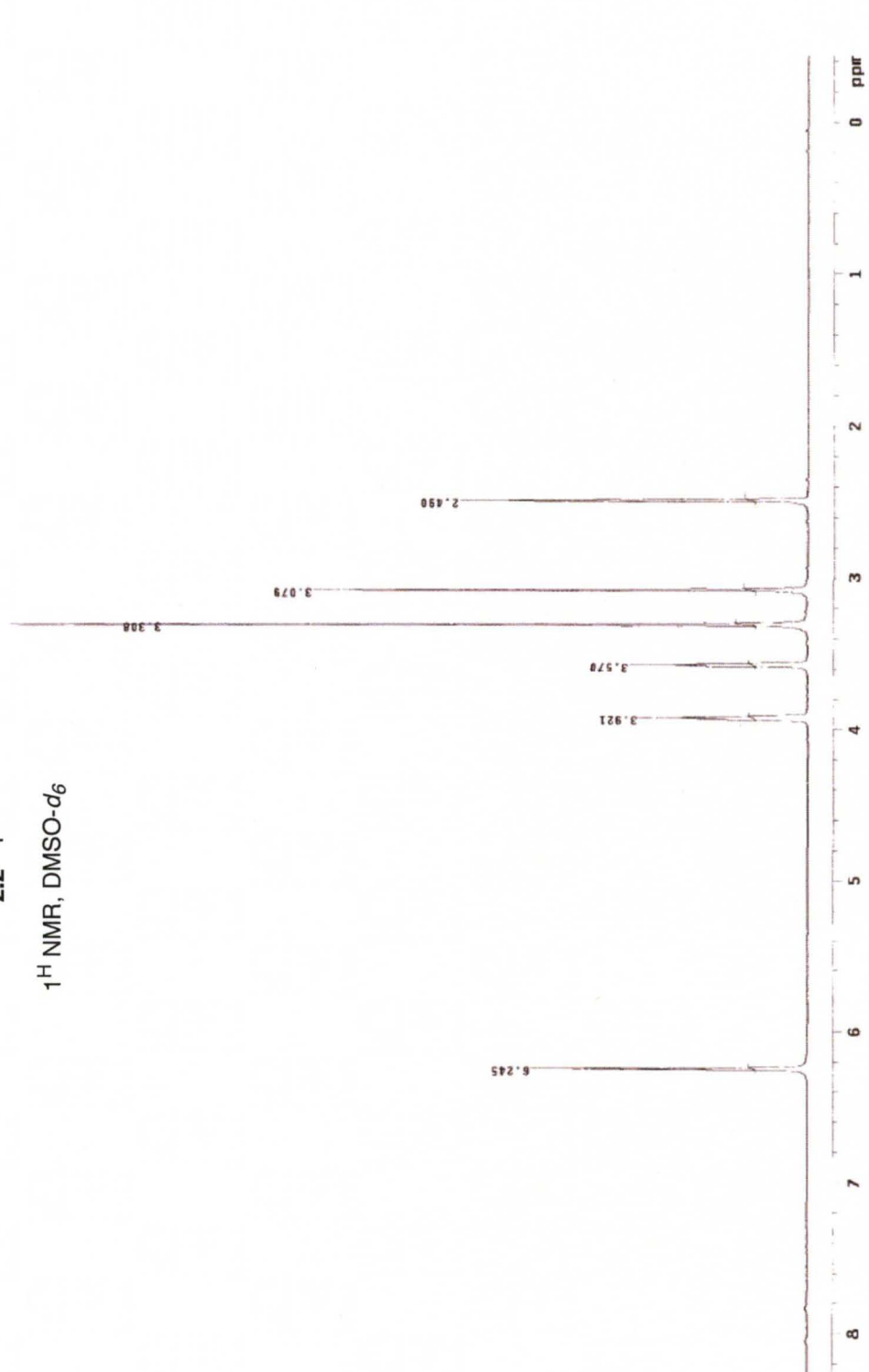


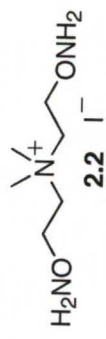
<sup>13</sup>C NMR, DMSO-d<sub>6</sub>



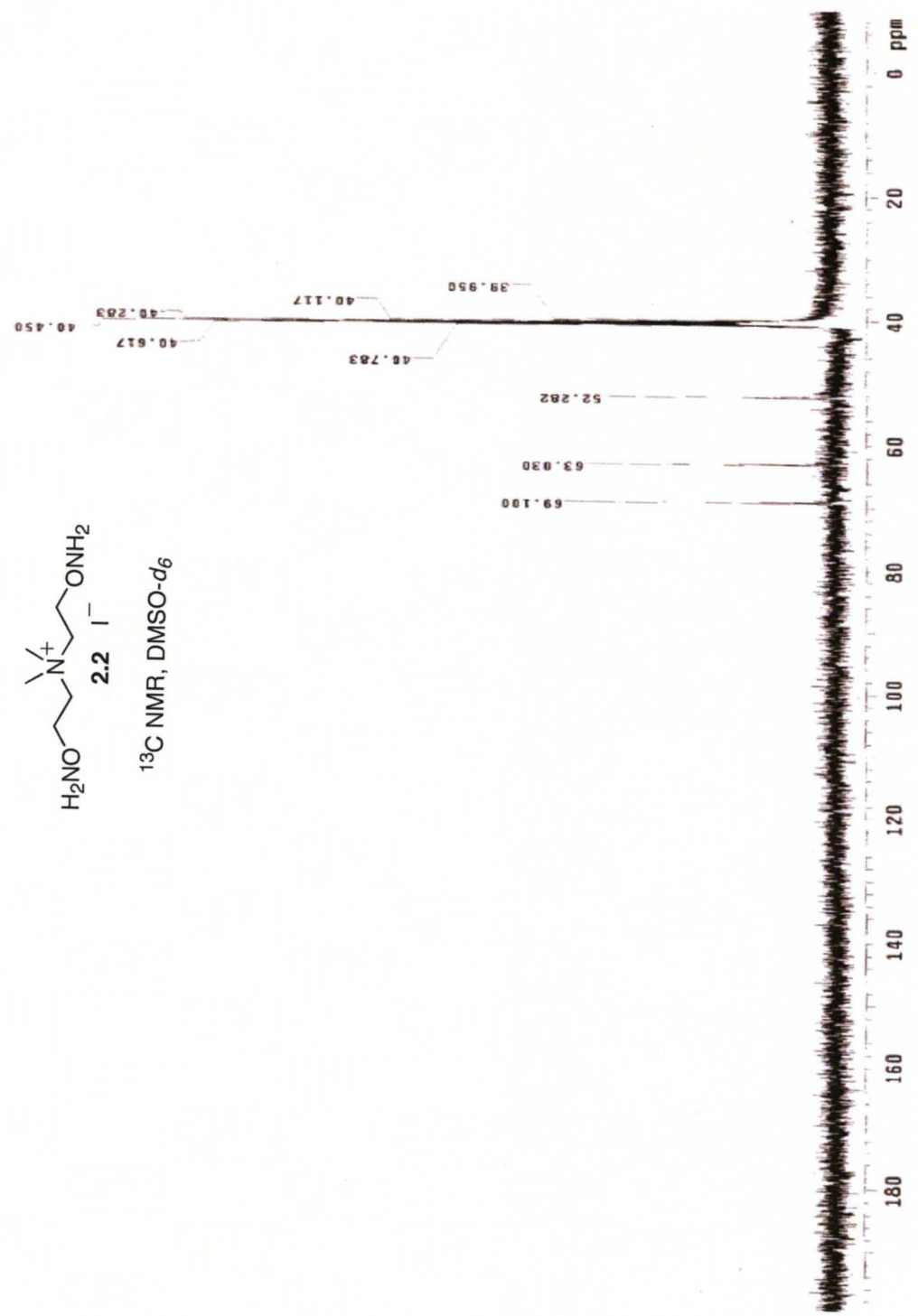


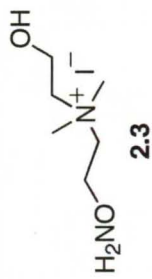
<sup>1</sup>H NMR, DMSO-d<sub>6</sub>



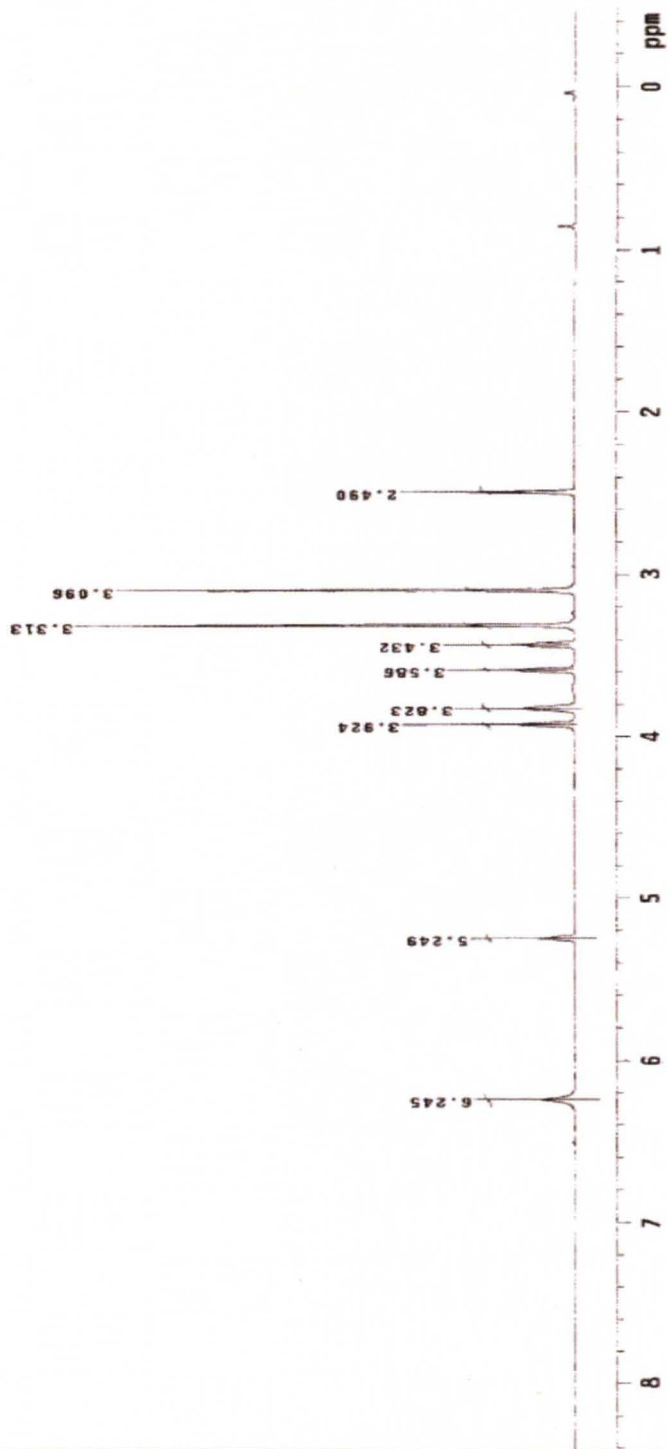


<sup>13</sup>C NMR, DMSO-d<sub>6</sub>





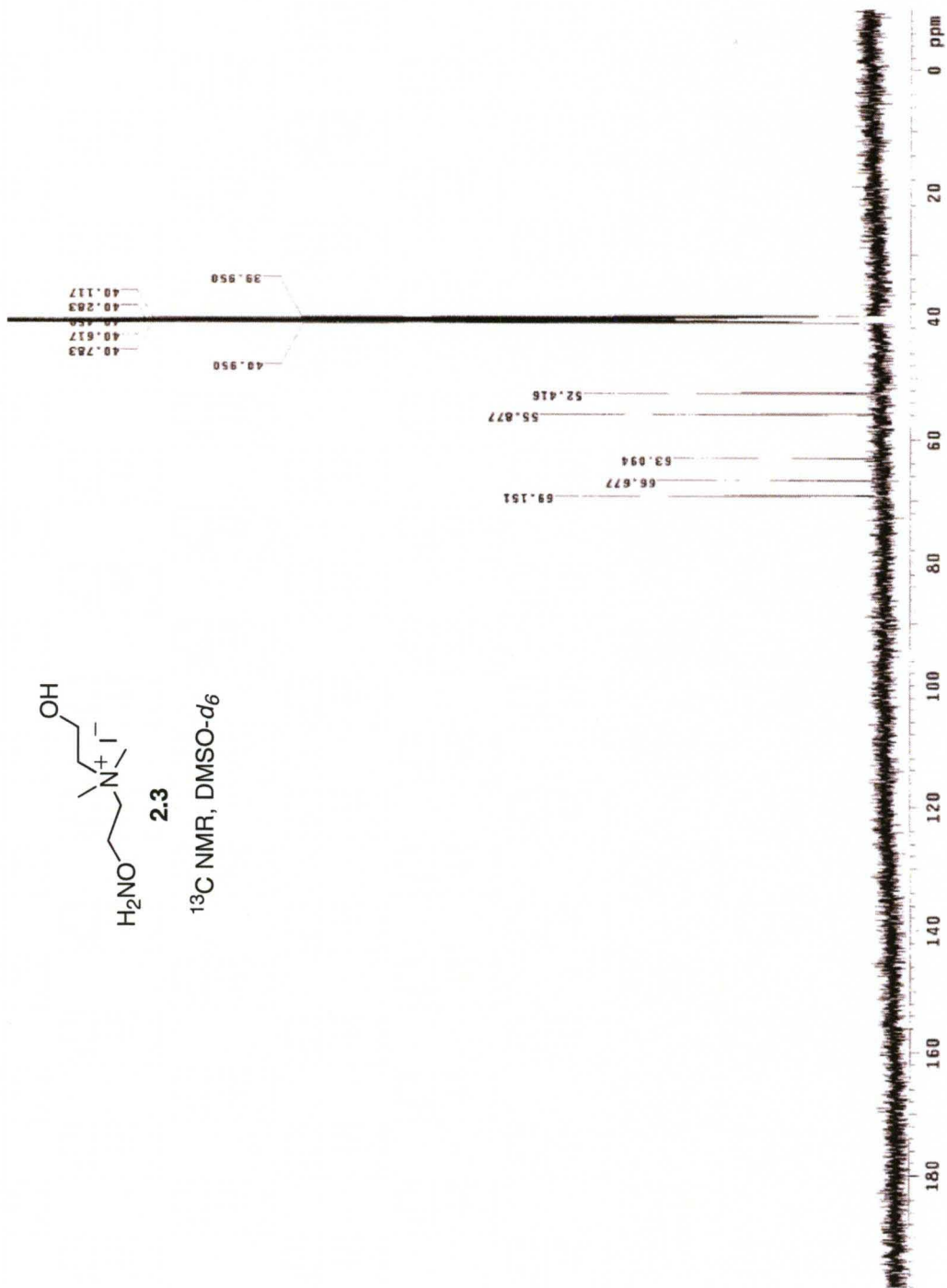
<sup>1</sup>H NMR, DMSO-d<sub>6</sub>

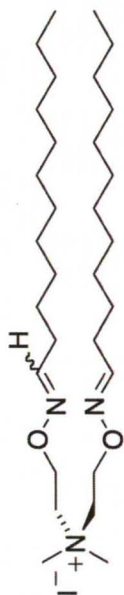




2.3

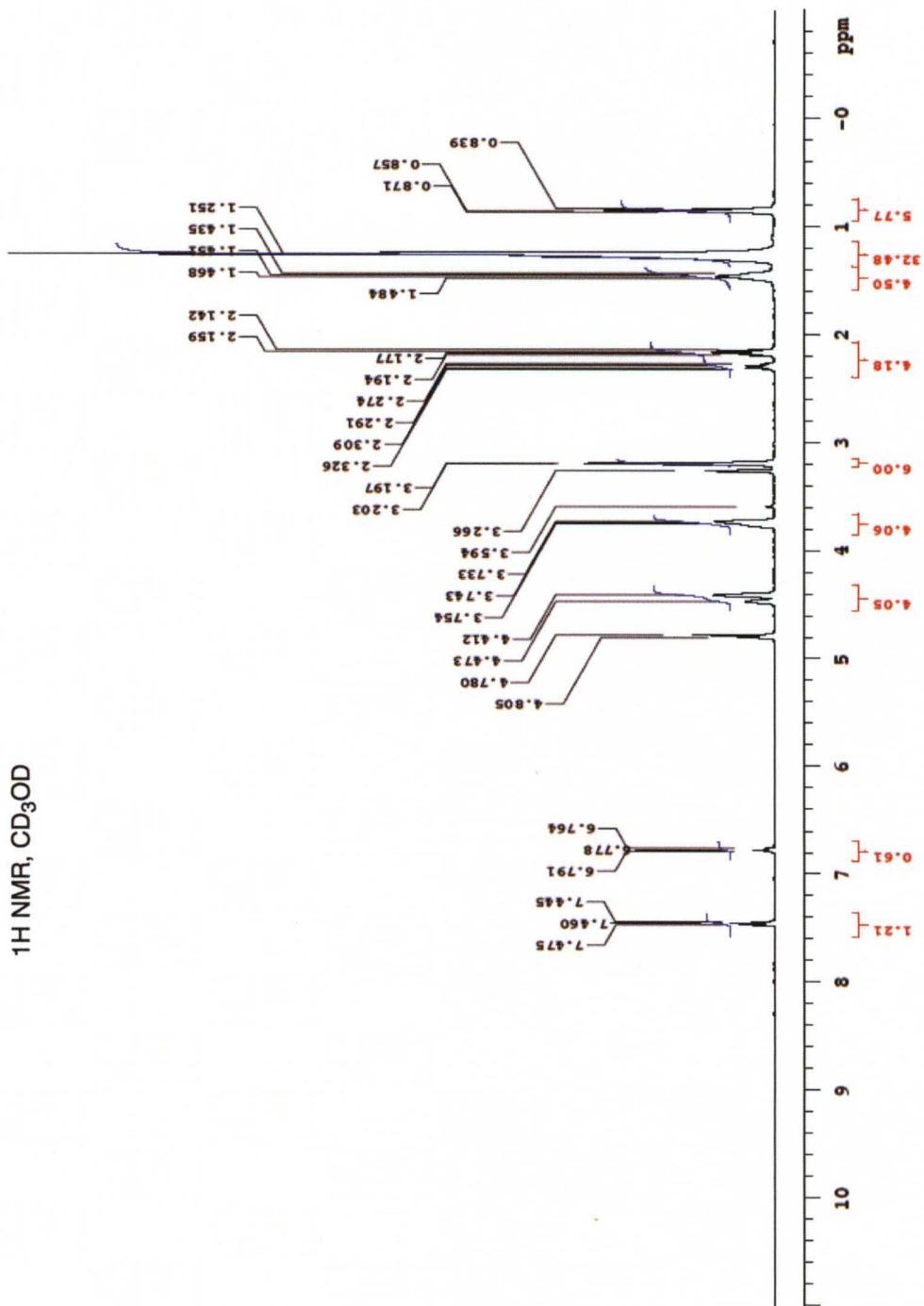
$^{13}\text{C}$  NMR,  $\text{DMSO-}d_6$

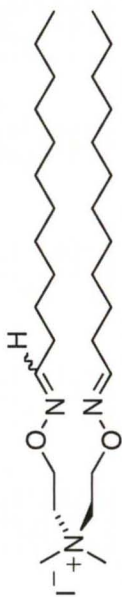




3.1

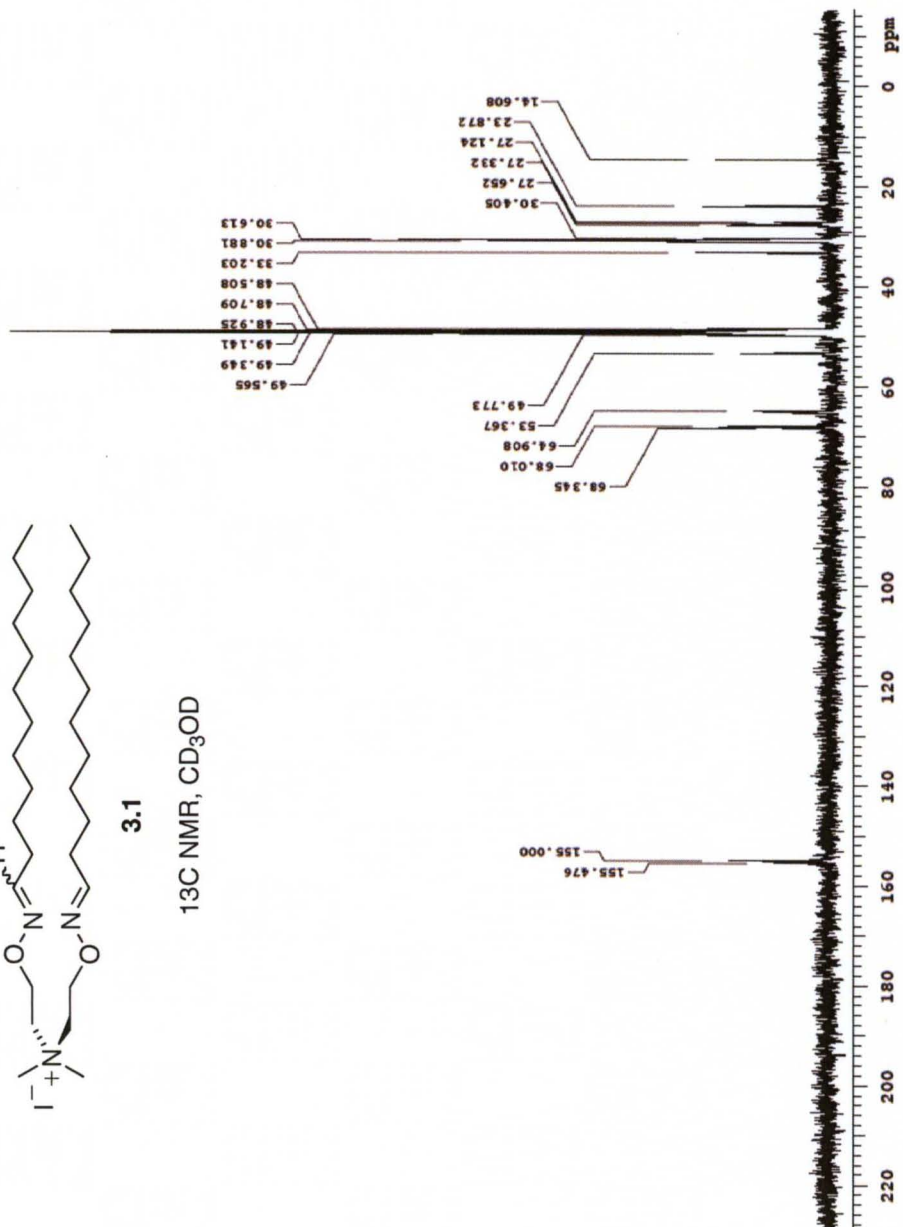
<sup>1</sup>H NMR, CD<sub>3</sub>OD



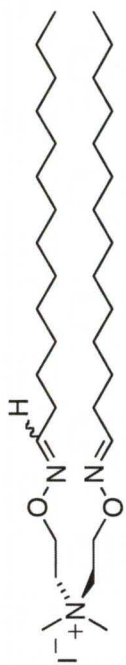


3.1

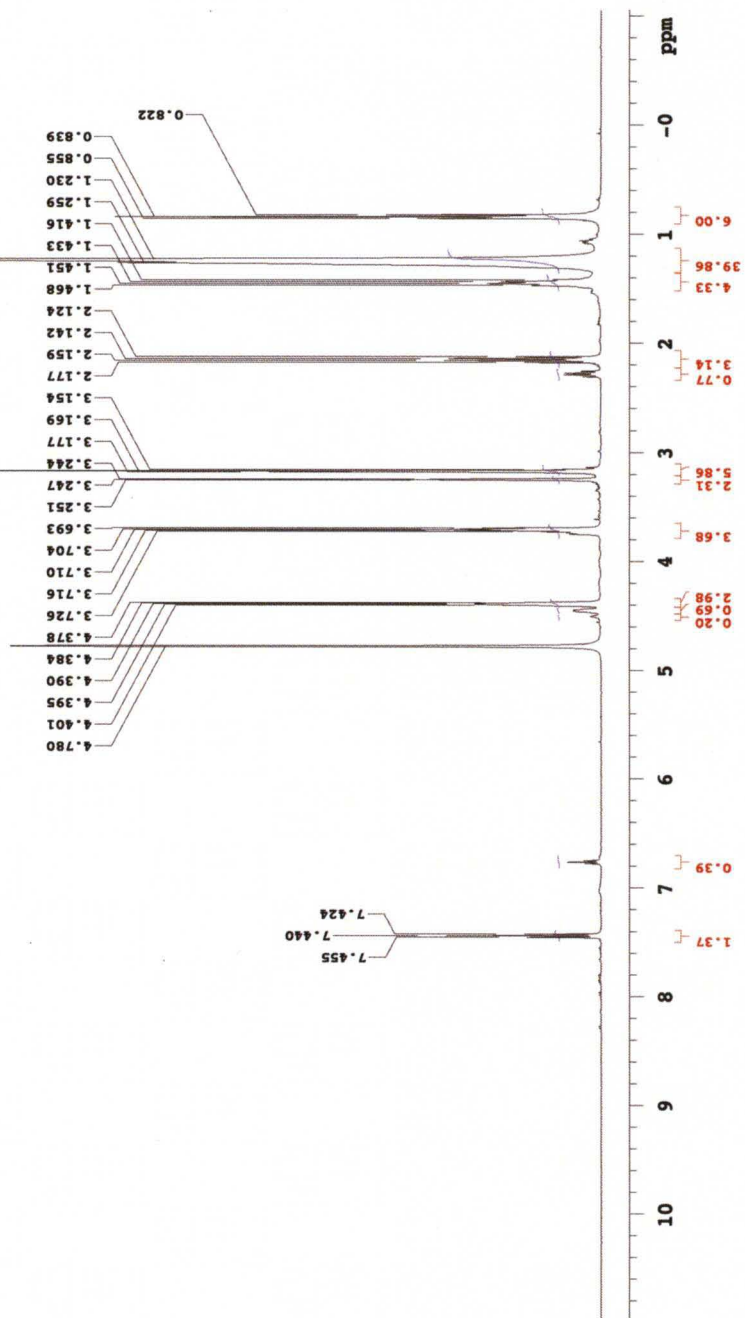
<sup>13</sup>C NMR, CD<sub>3</sub>OD

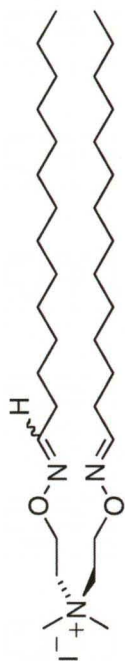




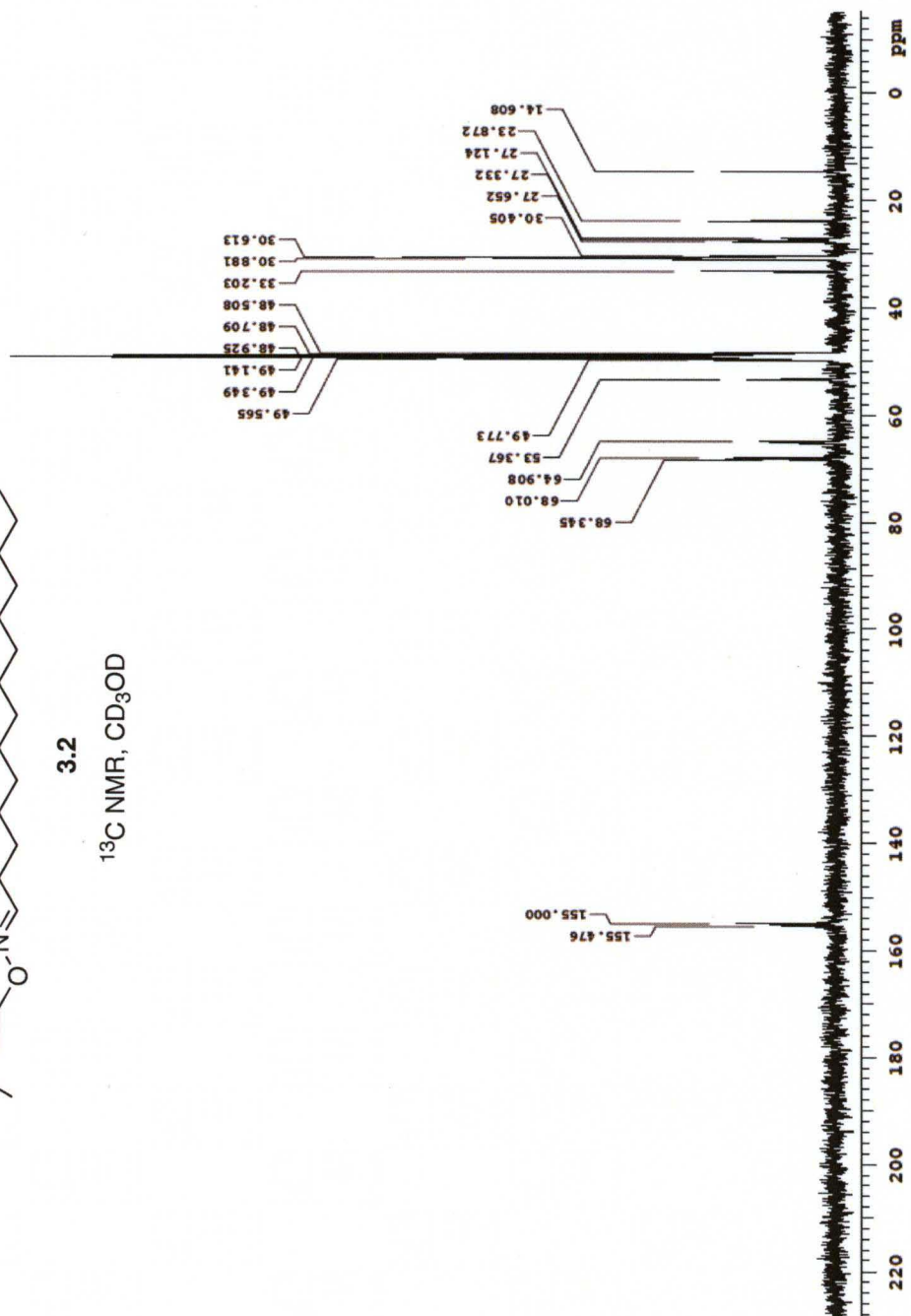


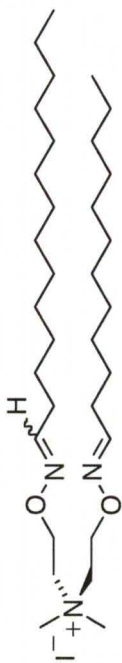
3.2  
<sup>1</sup>H NMR, CD<sub>3</sub>OD





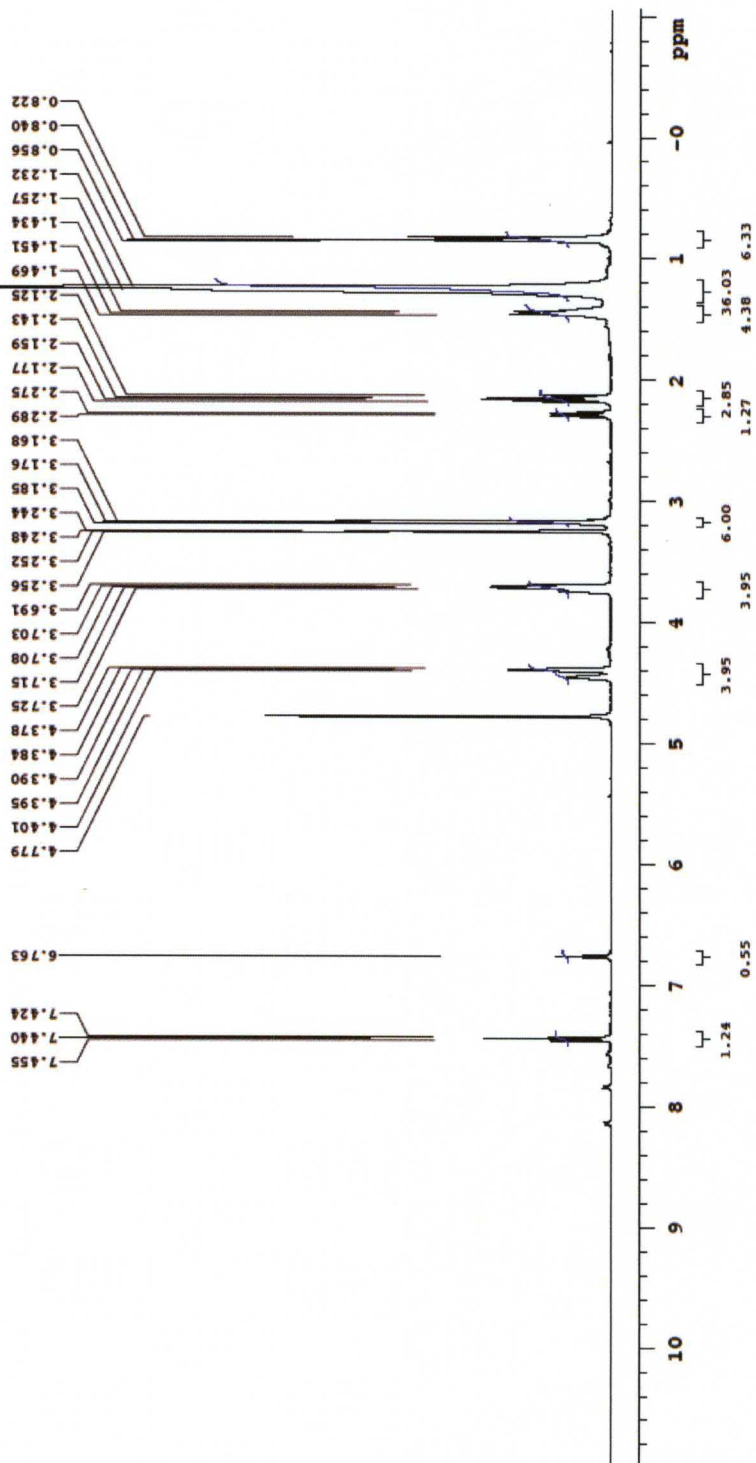
**3.2**  
 $^{13}\text{C}$  NMR,  $\text{CD}_3\text{OD}$

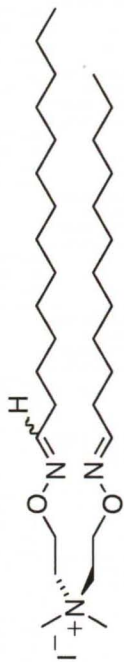




3.3

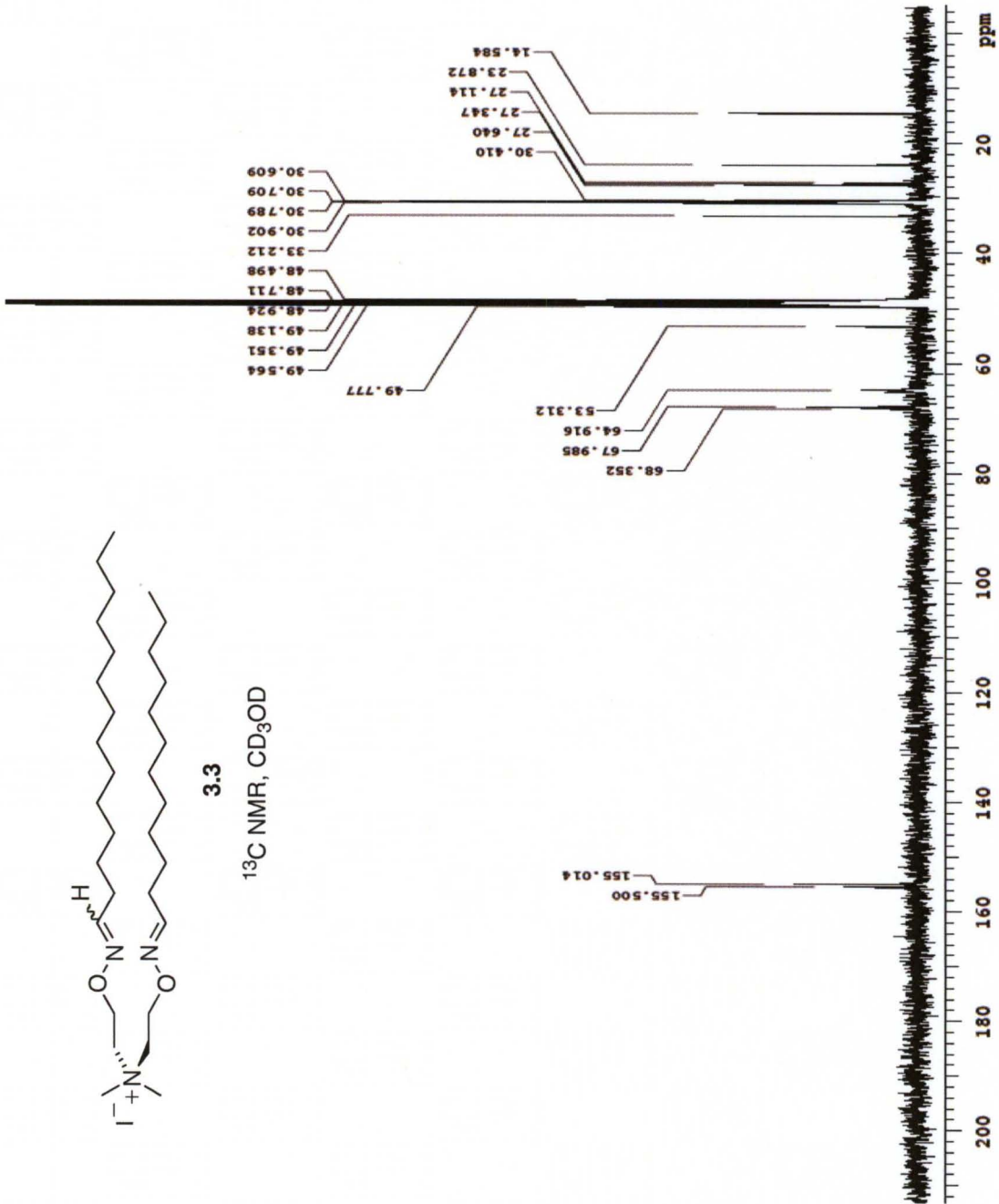
<sup>1</sup>H NMR, CD<sub>3</sub>OD

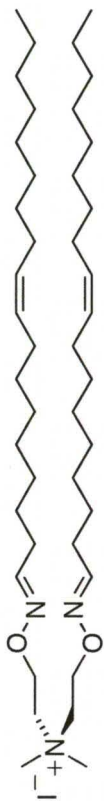




3.3

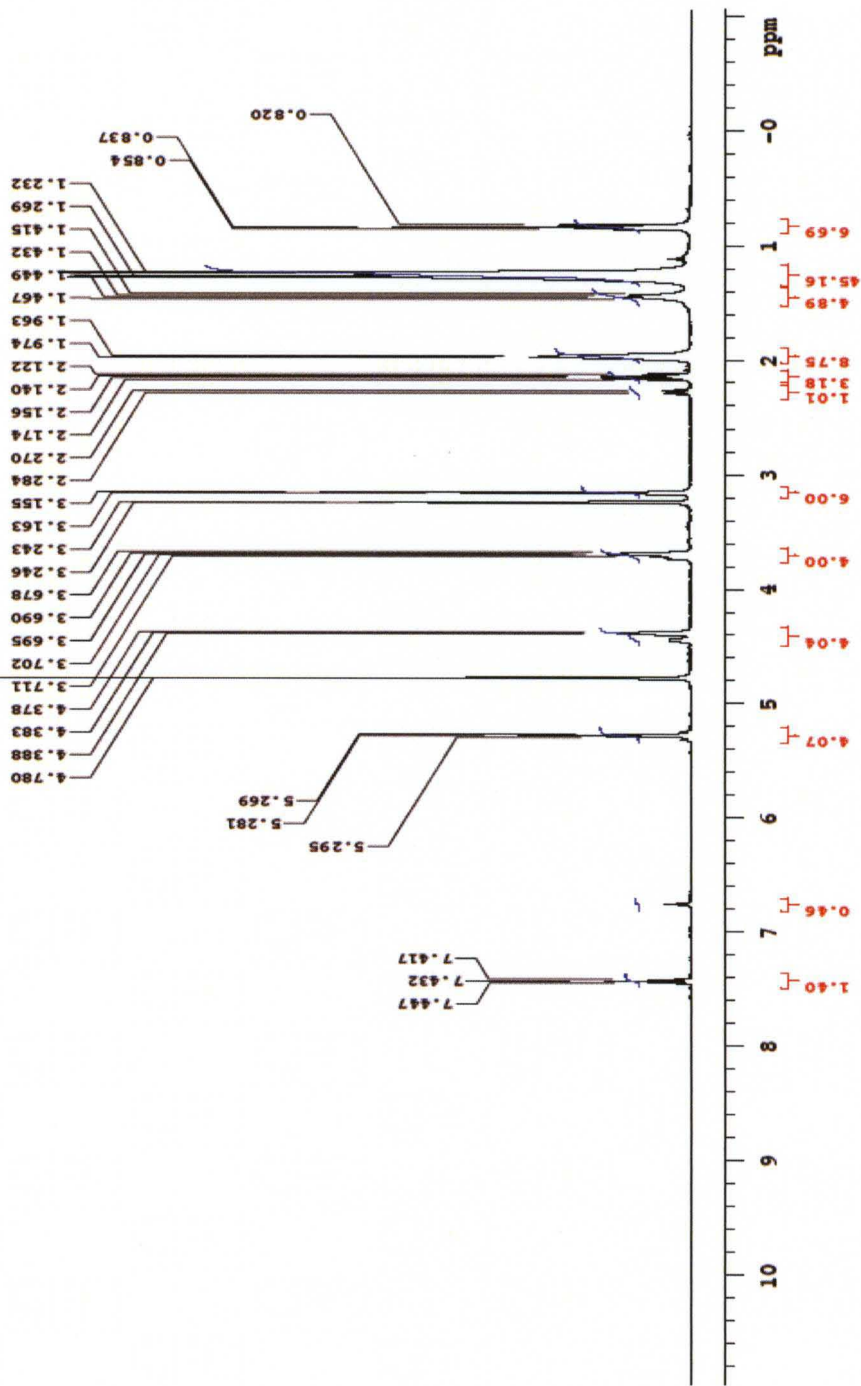
$^{13}\text{C}$  NMR,  $\text{CD}_3\text{OD}$

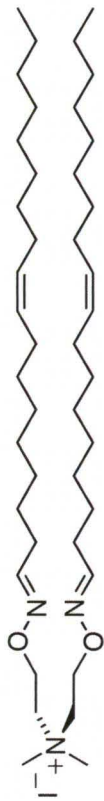




3.4

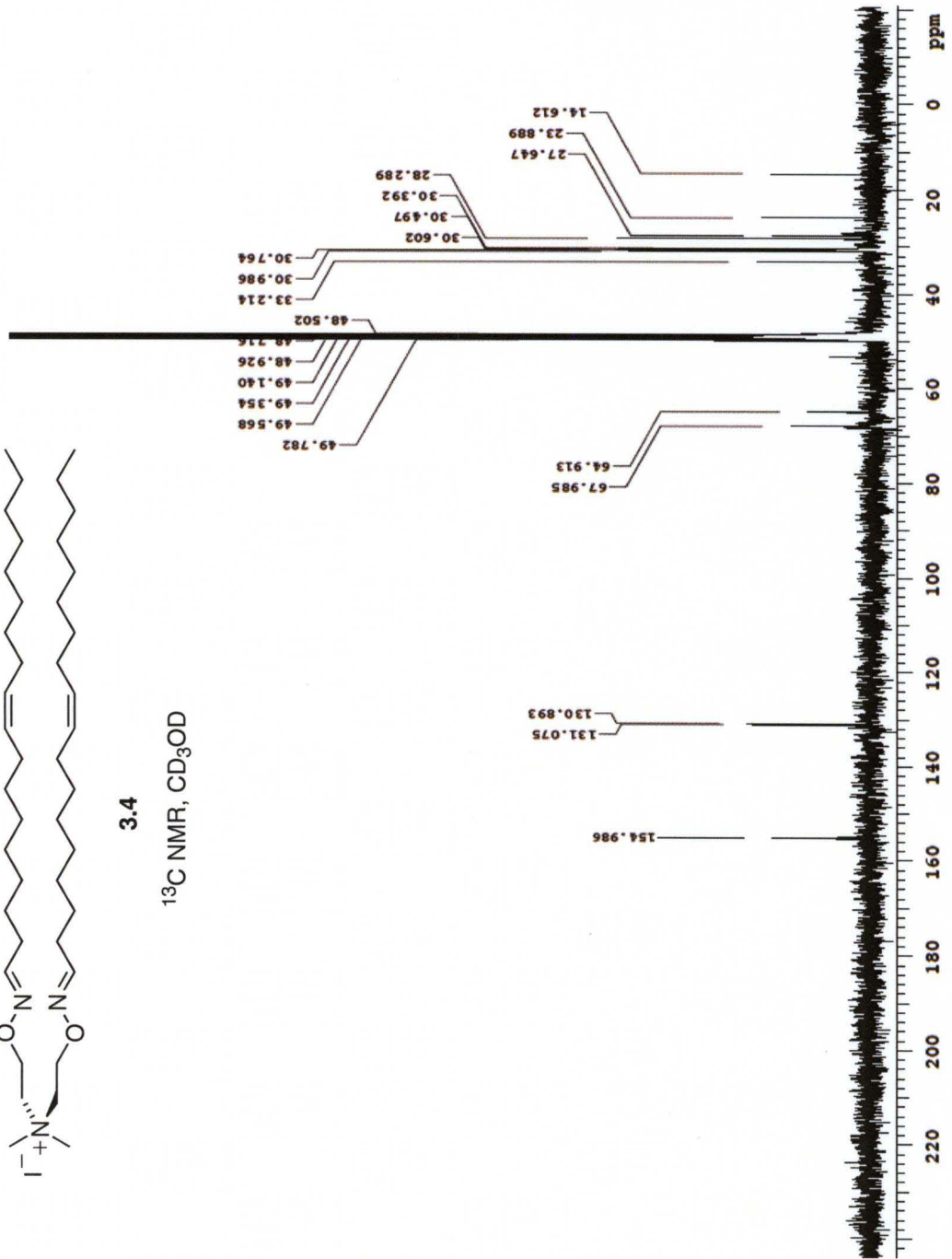
$^1\text{H NMR}$ ,  $\text{CD}_3\text{OD}$

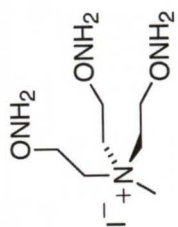




3.4

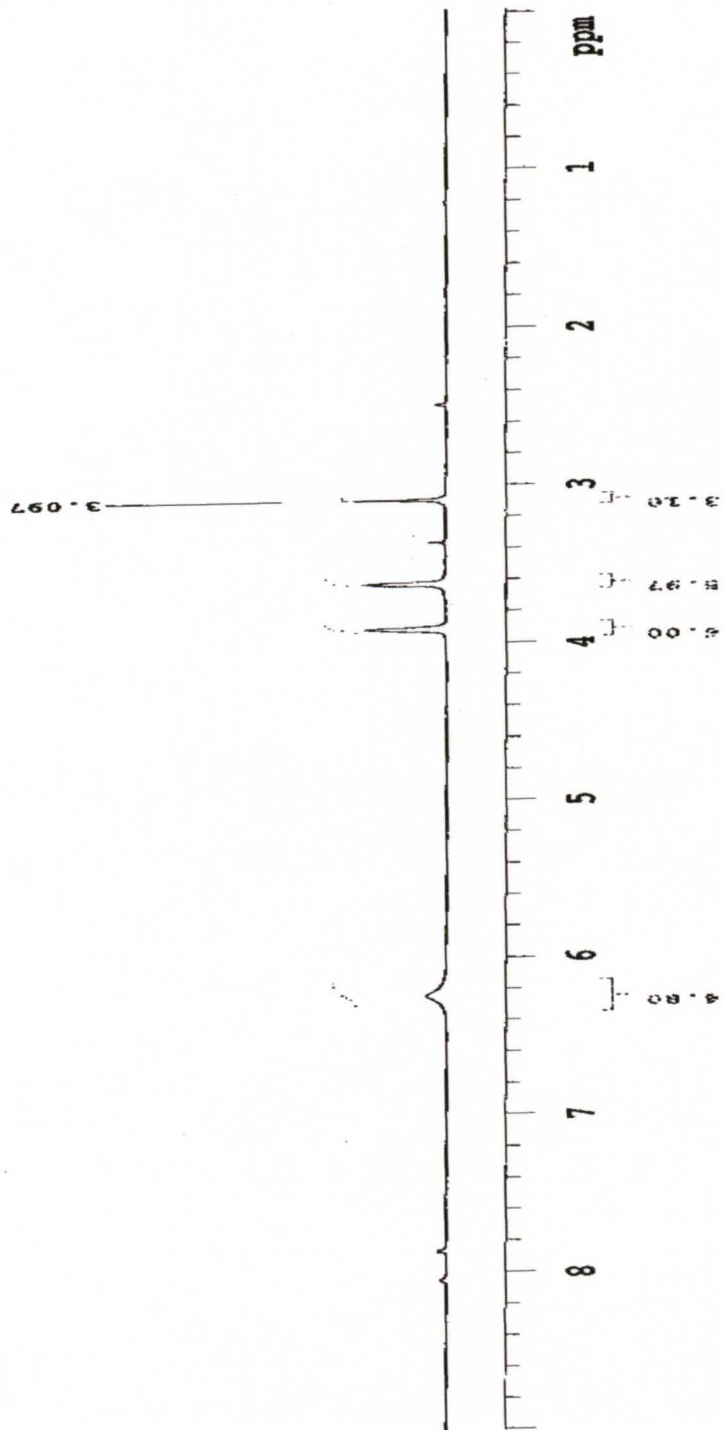
$^{13}\text{C}$  NMR,  $\text{CD}_3\text{OD}$

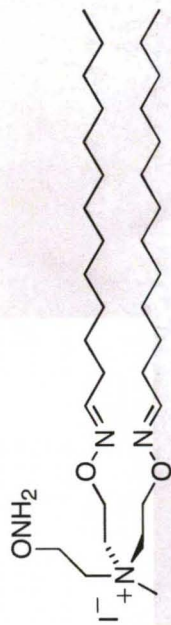




3.5

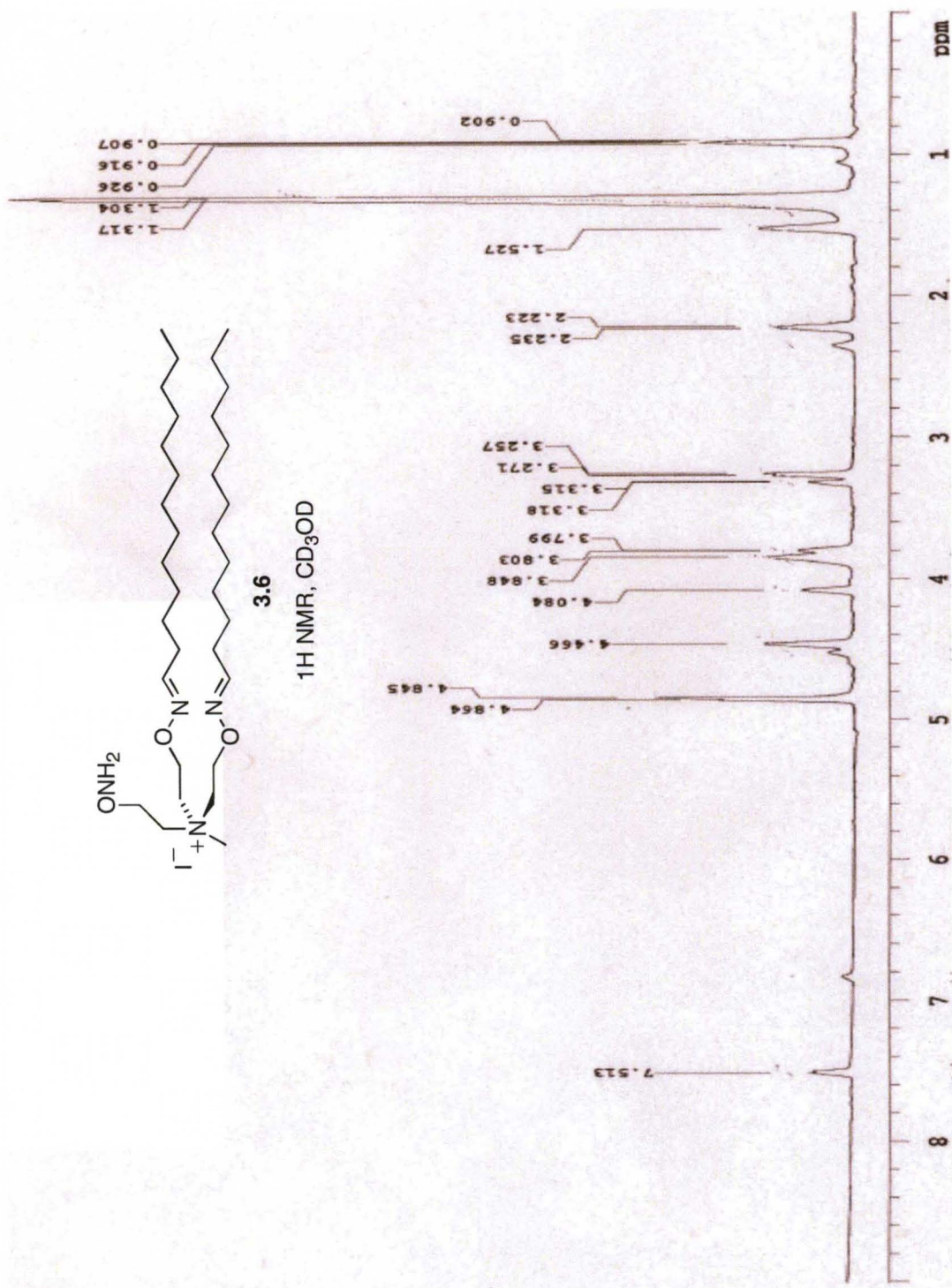
<sup>1</sup>H NMR, CD<sub>3</sub>OD



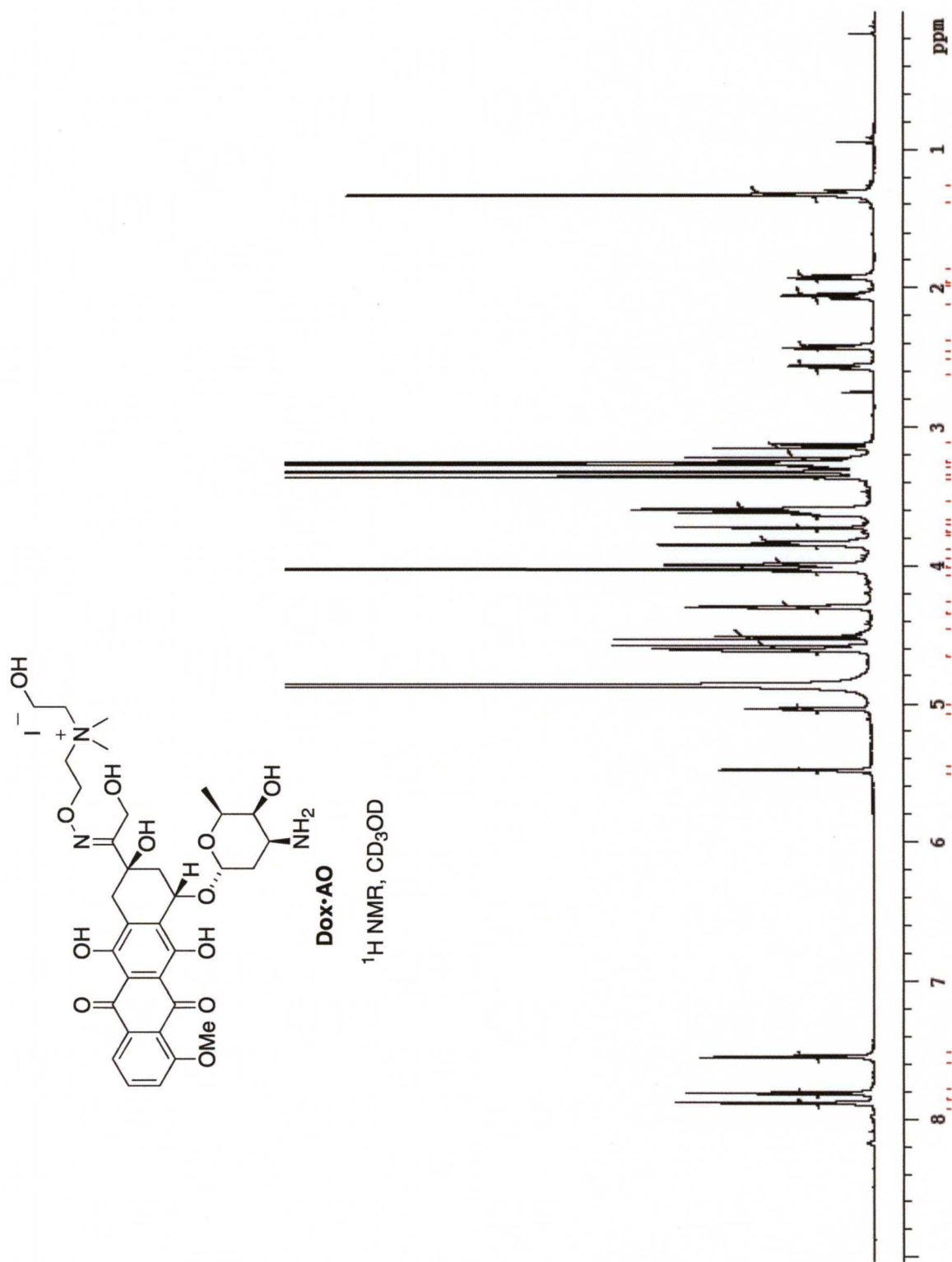


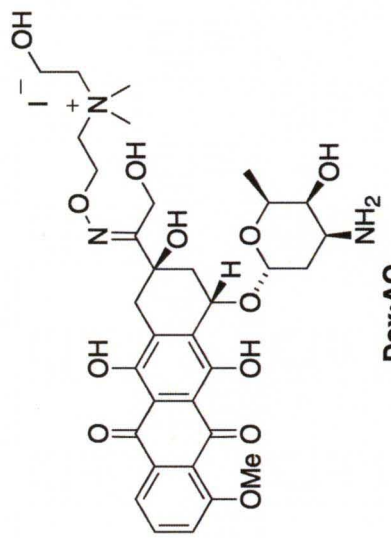
3.6

<sup>1</sup>H NMR, CD<sub>3</sub>OD

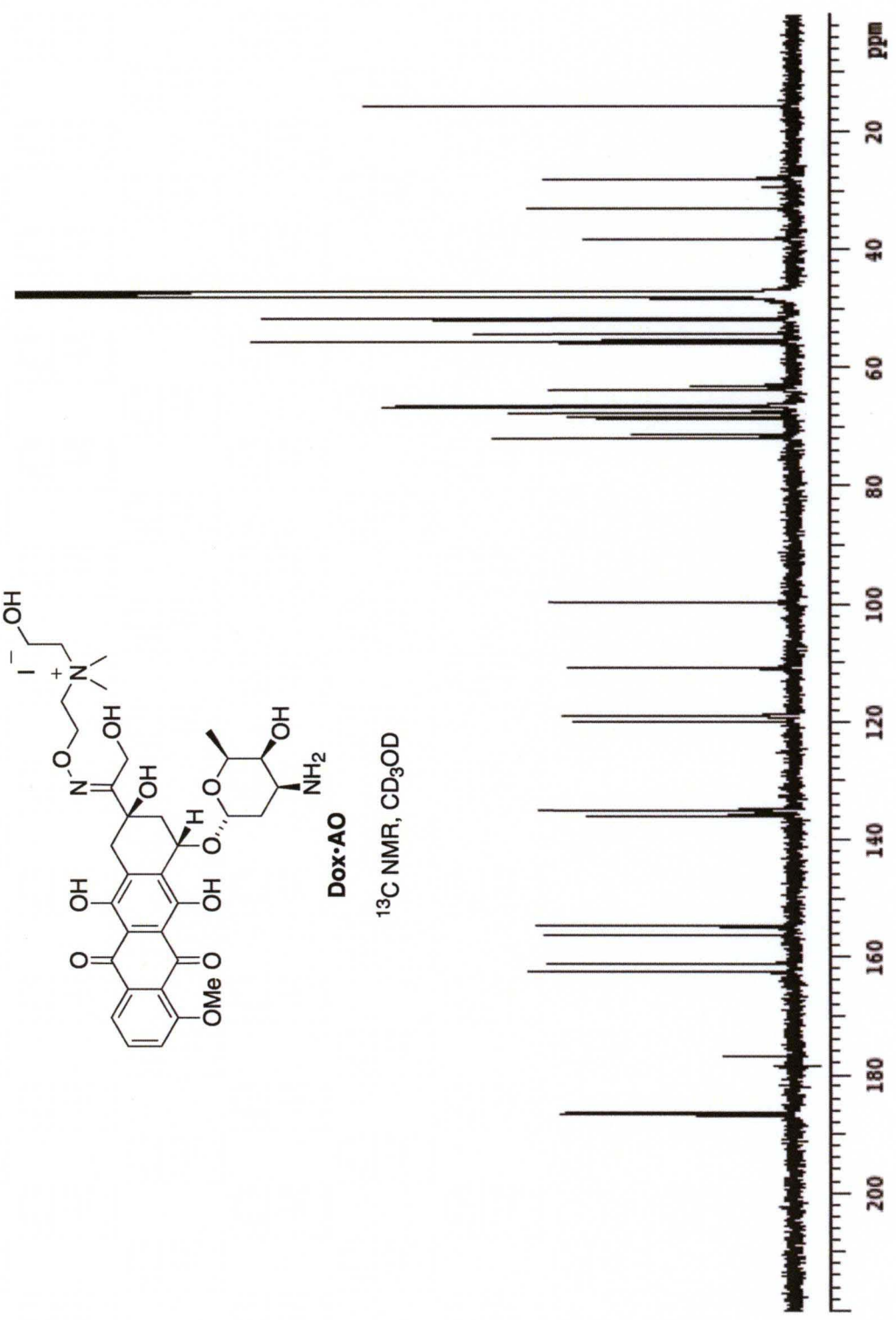








<sup>13</sup>C NMR, CD<sub>3</sub>OD



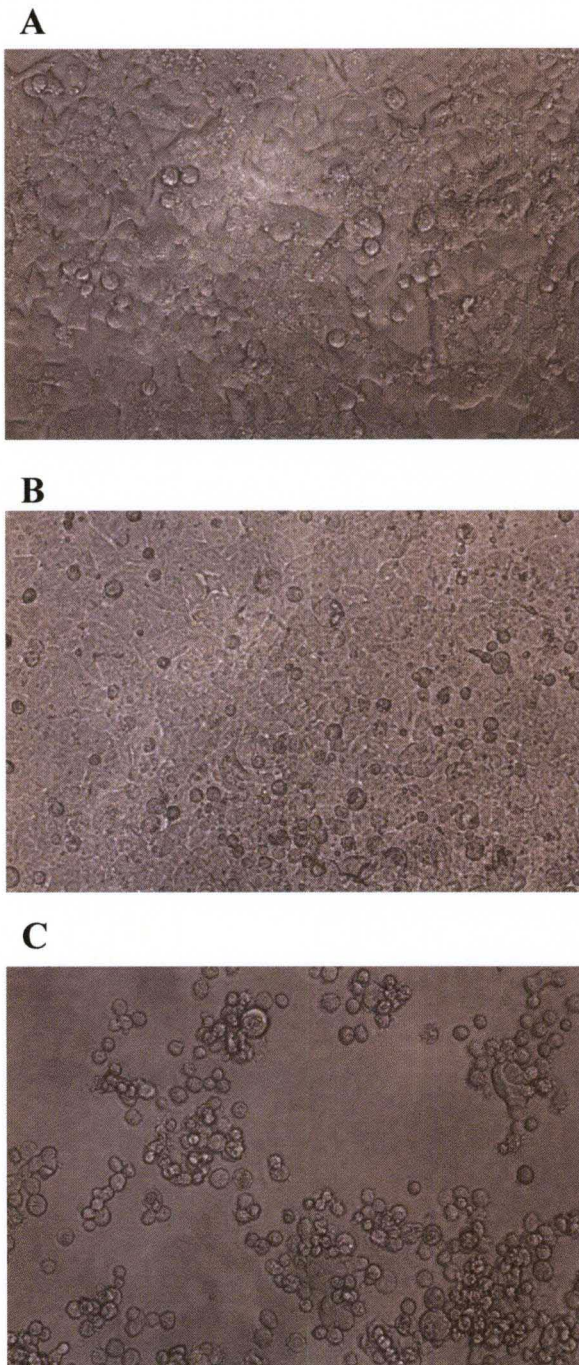


**Figure A.1.** Microscope images of MCF-7 cells after 48 h of treatment with Dox and Dox•AO . **A.** Untreated cells. **B.** Dox•HCl treatment. **C.** Cells treated with Dox•AO.

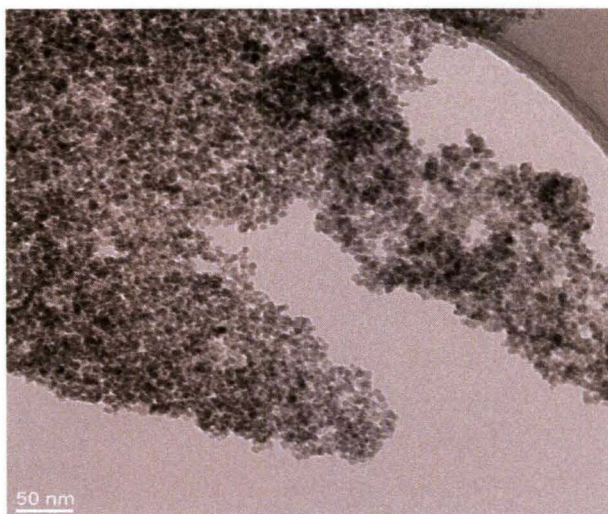


**Figure A.2.** TEM micrograph of  $\text{Fe}_3\text{O}_4$  nanoparticles.

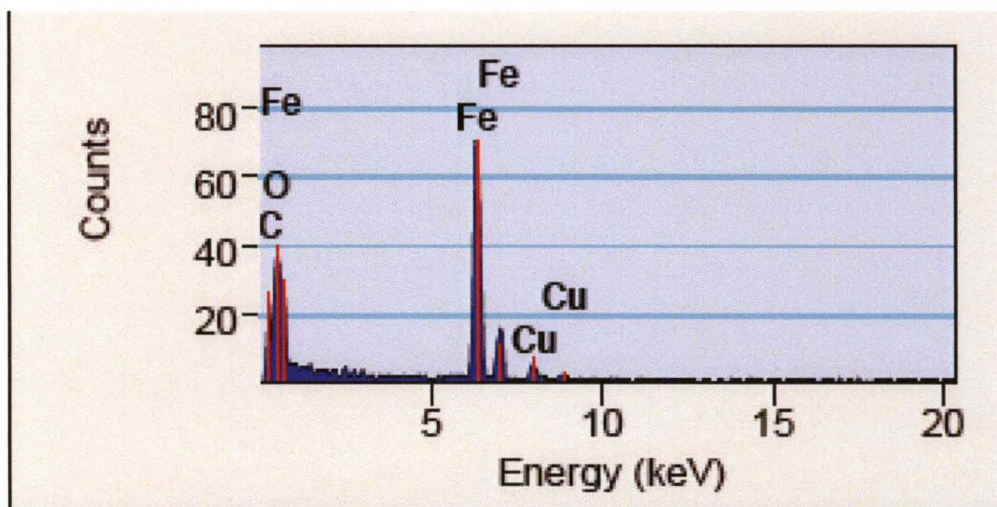


**Figure A.3.** EDX spectrum of NPs.

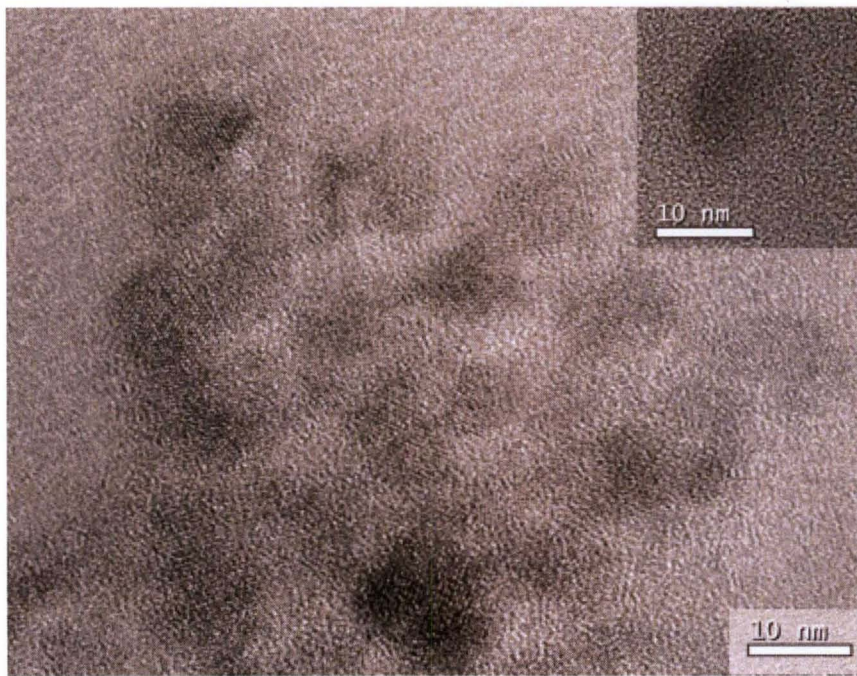


**Figure B.4.** TEM micrograph of dNP•AO•Dox particles; inset is a single particle.

## **APPENDIX B**

---

### **B.1. List of Patent and Publications**

### **B.2. Abstracts (and Title Pages) of Patent and Publications**

---

## B.1. Publications

This thesis work has led to one patent and several publications. The following list summarizes the publications that arose from my research and the Chapter(s) in which the work is described more fully. Also attached are the title pages of these works in the section B.2.

### Patent

Nantz, M. H. and Biswas, S. Nanoparticles for Drug Delivery. **PCT/US2010/53235**, Filed October 19, 2010. Patent pending (priority: Provisional Application 61/252,934, Filed October 19, 2009). [Chapter 4]

### Publications

1. Biswas, S.; Huang, X.; Badger, W. R.; Nantz, M. H. Nucleophilic Cationization Reagents. *Tetrahedron Letters* **2010**, *51*, 1727-1729. [Chapter 2-5]
2. Biswas, S.; Gordon, L. E.; Clark, G. J.; Nantz, M. H. Click Assembly of Magnetic Nanovectors for Gene Delivery. *Biomaterials* **2011**, *32*, 2683-2688. [Chapter 2]
3. Biswas, S.; Knipp, R. J.; Gordon, L. E.; Nandula, S. R.; Gorr, S.-U.; Clark, G. J.; Nantz, M. H. Hydrophobic Oxime Ethers: A Versatile Class of pDNA and siRNA Transfection Lipids. *ChemMedChem* **2011**, *6*, 2063-2069. [Chapter 3]
4. Fu, X-A; Li, M; Biswas, S; Nantz, M. H.; Higashi, R. A. A Novel Preconcentration Approach for Analysis of Ketones and Aldehydes in Breath. *Analyst* **2011**, *136*, 4662-4666. [Chapter 5]
5. Li, M; Biswas, S; Nantz, M. H.; Higashi, R. A.; Fu, X-A. A Novel Method for Detection of Ultra Trace Ketones and Aldehydes. *Analytical Chemistry* **2011**, **In Press**. [Chapter 5]
6. Biswas, S.; Gordon, L. E.; Clark, G. J.; Nantz, M. H. Externally Directed AMF-triggered Release of Doxorubicin from Magnetic Carriers. *Nano Letters* **2011**, manuscript in preparation. [Chapter 4]
7. Wang, J.; O'Toole, M. G.; Massey, A. P.; Biswas, S.; Nantz, M. H.; Achilefu, S. and Kang, K. A. Highly Specific, NIR Fluorescent Contrast Agent with Emission Controlled by Gold Nanoparticles. *Advances in Experimental Medicine and Biology* **2011**, *701*, 149-154. [this research, a side project, is not detailed in this thesis]

## B.2. Abstracts (and Title Pages) of Patent and Publications

SciFinder - Magnetic iron o...

11/28/11 6:17 PM

Explore •  
References

Explore •  
Substances

Explore •  
Reactions

Welcome souvik biswas | Sign Out

Author Name "Nantz, Michael" > references (150) > Magnetic

iron oxide nanopartic...

### Reference Detail

[Return](#)

[Previous](#) [Next](#)

## 5. Magnetic iron oxide nanoparticles for targeted drug delivery

By: **Nantz, Michael H.**; Biswas, Souvik  
Assignee: University of Louisville, USA

The invention provides magnetic nanoparticles comprising a core, wherein the nanoparticles comprise at least one therapeutic agent linked to the core via a hydrazone linkage or via an oxime ether linkage, methods for making said nanoparticles, and methods for using said nanoparticles.

### Patent Information

Patent No.	Kind	Date	Application No.	Date
WO 2011049972	A1	Apr 28, 2011	WO 2010-US53235	Oct 19, 2010

### Priority Application

US 2009-252934P	P	Oct 19, 2009
-----------------	---	--------------

### Indexing

Pharmaceuticals (Section 63-5)

### Concepts

Electromagnetic field

alternating; magnetic iron oxide nanoparticles for targeted drug delivery

Antibiotics

anthracycline; magnetic iron oxide nanoparticles for targeted drug delivery

### Quick Links

0 Tags, 0 Comments

### Patent Information

Apr 28, 2011  
WO 2011049972  
A1

### Application

Oct 19, 2010  
WO 2010-US53235

### Priority

Oct 19, 2009  
US 2009-252934P

### Source

*PCT Int. Appl.*  
43pp.  
Patent  
2011  
CODEN: PIXXD2

### Accession Number

2011:523642  
CAN 154:523682  
CAPLUS

### Language

English





## Nucleophilic cationization reagents

Souvik Biswas, Xuan Huang, Wesley R. Badger, Michael H. Nantz\*

Department of Chemistry, University of Louisville, Louisville, KY 40292, United States

### ARTICLE INFO

#### Article history:

Received 4 January 2010

Revised 20 January 2010

Accepted 25 January 2010

Available online 1 February 2010

### ABSTRACT

Nucleophilic cationization reagents fitted with aminoxy groups are described. Practical syntheses of mono- and bis-aminoxy tetraalkylammonium iodides including *N*-hydroxyethyl-functionalized analogs are reported. An oximation example using one of the reagents is presented to illustrate their use in synthesis of cationic materials.

© 2010 Elsevier Ltd. All rights reserved.

A wide variety of materials have been modified by the covalent attachment of quaternary ammonium functionality to furnish derivatives with overall positive charge.<sup>1</sup> This process, a derivatization known as cationization, typically proceeds via reaction of the substrate with an electrophilic reagent containing a quaternary ammonium salt. For example, the cationization of proteins is performed to enhance their intracellular delivery via adsorptive-mediated endocytosis.<sup>2</sup> The cationization of cellulose fibers (e.g., cotton) can improve the uptake of dyes in subsequent coloring operations.<sup>3</sup> These applications and others principally rely on cationization reagents of the type 1–5 depicted in Figure 1. Indeed, chlorohydrin **1**<sup>4</sup> and epoxide reagents **2**<sup>5</sup> and **3**<sup>6</sup> have been particularly useful for the cationization of carbohydrate domains in reactions with bases at elevated temperatures. The reagents **4**<sup>7</sup> and **5**<sup>8</sup> illustrate other permutations of reactive electrophilic groups used in reactions to derivatize materials with ammonium salts.

Of particular interest to us<sup>9</sup> is the use of quaternary ammonium salts attached to lipid- or polymer-frameworks as vehicles for the intracellular delivery of polynucleotides to mammalian cells.<sup>10</sup> We felt that a mild, more convenient procedure for direct attachment of ammonium ions to substrates would greatly improve our abilities to access new cationic materials. On considering alternative strategies, the chemospecific reaction between aminoxy and ketone or aldehyde carbonyl groups appeared to be an ideal, nucleophilic counterpart to current methods.<sup>11</sup> Given the ease of oximation and the robust nature of the oxime ether linkage, we targeted aminoxy reagents **6.1** and **6.2** (Fig. 2) for synthesis. Our interest in gene transfer materials also led us to prepare hydroxyethyl-functionalized analogs **7.1** and **7.2**. The benefit of hydroxyethylated polar domains in gene delivery is well documented.<sup>12</sup> Consequently, we disclose herein a general synthesis of the novel nucleophilic cationization reagents **6** and **7**.

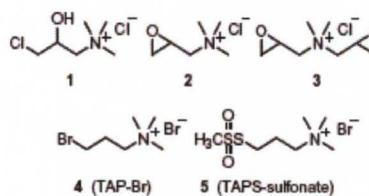


Figure 1. Common cationization reagents.

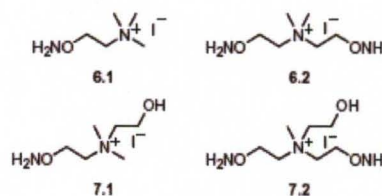
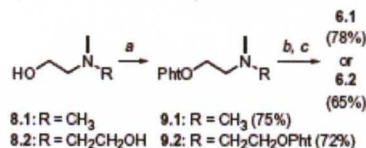


Figure 2. Cationic aminoxy reagents.

Reaction of the commercially available ethanolamines **8.1** and **8.2** (Scheme 1) with *N*-hydroxyphthalimide (NHP) under Mitsunobu



Scheme 1. Reagents and conditions: Pht = phthalimidoyl; (a) *N*-hydroxyphthalimide, PPh<sub>3</sub>, DIAD, THF, 0 °C to rt, 12 h; (b) CH<sub>2</sub>L sealed tube, 45 °C, 2 h; (c) H<sub>2</sub>NNH<sub>2</sub>·H<sub>2</sub>O, EtOH, H<sub>2</sub>O, rt, 12 h.

\* Corresponding author. Tel.: +1 502 852 8069; fax: +1 502 852 7214.  
E-mail address: michael.nantz@louisville.edu (M.H. Nantz).



## Click assembly of magnetic nanovectors for gene delivery

Souvik Biswas<sup>a</sup>, Laura E. Gordon<sup>b</sup>, Geoffrey J. Clark<sup>b</sup>, Michael H. Nantz<sup>a,\*</sup>

<sup>a</sup> Department of Chemistry, University of Louisville, Louisville, KY 40292, USA

<sup>b</sup> Department of Medicine, Brown Cancer Center, University of Louisville, Louisville, KY 40292, USA

### ARTICLE INFO

#### Article history:

Received 2 December 2010

Accepted 29 December 2010

Available online 20 January 2011

#### Keywords:

Nanoparticle

Oxidation

Aminoxy

Magnetofection

Magnetoplex

### ABSTRACT

Functionalization of iron oxide nanoparticles with quaternary ammonium ion-based aminoxy and oxime ether substrates provides a flexible route for generating magnetic gene delivery vectors. Using the MCF-7 breast cancer cell line, our findings show that pDNA magnetoplexes derived from the lipid-coated nanoparticle formulation dMPLP transfect in the presence of 10% serum with or without magnetic assistance at significantly higher levels than a commonly used cationic liposome formulation, based on luciferase assay. The present ion-pairing, click chemistry approach furnishes Fe<sub>3</sub>O<sub>4</sub> nanoparticles with lipid layers. The resultant magnetic nanovectors serve as transfection enhancers for otherwise transfection-inactive materials.

© 2011 Elsevier Ltd. All rights reserved.

### 1. Introduction

Since the seminal report by Mah's group on the use of magnetic nanoparticles to enhance viral-mediated transduction [1], much research effort has been directed toward the development of nano-sized magnetic vectors for intracellular delivery of polynucleotides [2]. Indeed, the rising interest in 'magnetofection', the term coined by Scherer et al. [3] to denote magnet-assisted gene delivery [4,5], has led to a plethora of new strategies for functionalizing magnetic particles to promote association with negatively charged oligonucleotides [6], DNA or siRNA [7]. The majority of approaches have relied on coating iron oxide nanoparticles or nanocomposites with cationic polymers, such as poly-L-lysine [8] or, in particular, polyethylenimine (PEI) [9–11]. The high positive charge [12] of PEI effectively promotes DNA transfer into cells. Additionally, the polyamine backbone of PEI enhances escape of DNA complexes entrapped within endosomes by means of a proton sponge effect that increases osmotic pressure and causes endosome rupture [13]. Magnetic PEI-coated nanoparticles generally are prepared by mixing suspensions of magnetite (Fe<sub>3</sub>O<sub>4</sub>) nanocrystals with solutions of linear or branched PEI [14]. More recently, an *in situ* preparation [15] involving precipitation of iron oxide in the presence of PEI and a method for covalent attachment [16] of PEI to chitosan-coated iron oxide nanoparticles have been described. Elaboration of PEI-coated iron oxide nanoparticles, such as by

addition of cationic peptide fragments [17] or single chain antibodies [18], is also an area under intense investigation. Irrespective of the mode of generation or subsequent functionalization, magnetic PEI-coated iron oxide nanovectors readily combine with polynucleotides on simple mixing to generate the corresponding magnetic, electrostatic charge-affinity complexes. The resultant 'magnetoplexes' (nomenclature derived by extrapolation of the established term magnetoliposome [19] and the terms lipoplex and polyplex [20]) have been used principally for gene delivery *in vitro*; however, successful magnetofection also has been demonstrated *in vivo* by externally applying a magnetic gradient to the treatment area, for example [21].

One concern that plagues applications involving PEI is the associated cellular toxicity. The high positive charge density of PEI disrupts cellular membranes [22]; thus, complications arising from vector toxicity afflict many PEI-based gene therapy approaches [23]. To overcome this limitation, a recent focus in the field of magnetofection has been to develop lipid-based magnetoplexes. This strategy has been realized in part by mixing preformed lipoplexes (cationic lipid:helper lipid:DNA) with magnetite [24] or by adding transfection-active cationic liposome formulations (cationic lipid:helper lipid) to either oleic acid-coated [25,26] or dextran-coated [27] magnetite prior to complexation with nucleic acids to form magnetoplexes.

Given that the molecular structure of cationic lipids has a profound influence on gene delivery [28], it is surprising that few magnetofection studies have exploited structure-activity optimizations offered by a modular, lipid-based approach. Our program on

\* Corresponding author. Tel.: +1 502 852 8059.  
E-mail address: [michael.nantz@louisville.edu](mailto:michael.nantz@louisville.edu) (M.H. Nantz).

DOI: 10.1002/cmdc.201100259

## Hydrophobic Oxime Ethers: A Versatile Class of pDNA and siRNA Transfection Lipids

Souvik Biswas,<sup>[a]</sup> Ralph J. Knipp,<sup>[a]</sup> Laura E. Gordon,<sup>[b]</sup> Seshagiri R. Nandula,<sup>[c]</sup> Sven-Ulrik Gorr,<sup>[c]</sup> Geoffrey J. Clark,<sup>[b]</sup> and Michael H. Nantz<sup>\*(a)</sup>

The manipulation of the cationic lipid structures to increase polynucleotide binding and delivery properties, while also minimizing associated cytotoxicity, has been a principal strategy for developing next-generation transfection agents. The polar (DNA binding) and hydrophobic domains of transfection lipids have been extensively studied; however, the linking domain comprising the substructure used to tether the polar and hydrophobic domains has attracted considerably less attention as an optimization variable. Here, we examine the use of an oxime ether as the linking domain. Hydrophobic oxime ethers were readily assembled via click chemistry by oximation of hy-

drophobic aldehydes using an aminoxy salt. A facile ligation reaction delivered the desired compounds with hydrophobic domain asymmetry. Using the MCF-7 breast cancer, H1792 lung cancer and PAR C10 salivary epithelial cell lines, our findings show that lipoplexes derived from oxime ether lipids transfect in the presence of serum at higher levels than commonly used liposome formulations, based on both luciferase and green fluorescent protein (GFP) assays. Given the biological compatibility of oxime ethers and their ease of formation, this functional group should find significant application as a linking domain in future designs of transfection vectors.

### Introduction

Cationic lipids and their derived liposomes have become the most well-studied and widely used synthetic, nonviral gene delivery vehicles since Felgner et al.<sup>[1]</sup> first disclosed DOTMA-mediated gene transfer in 1987.<sup>[2,3]</sup> Due to the major limitations of viral vectors, such as associated immune responses, limited polynucleotide carrying capacity and high cost,<sup>[4,5]</sup> cationic lipids remain an attractive alternative. The advantages of low immunogenicity, the ability to transfect RNA or DNA of nearly unlimited size,<sup>[6,7]</sup> and the relative ease of cationic lipid-plasmid DNA (pDNA) or RNA complex (lipoplex) formulation<sup>[8]</sup> continue to attract interest aimed at developing safer and more efficient cationic lipids for use as transfection agents.<sup>[9]</sup>

Cationic lipid molecules, such as the prototypical dual chain lipids DOTMA<sup>[1]</sup> and DOTAP<sup>[10]</sup> (Figure 1), contain a polar, positively charged (DNA binding) head group connected to a hydrophobic domain via a linking functionality. These three principal structural components of cationic glycerol-type lipids

have been extensively studied in efforts to improve lipid-mediated intracellular delivery of polynucleotides to mammalian cells.<sup>[11]</sup> Many structure-activity relationships have been determined,<sup>[12,13]</sup> particularly for the hydrophobic domain. Indeed, the hydrophobic domain's structural variables of chain length, degree of unsaturation, and domain asymmetry are among the strongest contributors to transfection efficacy.<sup>[14]</sup> Fewer direct structural comparisons of changes in the cationic lipid backbone, or linking domain, have been reported, with the most well-known comparison being that of the diether DOTMA versus the diester DOTAP.<sup>[15]</sup> The linking functionality, and to a lesser extent the cationic head group, seem to be the principal determinants of toxicity.<sup>[15-17]</sup> The linker determines conformational flexibility, degree of stability, and biodegradability. Among the most studied chemical functionalities comprising the linking domain of transfection lipids are the ether, ester, ortho ester,<sup>[18,19]</sup> carbamate,<sup>[20]</sup> amide,<sup>[21,22]</sup> and phosphono<sup>[23]</sup> moieties.

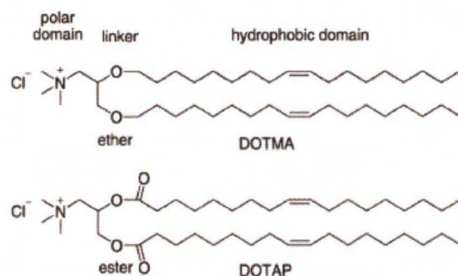


Figure 1. Structural domains of common transfection lipids.

[a] S. Biswas, R. J. Knipp, Dr. M. H. Nantz  
Department of Chemistry, University of Louisville  
2320 S. Brook Street, Louisville, Kentucky 40292 (USA)  
E-mail: michael.nantz@louisville.edu

[b] L. E. Gordon, Dr. G. J. Clark  
School of Medicine, Brown Cancer Center, University of Louisville  
529 S. Jackson Street, Louisville, Kentucky 40292 (USA)

[c] Dr. S. R. Nandula, Dr. S.-U. Gorr  
School of Dentistry, University of Minnesota, Moos Health Sciences Tower  
515 Delaware Street SE, Minneapolis, Minnesota 55455 (USA)

Supporting information for this article is available on the WWW under <http://dx.doi.org/10.1002/cmdc.201100259>.

Cite this: *Analyst*, 2011, **136**, 4662

www.rsc.org/analyst

## COMMUNICATION

## A novel microreactor approach for analysis of ketones and aldehydes in breath

Xiao-An Fu,<sup>a\*</sup> Mingxiao Li,<sup>a</sup> Souvik Biswas,<sup>b</sup> Michael H. Nantz<sup>b</sup> and Richard M. Higashi<sup>b,c,d</sup>

Received 19th July 2011, Accepted 19th August 2011

DOI: 10.1039/c1an15618g

We report a fabricated microreactor with thousands of micropillars in channels. Each micropillar surface is chemically functionalized to selectively preconcentrate gaseous ketones and aldehydes of exhaled breath and to enhance ultra-trace, rapid analysis by direct-infusion Fourier transform-ion cyclotron resonance (FT-ICR) mass spectrometry (MS). The micropillar reactive coating contains the quaternary ammonium aminoxy salt 2-(aminoxy)ethyl-*N,N,N*-trimethylammonium iodide (ATM) for capturing trace carbonyl VOCs by means of an oximation reaction. We demonstrate the utility of this approach for detection of C<sub>1</sub> to C<sub>12</sub> aldehydes and ketones in exhaled breath, but the approach is applicable to any gaseous sample.

Analysis of exhaled breath has been elevated to an international research frontier because of its potential and applicability in non-invasive health diagnosis, metabolite bioinformatics, and drug discovery.<sup>1-5</sup> The gaseous portion of breath is a complex mixture of atmospheric gases, water vapor, and trace volatile organic compounds (VOCs). In 1971, Pauling reported the first gas-chromatographic analysis of breath, and the study revealed the presence of a large number of VOCs in human breath.<sup>6</sup> A number of recent publications suggest that the analysis of exhaled breath promises to be a non-invasive diagnosis for early detection of particulate cancers since some VOCs in exhaled breath represent metabolic output of cancer tissues and cells.<sup>7-13</sup>

There are several critical challenges for the analysis of VOCs in exhaled breath, including ultra-trace concentrations of VOCs and interference of complex gas mixtures. Exhaled breath contains more than 200 VOCs. Recently, several reports indicate that some ketones and aldehydes in exhaled breath could be used for the diagnosis of lung cancer in its early stage.<sup>4,5,7,12,13</sup>

However, so far there is no established protocol for the analysis of all ketones or aldehydes in exhaled breath, in part due to their highly reactive nature. These carbonyl metabolites are produced in biochemical pathways as intermediates and some can be unique to

a given pathway or process. However, even common carbonyl metabolites can be attributed to specific processes when stable isotope labeled substrates are metabolized (e.g. by human subjects) and detected by mass spectrometry or NMR.<sup>14,15</sup> Volatile ketones and aldehydes are also generated from damaging oxidative reactions, such as lipid peroxidation.<sup>16-18</sup> Therefore, development of a new method for analysis of ketone and aldehyde VOCs in exhaled breath is a crucial first step to fulfilling the potential that breath analysis promises.

Ketones and aldehydes can be detected by proton transfer reaction mass spectrometry (PTR-MS)<sup>19-21</sup> or selected ion flow tube mass spectrometry (SIFT-MS) without any preconcentration process.<sup>22-25</sup> Most recently, solid phase microextraction (SPME) with adsorbed *O*-2,3,4,5,6-(pentafluorobenzyl)hydroxylamine hydrochloride (PFBHA) has been used for analysis of aldehydes in exhaled breath by gas chromatography-mass spectrometry (GC-MS).<sup>4,5</sup> SPME is a popular preconcentration method introduced a decade ago as a rapid extraction technique for analysis of volatile compounds from a variety of matrices.<sup>26</sup> However, the surface area of the SPME polymer extraction phase is small and aldehyde capture requires physical adsorption of PFBHA onto SPME first. In most cases, it is also extremely difficult to improve upon, or even determine the volume of air that is actually sampled by the SPME fiber. The quality of the fibers depends on the manufacturer, and the performance varies from batch to batch. Derivatization of ketones and aldehydes by reaction with 2,4-dinitrophenylhydrazine has also been used for analysis of carbonyl compounds in exhaled breath,<sup>16,27</sup> which has the advantage of converting volatile aldehydes and ketones into stable, easy-to-handle non-volatile analytes. However, this class of reagents was not designed to aid in detection by modern ultra-sensitive MS ion sources such as nanoelectrospray.

In this work, we describe a microreactor approach for chemoselective capture of gaseous ketones and aldehydes from gaseous samples such as exhaled breath. The microreactor was fabricated on a silicon wafer and charged with an aminoxy-functionalized quaternary ammonium salt. The high selectivity of the aminoxy moiety (R-ONH<sub>2</sub>) for reaction with ketone and aldehyde carbonyl groups suggested that an oximation reaction could be used to selectively capture ketone and aldehyde metabolites directly from the air, such as exhaled breath. For rapid analysis and identification of VOC adducts, we additionally turned to direct-infusion nanoelectrospray FT-ICR-MS analysis. This microscale sampling technique matched the samples sizes of the microreactor, and the ultra-high resolution FT-ICR-MS enables simultaneous analysis of the ketone and aldehyde adducts, while avoiding analytical interference from the capture

<sup>a</sup>Department of Chemical Engineering, University of Louisville, Louisville, KY, 40208, USA. E-mail: xiaofu@louisville.edu

<sup>b</sup>Department of Chemistry, University of Louisville, Louisville, KY, 40292, USA

<sup>c</sup>Center for Regulatory and Environmental Analytical Metabolomics (CREAM), University of Louisville, Louisville, KY, 40208, USA

<sup>d</sup>James Graham Brown Cancer Center, University of Louisville, Louisville, KY, 40292

## A Novel Method for Preconcentration and Analysis of Trace Volatile Carbonyl Compounds

Mingxiao Li<sup>a</sup>, Souvik Biswas<sup>b</sup>, Michael H. Nantz<sup>b</sup>,

Richard M. Higashi<sup>b, c</sup>, Xiao-An Fu<sup>\*a</sup>

Departments of <sup>1</sup>Chemical Engineering and <sup>2</sup>Chemistry, <sup>3</sup>Center for Regulatory and Environmental Analytical Metabolomics (CREAM), and <sup>4</sup> James Graham Brown Cancer Center, University of Louisville, Louisville, Kentucky 40292

**ABSTRACT:** This paper demonstrates a novel preconcentration approach for quantitative analysis of trace volatile ketones and aldehydes in air and in human breath. The approach is based on the fabricated microreactor chips on a silicon wafer. The microreactors have thousands of micropillars in the microfluidic channel for uniformly distributing gaseous sample flowing through the microreactors. The surfaces of the micropillars are functionalized with a quaternary ammonium aminoxy 2-(aminoxy)ethyl-*N,N,N*-trimethylammonium iodide (ATM) synthesized in-house for trapping trace ketones and aldehydes by means of an oximation reaction. The ATM adduct and unreacted ATM can be easily eluted from the microreactor with less than 40 microliter of methanol and directly analyzed by nanospray Fourier transform-ion cyclotron resonance (FT-ICR) mass spectrometry (MS). Ketones and aldehydes in a concentration of 1ppbv can be detected. The microreactor approach is suitable for quantitative analysis of ketones and aldehydes in exhaled breath.

**KEYWORDS:** Preconcentration, Microreactor, Breath Analysis, Ketones, Aldehydes

## Chapter 21

# Highly Specific, NIR Fluorescent Contrast Agent with Emission Controlled by Gold Nanoparticle

Jianting Wang, Martin O'Toole, Archna Massey, Souvik Biswas, Michael Nantz, Samuel Achilefu, and Kyung A. Kang

**Abstract** Nanoparticles are currently being intensively studied for *in vivo* molecular imaging because of their unique and beneficial properties. Among these particles, some metal particles possess strong surface plasmon fields that can effectively alter fluorescence. Using this fluorescence alteration, an NIR fluorophore based, nano-sized contrast agent for breast cancer diagnosis is being developed. The fluorophore is conjugated to gold nanoparticles (GNP) *via* a short spacer whose length was specially adjusted to have the strong plasmon field to quench the fluorescence. The spacer also has a special molecular sequence that can be cleaved by an enzyme secreted by targeted cancer cells. Normally, the entity does not fluoresce. If it is delivered to the cancer site, the short spacer would be cleaved by the enzyme secreted by the cancer cell at which point the fluorescence would be restored. This entity can incorporate a cancer targeting molecule for a cancer specific delivery. The entity specifically targets cancer cells and fluoresce only when the spacer is cleaved by a specific cancer secreting biomolecule, providing dual specificity for cancer diagnosis. In the future, this entity will be combined with cancer drugs for seamless detection and personalized therapy.

### 21.1 Introduction

Fluorescence contrast agents have been extensively used in clinical diagnosis. Naturally, the agents providing high specificity are highly desirable for molecular imaging. Recently, nanoparticles have been intensively studied as candidates for image contrast agents and drug delivery because their small size allows interactions with

---

Jianting Wang, Martin O'Toole, and Kyung A. Kang  
Department of Chemical Engineering, University of Louisville, Louisville, KY 40292, USA  
e-mail: kyung.kang@louisville.edu

Archna Massey, Souvik Biswas, and Michael Nantz  
Department of Chemistry, University of Louisville, Louisville, KY 40292, USA

Samuel Achilefu  
Department of Radiology, Washington University School of Medicine, St. Louis, MO 63110, USA

J.C. LaManna et al. (eds.), *Oxygen Transport to Tissue XXXII*, Advances in Experimental Medicine and Biology 701, DOI 10.1007/978-1-4419-7756-4\_21, 149  
© Springer Science+Business Media, LLC 2011

# CURRICULUM VITAE

## Souvik Biswas

National Cancer Institute  
Chemical Biology Laboratory  
Frederick, MD, 21702  
Phone: 502-762-2594  
email: souvik\_gre@yahoo.com

1338 Taney Avenue, Apt 302  
Frederick, MD, 21702

---

### RESEARCH INTERESTS

- **Nanotherapeutics**; developing multifunctional nanoparticle-based platforms for drug delivery and bio-imaging
- **Non-viral gene delivery**; designing synthetic nano-vectors (e.g., liposomes and nanoparticles) for gene transfer
- **Organic synthesis**; developing targeted delivery systems for therapeutic agents and synthesizing drug conjugates using

### RESEARCH EXPERIENCE

#### 2007-Present

##### Gene Delivery

- Preparation and characterization of cationic aminoxy-functionalized Fe<sub>3</sub>O<sub>4</sub> nanoparticles
- Synthesis, characterization, formulation and application of novel magnetic lipid particles for *in vitro* transfections
- Development of alternating magnetic field-induced heat shock protein (*hsp*) promoted gene delivery systems
- Design, formulation and optimization of cationic oxime ether lipids for gene transfer application

##### Alternating Magnetic Field (AMF)-Triggered Drug Delivery

- Preparation, characterization and formulation of magnetic nano-carriers for doxorubicin
- Demonstration of *in vitro* AMF-triggered drug release and cell death
- Presently working on 3-D organo-mimic of human tumor model to substantiate the principles listed above

##### Organic Synthesis

- Design and characterization of oxime ether conjugates of the anti-cancer drug doxorubicin
- Synthesis and characterization of novel cationic oxime ether lipids for targeted gene delivery

- Synthesis and characterization of novel aminooxy-based reagents for various bio-medical applications
- Solid phase and solution phase syntheses of peptide-fluorophore conjugates (e.g., cypate)
- Synthesis of a panel of hydroxyethyl-based cationic lipids for use in microchip breath analyzer

**2005-2006 (Post M.Sc. research; advisor: Prof. A. N. Maitra, University of Delhi, India)**

- Formulation of highly stable water dispersed silver nanoparticles as an antimicrobial agent
- Glucose sensing ability of entrapped glucose oxidase in hollow gold nanoparticles

**KEY SKILLS**

**Synthesis and Formulation**

- Expertise in designing drug and gene delivery systems and synthesizing drug conjugates using “click” chemistry
- Expertise in surface functionalization and surface conjugation of nanoparticles for biomedical applications
- Proficient at formulation of drug and gene delivery systems (e.g., liposomes, lipoplexes, and magnetoplexes)

**AMF-triggered Drug Delivery**

Experience with operating an alternating magnetic field generator for magnetic hyperthermia-induced drug delivery

**Molecular Biology**

- Experience with drug release studies in cancer cells; evaluation of cytotoxicity using multiple assays
- Operation of fluorescence microscopy (AMG EVOS microscope)
- Extensive experience with non-viral methods of mammalian cell transfection; including the use of nanoparticles, magnetofection, cationic lipids, and polymers
- Familiar with different transfection assay systems (luciferase and GFP vector)

**EDUCATION**

**Ph.D., Chemistry, December 2011**

Thesis Title: “Functionalized Nanoparticles for AMF-Induced Gene and Drug Delivery”

Thesis Advisor: Professor Michael H. Nantz

Department of Chemistry, University of Louisville, Louisville, KY, USA

**M.Sc., Chemistry, 2006**

Department of Chemistry, University of Delhi, Delhi, India

**B.Sc., Chemistry (with Honors), 2002**

University of Calcutta, Kolkata, India

**AWARD**

Asit Ganguly and Jean Scholarship, 2003-2005 (this award is presented annually to the top three students in the M.Sc. Chemistry program at the University of Delhi)



## PATENT and PUBLICATIONS

### Patent

1. Nantz, M. H. and Biswas, S. Nanoparticles for Drug Delivery. **PCT/US2010/53235**, Filed October 19, 2010. Patent pending (priority: Provisional Application 61/252,934, Filed October 19, 2009).

### Peer Reviewed Publications

1. Biswas, S.; Gordon, L. E.; Clark, G. J.; Nantz, M. H. Click Assembly of Magnetic Nanovectors for Gene Delivery. *Biomaterials* **2011**, *32*, 2683-2688.
2. Biswas, S.; Huang, X.; Badger, W. R.; Nantz, M. H. Nucleophilic Cationization Reagents. *Tetrahedron Letters* **2010**, *51*, 1727-1729.
3. Biswas, S.; Knipp, R. J.; Gordon, L. E.; Nandula, S. R.; Gorr, S.-U.; Clark, G. J.; Nantz, M. H. Hydrophobic Oxime Ethers: A Versatile Class of pDNA and siRNA Transfection Lipids. *ChemMedChem* **2011**, *6*, 2063-2069.
4. Fu, X-A; Li, M; Biswas, S; Nantz, M. H.; Higashi, R. A. A Novel Preconcentration Approach for Analysis of Ketones and Aldehydes in Breath. *Analyst* **2011**, *136*, 4662-4666.
5. Li, M; Biswas, S; Nantz, M. H.; Higashi, R. A.; Fu, X-A. A Novel Method for Detection of Ultra Trace Ketones and Aldehydes. *Analytical Chemistry* **2011**, **In Press**.
6. Biswas, S.; Gordon, L. E.; Clark, G. J.; Nantz, M. H. Externally Directed AMF-triggered Release of Doxorubicin from Magnetic Carriers. *Nano Letters* **2011**, manuscript in preparation.
7. Biswas, S.; Knipp, R. J.; Nantz, M. H. Smart Inorganic Nanoparticles for Doxorubicin Delivery. **2011**, manuscript in preparation.

### Conference Proceedings and Presentations

1. Biswas S.; Gordon, L. E.; Clark, G. J.; Nantz, M. H. Externally directed AMF-triggered release of doxorubicin from magnetic carriers. Poster no. 28; presented at the 7th Kentucky Innovation and Entrepreneurship Conference and 16th Kentucky EPSCoR Conference, Louisville, KY; May 26, 2011.
2. Biswas S.; Gordon, L. E.; Deb, B.; Mattingly, S. J.; Massey, A. P.; Clark, G. J.; Nantz, M. H. Magnetic Lipid Particles (MLPs): A New Class of Iron Oxide Nanoparticles for Gene Transfer. Poster no. 10; presented at the Inaugural Conference of the American Society for Nanomedicine, Potomac, MD; October 22-25, 2009.
3. Biswas S.; Gordon, L. E.; Deb, B.; Mattingly, S. J.; Massey, A.P.; Clark, G. J.; Nantz, M. H. Magnetic Lipid Particles (MLPs): A New Class of Iron Oxide Nanoparticles for Gene Transfer. Poster 18; presented at the 11<sup>th</sup> Annual IMD3 Symposium, Louisville, KY; March 10, 2009.

## TEACHING EXPERIENCE

- Invited lecturer for graduate level Advanced Organic Chemistry 679, Modern Methods of Organic Synthesis (University of Louisville, Spring 2011)
- Invited lecturer for undergraduate organic chemistry 341 and 342 (University of Louisville)
- Organic Chemistry Recitation: Graduate Teaching assistant (GTA) for Organic chemistry 341 and 342 (fall 2007-summer 2008, Department of Chemistry, University of Louisville)
- Organic Chemistry Laboratory: GTA for Organic chemistry lab 344 (2007 spring and summer, Department of Chemistry, University of Louisville)

## **INSTRUMENTATION**

NMR, FTIR, HPLC, Combiflash *rf* (automatic liquid chromatograph system), particle size analyzer

## **REFERENCES**

1. Professor Michael H. Nantz (Ph.D. Advisor)  
Department of Chemistry, University of Louisville  
Louisville, KY 40292  
Phone 502-852-8069  
Email: [michael.nantz@louisville.edu](mailto:michael.nantz@louisville.edu)
2. Professor Geoffrey J. Clark  
Department of Medicine, Brown Cancer Center  
University of Louisville, KY 40202  
Phone 502-852-4485  
Email: [geoff.clark@louisville.edu](mailto:geoff.clark@louisville.edu)
3. Professor Xiao-An Fu  
Chemical Engineering Department  
University of Louisville, KY 40292  
Phone 502-852-6349  
Email: [xiaoan.fu@louisville.edu](mailto:xiaoan.fu@louisville.edu)